Exelon Nuclear
200 Exelon Way
KSA3-N
Kennett Square, PA 19348

Telephone 610.765.5610
Fax 610.765.5755
www.exeloncorp.com

Exelon Nuclear

52.17

October 31, 2005

U.S. Nuclear Regulatory Commission
ATTN: Document Control Desk
Washington, DC 20555

Early Site Permit (ESP) Application for the Clinton ESP Site
Docket No. 52-007

Subject: Responses to Supplemental Draft Safety Evaluation Report (DSER) Items

Re: Letter, U.S. Nuclear Regulatory Commission (W. D. Beckner) to Exelon Generation Company, LLC, (M. Kray), dated August 26, 2005, Supplemental Draft Safety Evaluation Report for the Exelon Early Site Permit Application

Enclosed, as requested in the referenced letter, are responses to the open items identified in the subject supplemental DSER for the Exelon Generation Company, LLC (EGC) ESP. Also provided in the enclosures is information related to the proposed permit conditions, and the proposed action items that would need to be addressed in a combined license (COL) application that references the ESP.

Please contact Eddie Grant of my staff at 850-598-9801 if you have any questions regarding this submittal.

Sincerely yours,

Thomas P. Mundy

Thomas P. Mundy
Director, Project Development

D073

TPM/erg

cc: U.S. NRC Regional Office (w/ enclosures)
Mr. John P. Segala (w/ enclosures)

Enclosures

AFFIDAVIT OF THOMAS P. MUNDY

State of Pennsylvania

County of Chester

The foregoing document was acknowledged before me, in and for the County and State aforesaid, by Thomas P. Mundy, who is Director, Project Development, of Exelon Generation Company, LLC. He has affirmed before me that he is duly authorized to execute and file the foregoing document on behalf of Exelon Generation Company, LLC, and that the statements in the document are true to the best of his knowledge and belief.

Acknowledged and affirmed before me this 31st day of October, 2005.

My commission expires 10-6-07.

Vivia V. Gallimore

Notary Public

COMMONWEALTH OF PENNSYLVANIA
Notarial Seal
Vivia V. Gallimore, Notary Public
Kennett Square Boro, Chester County
My Commission Expires Oct. 6, 2007
Member, Pennsylvania Association Of Notaries

NRC Letter Dated: 08/26/2005

This letter provides response(s) to the following draft safety evaluation report (DSER) Supplement Open Items.

DSER Open Item 2.5.1-1

DSER Open Item 2.5.2-1

DSER Open Item 2.5.2-2

DSER Open Item 2.5.2-3

DSER Open Item 2.5.2-4

DSER Open Item 2.5.2-5

DSER Open Item 2.5.4-1

In addition, the following proposed Permit Condition(s) and COL Action Items are addressed in this enclosure.

DSER Permit Condition 2.5-1

DSER COL Action Item 2.5.4-1

DSER COL Action Item 2.5.4-2

DSER COL Action Item 2.5.4-3

DSER COL Action Item 2.5.4-4

DSER COL Action Item 2.5.4-5

DSER COL Action Item 2.5.4-6

DSER COL Action Item 2.5.5-1

DSER COL Action Item 2.5.6-1

NRC Letter Dated: 08/26/2005

NRC DSER Open Item 2.5.1-1

Section 2.5.1.3.1 - The staff considers the applicant's response to RAI 2.5.1-1 to be an adequate assessment of the latest geologic literature concerning the magnitudes for New Madrid characteristic earthquakes. The applicant revised its magnitudes for rupture set number 3 to reflect the changes made by Bakun and Hooper (2004). In addition, the applicant added two new models based on its review of the latest literature and communications with researchers. The applicant assessed the impact of these additions and revisions by reevaluating its PSHA and found an increase (3 to 4 percent) in the 1 Hertz (Hz) ground motion hazard curve at the mean 10-4 and mean 10-5 hazard levels. However, the applicant did not incorporate this new information into its PSHA or subsequent SSE ground motion spectrum and indicated that the ESP application did not need to be updated as a result of its response to RAI 2.5.1-1. The applicant's failure to incorporate this information into its PSHA or SSE, and to explain why it did not update the SSAR to reflect the corrected magnitude estimates, renders its response to RAI 2.5.1-1 incomplete. This is Open Item 2.5.1-1. Further discussion of this open item, as it relates to NMSZ rupture sequence modeling, is provided in SER Section 2.5.2.3.3.

Section 2.5.2.3.3 - The staff considers the applicant's rationale for not updating its seismic hazard characterization of the NMSZ to be inadequate. In response to the staff's RAIs, the applicant has updated both the magnitudes for the NMSZ characteristic earthquake rupture sets (RAI 2.5.1-1) and rupture sequence modeling (RAI 2.5.2-5). However, for both updates, the applicant only performed limited sensitivity analyses and did not update either its PSHA or SSE. The staff considers both of these updates to the NMSZ characteristic earthquake modeling to be of sufficient importance to justify updating both the PSHA and SSE for the ESP site. Therefore, as part of Open Item 2.5.1-1, which covers the appropriate magnitudes for NMSZ characteristic earthquakes and is described in SER Section 2.5.1.3.1, the applicant needs to incorporate the latest relevant information on the NMSZ into its PSHA, calculation of the SSE, and the appropriate sections of the SSAR.

EGC RAI ID: SOI2-1

EGC RESPONSE:

The EGC PSHA is herein updated to incorporate the modification to the modeling of "characteristic" New Madrid earthquake described in its response to RAI 2.5.1-1 and RAI 2.5.2-5. Based on further consideration of the issues, EGC intends to use the following characterization of this seismic source.

Characteristic Magnitudes and Rupture Sequences

In response to RAI 2.5.1-1, EGC presented an updated characterization of the magnitudes of "characteristic" or repeating large magnitude New Madrid earthquakes. This updated characterization incorporated the final published assessment of Bakun and Hopper (2004) and additional models based on review of the literature and discussion with researchers. This updated characterization consists of the six alternative rupture sets are listed in Table 2.5.1-1-1. Further, in response to RAI-2.5.2-5, EGC presented an updated characterization of two alternative models for rupture scenarios of the three New Madrid faults. In Model A, all ruptures of the three New Madrid fault sources are similar in size to the 1811-1812 earthquakes. In Model B, 1/3 of the sequences consist of ruptures similar in size to the 1811-1812 ruptures (i.e. the same as Model A), 1/3 of

the sequences contain a smaller rupture of the New Madrid North fault, and 1/3 of the sequences contain a smaller rupture of the New Madrid South fault. For those sequences that contain smaller ruptures of the New Madrid North or New Madrid South faults, the difference in magnitude from the 1811-1812 ruptures is set to be no more than ½ magnitude unit, and no ruptures were allowed to be less than **M** 7. In addition, all three earthquakes are included in the hazard calculation in all rupture sequences. Model A (always full ruptures) is given a weight of 2/3 and Model B a weight of 1/3 based on the difficulties in estimating the size of the pre 1811-1812 ruptures. The resulting magnitudes are listed in Table 2.5.1-1-1. In the PSHA calculation the moment magnitudes listed in Table 2.5.1-1-1 are converted into m_b magnitudes using the three alternative m_b versus **M** relationships described in Section 4.1.4 of Appendix B to the FSAR.

Earthquake Cluster Occurrence Frequencies

In response to RAI 2.5.2-5, EGC presented updated calculations of the occurrence rate for rupture sequences on the three New Madrid faults. These updated calculations involved use of the Brownian Passage Time (BPT) model developed by Matthews et al. (2002) and used by Working Group (2003) to assess the probabilities of large earthquakes in the San Francisco bay region as the preferred model for estimating real-time recurrence of repeating earthquakes on individual faults. In response to Open Item 2.5.1-1, the real-time recurrence rates for the repeating New Madrid earthquake sequences are computed using the BPT model. The data required for this calculation are the simulated data set of possible dates for the 1450 A.D. and 900 A.D. rupture sequences described in Attachment 2 to Appendix B of the FSAR. Two modifications to the calculation presented in the Response to RAI 2.5.2-5 will be included. First, the elapsed time since the last sequence (1811-1812) will be extended to include the time period through October 2005. Second, the time period of interest will be extended from 50 years to 60 years. This extended time period will cover the 20-year life of the ESP and a 40-year design life of a new plant.

The calculation of the occurrence times presented in the response to RAI 2.5.2-5 were based on the estimated dates for previous New Madrid earthquakes derived from radio-carbon dating of paleoliquifaction features in the north-east portion of the New Madrid seismic zone in the vicinity of the New Madrid North fault (Attachment 2 to Appendix B of the FSAR). These analyses were repeated using data from the central and southwestern portions of the New Madrid seismic zone. All three sets of data produce essentially the same estimates of mean return period. Figure 2.5.1-1-1 shows the uncertainty distributions for mean repeat time derived from the three data sets assuming a Poisson recurrence model. The updated occurrence rates of equivalent annual frequency of New Madrid earthquake sequences were computed by combining the estimated dates for prehistoric earthquakes from all three sections of the seismic zone. Figure 2.5.1-1-2 shows the resulting distributions for mean repeat time derived using the Poisson and BPT models. Table 2.5.1-1-2 lists the resulting distributions for equivalent annual frequency of New Madrid clusters.

Updated Logic Tree

The revised logic tree for the New Madrid repeating earthquake source is shown on Figure 2.5.1-1-3. The Poisson and renewal recurrence models are given equal weight. The renewal model is considered more appropriate on a physical basis for the behavior of characteristic earthquakes on active faults. The Working Group (2003) applied weights of 0.7 and 0.6 to non-Poissonian behavior for the San Andreas and Hayward faults, respectively. For other, less active sources, they assigned a weight of 0.5 or less

to non-Poissonian behavior. While the New Madrid faults are not plate boundary faults, they exhibit behavior that is similar to that expected for an active plate boundary fault. Equal weights represent maximum uncertainty as to which is the more appropriate model. The mean equivalent annual frequency of New Madrid sequences computed from the logic tree is 2.0×10^{-3}/yr or a repeat time of 500 years.

Note that in the response to RAI 2.5.2-5, EGC assigned a weight of 0.6 to non-Poissonian behavior based on the weighting assigned by the Working Group (2002) to faults that clearly exhibited repeated earthquakes. In the updated logic tree presented here, that weight was reduced to 0.5 to reflect the uncertainty in applying a model based on the behavior of plate-boundary faults to a seismic source in the interior of a stable continental region.

ASSOCIATED EGC ESP APPLICATION REVISIONS:

The references to Bakun and Hopper (2003, in press) utilized in SSAR Appendix B will be updated to reflect the Bakun and Hopper (2004) final published assessment. In addition, the PSHA material dependent upon this information will also be updated to reflect the above response. These changes will include:

1) Revision of SSAR, Appendix B, Section 4.1.1 text.

2) Revision of SSAR, Appendix B, Section 4.1, Tables 4.1-1, 4.1-2, and 4.1-3.
For example, SSAR Appendix B, Table 4.1-2 will be updated with the information in the open item response Table 2.5.1-1-1.

3) Revision of SSAR, Appendix B, Section 4.1, Figures 4.1-1, 4.1-3, 4.1-9 thru 4.1-16, 4.1-19 thru 4.1-21.
For example, SSAR Appendix B, Figure 4.1-1 will be updated with the information in the open item response Figure 2.5.1-1-3, and SSAR Appendix B, Figure 4.1-3 will be updated with the information in the open item response Table 2.5.1-1-2, and Figures 2.5.1-1-1 and 2.5.1-1-2.

4) Revision of SSAR, Appendix B, Section 4.2, Figures 4.2-19 thru 4.2-26.

5) Revision of SSAR, Appendix B, Section 4.3, Tables 4.3-1 and 4.3-2.

6) Revision of SSAR, Appendix B, Attachment 2, Section 1.2.2 text.

7) Revision of SSAR, Appendix B, Section 4.1, Tables B-2-1 and B2-2.

8) Revision of SSAR, Appendix B, Section 4.1, Figure B2-2.

The details of the revisions identified in Items 1) through 8) above are in process and will be provided in the upcoming Revision 1 of the EGC ESP Application.

ATTACHMENTS:

Tables 2.5.1-1-1 and 2.5.1-1-2

Figures 2.5.1-1-1 through 2.5.1-1-3

TABLE 2.5.1-1-1

REVISED MAGNITUDE DISTRIBUTIONS FOR CHARACTERISTIC NEW MADRID EARTHQUAKES

Characteristic Earthquake Rupture Set [weight]	Rupture Sequence Model [weight]	Characteristic Magnitude for Individual Faults (moment magnitude, M)		
		New Madrid South	Reelfoot Thrust	New Madrid North
1 [0.1667]	A [0.667]	7.8	7.7	7.5
	B [0.333]	7.8 or 7.3*	7.7	7.5 or 7.0*
2 [0.1667]	A [0.667]	7.9	7.8	7.6
	B [0.333]	7.9 or 7.4*	7.8	7.6 or 7.1*
3 [0.25]	A [0.667]	7.6	7.8	7.5
	B [0.333]	7.6 or 7.1*	7.8	7.5 or 7.0*
4 [0.0833]	A [0.667]	7.2	7.4	7.2
	B [0.333]	7.2 or 7.0*	7.4	7.2*
5 [0.1667]	A [0.667]	7.2	7.4	7.0
	B [0.333]	7.2 or 7.0*	7.4	7.0*
6 [0.1667]	A [0.667]	7.3	7.5	7.0
	B [0.333]	7.3 or 7.0*	7.5	7.0*

* For Model B 1/3 of rupture sequences contain smaller New Madrid North magnitudes, 1/3 contain smaller New Madrid South magnitudes and 1/3 contain full ruptures on all three faults.

TABLE 2.5.1-1-2

EARTHQUAKE FREQUENCIES FOR REPEATING NEW MADRID EARTHQUAKE SEQUENCES

Recurrence Model	Weight	Mean Repeat Time (years)	Equivalent Annual Frequency
Poisson	0.10108	161	6.20E-03
	0.24429	262	3.82E-03
	0.30926	410	2.44E-03
	0.24429	694	1.44E-03
	0.10108	1,563	6.40E-04
Renewal (BPT), $\alpha = 0.3$	0.10108	333	3.39E-03
	0.24429	410	1.07E-03
	0.30926	485	3.02E-04
	0.24429	574	5.95E-05
	0.10108	709	4.30E-06
Renewal (BPT), $\alpha = 0.5$	0.10108	316	4.85E-03
	0.24429	440	2.18E-03
	0.30926	573	8.89E-04
	0.24429	746	2.58E-04
	0.10108	1,032	2.97E-05
Renewal (BPT), $\alpha = 0.7$	0.10108	325	4.45E-03
	0.24429	506	2.25E-03
	0.30926	719	1.02E-03
	0.24429	1,011	3.37E-04
	0.10108	1,521	4.49E-05

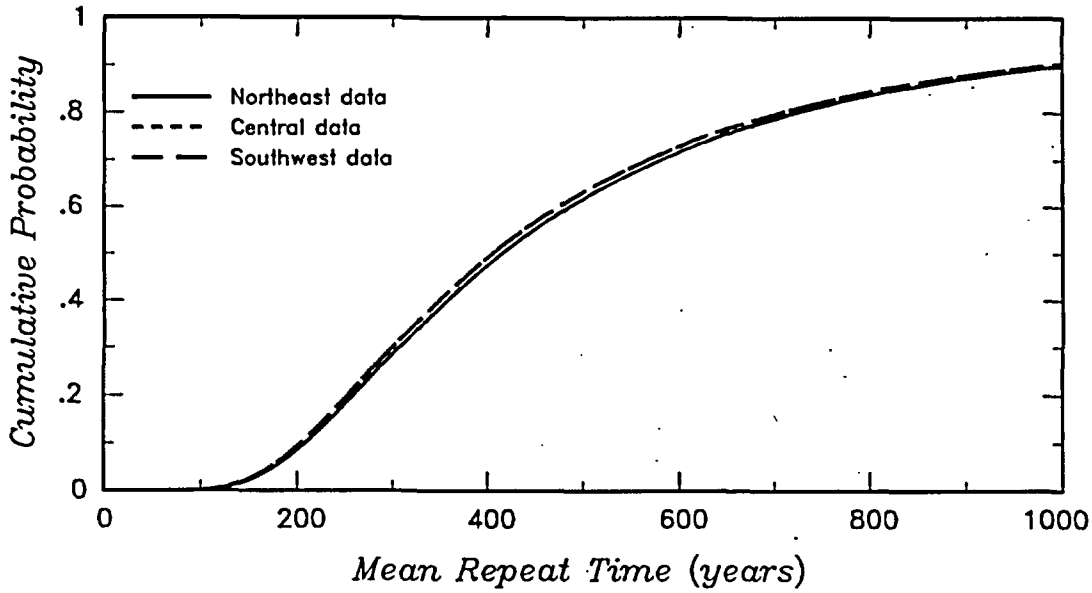

Figure 2.5.1-1-1: Comparison of mean repeat time distributions computed assuming a Poisson model for prehistoric earthquake dates developed from data in the three sections of the New Madrid seismic zone

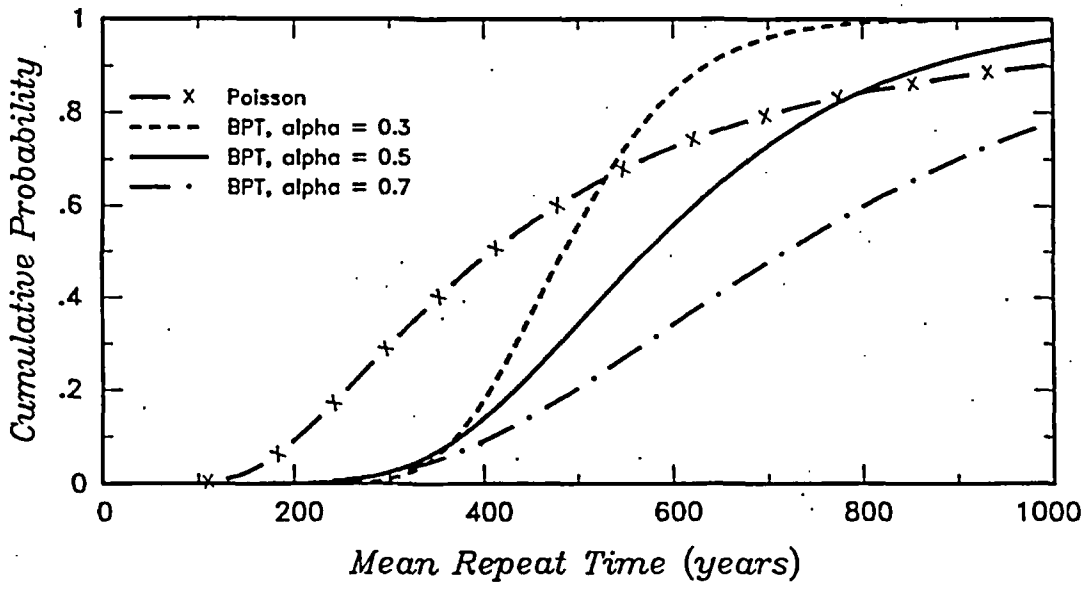

Figure 2.5.1-1-2: Updated distributions for mean repeat time computed by combining the estimates of prehistoric earthquake dates for the three portions of the New Madrid seismic zone

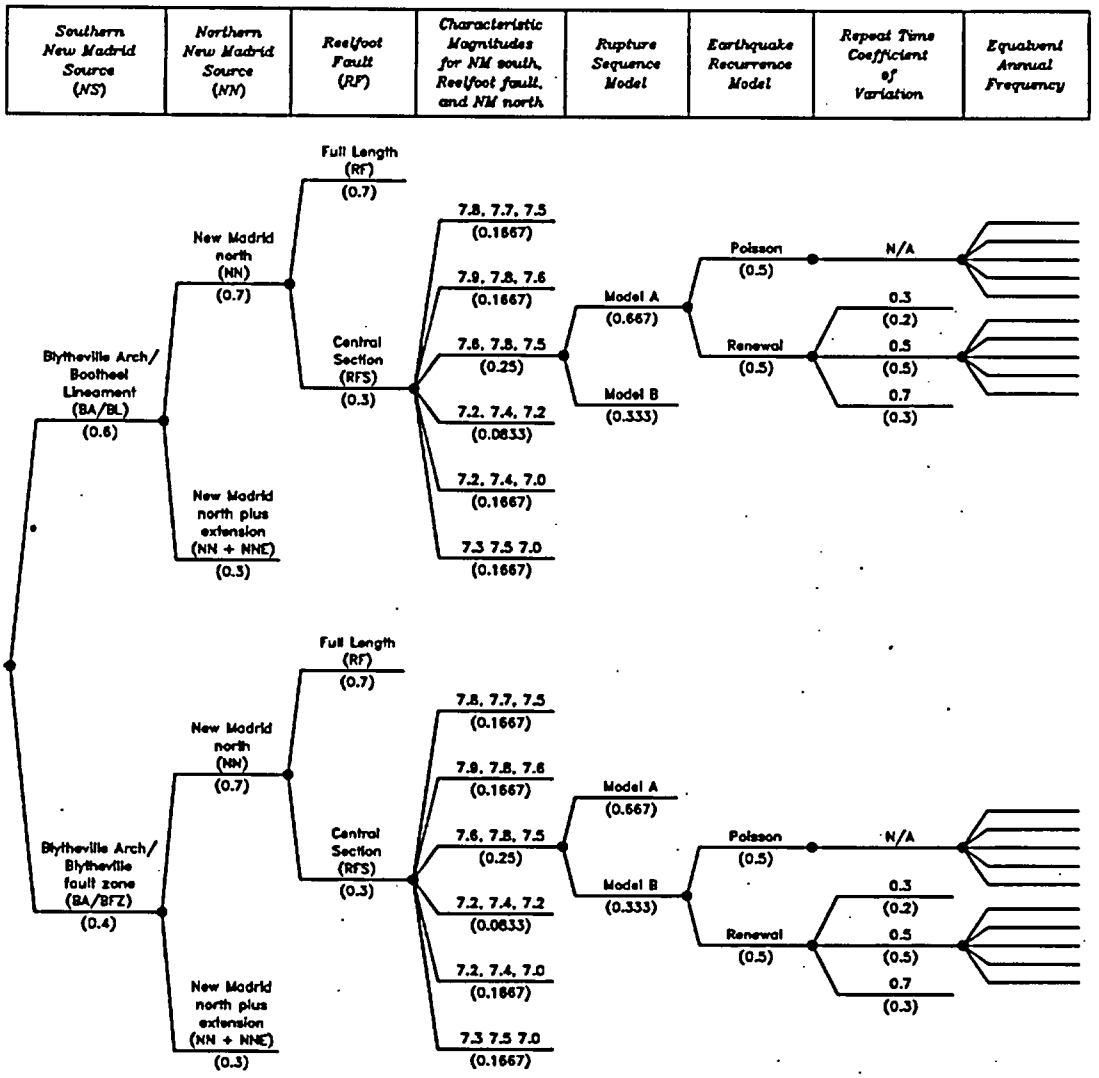

Figure 2.5.1-1-3: Updated logic tree for the New Madrid source of repeating (characteristic) earthquakes

(Note: The Equivalent Annual Frequency values and weights (right hand column of the logic tree) are given in Table 2.5.1-1-2. The appropriate values are indicated by the Recurrence Model (Poisson or Renewal) and for the renewal model, by the alternative values for the coefficient of variation, α.)

NRC Letter Dated: 08/26/2005

NRC DSER Open Item 2.5.2-1

Section 2.5.2.3.3 - In RAI 2.5.2-3, the staff asked the applicant to describe how the recent EPRI ground motion study converted the distance measure used for each of the attenuation relationships to a common measure. Specifically, the 13 CEUS attenuation relationships selected by the EPRI ground motion experts each use one of two different distance measures. In response to RAI 2.5.2-3, the applicant provided a description of the method it used to convert the "point-source" distance measure to the more commonly used Joyner-Boore distance measure. In EPRI ground motion clusters 1, 2, and 4, all but two of the individual models (Frankel et al. (1996) and Atkinson and Boore (1995)) use the Joyner-Boore distance, which is the closest distance from the site to the surface projection of the fault rupture in kilometers. The other two ground model attenuation relationships use the hypocentral distance, which is the distance from the site to the earthquake focus in kilometers. To convert the point-source distance to the Joyner-Boore distance, the applicant described the following method:

> These two relationships [Frankel et al. (1996) and Atkinson and Boore (1995)] were converted to Joyner-Boore distance by simulating a data set in terms of moment magnitude and Joyner-Boore distance and fitting this simulated data set. At a given Joyner-Boore distance, earthquake point source depths were simulated for a range of magnitudes using the point-source depth distributions for the CEUS proposed by Silva et al. (2002). These consist of lognormal distributions with the parameters listed in the table of Point-Source Depth Distribution Parameters from Silva et al. 2002.

For each simulation, the depth and the Joyner-Boore distance were used to compute the corresponding point source distance. The median ground motion for the given magnitude and point source distance were then computed using the Frankel et al. (1996) and Atkinson and Boore (1995) relationships. The resulting simulated data sets were then fit with an appropriate functional form to provide ground motion relationships in terms of moment magnitude and Joyner-Boore distance consistent with the other relationships in Clusters 1 and 2.

The applicant's description, given above, of the EPRI study's distance conversion process is vague on several key points. The applicant did not adequately describe or provide the bases for (1) the simulated data set, (2) the functions that EPRI used to fit the simulated data set, (3) the point-source depth distributions for the CEUS proposed by Silva et al. (2002), and (4) the final "appropriate" functions used to provide ground motion relationships in terms of Mw and Joyner-Boore distance. In addition, the applicant did not provide an overall or general explanation of the distance-conversion method nor any indication of the adequacy of the final distance conversion. The staff's request for further clarification and elaboration of the EPRI study distance-conversion method is Open Item 2.5.2-1.

EGC RAI ID: SOI2-2

EGC RESPONSE:

Hypocenter to Joyner-Boore Distance Conversion and Point-Source Depth Distributions

The EPRI (2004) model for central and eastern US (CEUS) ground motions was constructed from a set of individual ground motion models that were grouped into four clusters. These models fundamentally use three types of ground motion distance measures. Most of the models use the so-called "Joyner-Boore" distance (r_{JB}) which represents the closest distance to the surface projection of the earthquake rupture plane. This distance measure was first used in developing ground motion models from empirical strong motion data (e.g., Joyner and Boore, 1981). The single model that makes up Cluster 4 and most of the models in Clusters 1 and 2 use the r_{JB} distance measure. The distance measure that is used in most ground motion models developed from empirical strong motion data is the closest distance to the fault rupture plane (r_{CLD}) (e.g., Abrahamson and Silva, 1997). All of the models that make up Cluster 3 were hybrid models based on scaling western U.S. empirical models to CEUS conditions and they use the r_{CLD} distance measure. The remaining distance measures used by one model in Cluster 1 (Frankel et al., 1996) and one in Cluster 2 (Atkinson and Boore, 1995) is hypocentral distance. This distance arises out of the development of the stochastic point source numerical models for ground motion estimation (e.g., Hanks and McGuire, 1981; Boore, 1983) in which the distance was measured to the point representing the energy release. This point has been interpreted as the hypocenter for small earthquakes and variously interpreted as the hypocenter, asperity, or energy center for large earthquakes. For example, Boore (1983) refers to distance as "the distance to the fault" and EPRI (1993) refers to the "distance to the equivalent point source." In their calibration of the point source stochastic model, Silva et al. (1996) consider the distance in the point source calculations to be the closest distance to the surface projection of the fault, R_{JB}, combined with the depth to the largest asperity. Frankel et al. (2002) use a similar interpretation of distance in computing hazard in the CEUS using the Frankel et al (1996) stochastic point-source ground motion model. Frankel et al. (2002) place randomly oriented faults at each seismicity grid point and compute the "hypocentral" distance to be used for the Frankel et al. (1996) as r_{JB} combined with a depth of 5 km. Frankel et al. (1996, 2002) also impose a minimum value of 10 km for the computed "hypocentral" distance.

The Atkinson and Boore (1995) and Frankel et al. (1996) ground motion models are defined in terms of tables of median ground motion values for a range of magnitudes and hypocentral distances. EPRI (2004) developed functional forms to represent these models in their analysis. The first step was to fit a functional form to the tabular data. Figures 2.5.2-1-1 and 2.5.2-1-2 show the tabulated data and the resulting fits using the functional form

$$\ln(SA) = C_1 + C_2 m + C_3 m^2 + (C_4 + C_5 m) \times \min[\ln(r), \ln(70)] + (C_6 + C_7 m) \times \max[\ln(r/130), 0] + C_8 r \quad \text{Eq. (1)}$$

for Atkinson and Boore (1995) data (Figure 2.5.2-1-1) and

$$\ln(SA) = C_1 + C_2 m + C_3 m^2 + (C_4 + C_5 m) \times \min\{\ln(r), \ln(70)\} + (C_6 + C_7 m) \times \max[\min\{\ln(r/70), \ln(130/70)\}, 0] + (C_8 + C_9 m) \times \max\{\ln(r/130), 0\} + C_{10} r \quad \text{Eq. (2)}$$

for Frankel et al. (1996) data (Figure 2.5.2-1-2) where m is moment magnitude and r is equivalent point-source distance. These forms were chosen to match the characteristics of the ground motion simulation models used in developing the tabular data, in particular the form of distance attenuation. For ease in comparing these two relationships with the other models within their respective clusters, the "hypocentral" distance versions were converted into r_{JB} version by the following process. A synthetic data set was created by simulating data for a specific set of r_{JB} values using a distribution of equivalent point source depths. The point source depth distributions developed by Silva et al. (2002) were used in generating the synthetic data. These point source depth distributions were developed from the hypocentral depth distributions published by EPRI (1993) accounting for adjustments from hypocentral to asperity depth as a function of earthquake magnitude. Table 2.5.2-1-1 gives the parameters of these distributions. For comparison, EPRI-SOG (1988) used a fixed depth of 10 km in applying the stochastic point source ground motion models and Frankel et al (1996) used a fixed depth of 5 km with a minimum hypocentral depth of 10 km. Figure 2.5.2-1-3 shows examples of the simulated data for the Frankel et al. (1996) ground motion model. The simulated data were then fit by modified versions of Equations (1) and (2) to add a "fictitious depth" term to convert r_{JB} into equivalent point source distance. The modified functional forms are:

$$\ln(SA) = C_1 + C_2 m + C_3 m^2 + (C_4 + C_5 m) \times \min[\ln(r'), \ln(70)] + (C_6 + C_7 m) \times \max[\ln(r'/130), 0] + C_8 r' \quad \text{Eq. (3)}$$

$$r' = \sqrt{r_{JB}^2 + h^2} \qquad h = \exp(C_9 + C_{10} m)$$

for Atkinson and Boore (1995), and

$$\ln(SA) = C_1 + C_2 m + C_3 m^2 + (C_4 + C_5 m) \times \min\{\ln(r'), \ln(70)\} + (C_6 + C_7 m) \times \max[\min\{\ln(r'/70), \ln(130/70)\}, 0] + (C_8 + C_9 m) \times \max\{\ln(r'/130), 0\} + C_{10} r' \quad \text{Eq. (4)}$$

$$r' = \sqrt{r_{JB}^2 + h^2} \qquad h = \exp(C_{11} + C_{12} m)$$

for Frankel et al. (1996) where m is moment magnitude and r_{JB} is Joyner-Boore distance.

Figure 2.5.2-1-4 compares median ground motion estimates for the EPRI (2004) and the Frankel et al. (2002) implementation of the Frankel et al. (1996) ground motion model in terms of r_{JB}. The EPRI (2004) implementation provides a smooth variation with distance and results in somewhat higher median ground motions at very small values of r_{JB}. Also shown on Figure 2.5.2-1-4 are the median ground motion estimates for the Frankel et al. (1996) ground motion model using the EPRI-SOG (1988) implementation of a fixed depth of 10 km.

Conversion to Epicentral Distance for PSHA Calculations

Probabilistic seismic hazard analysis (PSHA) formulations typically use two representations of individual earthquakes. When the seismic source is a specific fault, (e.g., the San Andreas Fault in California or the Reelfoot Thrust at New Madrid), then earthquakes are typically modeled as extended ruptures (either as lines or planes) with the size of the rupture defined as a function of earthquake magnitude. When the seismic source is a zone used to represent randomly occurring earthquakes without specific orientations, then earthquakes are often modeled as point-sources, with the point nominally representing the epicenter of the earthquake. In performing the PSHA, it is important to use ground motion models that are formulated with the same distance measure that is being used in the calculation.

PSHA calculations for the EGC ESP site were based on the EPRI-SOG (1988) seismic source model. In that model, earthquakes were represented by points in space, as is typically done in modeling source zones. However, the ground motion model developed by EPRI (2004) is defined in terms of minimum distance to earthquake rupture (either r_{JB} or r_{CLD}). Therefore, proper use of the EPRI (2004) ground motion model in conjunction with the EPRI-SOG (1988) seismic source models required conversion of the distance measures. EPRI (2004) developed a set of conversion relationships based on the assumption that the points in space in the EPRI-SOG (1988) seismic source models represent earthquake epicenters (the spatial distributions of earthquake frequencies in the EPRI-SOG model were developed from epicenter locations) and the rupture orientations are uniformly distributed over azimuths of 0° to 360° (no preferred orientation) using the following process.

For a given moment magnitude and epicentral distance, a set of possible rupture orientations was simulated. The rupture size was obtained using the relationship for CEUS earthquakes proposed by Somerville et al. (2001) for eastern North America (Figure 2.5.2-1-5):

$$\ln(\text{Rupture Area}) = -10.106 + 2.303M \qquad \text{Eq. (5)}$$

The length and width of ruptures was defined by specifying a magnitude-dependent aspect ratio (L:W) that is 1 at M 4 and either 2 or 3 at M 7 for reverse or strike-slip earthquakes, respectively. The rupture width was assumed to be limited by a maximum seismogenic crustal thickness of 25 km and the fault dip. Strike-slip earthquakes were assumed to have a dip of 90° and reverse earthquakes were assumed to have a dip of 40°, the average dip of reverse earthquakes in intra-continental regions found by Sibson and Xie (1998). Figure 2.5.2-1-6 compares the resulting variations of rupture length versus magnitude with the Wells and Coppersmith (1994) relationship for surface rupture length, all slip types, based on world-wide earthquake data used by Frankel et al. (2002). Difference between the EPRI (2004) and Wells and Coppersmith (1994) estimates of rupture length reflect the fact that Somerville et al. (2001) found that rupture sizes for CEUS earthquakes were approximately half the size of those in active tectonic regions, which dominate the Wells and Coppersmith (1994) data set. In contrast, Wells and Coppersmith (1994) found that the limited data they had from stable continental regions were not inconsistent with the relationships based on world-wide data. The Somerville et al. (2001) relationships were used to develop the EPRI (2004) distance adjustments because they were based specifically on eastern North America data.

At each epicentral distance ruptures were simulated for azimuths spaced at 10° between 0° and 180°. Two sets of simulations were developed. In the first set, the ruptures were centered on the epicenter and in the second set the ruptures were randomly placed on the epicenter such that the epicenter was uniformly distributed along the length of

rupture. An equal number of strike slip (dip 90°) and reverse (dip 40°) ruptures were simulated for each magnitude at each epicentral point. Using the median ground motion model for a cluster, the median ground motions were computed at the site for each simulated rupture using the corresponding distance measure for that cluster (e.g., r_{JB} for Cluster 2). Mathematically, for the i^{th} rupture at the j^{th} epicentral distance, the median ground motion for the Cluster 2 model, designated $\ln[SA]_{ij}$, is computed from

$$\ln[SA|m]_{ij} = medianCluster2Model(m, r_{JB|rupture_i, r_j^{Epicenter}}) \quad \text{Eq. (6)}$$

where $r_{JB|rupture_i, r_j^{Epicenter}}$ is the Joyner-Boore distance for the i^{th} rupture of magnitude m located at the j^{th} epicentral distance, $r_j^{Epicenter}$. The geometric mean of these individual median ground motion values was then computed. This value represents the average value of ln(ground motion) for a random rupture with the specified epicentral distance.

$$\overline{\ln[SA|m]_j} = \frac{1}{N}\sum_i \ln[SA|m]_{ij} \quad \text{Eq. (7)}$$

where N is the total number of ruptures simulated at the j^{th} epicentral distance for magnitude m. The median cluster model was then inverted to determine the distance that produces this same ground motion level.

$$\overline{\ln[SA|m]_j} = medianCluster2Model(m, r_{JB|r_j^{Epicenter}}^{Equivalent}) \quad \text{Eq. (8)}$$

In other words this equivalent value Joyner-Boore distance, $r_{JB|r_j^{Epicenter}}^{Equivalent}$, when entered into the median ground motion model for Cluster 2, produces the same level of ground motion as the geometric mean of all of the ground motions for the simulated ruptures at the j^{th} epicentral distance. Figure 2.5.2-1-7 shows plots of the equivalent Joyner-Boore distance versus epicentral distance for the Cluster 2 median model. An algebraic relationship was then fit to the simulated data to provide a readily usable relationship for PSHA applications. These relationships are of the form

$$r_{JB}^{Equivalent} = r^{Epicentral} \times \{1 - 1/\cosh(C_1 + C_2(\mathrm{M}-6) + C_3 \ln(r'))\}$$
$$r' = \sqrt{(r^{Epicentral})^2 + h'^2}, \quad h' = \exp\{C_4 + C_5(\mathrm{M}-6)\} \quad \text{Eq. (9)}$$

for Clusters 1, 2, and 4; and of the form

$$r_{CLD}^{Equivalent} = \sqrt{\left[r^{Epicentral} \times \{1 - 1/\cosh(C_1 + C_2(\mathrm{M}-6) + C_3 \ln(r'))\}\right]^2 + CC^2}$$
$$r' = \sqrt{(r^{Epicentral})^2 + h'^2}, \quad h' = \exp\{C_4 + C_5(\mathrm{M}-6)\}, \quad CC = \exp(C_6) \quad \text{Eq. (10)}$$

for Cluster 3, which used closest distance to rupture rather than Joyner-Boore distance. The form of the algebraic functions was selected to match the variation of the simulated data with magnitude and distance and does not have a specific physical basis.

The random orientation of ruptures about an epicentral location introduces an additional source of aleatory variability in estimating site ground motions. This additional aleatory variability was computed from the set of values of $\ln[SA]_{ij}$ by the expression

$$\sigma^2_{\text{Additional Epicentral Distance Aleatory}}(m, r_j^{Epicentral}) = \frac{1}{N}\sum_i \left(\ln[SA|m]_{ij} - \overline{\ln[SA|m]_j}\right)^2 \quad \text{Eq. (11)}$$

Figure 2.5.2-2-8 shows the computed values of the additional aleatory variability for Cluster Model 2. Again to provide a readily usable relationship for PSHA applications, these simulated data points were fit with an algebraic function of the form

$$\sigma_{\text{Additional Epicentral Distance Aleatory}} = \exp\{C_1 + C_2(\mathbf{M}-6) + C_3(\mathbf{M}-6)^2\} \times [1 - 1/\cosh(f_A)] \times \frac{1}{\cosh(f_B)}$$

$$f_A = \exp\{C_4 + C_5(\mathbf{M}-6)\} + \exp\{C_6 + C_7(\mathbf{M}-6)\} \times r^{Epicentral}$$

$$f_B = \exp\{C_8 + C_9(\mathbf{M}-6)\} \times \ln(r'/h)$$

$$r' = \sqrt{(r^{Epicentral})^2 + h^2}, \quad h = \exp\{C_{10} + C_{11}(\mathbf{M}-6)\}$$

Eq. (12)

The total aleatory variability used in the PSHA calculation based on epicentral distance is then determined by the relationship

$$\sigma_{\text{Epicentral Total Aleatory}} = \sqrt{\sigma^2_{\text{Extended Source Aleatory}} + \sigma^2_{\text{Additional Epicentral Distance Aleatory}}} \qquad \text{Eq. (13)}$$

Summary

The above discussion provides a detailed description of the distance conversion process used in the EPRI (2004) CEUS ground motion model. The itemized requests in the Open Item are addressed as follows. Item (1) is addressed by the description of the simulated data sets of ruptures generated at epicentral distances in the range of 1 to 1000 km for magnitudes between M 5 and 8. Item (2) is addressed by the descriptions of Equations (9), (10), and (12). Item (3) is addressed by reference to the source for the Silva et al. (2002) point source depth distributions, being the EPRI (1993) study, and by comparing the effect of these depth distributions to other implementations (Figure 2.5.2-1-4). Item (4) is addressed in that the "appropriate" functions are smooth algebraic relationships that provide a good fit to the simulated data. The adequacy of the distance conversion method is justified in that the smooth algebraic relationships produce values of the equivalent Joyner-Boore or rupture distance that reproduce the effect of averaging over a suite of randomized ruptures. Figures 2.5.2-1-9 and 2.5.2-1-10 compare probabilities of exceedance as a function of epicentral distance for M 5.5, 6.5, and 7.5 earthquakes computed using the EPRI (2004) distance adjustment relationships to those obtained by simulating the approach used in the USGS 2002 national hazard map development (Frankel et al., 2002). The simulated USGS approach results in Figure 2.5.2-1-9 were computed using the Wells and Coppersmith (1994) relationship employed by Frankel et al. (2002) while the simulated USGS approach results in Figure 2.5.2-1-10 were computed using the rupture length relationship for strike-slip used in the EPRI (2004) model (see Figure 2.5.2-1-6). As indicated by the comparisons in Figure 2.5.2-1-10, the EPRI (2004) conversion process is able to produce results equivalent to simulation of random rupture orientations when the same rupture dimensions are used. The differences between the EPRI (2004) and simulated USGS results shown on Figure 2.5.2-1-9 are primarily at large distances for large magnitude earthquakes an can be attributed to use of different rupture dimension relationship.

References

Abrahamson, N. A., and W. J. Silva. "Empirical Response Spectral Attenuation Relations for Shallow Crustal Earthquakes." *Seismological Research Letters*. Vol. 68, No. 1, pp. 9-23. 1997.

Atkinson, G.M., and D.M. Boore.. "Ground Motion Relations for Eastern North America." *Bulletin of the Seismological Society of America.* Vol. 85. No. 1. pp. 17-30. 1995.

Boore, D.M. "Stochastic Simulation of High-Frequency Ground Motions Based on Seismological Models of the Radiated Spectra." *Bulletin of the Seismological Society of America.* Vol. 73. pp. 1865-1894. 1983.

Electric Power Research Institute (EPRI). "*Guidelines for Determining Design Basis Ground Motions.*" Technical Report 102293. EPRI. Palo Alto, California. Vol. 1. 1993.

EPRI. "CEUS Ground Motion Project Final Report." Technical Report 1009684. EPRI. Palo Alto, California. 2004.

EPRI-SOG. "*Seismic Hazard Methodology for the Central and Eastern United States.*" Technical Report NP-4726-A. EPRI. Palo Alto, California. Vols. 1-10. 1988.

Frankel, A., C. Mueller, T. Barnhard, D. Perkins, E.V. Leyendecker, N. Dickman, S. Hanson, and M. Hopper. *National Seismic-Hazard Maps; Documentation.* U.S. Geological Survey (USGS) Open-File Report 96-532. 110 pp. 1996.

Frankel, A.D., M.D. Petersen, C.S. Mueller, K.M. Haller, R.L. Wheeler, E.V. Leyendecker, R L. Wesson, S.C. Harmsen, C.H. Cramer, D.M. Perkins, and K.S. Rukstales. *Documentation for the 2002 Update of the National Seismic Hazard Maps.* USGS Open-File Report 02-420. 33 pp. 2002.

Hanks, T.C., and R.K. McGuire. "The Character of High-Frequency Ground Motion." *Bulletin of the Seismological Society of America.* Vol. 71, pp. 2071-2095. 1981.

Joyner, W.B., and D.M. Boore. "Peak Horizontal Acceleration and Velocity from Strong-Motion Records Including Records from the 1979 Imperial Valley, California, Earthquake." *Bulletin of the Seismological Society of America.* Vol. 71, pp. 2011-2038. 1981.

Sibson, R. H., and G. Xie. "Dip Range for Intracontinental Reverse Fault Ruptures: Truth Not Stranger than Friction." *Bulletin of the Seismological Society of America.* v. 88, p. 1014-1022. 1998.

Silva W.J., N. Abrahamson, G. Toro, and C. Costantino. *Description and Validation of the Stochastic Ground Motion Model.* Report prepared by Pacific Engineering and Analysis. El Cerrito, CA for the Engineering Research and Applications Division, Department of Nuclear Energy, Brookhaven National Laboratory. Contract No. 770573. 1996

Silva, W. J., N. Gregor, and R. Darragh. "*Development of Regional Hard Rock Attenuation Relations for Central and Eastern North America.*" Pacific Engineering and Analysis. El Cerrito, CA: 2002.

Somerville, P., N. Collins, N. Abrahamson, R. Graves, and C. Saikia. 2001. *Ground Motion Attenuation Relations for the Central and Eastern United States.* Final Report to U.S. Geological Survey. 2001.

Wells, D.L., and K.J. Coppersmith. New Empirical Relationships among Magnitude, Rupture Length, Rupture Area, and Surface Displacement." *Bulletin of the Seismological Society of America.* Vol. 84, pp. 974-1002. 1994.

ASSOCIATED EGC ESP APPLICATION REVISIONS:

None

ATTACHMENTS:

Table 2.5.2-1-1

Figures 2.5.2-1-1 through 2.5.2-1-10

Table 2.5.2-1-1

Lognormal Point-Source Depth Distribution Parameters Used in Developing the EPRI (2004) CEUS Ground Motion Model

Magnitude M	Minimum Depth (km)	Median Depth (km)	Maximum Depth (km)	$\sigma_{ln(D)}$
4.5	2	6	15	0.6
5	2	6	15	0.6
5.5	2	6	15	0.6
6	3	7	17	0.6
6.5	4	8	20	0.6
7	4.5	9	20	0.6
7.5	5	10	20	0.6
8	5	10	20	0.6
8.5	5	10	20	0.6

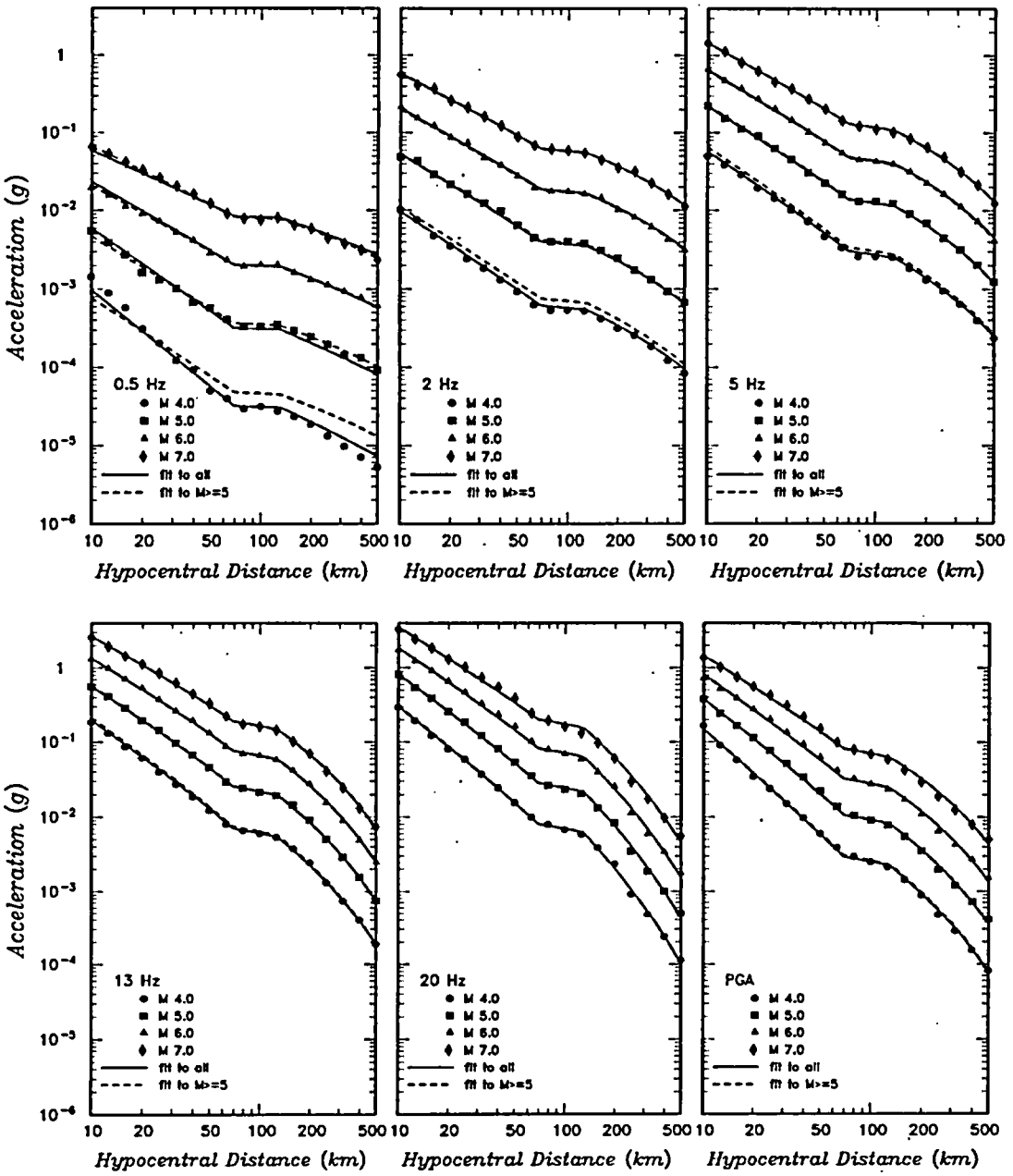

Figure 2.5.2-1-1: Fit of Equation (1) to Atkinson and Boore (1995) simulated ground motion data for hard rock conditions

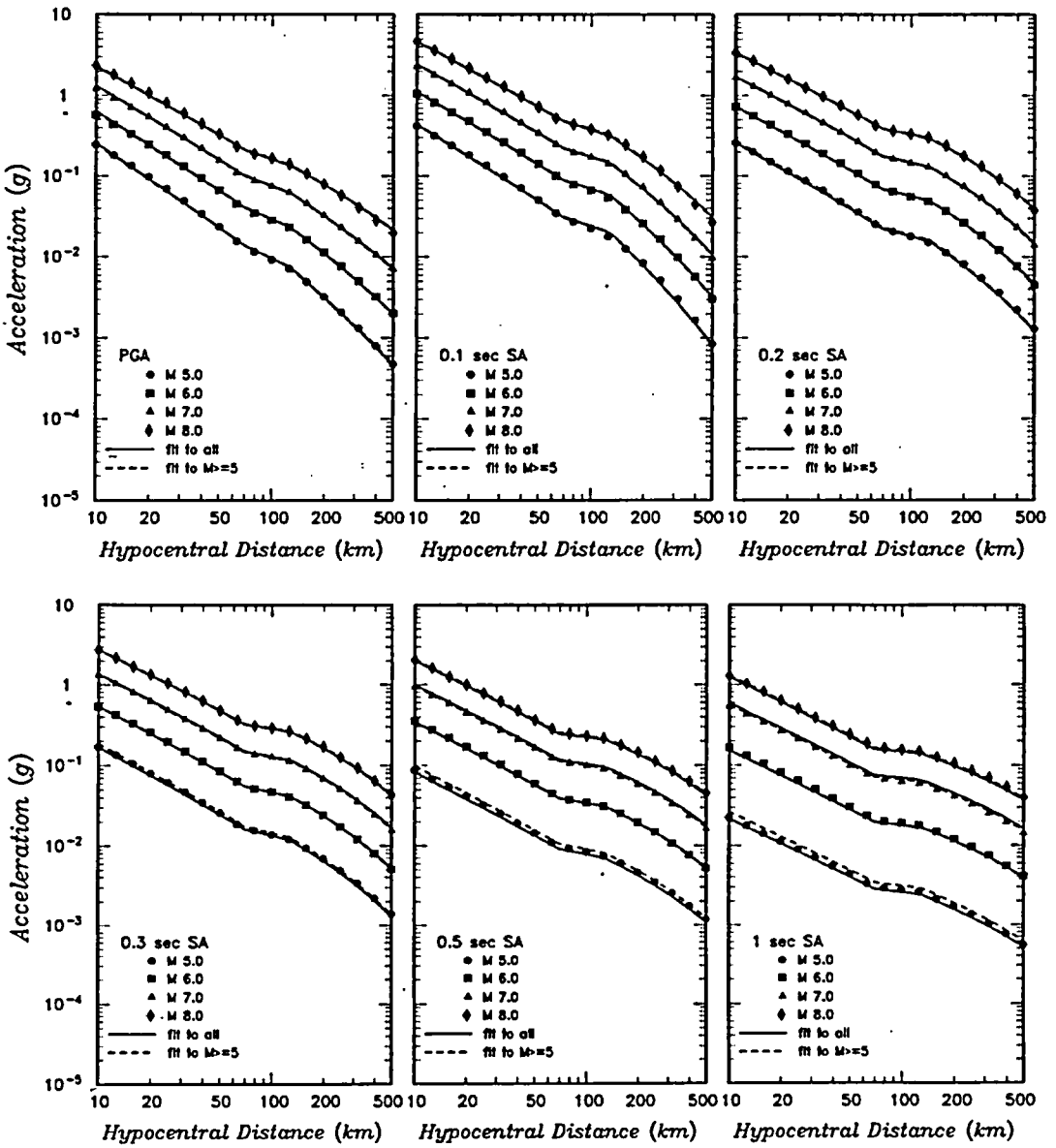

Figure 2.5.2-1-2: Fit of Equation (2) to Frankel et al. (1996) simulated ground motion data for hard rock conditions

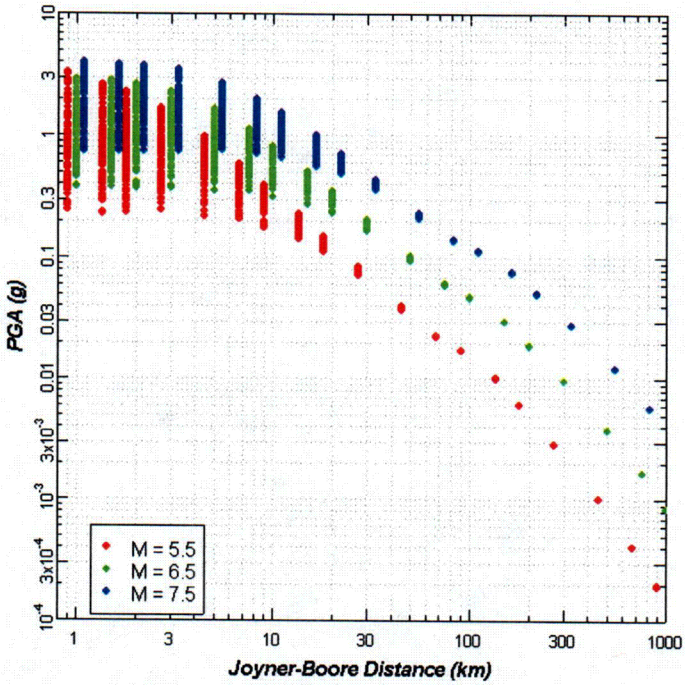

Figure 2.5.2-1-3: Example simulated data set for ground motions as a function of r_{JB} for the Frankel et al. (1996) ground motion model

Note for purposes of plotting, the points for **M** 5.5 and 7.5 are offset ±10% in distance about the points for **M** 6.5

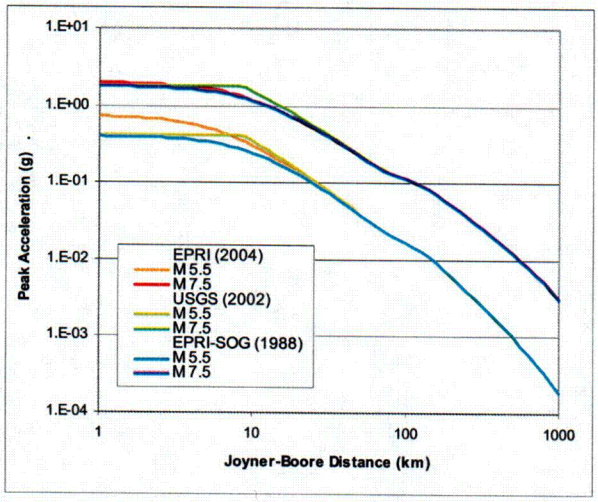

Figure 2.5.2-1-4: Comparison of EPRI (2004), USGS (Frankel et al., 2002), and hypothetical EPRI-SOG (1988) implementation of the Frankel et al. (1996) ground motion model in terms of r_{JB}

C01

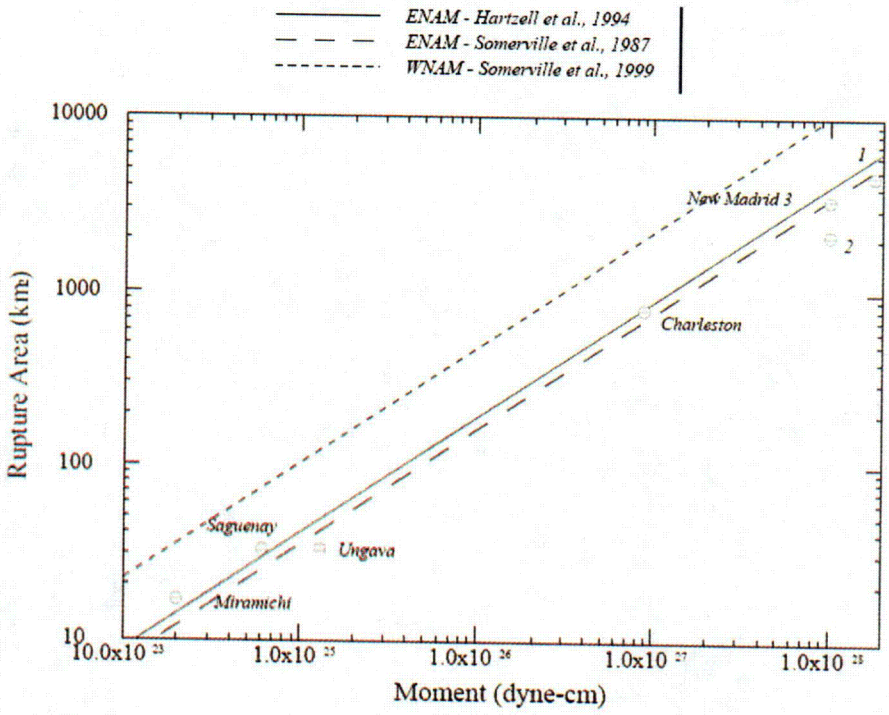

Figure 2.5.2-1-5: Rupture area scaling relationships for eastern North America (ENAM) and western North America (WNAM) from Somerville et al. (2001)

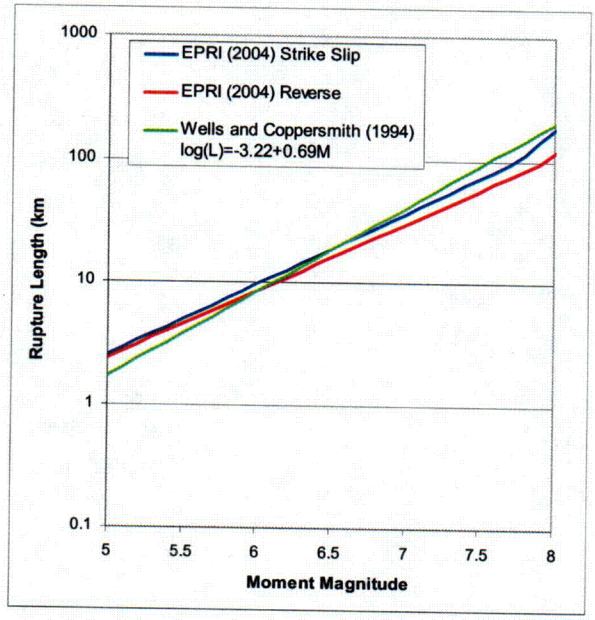

Figure 2.5.2-1-6: Rupture lengths as a function of magnitude used by EPRI (2004) compared to Wells and Coppersmith (1994) relationship for surface rupture, all slip types, used by Frankel et al. (2002)

C02

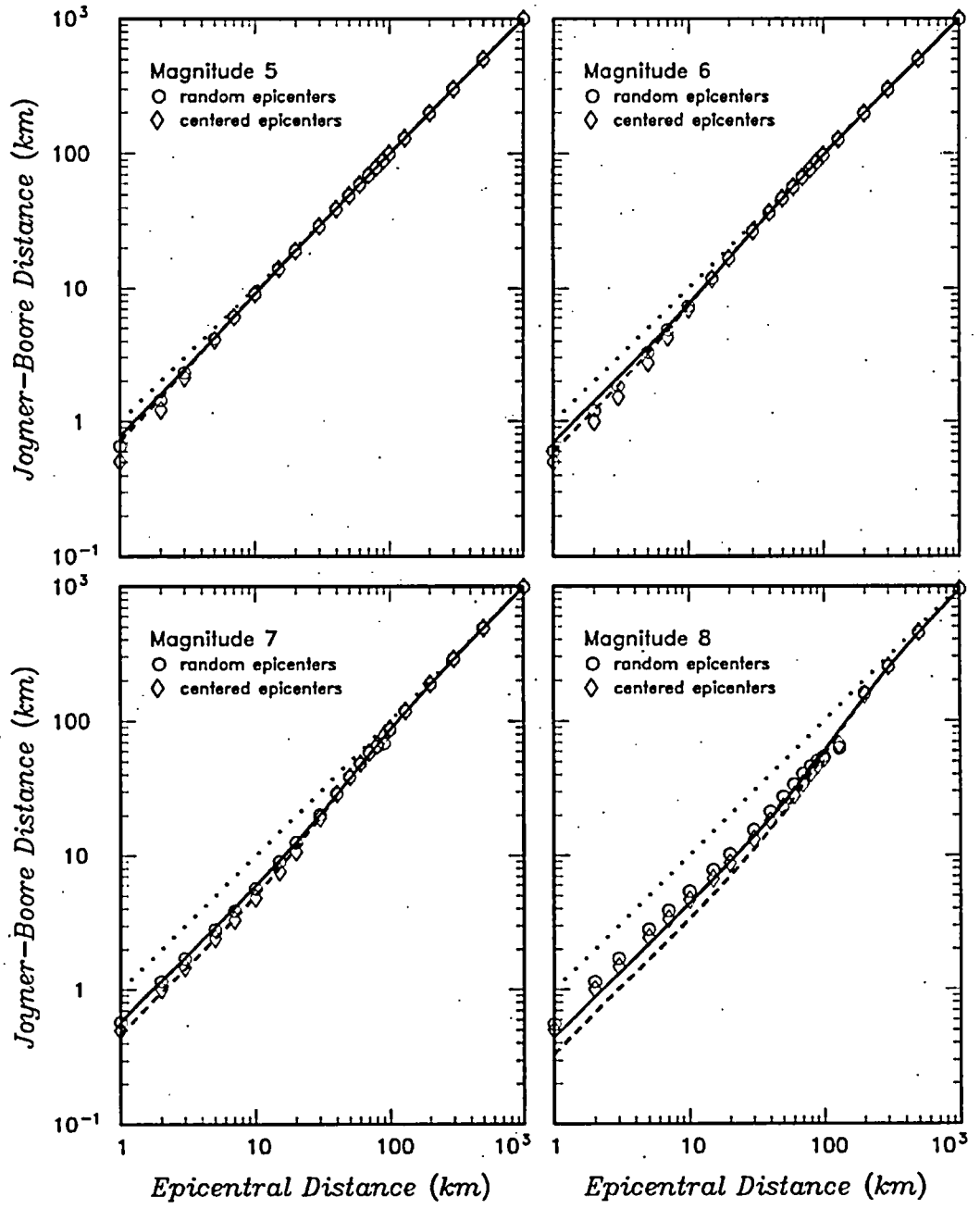

Figure 2.5.2-1-7: Plot of equivalent Joyner-Boore distance versus epicentral distance for the Cluster 2 median model

The points show the values of $r_{JB|r_j}^{Equivalent}$ computed at each epicentral distance.

The lines show the algebraic relationships fit to the simulated data.

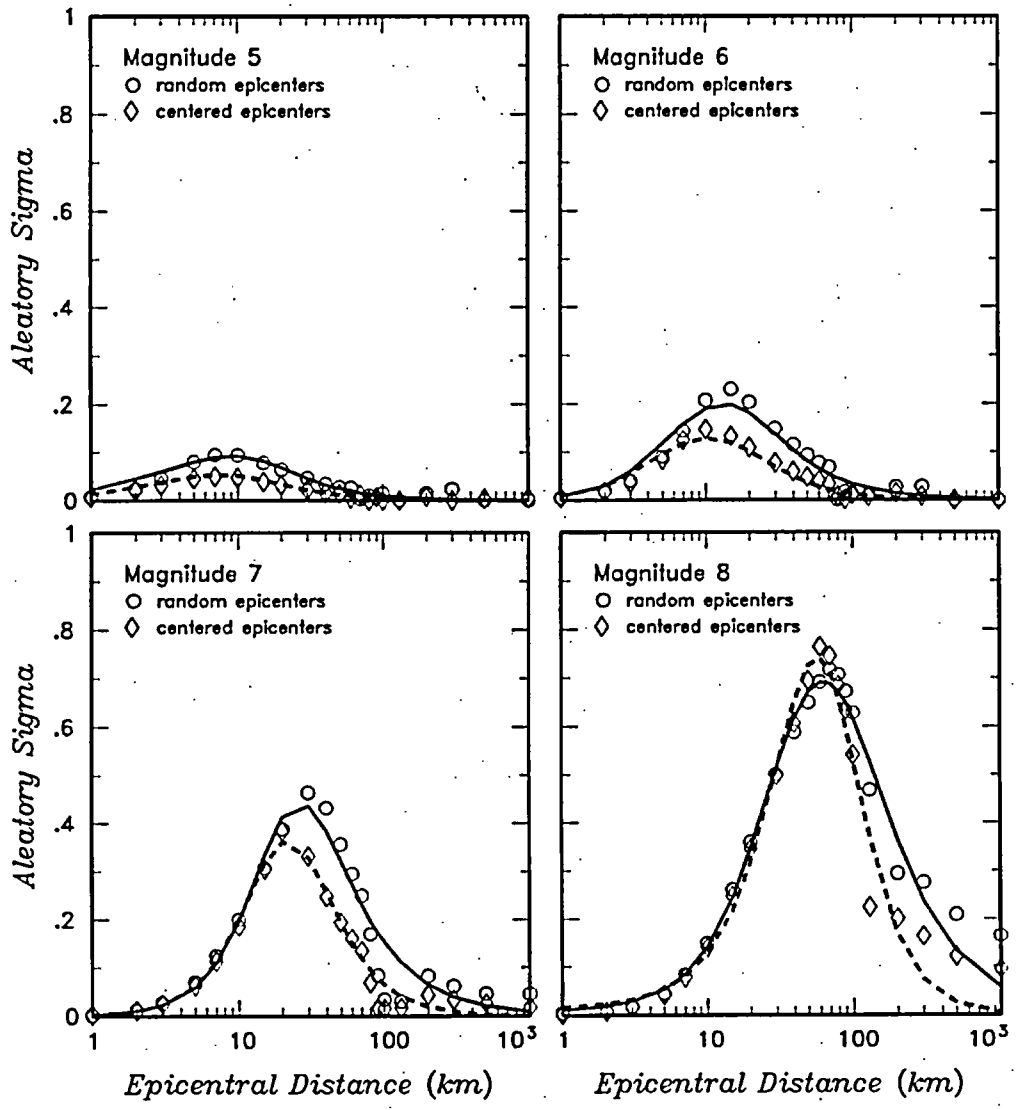

Figure 2.5.2-1-8: Plot of additional aleatory variability versus epicentral distance for the Cluster 2 median model

The points show the values of $\sigma^2_{\text{Additional Epicentral Distance Aleatory}}$ computed at each epicentral distance. The lines show the algebraic relationships fit to the simulated data.

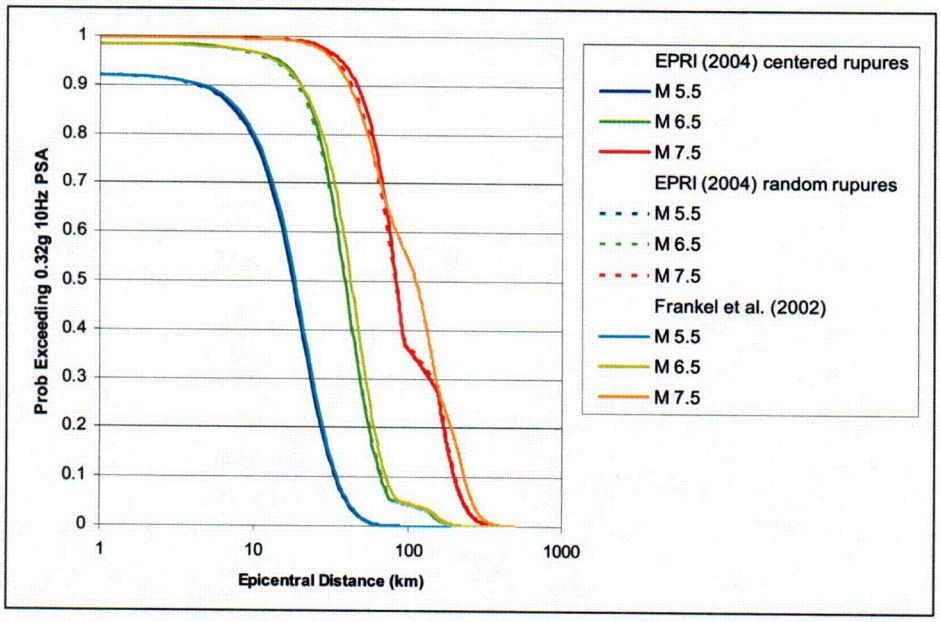

Figure 2.5.2-1-9: Comparison of the probability of exceeding a 0.32g 10-Hz spectral acceleration (based on the median model for Cluster 2) as a function of epicentral distance

Plot shows the results for the two EPRI (2004) distance conversions and simulation of the approach used by the USGS (Frankel et al., 2002)

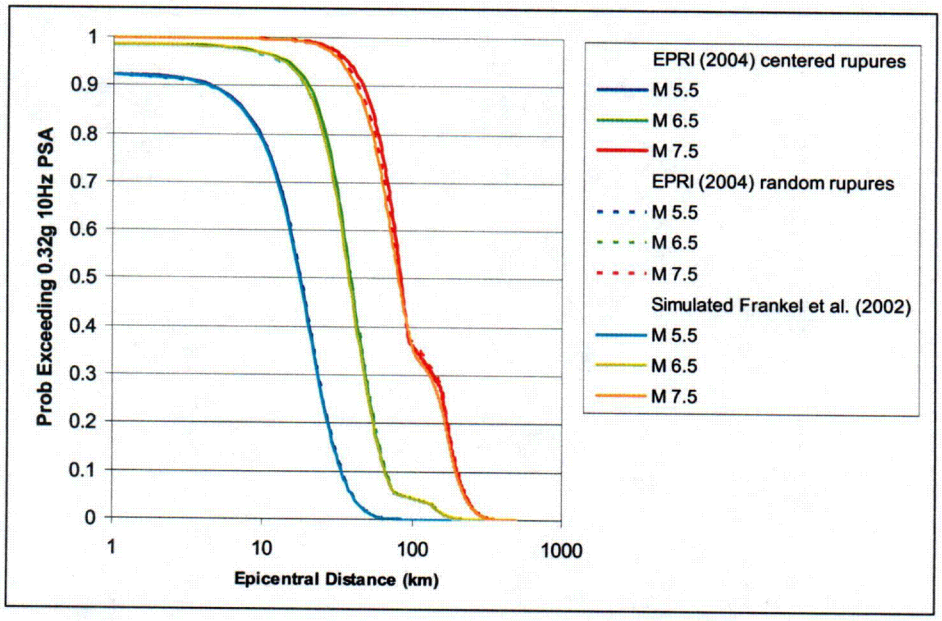

Figure 2.5.2-1-10: Comparison of the probability of exceeding a 0.32g 10-Hz spectral acceleration (based on the median model for Cluster 2) as a function of epicentral distance

Plot shows the results for the two EPRI (2004) distance conversions and simulation of the approach used by the USGS using the EPRI (2004) rupture length relationship.

C03

NRC Letter Dated: 08/26/2005

NRC DSER Open Item 2.5.2-2

Section 2.5.2.3.5 - Based on the large range in S-wave velocities for some of the soil layers (Table 5-2 of SSAR Appendix A) and the differences in SPT blowcount values for ESP borings B1 and B4 compared to those of B2 and B3, the staff in RAI 2.5.4-4 requested that the applicant justify the appropriateness of using a single "average" soil column for the site response analyses rather than including a number of different base-case soil columns. In response to RAI 2.5.4-4, the applicant stated that the variations in S-wave velocity and SPT blowcounts result from "changes in the depositional conditions during formation of the soil profile and the geologic history of the site following deposition." The applicant further stated that for the ESP site, the geologic history includes the advance and retreat of a substantial thickness of ice during the last ice age. This ice loaded the material located below approximately 50 ft, which led to very dense or hard soil conditions (i.e., overconsolidation) by the ice load. Because of the ice loading, the variability of the soil existing below 50 ft after initial formation has been reduced. In contrast, the applicant reported that the soil in the upper 50 ft was formed by fluvial (river) and aeolian (wind) processes, resulting in more variability both vertically and horizontally.

Regarding the modeling of this variability in soil properties, the applicant stated the following:

> In recognition of the natural variability of the soil, the standard approach for site response analyses is to account for the likely variation in soil layering and soil properties within a specific layer by considering different combinations of soil property and soil profile conditions that could exist at a site. One method for evaluating these variations is by manually creating independent soil columns, as suggested in the RAI. The alternative that was taken during the EGC ESP site ground motion response studies was to statistically create a large number of profiles, or realizations, and conduct the site response analyses using these profiles.

The applicant concluded its response to RAI 2.5.4-4 by stating that the randomization process used to develop the transfer functions at the ESP site allows the uncertainty in soil layering and soil properties to be considered during the evaluation of site response effects.

The staff reviewed the applicant's response and found that the large variability in strength and stiffness of the site soils, as demonstrated by the S-wave velocities and SPT blowcounts from the relatively few borings taken at the EGC ESP site, indicates a potentially large epistemic uncertainty in site profiles that cannot easily be captured directly by the randomization process. For the 60 realizations of the site soil column described in the applicant's response, the staff presumes that they were selected using a single base-case velocity profile with associated large values of sigma for the S-wave velocities. The probabilistic procedure in which a single base-case velocity profile is used based on the best estimate (or average) layer velocities generally leads to a mean surface response spectrum primarily controlled by the mean velocity profile. The influence of variability in the velocities (plus/minus one-sigma values) is generally of lower importance than the mean velocity profile in this calculation. For such cases, in which large variability (in layer S-wave velocities) is encountered, it is better (especially for cases in which a small database is available to define mean properties) to use at least two base-case profiles in the calculations. For each base-case profile, a reasonable uncertainty in velocities should also be modeled. Both sets of data are then

used to span the sparse data available for the site. The envelope of the site amplification functions from each base-case is then used to define the surface response. Because the site response is largely influenced by the mean velocity profile and not as much by the variability, the applicant needs to develop more than one bounding base-case site velocity model and use these models to evaluate their impact on the surface response spectrum to address the issue of site variability indicated in the available data. The guidance presented in Section 2.5.4.1 of RS-002 specifies that an unambiguous representation of site conditions needs to be presented in the SSAR. On the basis discussed above, the staff finds that RAI 2.5.4-4 remains unresolved. This is Open Item 2.5.2-2.

EGC RAI ID: SOI2-3

EGC RESPONSE:

As noted in this open issue, the site amplification factors for the EGC ESP Site were determined by conducting ground response studies using 60 realizations of the site soil column. The realizations accounted for potential variations in the soil properties and soil layering at the site. The randomization process used to develop the realizations was based on the geometric mean value of the shear wave velocity recorded during P-S Suspension logging tests with variations introduced to account for horizontal and vertical variability in soil response and soil layering. This approach for evaluating site response is becoming the standard practice for important facilities (e.g., NUREG/CR-6728) and is normally considered to be appropriate, as long as the geometric mean velocity profile is representative of the area being modeled. If, however, the site is characterized spatially by distinctly different soil profiles, as represented by the geometric mean shear wave velocity and its variation (e.g., a soft area located within an otherwise stiff material), then a single mean geometric profile is not necessarily a good model for the site. The potential for such variations can be determined by evaluating the spatial variation in key soil properties, such as shear wave velocity, with depth.

Additional reviews of the geotechnical information from the EGC ESP Site and the CPS Site were performed to determine if the soil properties appeared to be randomly distributed within the footprint area or occurred in distinct areas. This evaluation was made first by comparing shear wave velocities within the upper 100 feet of the soil profile for results obtained by the P-S Suspension Logging method and the seismic cone penetrometer method at the EGC ESP Site and by the downhole shear wave velocity method at the CPS site. The shear wave velocity is the fundamental soil property used in the site response analysis, and therefore an identification of distinctly different velocities in different areas could indicate the site needs to be represented by more than one geometric mean profile. The results of these velocity comparisons are shown in Figure 2.5.2-2-1 for the upper 100 feet of soil profile and in Figure 2.5.2-2-2 for the entire soil profile at the ESP EGC Site. These two profiles show that the velocities at the EGC ESP Site obtained by the two geophysical testing methods are similar and do not show distinct velocities as the individual velocity profiles cross each other at various depths. These velocities also are consistent with the average downhole shear wave velocity results from the CPS Site. This similarity in velocity values suggests that a single geometric mean profile is appropriate for developing the realizations for the variability study.

A similar comparison was performed for Standard Penetration Test (SPT) blowcounts from the EGC ESP Site and from the CPS Site for the upper 100 feet of soil profile. Generally, the variation in SPT blowcounts with depth will be greater than the variation of

shear wave velocities over the same depth interval. This greater variability – even for uniform soil conditions – results from small test variations inherent to the SPT method and from the significant effects that gravels will have on individual measurements of SPT blowcount. These gravel particles can result in sharp increases in the blowcount as the SPT sampler drives the gravel into the sampler or out of the way of the sampler. The higher blowcounts are not always characteristic of the soil conditions, particularly if the gravel particles are in an overall finer matrix of silt and clay-size material, such as occurs at many locations within the EGC ESP and CPS Sites.

Figure 2.5.2-2-3 shows the resulting SPT blowcounts for the upper 100 feet of soil profile at the EGC ESP Site. Superimposed on this plot are the means of the blowcounts recorded at the CPS and EGC ESP Sites. This comparison shows that while there are sharp changes in the blowcounts recorded at the four EGC ESP boreholes, most likely indicative of gravel particles, there is no strong evidence from the individual plots or from the comparison to the mean values that the site soil profile should be represented by more than a single average profile. The individual profiles of STP blowcount cross each other at various depths in a similar fashion to the velocity profiles shown on Figure 2.5.2-2-1. As a further evaluation of any trends in SPT blowcount data, the spatial variation in mean blowcounts for each stratigraphic unit was also compared. These plots are provided in Figures 2.5.2-2-4 through 2.5.2-2-7. These plots also show considerable variation in the mean for each layer; however, there is no distinctive trend which would suggest that the EGC ESP Site differs substantially within its perimeter or from average conditions throughout the area.

The data comparisons shown in Figures 2.5.2-2-1 through 2.5.2-2-7 indicate that some soil variability occurs in the upper 50 to 60 feet of soil profile. This variability will be decreased during any construction at the site by the use of a structural fill within the upper 60 feet of soil profile. The use of a structural fill is related to the consistency of the existing soil conditions within the upper 50 to 60 feet. Soil in this zone is either normally consolidated or lightly overconsolidated. In this context normally consolidated means that the soil has not been loaded above its current state of stress, while overconsolidated refers to the soil being loaded to higher than its existing stress state. For the EGC ESP and CPS Sites overconsolidation occurred during the last glaciation when the site was loaded by the weight of ice. As discussed in Section 2.5.4.5 of the EGC ESP SSAR, the upper 50 feet of soil at the CPS Site were excavated and replaced with a structural fill during construction to remove material that was potentially compressible. Similar compressible material was identified in the upper 60 feet of soil profile at the EGC ESP Site. Some cohesionless layers located in the upper 60 feet at the EGC ESP Site were also determined to have a potential for liquefaction under the SSE, as discussed in Section 2.5.4.8 of the EGC ESP. These undesirable soil conditions led to the conclusion that the upper 60 feet of soil located below the footprint of the Category 1 structures at the EGC ESP Site would have to be removed and replaced with a structural backfill. This backfill will exhibit properties that are resistant to settlement and liquefaction. From a variability standpoint, soil conditions for the structural fill in the upper 60 feet will be much more uniform than existing conditions.

It was concluded from this re-evaluation of data that while both the shear wave velocity and the SPT blowcounts vary within the EGC ESP Site footprint, the data do not indicate any systematic spatial pattern that would suggest distinctly different velocity profiles in different areas of the site. This conclusion suggests that the observed variability is adequately captured by the profile randomization process. The variability is highest in the upper 60 feet of soil profile. However, these materials will be removed during construction, as required by proposed Permit Condition 2.5-1. The engineering fill that

replaces soil in the upper 60 feet will result in a more uniform condition, further supporting the use of a single geometric mean velocity profile for the site response analyses.

ASSOCIATED EGC ESP APPLICATION REVISIONS:

None

ATTACHMENTS:

Figures 2.5.2-2-1 through 2.5.2-2-7

Figure 2.5.2-2-1
Comparison of Vs vs. Depth - Upper 100 feet

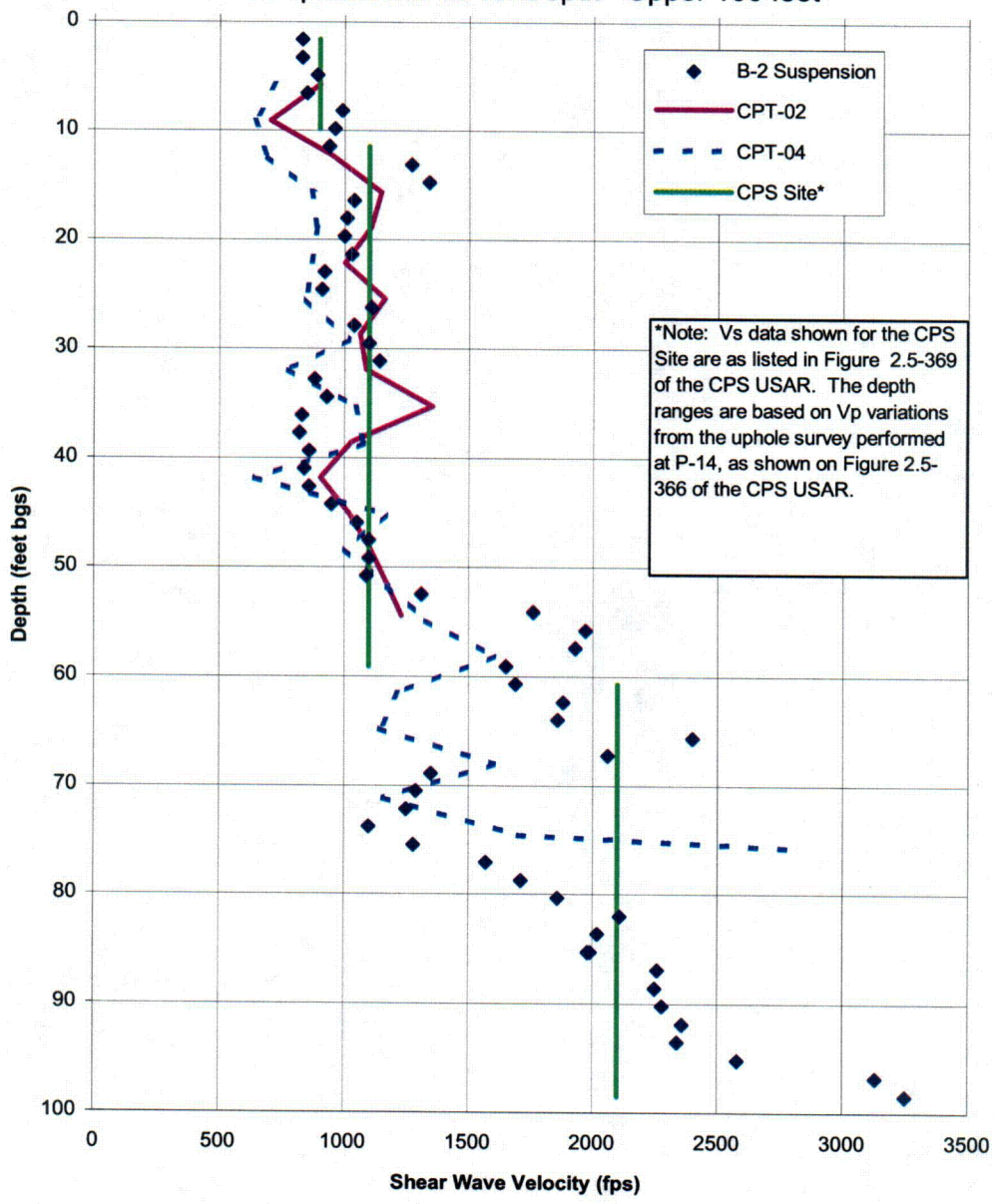

C04

Figure 2.5.2-2-2
Comparison of Vs vs. Depth - Full Profile

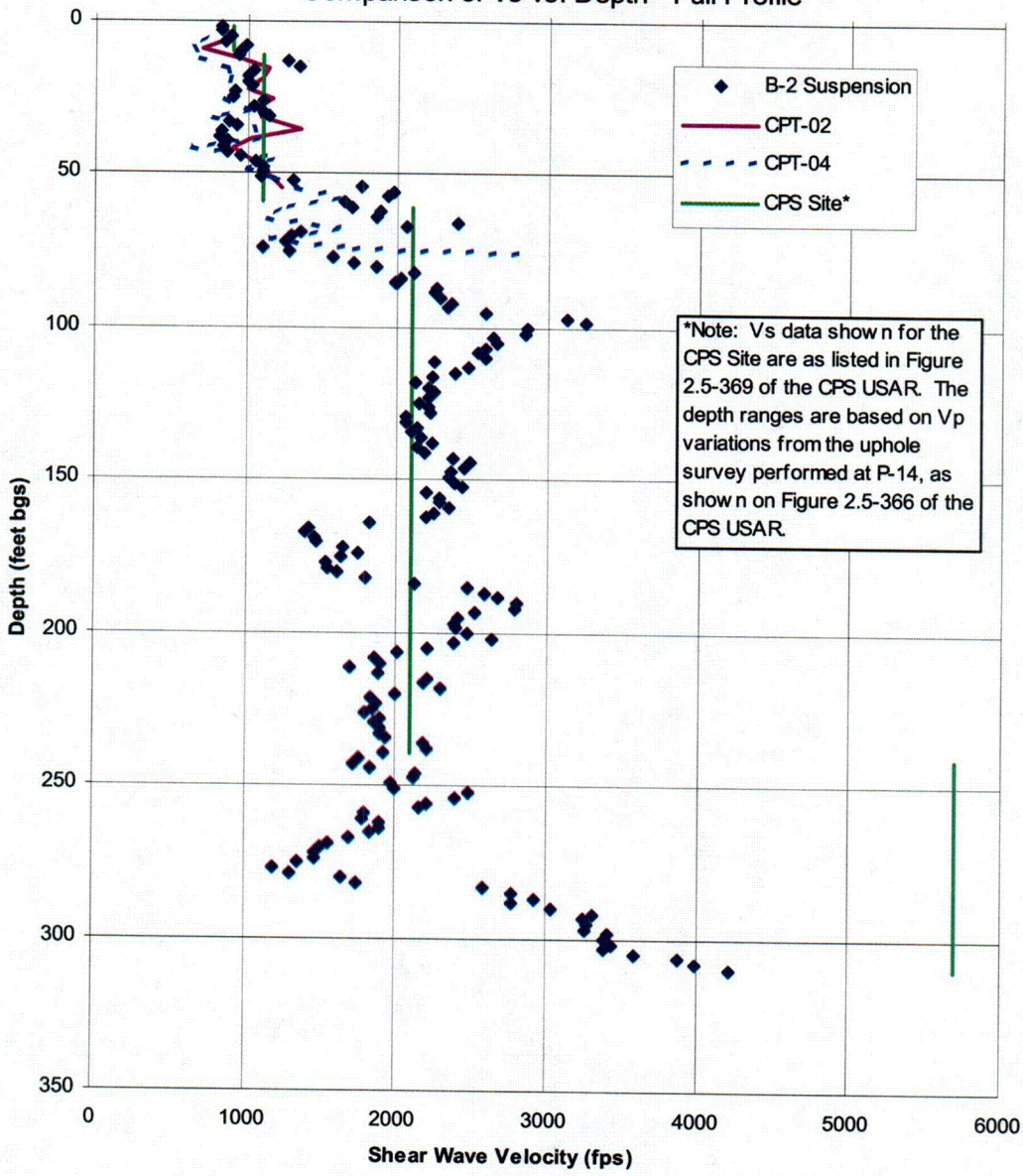

C05

Figure 2.5.2-2-3
Variation in Uncorrected Blowcount with Depth

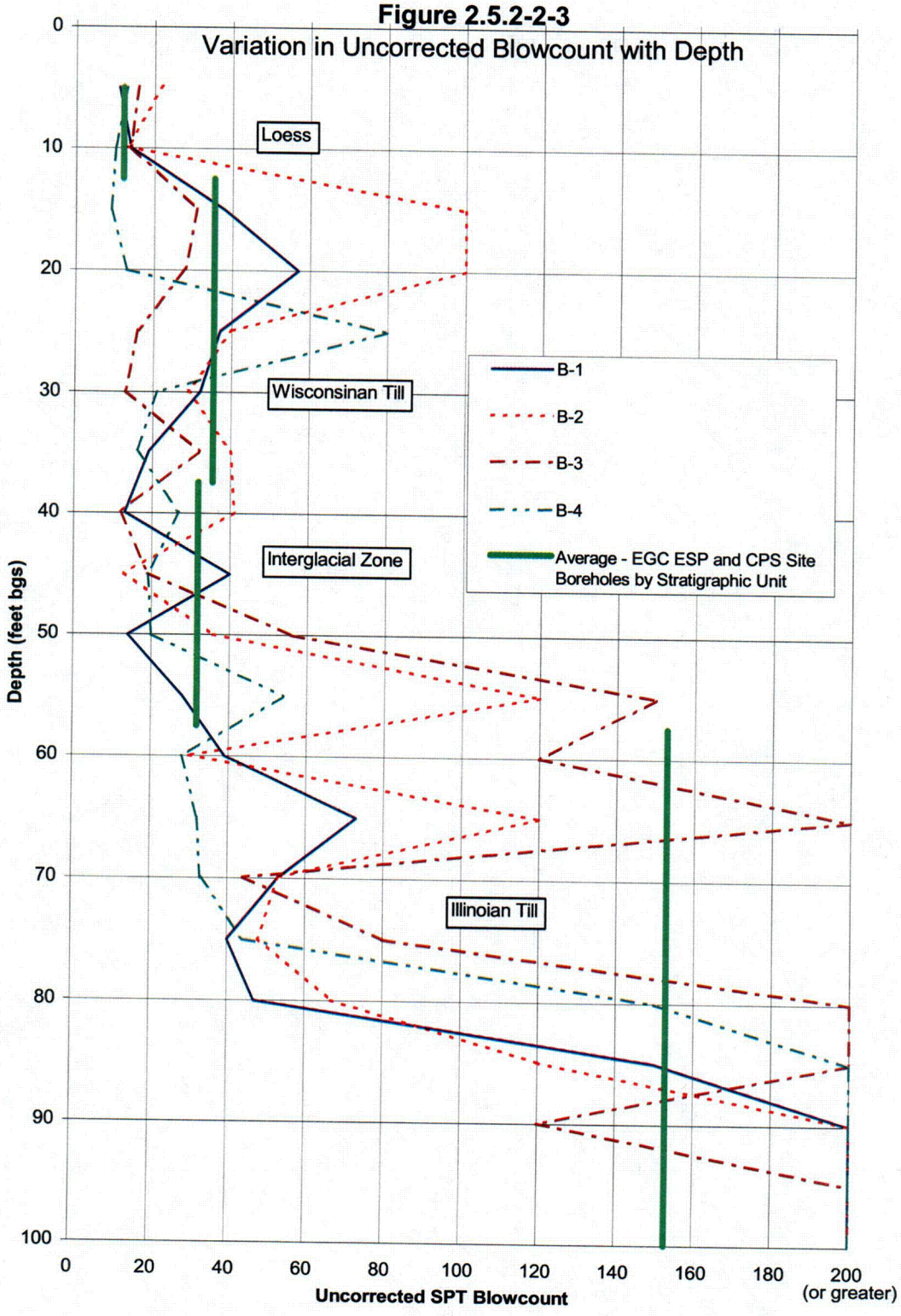

C06

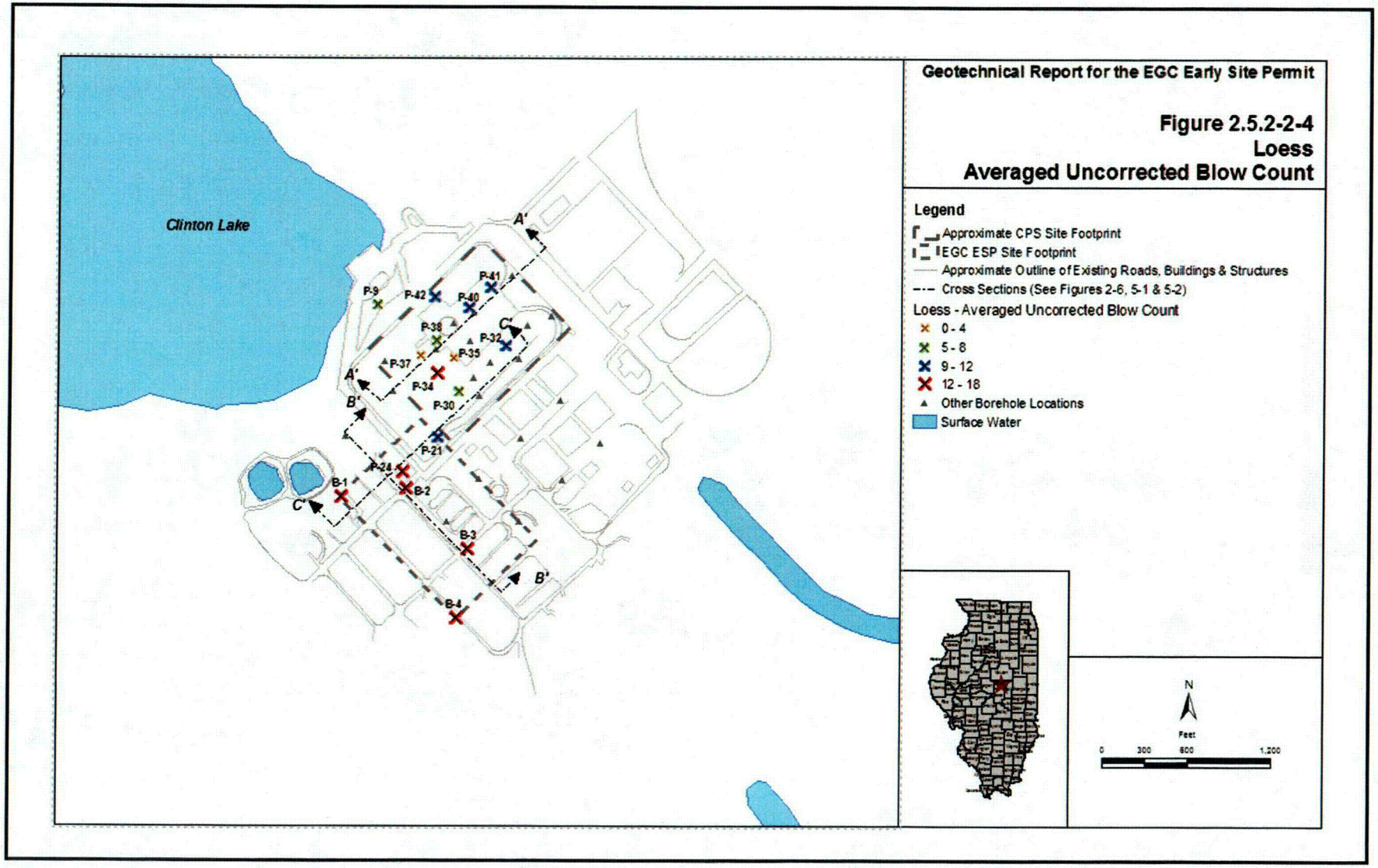
Clinton Lake
A'
B'
C'
P-9
P-42
P-41
P-40
P-38
P-32
P-35
P-37
P-34
P-30
P-21
P-24
B-1
B-2
B-3
B-4
Geotechnical Report for the EGC Early Site Permit
Figure 2.5.2-2-4
Loess
Averaged Uncorrected Blow Count
Legend
Approximate CPS Site Footprint
EGC ESP Site Footprint
Approximate Outline of Existing Roads, Buildings & Structures
Cross Sections (See Figures 2-6, 5-1 & 5-2)
Loess - Averaged Uncorrected Blow Count
0 - 4
5 - 8
9 - 12
12 - 18
Other Borehole Locations
Surface Water
N
Feet
0
300
600
1,200

C07

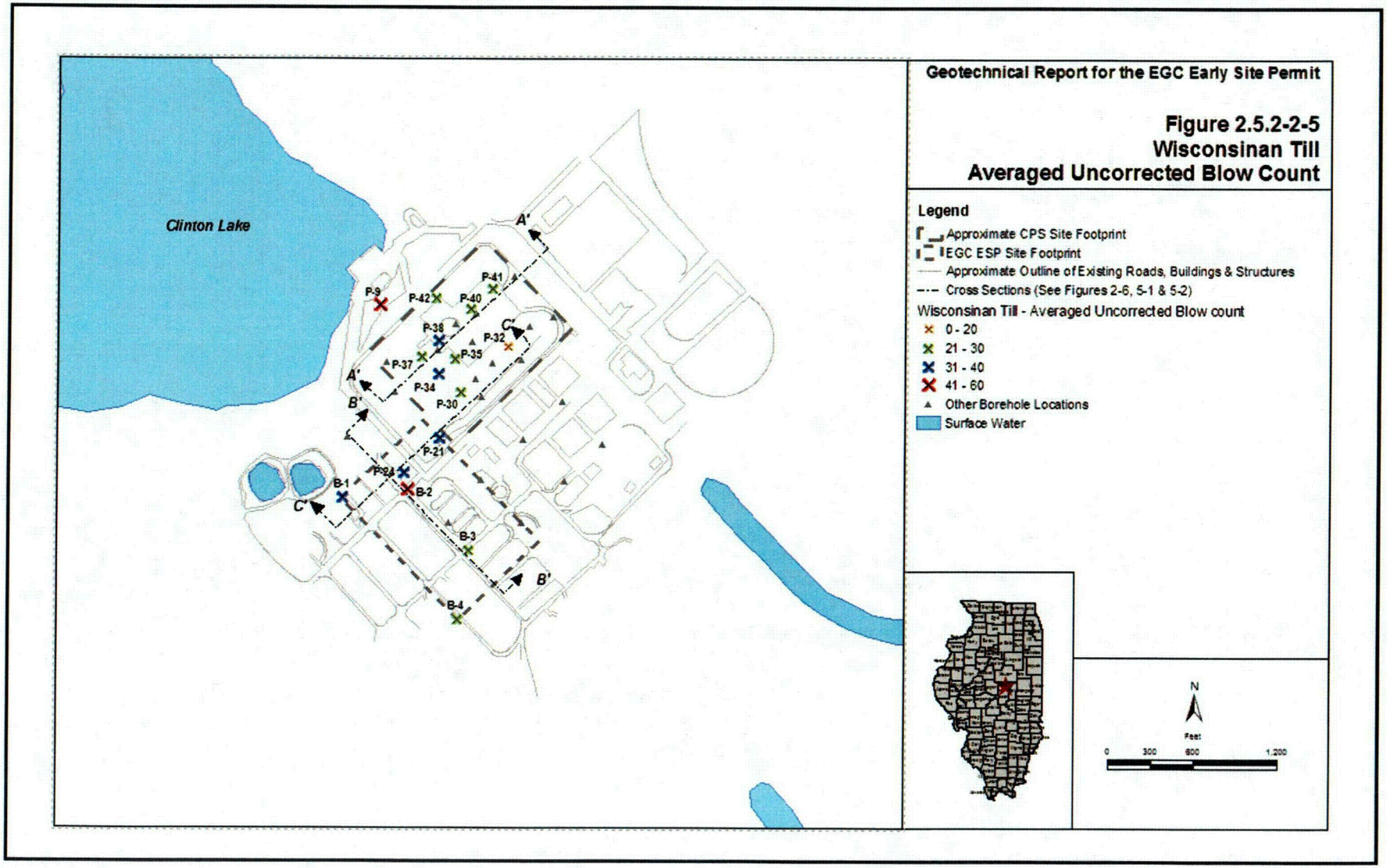
Clinton Lake
A'
P-9
P-42
P-40
P-41
P-38
C'
P-32
P-35
P-37
A'
P-34
B'
P-30
P-21
P-24
B-1
B-2
C'
B-3
B'
B-4
Geotechnical Report for the EGC Early Site Permit
Figure 2.5.2-2-5
Wisconsinan Till
Averaged Uncorrected Blow Count
Legend
Approximate CPS Site Footprint
EGC ESP Site Footprint
Approximate Outline of Existing Roads, Buildings & Structures
Cross Sections (See Figures 2-6, 5-1 & 5-2)
Wisconsinan Till - Averaged Uncorrected Blow count
0 - 20
21 - 30
31 - 40
41 - 60
Other Borehole Locations
Surface Water
N
Feet
0
300
600
1,200

C08

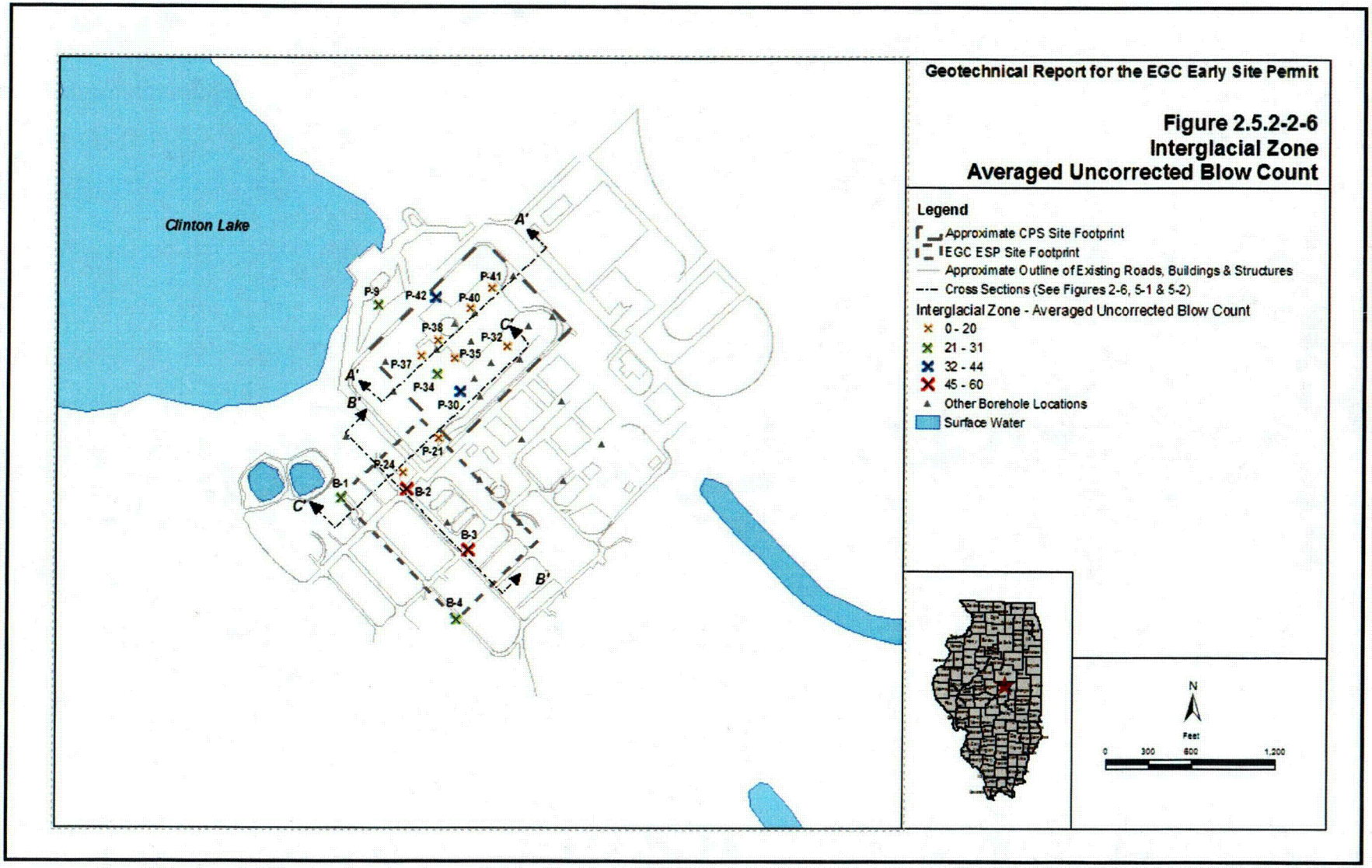
Geotechnical Report for the EGC Early Site Permit
Figure 2.5.2-2-6
Interglacial Zone
Averaged Uncorrected Blow Count
Legend
Approximate CPS Site Footprint
EGC ESP Site Footprint
Approximate Outline of Existing Roads, Buildings & Structures
Cross Sections (See Figures 2-6, 5-1 & 5-2)
Interglacial Zone - Averaged Uncorrected Blow Count
0 - 20
21 - 31
32 - 44
45 - 60
Other Borehole Locations
Surface Water
Clinton Lake
A'
B'
C'
P-9
P-42
P-40
P-41
P-38
P-32
P-35
P-37
P-34
P-30
P-21
P-24
B-1
B-2
B-3
B-4
N
Feet
0
300
600
1,200

C09

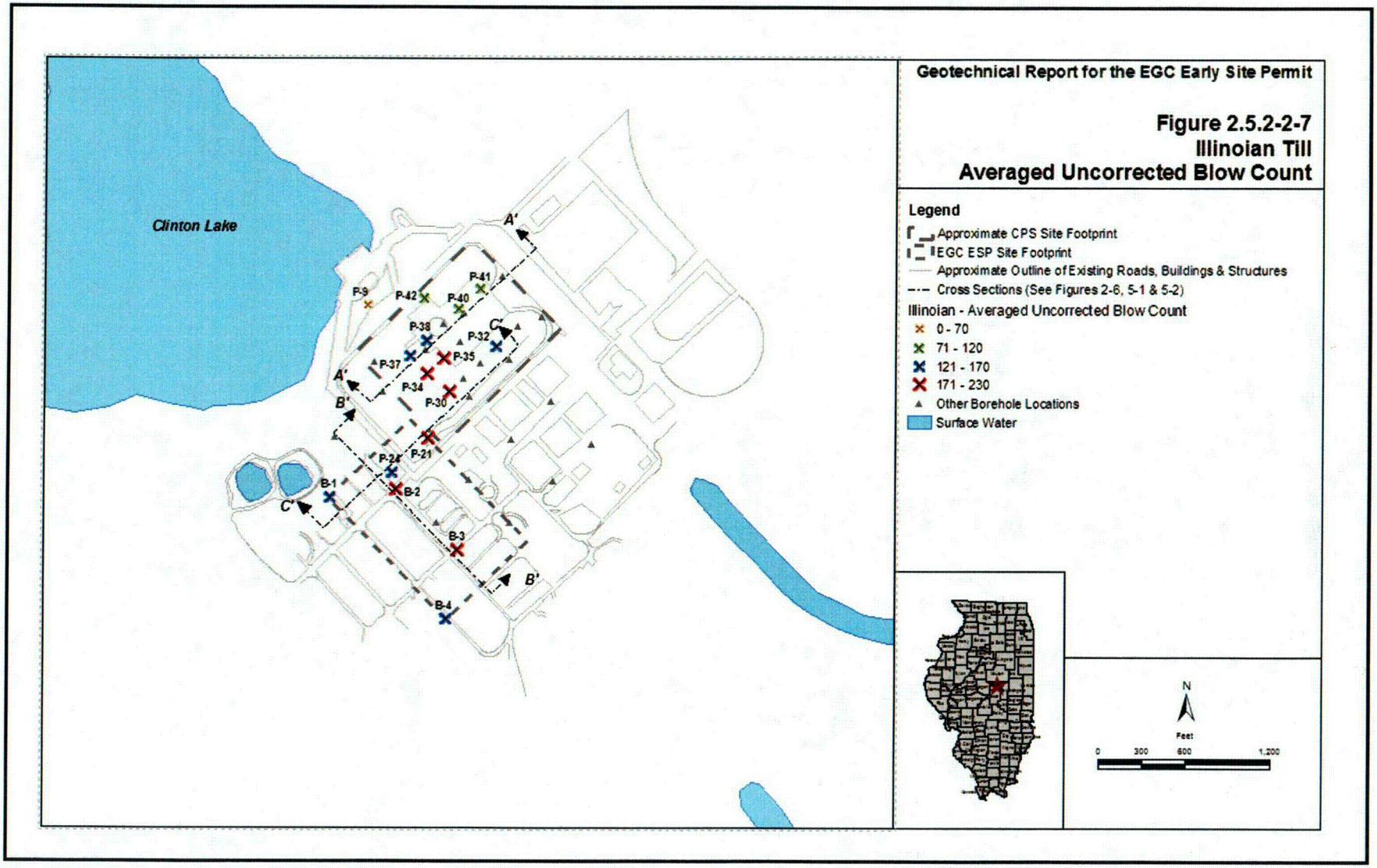
Clinton Lake
A'
C'
A'
B'
C'
B'
P-9
P-42
P-41
P-40
P-38
P-32
P-37
P-35
P-34
P-30
P-21
P-24
B-1
B-2
B-3
B-4
Geotechnical Report for the EGC Early Site Permit
Figure 2.5.2-2-7
Illinoian Till
Averaged Uncorrected Blow Count
Legend
Approximate CPS Site Footprint
EGC ESP Site Footprint
Approximate Outline of Existing Roads, Buildings & Structures
Cross Sections (See Figures 2-6, 5-1 & 5-2)
Illinoian - Averaged Uncorrected Blow Count
0 - 70
71 - 120
121 - 170
171 - 230
Other Borehole Locations
Surface Water
N
Feet
0
300
600
1,200

C10

NRC Letter Dated: 08/26/2005

NRC DSER Open Item 2.5.2-3

Section 2.5.2.3.5 - The staff finds that both of the issues it raised in RAI 2.5.4-7 were not adequately resolved by the applicant. The first issue is the impact of the highly plastic clay soils at the site on the assumption of the independence of the modulus reductions and material damping curves from the specific soil type. The second issue concerns the use of the 15 percent damping cutoff and its impact on the final site surface response spectra. The applicant should rerun its site response analysis using appropriate shear modulus and damping curves for the clay soils and at the same time implement the 15 percent damping cutoff. The combination of these two unresolved issues, described above, constitute Open Item 2.5.2-3.

EGC RAI ID: SOI2-4

EGC RESPONSE:

This response is presented in two parts. The first addresses the question on soil plasticity; the second deals with the 15 percent damping cutoff.

Soil Plasticity

Plasticity is a term used during the classification of fine-grained soils – that is silts and clays. Laboratory Atterberg limits tests are normally conducted to determine the plasticity of the soil, and the plastic index from the Atterberg limits test is the normal measure of plasticity. The open item suggests that soils at the EGC ESP Site are highly plastic. This description could have implications on the appropriateness of the EPRI standard shear modulus and material damping curves at the EGC ESP Site. If the soils are highly plastic, the EPRI standard curves may not be representative.

In response to this Open Issue, Casagrande classification charts were prepared to show the plasticity of soils from each of the primary soil layers. These layers are described in Section 2.5 and Appendix A of the EGC ESP SSAR. The Casagrande classification chart shows the comparison of plastic index to the liquid limit. Soils with a liquid limit of less than 50 are normally classified as either low plasticity clays or silts; soils with liquid limits greater than 50 are considered highly plastic silts and clays.

These plasticity plots are presented in Figures 2.5.2-3-1 through 2.5.2-3-6. The plots show that with the exception of one test result, the Atterberg limits tests on samples from the EGC ESP and the CPS Sites have a liquid limit of less than 50. Based on the Unified Soil Classification System (USCS), these soils are described as silts and clays with low plasticity. This description is consistent with that used for the EPRI standard modulus and damping curves.

As an additional support for use of the EPRI curves, comparisons in Figure 5-20 of Appendix A of the EGC ESP SSAR show that the modulus reduction curve, G/G_{max}, obtained from resonant column/cyclic torsion tests is consistent with the Vucetic and Dobry (1991) curves for plastic index of 15. Figures 4.2-2 through 4.2-6 of Appendix B of the EGC ESP SSAR show that the laboratory data obtained from resonant column/cyclic torsion tests conducted on intact soil samples from the EGC ESP exploration program are also very similar to the EPRI standard modulus and damping curves.

The conclusion from this review is that the soils are best described as low plasticity silts and clays and appropriately modeled by the EPRI standard curves.

15 Percent Damping Cutoff

This issue deals with the maximum material damping value that should be used during site response analyses. The EPRI material damping curves exceed 15 percent when the imposed shearing strains during the site response analysis reach from approximately 0.1 to 0.5 percent, depending on the depth (or confining pressure). At 1 percent shearing strain the damping in the EPRI material damping curves can range from approximately 22 to 30 percent.

As the material damping value increases, particularly above 15 percent, the level of site response can decreases. In view of the uncertainties in both the equivalent linear method used to conduct site response studies, as well as the difficulties of obtaining material damping measurements in laboratory tests under a combination of higher shearing strain and confining pressures, it has been suggested during some past site response studies that the level of material damping should be limited to 15 percent to account for the uncertainties in material damping above this level.

Previously in response to RAI 2.5.4-7, additional site response analyses were conducted with the 15 percent damping limitation. Results of these additional analyses indicated that the damping cutoff had less than a 2 percent effect on the site amplification factors, and these effects occurred primarily at higher frequencies, between 10 and 100 Hz. This effect is negligible and therefore no changes in the SSE were suggested.

In response to this Open Issue, further evaluation of the appropriateness of 15 percent cutoff was made. This evaluation involved contacting Dr. K.H. Stokoe, Professor of Civil Engineering at the University of Texas at Austin, to discuss the physical mechanisms that could limit damping at higher shearing strain levels. Dr. Stokoe conducted the resonant column/cyclic torsion tests on intact samples of soil from the EGC ESP Site; he is also an expert on modeling the cyclic response of soil using laboratory testing methods. Dr. Stokoe indicated awareness of the 15 percent cutoff from previous work at the Savannah River site. While he was unable to provide test data to support using the 15 percent limit on damping, he suggested that in the absence of laboratory test data at high shearing strain levels that would support material damping values of 15 percent or more, it was not unreasonable to limit the laboratory-derived damping value.

In view of the continued concern on the use of damping values greater than 15 percent by the Staff and the absence of laboratory data that would support higher values, as noted by Dr. Stokoe, EGC will revise the SSE for the site to include site amplification factors that have a 15 percent cutoff on damping.

ASSOCIATED EGC ESP APPLICATION REVISIONS:

The EGC October 11, 2004, response to RAI 2.5.4-2, included the following associated EGC ESP application revisions. Each of this is repeated and followed by a bullet identifying any necessary revisions to incorporate the 15% damping cutoff.

1) Revise SSAR, Chapter 2, Section 2.5.2.5, 3rd paragraph, 2nd bullet, second sentence, from:

In general, the modulus and damping data are consistent with the EPRI (1993a) relationships, except that the laboratory data tend to show higher damping levels at very low shearing strains.

To read:

In general, the modulus and damping data are consistent with the EPRI (1993a) relationships, except that the resonant column data tend to show higher damping levels at very low shearing strains. The higher damping from the resonant column tests is attributed to rate-of-loading effects. Damping values from torsional shear tests, which are conducted at frequencies of loading more consistent with predominant free-field ground motions, is very consistent with EPRI damping values.

- No changes are necessary for the above revision.

2) Revise SSAR, Chapter 2, Section 2.5.2.5, 5th paragraph, from:

The site response analyses were conducted using randomized shear wave velocity profiles and soil modulus and damping relationships to account for variation in the dynamic soil properties across the EGC ESP Site. The depth to hard rock was also randomized to reflect its uncertainty. The site response also assumed that the sedimentary rock below 300 ft remains linear during earthquake shaking. Damping in the rock was based on published information. Additional details about the generation of profiles for the site response analyses are included in Sections 4.2.1 and 4.2.2 of Appendix B.

To read:

The site response analyses were conducted using randomized shear wave velocity profiles and soil modulus reduction and material damping relationships to account for variation in the dynamic soil properties across the EGC ESP Site. In the absence of consensus within the profession and since these were free-field ground response analyses, rather than soil-structure analyses described in the SRP Section 3.7.2, material damping in the randomized sets of material damping curves was not capped at 15 percent. The depth to hard rock was also randomized to reflect its uncertainty. This randomization process resulted in 60 independent soil columns that were used in evaluating site response effects. The site response also assumed that the sedimentary rock below 300 ft remains linear during earthquake shaking. Damping in the rock was based on published information. Additional details about the generation of profiles for the site response analyses are included in Section 4.2.1 and 4.2.2 of Appendix B.

- The above revision is now revised to read:

The site response analyses were conducted using randomized shear wave velocity profiles and soil modulus reduction and material damping relationships to account for variation in the dynamic soil properties across the EGC ESP Site. Material damping in the randomized sets of material damping curves was capped at 15 percent, as recommended by NRC. The depth to hard rock was also randomized to reflect its uncertainty. This randomization process resulted in 60 independent soil columns that were used in evaluating site response effects. The site response also assumed that the sedimentary rock below 300 ft remains linear during earthquake shaking. Damping in the rock was based on published information. Additional details about the generation of profiles for the site response analyses are included in Section 4.2.1 and 4.2.2 of Appendix B.

3) Revise SSAR, Chapter 2, Section 2.5.4.2, 4th paragraph, from:

Dynamic properties obtained for the EGC ESP Site were considered but not used explicitly for the site response studies described previously in Section 2.5.2.6. Rather, the EPRI modulus and damping curves were used as the base case for the site response analyses. The rationale for using the EPRI curves rather than the EGC ESP Site data was that a much larger database was used to develop the EPRI curves and, therefore, average EPRI results are expected to be representative of conditions at the EGC ESP site if an extensive dynamic testing program had been conducted. It is important to note that the dynamic test results for the EGC ESP Site are very consistent with the EPRI curves, indicating that use of the EPRI curves is acceptable. A comparison of the EPRI and EGC ESP Site cyclic test results is included in Figures 5-20 and 5-21 of Appendix A.

To read:

Dynamic properties obtained for the EGC ESP Site were considered but not used explicitly for the site response studies described previously in Section 2.5.2.6. Rather, the EPRI modulus and damping curves were used as the base case for the site response analyses. According to EPRI (1993a), the EPRI modulus reduction and material damping curves were developed to account for the variations in soil shear modulus and material damping that occur with shearing strain and soil confining pressure - with soil confining pressure being approximated within the set of curves by the depth below the ground surface. EPRI (1993a) indicates that these curves are appropriate for use in "gravelly sands to low plasticity silty or sandy clays", which is consistent with the soil conditions at the EGC ESP Site. The rationale for using the EPRI curves rather than the EGC ESP Site data was that a much larger database was used to develop the EPRI curves and, therefore, average EPRI results are expected to be representative of conditions at the EGC ESP Site. It is important to note that the dynamic test results for the EGC ESP Site are very consistent with the EPRI curves, indicating that use of the EPRI curves is acceptable. A comparison of the EPRI and EGC ESP Site cyclic test results is included in Figures 5-20 and 5-21 of Appendix A.

- The above revision is revised to include the following additional sentence at the end of the above stated revision:

During site response analyses, material damping was capped at 15 percent, as recommended by NRC.

4) Revise SSAR, Appendix A, Section 5.2.4.2, 8th paragraph, from:

In view of the good comparison between the measured modulus and damping data for the samples from the EGC ESP Site and the published EPRI values of modulus ratio and damping ratio, it was concluded that the conditions at the EGC ESP Site could be adequately represented by the EPRI soil model when developing a site response model, as discussed in both Section 2.5 and Appendix B of the SSAR. Variations noted between the published EPRI curves and those obtained by laboratory testing reflect the normal variation that can be expected when testing soil samples. These variations are accounted for during ground response modeling by introducing a variation between the upper and lower bound modulus and damping ratio curves.

To read:

In view of the good comparisons between the measured modulus and damping data for the samples from the EGC ESP Site and the published EPRI values of modulus ratio and damping ratio, it was concluded that the conditions at the EGC ESP Site could be adequately represented by the EPRI soil model when developing a site response model, as discussed in both Section 2.5 and Appendix B of the SSAR. According to EPRI (1993), the EPRI modulus and damping curves were developed to account for the variations in soil shear modulus and material damping with shearing strain and soil confining pressure - with soil confining pressure being approximated within the set of curves by the depth below the ground surface. EPRI (1993) indicates that these curves are appropriate for use in "gravelly sands to low plasticity silty or sand clays", which is consistent with the soil conditions at the EGC ESP Site. Variations noted between the published EPRI curves and those obtained by laboratory testing reflect the normal variation that can be expected when testing soil samples, including the effects of soil disturbance as represented by the shear wave velocity ratio tabulated in Table 5-3. These variations are accounted for during ground response modeling by introducing sets of randomized modulus reduction and material damping curves that account for uncertainty in these curves through the use of variability terms explicitly determined from a study testing of rock and soil samples (Silva et al., 1996), as discussed in Section 4.2.2 of Appendix B in the EGC ESP SSAR.

- The above revision is revised to include the following additional sentence at the end of the above stated revision:

Material damping values in the site response analyses were capped at 15 percent, as recommended by NRC.

5) Revise SSAR, Appendix B, Section 4.2.1, 4th paragraph, from:

A set of shear modulus reduction and damping tests were performed on samples taken from borings at the EGC ESP Site, as described in the EGC ESP Geotechnical Report (SSAR Appendix A). Figures 4.2-2 through 4.2-6 show the test results compared to the generic modulus reduction (G/Gmax) and damping relationships developed by EPRI (1993). (Note that one test sample produced what are considered to be erroneous values of modulus reduction and high damping values, as discussed in Appendix A to the SSAR. The test data from that sample were not included in developing the site dynamic properties and are not shown here.) In general, the site data are consistent with the EPRI (1993) relationships, except that the site data tend to show higher damping levels at very low shear strains. The EPRI (1993) curves are shown together on Figure 4.2-7, illustrating the effect of increasing confining pressure (increasing depth) on the nonlinear behavior of soils.

To read:

A set of shear modulus reduction and damping tests were performed on samples taken from borings at the EGC ESP Site, as described in the EGC ESP Geotechnical Report (SSAR Appendix A). Figures 4.2-2 and 4.2-6 show the test results compared to the generic modulus reduction (G/Gmax) and damping relationships developed by EPRI (1993). (Note that one test sample produced what are considered to be erroneous values of modulus reduction and high damping values, as discussed in Appendix A to the SSAR. The test data from that sample were not included in developing the site dynamic properties and are not shown here.) In general, the site data are consistent with the EPRI (1993) relationships, except that the resonant column data tend to show higher

damping levels at very low shearing strains. The higher damping from the resonant column tests is attributed to rate-of-loading effects. Damping values from torsional shear tests, which are conducted at frequencies of loading more consistent with predominant free-field ground motions, is very consistent with EPRI damping values. The EPRI (1993) curves are shown together on Figure 4.2-7, illustrating the effects of increasing confining pressure (increasing depth) on the nonlinear behavior of soil. According to EPRI (1993), the EPRI modulus and damping curves were developed to account for the variations in soil shear modulus and material damping with shearing strain and soil confining pressure - with soil confining pressure being approximated within the set of curves by the depth below the ground surface. EPRI (1993) indicates that these curves are appropriate for use in "gravelly sands to low plasticity silty or sand clays", which is consistent with the soil conditions at the EGC ESP Site.

- The above revision is revised to include the following additional sentence at the end of the above stated revision:

Material damping values were capped at 15 percent, as recommended by NRC.

In addition to revisions to the responses to RAI 2.5.4-2, the following associated EGC ESP application revisions will also be necessary to incorporate the 15% damping cutoff.

6) Revision of SSAR, B, Section 2.5, Figures 2.5-8, 2.5-11, and 2.5-12.

7) Revision of SSAR, Appendix B, Section 4.2.2, text.

8) Revision of SSAR, Appendix B, Section 4.2, Figures 4.2-14 thru 4.2-18, and 4.2-23 thru 4.2-26, 4.3-1 and 4.3-6.

9) Revision of SSAR, Appendix B, Section 4.3, Figures 4.3-1 and 4.3-6.

The details of the revisions identified in Items 6) through 9) above are in process and will be provided in the upcoming Revision 1 of the EGC ESP Application.

ATTACHMENTS:

Figures 2.5.2-3-1 through 2.5.2-3-6

Figure 2.5.2-3-1
Loess Plasticity Chart

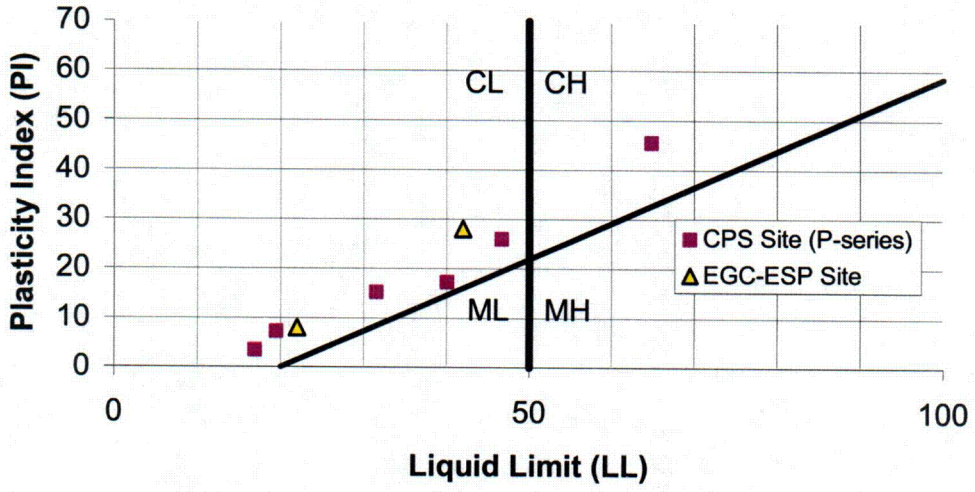

Figure 2.5.2-3-2
Wisconsinan Plasticity Chart

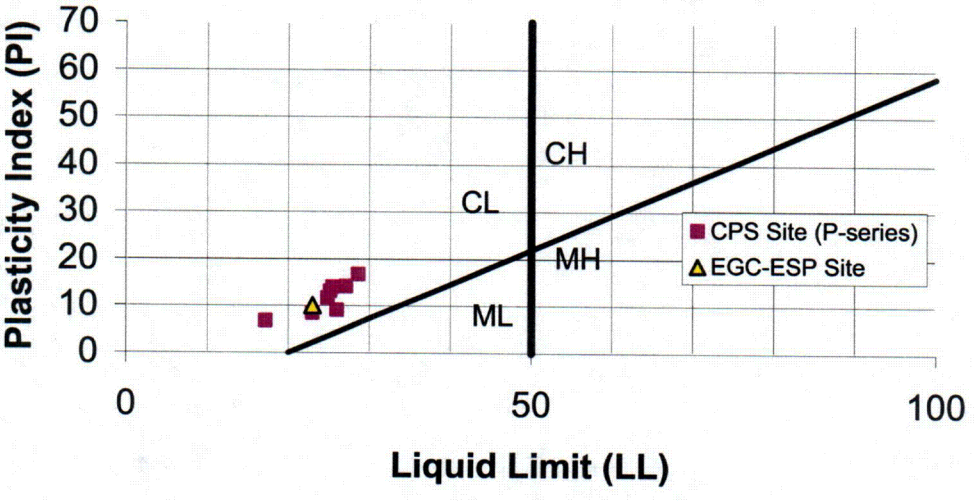

C11

Figure 2.5.2-3-3
Interglacial Plasticity Chart

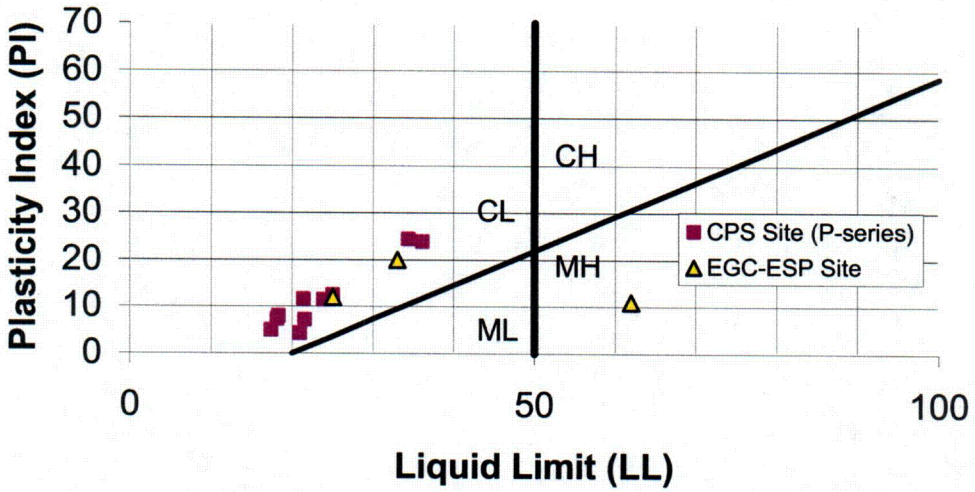

Figure 2.5.2-3-4
Illinoian Plasticity Chart

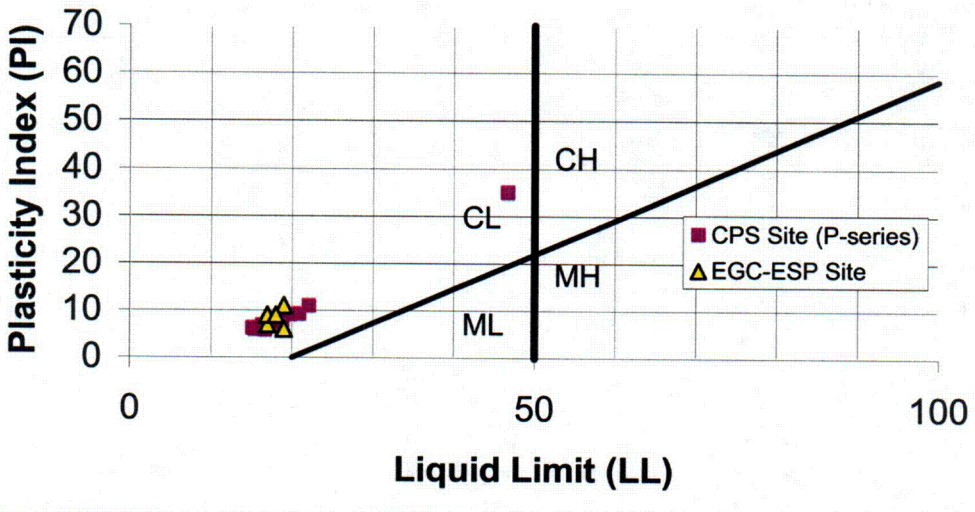

C12

Figure 2.5.2-3-5
Lacustrine Plasticity Chart

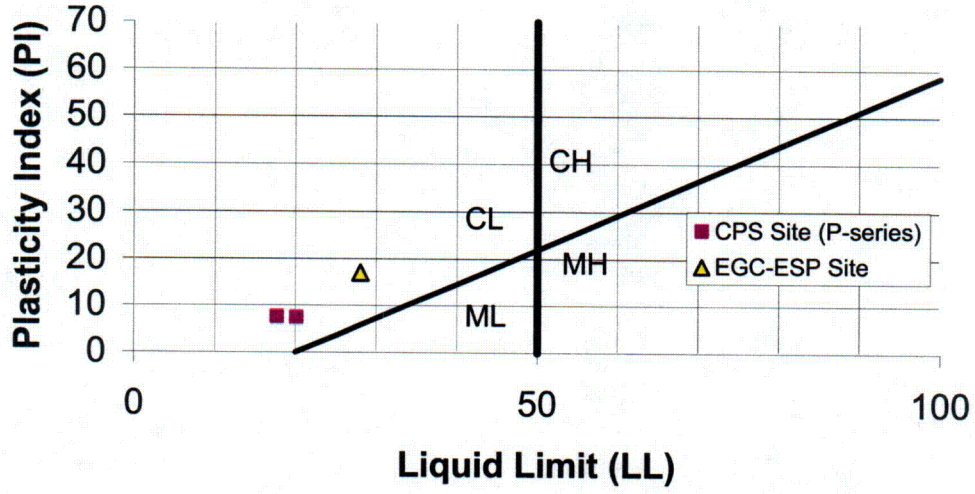

Figure 2.5.2-3-6
Pre-Illinoian Plasticity Chart

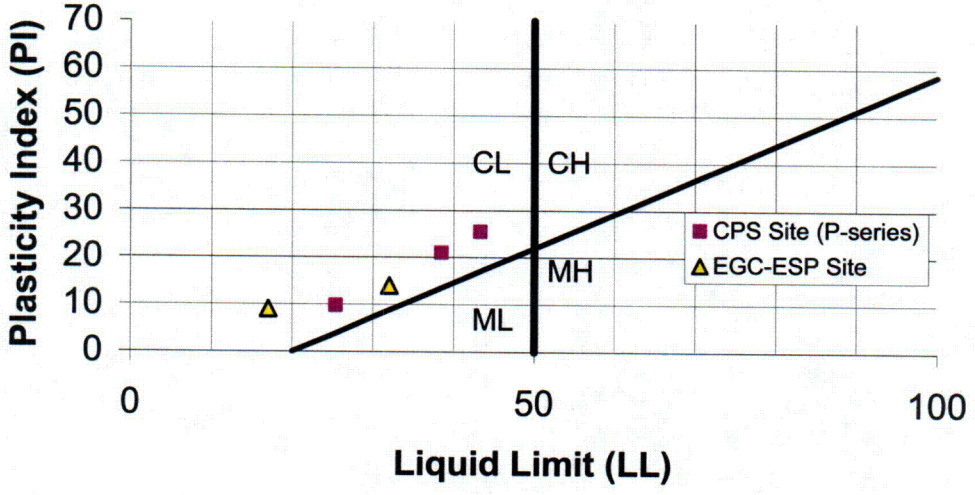

C13

NRC Letter Dated: 08/26/2005

NRC DSER Open Item 2.5.2-4

Section 2.5.2.3.6 - To determine the appropriateness of the target 10-5 annual performance goal and performance based approach for the Clinton ESP site, the staff reviewed the applicant's final SSE. As shown previously in SER Section 2.5.2.1.6, the final SSE using the performance-based approach is calculated by multiplying the DF and 10-4 surface UHRS. Since, by definition, the DF is at least 1.0, the final SSE ground motion spectrum will be at least the 10-4 UHRS and higher, depending on the value of the amplitude ratio (AR) for the 10-4 and 10-5 hazard curves. For the Clinton ESP site, the DF values from 2.5 to 100 Hz are very close to 1.0, implying that the final SSE, while meeting the target 10-5 annual performance goal, is essentially the 10-4 surface UHRS. This result is clearly shown by Figure 2.5.2-8 below, which shows the 10-4 and 10-5 surface UHRS along with the final SSE.

The high-frequency and low-frequency controlling earthquakes that provide the largest contribution to these two hazard levels (10-4 and 10-5) for the ESP site were shown previously in SER Section 2.5.2.1.4.

Because the performance-based SSE is essentially the 10-4 surface UHRS, the corresponding controlling earthquakes for the ESP site are mb 6.5 at 83 km (52 mi) (high frequency) and mb 7.2 at 320 km (199 mi) (low frequency). These two earthquakes correspond to events in the WVSZ and NMSZ, respectively. Both of these events are somewhat distant from the ESP site. In contrast, the mean 10-5 high-frequency controlling earthquake (mb 6.2 at 24 km (15 mi)) represents a local earthquake from the central Illinois seismic zone. Figure 2.5.2-9, reproduced from Figure 4.2-19 in SSAR Appendix B and shown previously in SER Section 2.5.2.1.4, shows the 10-4 and 10-5 UHRS together with the ground motion response spectra for these two sets of controlling earthquakes.

Since, as shown above in Figures 2.5.2-8 and 2.5.2-9, the high-frequency 10-5 controlling earthquake ground motion response spectrum from a local earthquake in the central Illinois seismic zone is significantly larger than the SSE ground motion response spectrum, the staff believes that the final performance-based SSE does not adequately represent the seismic hazard for the ESP site.

The seismic hazard for the central Illinois basin/background source zone, which encompasses the ESP site, is dominated by the Springfield earthquake. Paleoliquefaction studies in the area have found evidence that one or, more likely, two prehistoric earthquakes occurred 5900 to 7400 years ago near Springfield, Illinois, approximately 30 mi southwest of the ESP site (McNulty and Obermeier, 1999). These earthquakes were large enough to generate liquefaction features, with magnitude estimates ranging between 6.2 and 6.8 for the larger event and at least 5.5 for the second event. In addition to the Springfield events, geologists have discovered paleoliquefaction features further south near Shoal Creek. The estimated magnitude and

regional and local liquefaction studies, as well as the historical seismicity, indicate that there is a significant seismic hazard within the central Illinois basin/background seismic source zone. This seismic hazard is quantified by the ground motion from the 10-5 high-frequency controlling earthquake, appropriately scaled to the 5- and 10-Hz hazard curves, with a magnitude of 6.2 at a distance of 24 km (15 mi) from the site.

The opening paragraph of 10 CFR 100.23 states the following:

> This section sets forth the principal geologic and seismic considerations that guide the Commission in its evaluation of the suitability of the proposed site and adequacy of the design bases established in consideration of the geologic and seismic characteristics of the proposed site, such that, there is a reasonable assurance that a nuclear power plant can be constructed and operated at the proposed site without undue risk to the health and safety of the public.

In addition, GDC 2 in Appendix A to 10 CFR Part 50 states the following:

> Structures, systems, and components important to safety shall be designed to withstand the effects of natural phenomena such as earthquakes, tornadoes, hurricanes, floods, tsunami, and seiches without loss of capability to perform their safety functions. The design bases for these structures, systems, and components, shall reflect: (1) Appropriate consideration of the most severe of the natural phenomena that have been historically reported for the site and surrounding area, with sufficient margin for the limited accuracy, quantity, and period of time in which the historical data have been accumulated, . . .

It is the staff's position that the SSE developed by the applicant using the target 10-5 annual performance goal and performance-based approach does not provide a design-basis ground motion that adequately reflects the seismic characteristics of the proposed site. Furthermore, the applicant's SSE does not represent ground motion from the most severe local earthquake as required by GDC 2. The staff does not view the use of the phrase "historically reported" in GDC 2 as limiting the use of paleoliquefaction features as legitimate indicators of earthquake activity or as limiting the size of the design basis ground motion for prospective nuclear sites. RG 1.165, which describes the geologic investigations necessary to meet the requirements of 10 CFR 100.23, defines capable earthquake sources as the "presence of surface or nearsurface deformation of landforms or geologic deposits of a recurring nature within the last approximately 500,000 years or at least once in the last approximately 50,000 years." Both of these dates extend far back into the prehistory of the North American continent. In addition, RG 1.165 recommends that the design-basis ground motion (SSE) be determined using a reference probability of median 10-5, which corresponds to a median ground motion return period of 100,000 years. To determine ground motions with this return period in the CEUS requires the use of paleoliquefaction features to estimate prehistoric earthquake magnitudes and locations.

In conclusion, the staff finds that the applicant's SSE does not represent a ground motion of adequate severity to represent the seismic hazard for the ESP site. Based on this conclusion, the staff does not accept the use of the performance-based threshold with the target 10-5 annual performance goal as a suitable method for the determination of the SSE for the Clinton ESP site. This is Open Item 2.5.2-4.

EGC RAI ID: SOI2-5

EGC RESPONSE:

The DSER raises several issues in this item relating to the representation of prehistoric earthquakes in the PSHA for the EGC ESP site, the relationship between the controlling earthquakes defined from that PSHA and the Springfield earthquake, and the adequacy of the SSE ground motions developed from application of the ASCE 45-05 approach to represent ground motion from the controlling earthquakes. These issues are addressed below.

Incorporation of Prehistoric Earthquake Data into the EGC ESP PSHA

The development of the PSHA model for the EGC ESP site is described in Appendix B to the SSAR. The starting point is the EPRI-SOG (1988) seismic hazard model which has been accepted by the U.S. Nuclear Regulatory Commission as an appropriate seismic hazard model (Regulatory Guide 1.165). The seismic sources developed in the EPRI-SOG (1988) study that are important to the seismic hazard at the EGC ESP site can be divided into three general groups. The first group is seismic sources associated with the New Madrid seismic zone located approximately 320 kilometers (200 miles) or more to the south (see Figure 2.5.2-4-1). The second group is seismic sources representing the seismicity in southern Illinois and southern Indiana, often designated the Wabash Valley. These sources lie in the range of 100 to 175 kilometers from the EGC ESP site. The third group represents the low level seismicity in central Illinois where the EGC ESP site is located. The EPRI SOG experts either defined a local source zone for central Illinois or modeled the EGC ESP site region to be part of a large background source representing the stable craton of central North America.

Section 2 of Appendix B to the SSAR summarizes the information on prehistoric earthquakes that are important to assessing the seismic hazard at the EGC ESP site. There have been a number of investigations that have identified prehistoric earthquakes in the New Madrid area that are inferred to have been similar in size to the earthquakes of the 1811-1812 sequence. These earthquakes are thought to have occurred within the area of concentrated seismicity that comprises the New Madrid seismic zone (Figure 2.5.2-4-1). As discussed in Section 3 of Appendix B to the SSAR, the location of these prehistoric earthquakes is well represented by the New Madrid seismic sources developed in the EPRI-SOG (1988) study. A second set of studies has identified prehistoric earthquakes in southern Indiana and southern and central Illinois. The locations of these earthquakes are shown in part (a) of Figure 2.5.2-4-2. Shown in part (b) of Figure 2.5.2-4-2 are the EPRI-SOG (1988) seismic sources for the New Madrid and southern Illinois/southern Indiana regions. With the exception of the Springfield earthquake, all of the identified prehistoric earthquakes lie with the EPRI-SOG (1988) seismic sources for the southern Illinois/southern Indiana region. The energy center for the Springfield earthquake is placed 60 kilometers southwest of the EGC ESP site. This location places the Springfield earthquake within the EPRI-SOG seismic source zones that contain the EGC ESP site. This earthquake is estimated to have occurred between 5,900 and 7,400 years ago. The estimated magnitude reported in Appendix B to the SSAR is in the range of **M** 6.2 to 6.8. A second, smaller earthquake, ~**M** 5.5, may have occurred in the same area. There is no identifiable cluster of historical seismicity in this area (Figure 2.5.2-4-1) and no clearly defined potentially seismogenic structure. Additional field reconnaissance in the area around the EGC ESP site (described in Attachment 1, Appendix B to the SSAR) did not find evidence for other prehistoric earthquakes similar in size to, or larger than, the

Springfield earthquake. Isolated liquefaction features were found that may represent evidence for possible older, low-magnitude prehistoric earthquakes that may have occurred in central Illinois; or may represent the effects of large distant earthquakes.

The conclusion reached is that no additional seismic sources have been identified by post EPRI-SOG (1988) studies. The prehistoric earthquakes in the New Madrid region are represented by the EPRI-SOG New Madrid sources, and the prehistoric earthquakes in southern Illinois and southern Indiana are represented by the EPRI-SOG seismic sources in these regions. The Springfield earthquake is interpreted to be an isolated moderate magnitude earthquake that could occur anywhere in the site region, rather than an earthquake associated with an identifiable seismic source located near Springfield, approximately 60 kilometers to the southwest of the EGC ESP site.

Sections 3.1.2, 3.1.3 and 4.1 of Appendix B to the SSAR present the assessment of the impact of the prehistoric earthquake data on the characterization of seismic sources for the EGC ESP site in terms of earthquake occurrence rates and maximum magnitudes.

Figure 2.5.2-4-3 shows representative seismic sources used to assess the implications of the prehistoric earthquake data on earthquake occurrence rates. As discussed in Section 3.1.2 of Appendix B to the SSAR, earthquake frequencies within these sources computed using the earthquake catalog updated to include post EPRI-SOG seismicity are very similar to earthquake frequencies computed using just the EPRI-SOG (1988) catalog. Figure 2.5.2-4-4 compares the earthquake frequencies computed using the updated catalog with estimated earthquake frequencies for large earthquakes based on the prehistoric earthquake data. For the New Madrid sources, extrapolation of the earthquake frequencies based on recorded small magnitude seismicity under estimates the frequency of large earthquakes based on the 1811-1812 earthquakes and prehistoric earthquake sequences in approximately 900 AD and 1450 AD. As discussed in Section 4.1.1 of Appendix B to the SSAR, the EPRI-SOG seismic sources for New Madrid were modified to include a source of large magnitude earthquakes with an average repeat time of approximately 500 years in order to adequately represent the frequency of large earthquakes in the New Madrid region inferred from the paleoliquefaction data.

For the Wabash Valley sources, extrapolation of seismicity rates based on historical seismicity adequately predicts the frequency of large magnitude earthquakes inferred from prehistoric earthquake data (six earthquakes of $m_b > 6$ in 8,000 years). A similar conclusion was reached by Wheeler and Cramer (2002). Similarly for the central Illinois source, extrapolation of seismicity rates based on historical seismicity adequately predicts the frequency of large magnitude earthquakes inferred from prehistoric earthquake data (one earthquake of $m_b > 6$ in 8,000 years). Therefore, no modification of the EPRI-SOG earthquake occurrence rates for these sources was needed to capture the frequency of large earthquakes inferred from the paleoliquefaction data.

Sections 3.1.3 and 4.1 of Appendix B to the SSAR discuss the implication of the estimated sizes of the prehistoric earthquakes to the maximum magnitude distributions for the EPRI-SOG seismic sources. The maximum magnitude distributions for the New Madrid seismic sources adequately represents the size of prehistoric New Madrid earthquakes because these events are inferred to have been similar in size to the 1811-1812 earthquakes. The estimated magnitude for the largest prehistoric Wabash Valley earthquake is in the range of **M** 7.2 to 7.8, near the upper end of the EPRI-SOG maximum magnitude distributions for these sources. The estimated magnitude for the Springfield earthquake is in the range of **M** 6.2 to 6.8, at the upper end of the EPRI-SOG

maximum magnitude distributions for seismic sources that encompass central Illinois. As a result of these comparisons, the maximum magnitude distributions for southern Illinois/southern Indiana sources and central Illinois sources were modified to reflect the estimated sizes of these earthquakes (Section 4.1.2 and 4.1.3 of Appendix B to the SSAR). Figures 2.5.2-4-5 and 2.5.2-4-6 compare the composite EPRI-SOG maximum magnitude distributions converted from m_b magnitude to **M** magnitude with the updated maximum magnitude distributions for these sources.

In summary, the data for prehistoric earthquakes in the region indicated that the EPRI-SOG seismic source characterization should be modified to include more frequent large-magnitude earthquakes in the New Madrid region and to increase the maximum magnitude distributions for southern Illinois/southern Indiana and central Illinois sources to accommodate the inferred sizes of the largest prehistoric earthquakes. These modifications were implemented in the PSHA conducted for the EGC ESP site.

Determination of Controlling Earthquakes

Controlling earthquakes, as defined in Regulatory Guide 1.165, are computed from de-aggregation of the seismic hazard in terms of the contributions of earthquakes in different magnitude and distance intervals. The process of de-aggregation is illustrated on Figure 2.5.2-4-7 using the example central Illinois seismic source shown on Figure 2.5.2-4-3. The figure shows detailed de-aggregation of the components of a PSHA calculation into 0.1 magnitude intervals and 1-km distance interval. The top plot shows the magnitude-distance density for earthquake occurrence rates. The seismicity in the central Illinois source does not show clustering and thus can be represented by assuming for this illustrative example that the spatial distribution of earthquakes is uniform. Given this assumption, the number of earthquakes that occur in any region R is directly proportional to the area of R. Therefore, the relative number of earthquakes that occur at an epicentral distance $r \pm \Delta r/2$ from the site is proportional to r as the area encompassed by annular rings of radius $r \pm \Delta r/2$ is approximately equal to $2\pi r \Delta r$. The earthquake occurrence frequencies for the source are modeled using the standard truncated exponential recurrence model (Figure 2.5.2-4-4). Therefore, the relative frequency of earthquakes of different magnitudes is proportional to $10^{-0.78mb}$. As a result, the relative frequency of earthquakes increases with increasing epicentral distance and decreases with increasing magnitude. The peak of the de-aggregation of the earthquake occurrence rates is located at the lowest magnitude considered (m_b 5.0) and at large distances. The magnitude-distance density for earthquake rates shown at the top of Figure 2.5.2-4-7 begins to decrease at distances beyond about 100 km due to the finite dimensions of the example source. The ridges in the density are caused by edge effects from the rectangular source boundaries.

The lower left plot in Figure 2.5.2-4-7 shows the magnitude-distance distribution for the conditional probability of exceeding 0.32g 10-Hz spectral acceleration. This distribution was computed using the median model for Cluster 2 from the EPRI (2004) ground motion model. The 10-Hz spectral acceleration level of 0.32g is equal to the 10^{-4} exceedance frequency computed for the EGC ESP site. The conditional probability of exceedance decreases with increasing distance and increases with increasing magnitude – the opposite trend from that for the magnitude-distance de-aggregation of the earthquake occurrence rates.

The product of the earthquake occurrence rates and the conditional probability of exceedance is the frequency of exceedance (the hazard). The lower right plot in Figure 2.5.2-4-7 shows the magnitude-distance de-aggregation of the frequency of

exceedance. The peak (mode) of this distribution occurs at m_b 5 and at an epicentral distance of 8 km. As epicentral distance increases, the conditional probability of exceedance decreases much more rapidly than the frequency of earthquakes increases, thus producing higher contributions to hazard at close distances. On the other hand, as magnitude increases, the increase in the conditional probability of exceedance at these short epicentral distances is less rapid than the decrease in earthquake frequencies, thus resulting in higher contributions from smaller magnitude earthquakes.

As defined in Regulatory Guide 1.165, the magnitude and distance for the controlling earthquake are computed as the weighted mean magnitude and weighted mean distance for earthquakes contributing to the hazard. The weights are defined by the magnitude-distance de-aggregation of the frequency of exceedance; i.e., the lower right plot of Figure 2.5.2-4-7. For the example de-aggregation, the weighted mean magnitude is m_b 5.8 and the weighted mean epicentral distance is 24 km.

The Springfield earthquake represents an event near the largest size expected to occur in the source zone and at a relatively large distance (approximately 60 km epicentral distance). Because there is no concentration of seismicity at Springfield, there is no peak in the magnitude-distance distribution of earthquake frequencies at that distance, and earthquakes of comparable size can occur closer to the site. Because earthquakes smaller than the Springfield earthquake occur much more frequently, they have a larger contribution to the hazard. As a result, the procedure outlined in Regulatory Guide 1.165 would not identify the Springfield earthquake as a controlling earthquake. In addition, it would not appear as a peak (mode) in the magnitude-distance de-aggregation of the hazard.

The de-aggregation of the hazard for the EGC ESP site reflects the contributions of the three groups of sources identified above. The example de-aggregation presented in Figure 2.5.2-4-7 was extended to include the contribution from all three of the example seismic sources shown on Figure 2.5.2-4-3. Figure 2.5.2-4-8 shows the composite magnitude-distance de-aggregations computed for these three sources. The top plot shows the de-aggregation of the combined earthquake frequencies. The higher seismicity in the New Madrid and Wabash Valley sources (Figures 2.5.2-4-1 and 2.5.2-4-4) produces large peaks in that magnitude-distance de-aggregation of earthquake frequencies at large distances from the site. The contribution from the central Illinois source now appears as a low level rise in the distance range of 0 to 100 km, reflecting the lower level of earthquake activity in central Illinois compared to the Wabash Valley and New Madrid regions. The three sharp large-magnitude peaks represent the three New Madrid fault sources with earthquakes occurring approximately every 500 years. The lower right plot of Figure 2.5.2-4-8 shows the magnitude-distance de-aggregation of the combined frequency of exceeding 0.32g 10-Hz spectral acceleration from all sources. The individual contributions of the three example sources can be seen in these results. The contribution from the central Illinois source appears at small magnitudes and small epicentral distances, as was seen in Figure 2.5.2-4-7. The contribution from the Wabash Valley source is indicated by the broad peak between distances of 100 and 200 km at larger magnitudes. Because of the large distance to the source, large magnitude earthquakes are the major contributor to the hazard from this source. The contribution from the New Madrid fault sources is again shown by the three sharp, large magnitude peaks between 350 and 450 km from the site.

Figures 2.5.2-4-9 and 2.5.2-4-10 present details of the calculation of controlling earthquakes for the 10^{-4} and 10^{-5} mean frequency of exceedance ground motions (the

average for 5 and 10 Hz spectral acceleration). These results are based on the full PSHA calculations for the EGC ESP site presented in Section 4.1 and 4.2 of Appendix B to the SSAR. The 3-D histograms shown on these figures represent the same type of information shown on the lower right of Figure 2.5.2-4-8. The magnitude and distance intervals used in the de-aggregation are those recommended in Appendix C of Regulatory Guide 1.165. Indicated on the figures are the contributions from the three groups of seismic sources. The histogram for the 10^{-4} hazard shows peaks in the contributions for all three source groups. The calculation of magnitude and distance for the controlling earthquake is illustrated by the table shown on the upper left of Figure 2.5.2-4-9. The three modes are indicated by the larger percent contributions identified for the three source groups. The weighted mean magnitude and distance, in essence, represent weighted averages for these three modes. For the case of the 10^{-4} hazard, the resulting controlling earthquake actually lies at a low point in the magnitude-distance de-aggregation. For the 10^{-5} hazard, Figure 2.5.2-4-10, the relative contribution from the local central Illinois sources increases because the large, distant earthquakes in the Wabash Valley/southern Illinois and New Madrid sources are much less likely to produce this higher level of ground motion. As a result, the controlling earthquake is dominated by the central Illinois source and the resulting mean magnitude and distance are smaller than those computed for the 10^{-4} hazard. Table 2.5.2-4-1 lists the controlling earthquakes computed for the 10^{-4} and 10^{-5} hazard levels from the PSHA conducted for the EGC ESP site.

Relationship between Uniform Hazard and Controlling Earthquake Response Spectra

As described in Regulatory Position 4 and Appendix F of Regulatory Guide 1.165, the controlling earthquakes are used to develop appropriate spectral shapes for the SSE ground motions because the controlling earthquake represents the weighted contributions of the distribution earthquake magnitudes and distances contributing to the site hazard. Response spectra are computed for the controlling earthquake magnitude and distance using appropriate ground motion data or models. Section 2.5.2.6 of the Standard Review Plan calls for the use of the 84th percentile response spectra. The response spectra for the controlling earthquakes are then scaled to match the uniform hazard response spectra in the appropriate frequency range. This process is illustrated in Figure 2.5.2-4-11. Part (a) of the figure shows median and 84th-percentile response spectra for the 5 and 10 Hz controlling earthquake for the 10^{-4} hazard. These were computed using the weighted combination of the EPRI (2004) ground motion models, including the adjustment from epicentral to Joyner-Boore or rupture distance and the three alternative conversions from m_b to **M** magnitudes used in the ESP EGC PSHA (Appendix B, Section 4.1.4 of the SSAR). Listed on the plot are the scaling factors required to scale the median and 84th-percentile response spectrum up to match the 10^{-4} UHS at 5 and 10 Hz for hard rock conditions. Part (b) of Figure 2.5.2-4-11 shows the scaled high frequency and low frequency controlling earthquake spectra scaled to match the 10^{-4} UHS. As indicated in Table 2.5.2-4-1, the controlling earthquake spectrum for the average of 1 and 2.5 Hz motions is based on the contributions from earthquakes at distances greater than 100 km, as specified in Appendix C of Regulatory Guide 1.165. As indicated on Figure 2.5.2-4-11, the scaling factors for the 84th-percentile spectrum are greater than 1, indicating that the 10^{-4} UHS is higher than the 84th-percentile spectrum for the controlling earthquakes defined by the process given in Regulatory Guide 1.165.

The site response methodology used to develop soil surface motions for the EGC ESP site is Method 2B described in NUREG/CR-6728 (McGuire et al., 2001). In that

approach, a distribution of earthquake sizes is used to represent the rock ground motions rather than a single earthquake representing the controlling earthquake. Termed de-aggregation earthquakes, these earthquakes are defined to represent of earthquakes contributing to the hazard at the site. The de-aggregation earthquakes defined for the EGC ESP site are listed in Table 2.5.2-4-1 along with the weights that represent their relative contribution to the site hazard. These three de-aggregation earthquakes are also representative of the three seismic source groups that contribute to the site hazard and of the three modes of the magnitude-distance de-aggregation of the hazard. This approach is designed to appropriately represent the ground motions contributing to the site hazard in the site response analyses in order to develop hazard-consistent response spectra at the ground surface.

In the DSER, the Staff expressed concern that "...the applicant's SSE does not represent ground motion from the most severe local earthquake..." as represented by the prehistoric Springfield earthquake. A direct comparison of the SSE developed from the site PSHA with deterministic response spectra for a specific earthquake is not part of the process specified for the applicant in Regulatory Guide 1.165. However, in response to the Staff's concerns, a comparison of ground motions representative of the Springfield earthquake and the results of the PSHA for the EGC ESP site is presented in Figure 2.5.2-4-12. As discussed in the DSER, the SSE ground motions are similar to the 10^{-4} hazard ground motions for spectral frequencies above 2 Hz. Therefore, comparisons are made between the rock 10-4 UHS and estimated ground motions for the Springfield event. In Section 4.1.3 of Appendix B to the SSAR, the following distribution for the size of the Springfield earthquake was developed: **M** 6.2 (0.4), **M** 6.4 (0.3), **M** 6.6 (0.2), and **M** 6.8 (0.1). The left hand plot on Figure 2.5.2-4-12 shows the median and 84^{th}-percentile response spectra developed using the distribution of EPRI (2004) ground motion models combined with the distribution for the size of the Springfield earthquake. The ground motion models used were those for Clusters 1, 2, and 3, the same set used to compute the hazard from the central Illinois sources. Including models from Cluster 4 in the calculation would produce slightly lower motions. The estimated energy center for the Springfield earthquake was taken to represent the earthquake epicenter, and the distance adjustment models developed in EPRI (2004) were applied to the calculation. Listed on the Figure are the scale factors needed to scale the estimated Springfield earthquake spectra up to match the 10^{-4} UHS at an average of 5 and 10 Hz spectral frequencies.

Recently, Olson et al. (2005 in press) have developed updated relationships for estimating the magnitude of prehistoric earthquakes from the extent of the area of associated paleoliquefaction features. Use of this updated relationship would give a magnitude of **M** 6.3 for the Springfield earthquake. Dr. Steven Obermeier, one of the authors of Olson et al. (2005, in press) and an author of previous estimates of the size of the Springfield earthquake discusses this new estimate in the letter attached to this response. The estimated magnitude of **M** 6.3 is consistent with the higher weight given to lower magnitudes in the distribution developed in Appendix B to the SSAR. The right hand plot in Figure 2.5.2-4-12 compares the response spectra for an **M** 6.3 earthquake at Springfield to the 10^{-4} UHS. The scale factors to match the 10^{-4} UHS are slightly larger for this updated magnitude estimate.

Summary

In summary, recent information on prehistoric earthquakes in the region was incorporated into the updated PSHA model for the EGC ESP site. This updated model appropriately represents the location, size, and frequency of large earthquakes inferred from these data. The definition of controlling earthquakes followed directly the procedure specified in Appendix C of Regulatory Guide 1.165. It is demonstrated that this procedure is not expected to identify the Springfield earthquake as a controlling earthquake and that the SSE response spectrum envelopes response spectra for the controlling earthquakes, and envelopes estimated response spectra for the Springfield earthquake. Therefore, EGC concludes that the SSE *does* represent a ground motion of adequate severity to represent the seismic hazard for the EGC ESP site.

References

EPRI. "CEUS Ground Motion Project Final Report." Technical Report 1009684. *Electric Power Research Institute*. Palo Alto, California. 2004.

EPRI-SOG. "*Seismic Hazard Methodology for the Central and Eastern United States.*" Technical Report NP-4726-A. Electric Power Research Institute. Palo Alto, California. Vols. 1-10. 1988.

McGuire, R.K., W.J. Silva, and C.J. Costantino. "Technical Basis for Revision of Regulatory Guidance on Design Ground Motions: Hazard- and Risk-Consistent Ground Motion Spectra Guidelines." U.S. Nuclear Regulatory Commission Technical Report NUREG/CR-6728. 2001.

Olson, S.M., R.A. Green, and S.F. Obermeier. "Revised Magnitude Bound Relation for the Wasatch Valley Seismic Zone of the Central United States." *Seismological Research Letters*. 2005 in press.

Wheeler, R.L., and C.H. Cramer. "Updated Seismic Hazard in the Southern Illinois Basin—Geological and Geophysical Foundations for Use in the 2002 USGS National Seismic-Hazard Maps." *Seismological Research Letters*. Vol. 73, No. 5. pp. 776-791. 2002.

ASSOCIATED EGC ESP APPLICATION REVISIONS:

None

ATTACHMENTS:

Table 2.5.2-4-1

Figures 2.5.2-4-1 through 2.5.2-4-12

1) Memo from S. Obermeier re: recent papers about paleoseismicity in Illinois

Table 2.5.2-4-1

ROCK HAZARD CONTROLLING AND DE-AGGREGATION EARTHQUAKES

(From SSAR Appendix B, Table 4.1-3

Hazard	Controlling Earthquake		De-aggregation Earthquakes		
	Magnitude (m_b)	Distance (km)	Magnitude (m_b)	Distance (km)	Weight
Mean 10^{-4} 5 and 10 Hz	6.5	83	5.7	15	0.377
			6.7	153	0.322
			7.2	375	0.301
Mean 10^{-4} 1 and 2.5Hz	7.0 7.2*	223 320*	5.9	15	0.093
			6.8	166	0.240
			7.3	379	0.667
Mean 10^{-5} 5 and 10 Hz	6.2	24	5.8	11	0.733
			6.8	140	0.149
			7.4	380	0.118
Mean 10^{-5} 1 and 2.5Hz	7.0 7.3*	134 320*	6.0	12	0.212
			6.9	155	0.220
			7.4	381	0.568

*computed using earthquakes with distances > 100 km

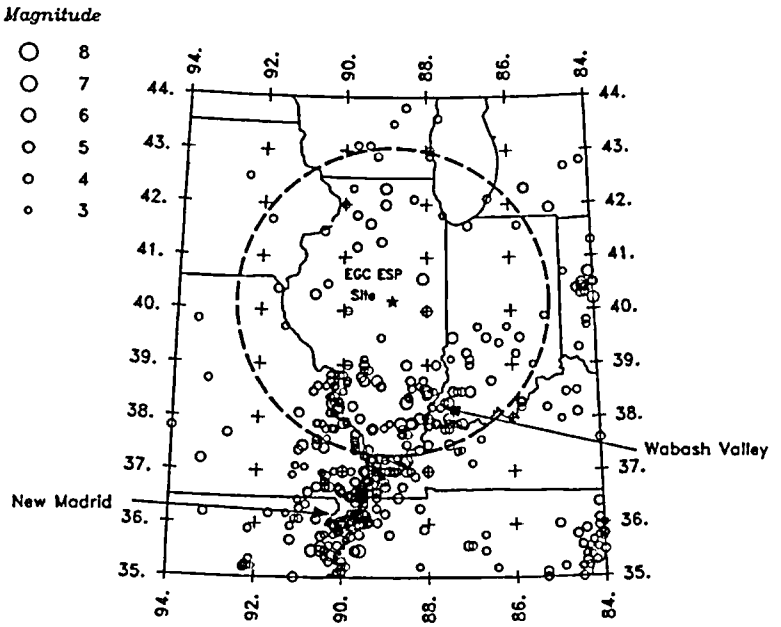

SSAR Appendix B, Figure 2.1-1

Figure 2.5.2-4-1: Seismicity in the region surrounding the EGC ESP site.

(a)

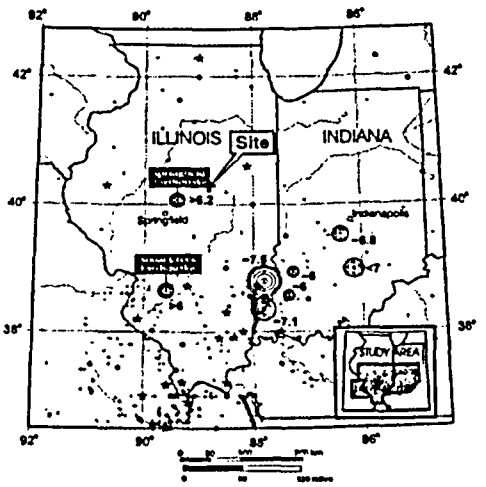

SSAR Appendix B, Figure 2.1-14

(b)

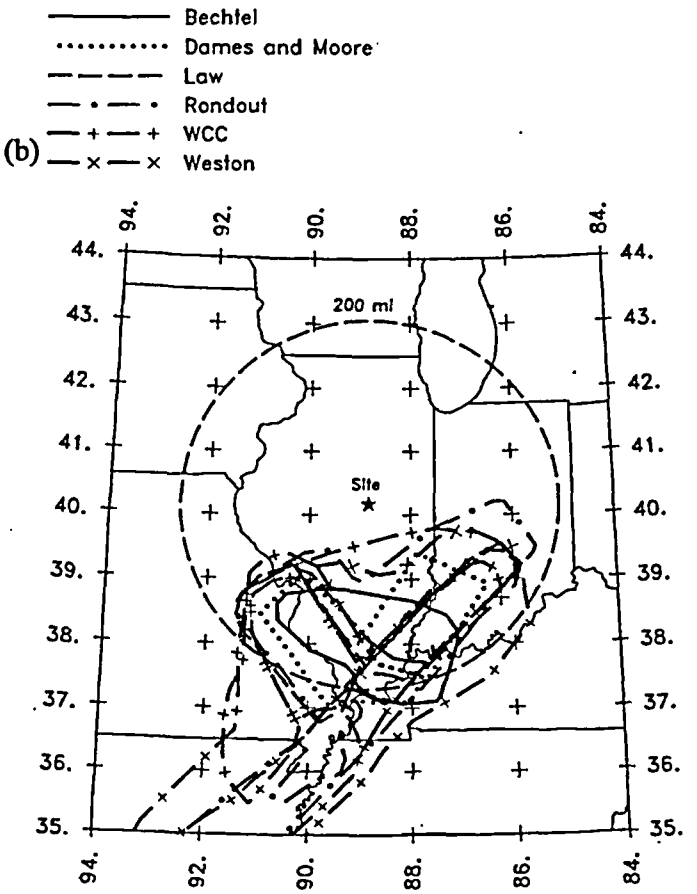

SSAR Appendix B, Figure 3.1-1

Figure 2.5.2-4-2: (a) Location of prehistoric earthquakes in Illinois and Indiana inferred from paleoliquefaction studies. (b) EPRI-SOG (1988) seismic sources for the New Madrid and southern Illinois/southern Indiana regions.

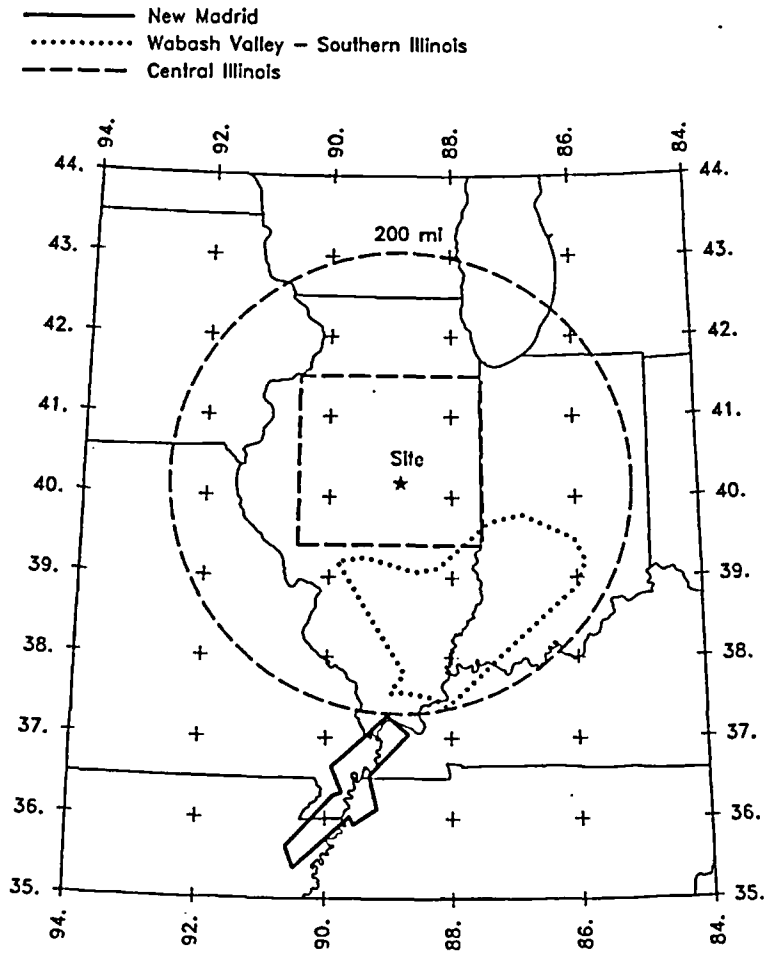

SSAR Appendix B, Figure 3.1-4

Figure 2.5.2-4-3: Representative seismic sources used to assess earthquake frequencies and example hazard de-aggregation.

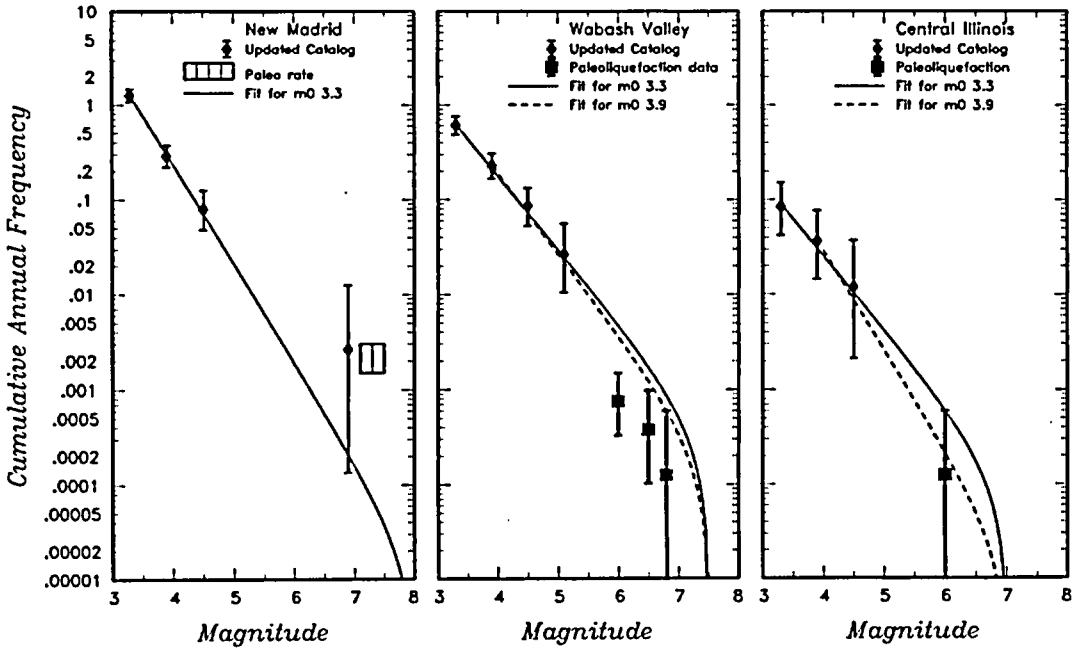

SSAR Appendix B, Figure 3.2-6

Figure 2.5.2-4-4: Earthquake frequencies computed from historical seismicity and from paleo-earthquake data for the three representative seismic sources shown in Figure 2.5.2-4-3.

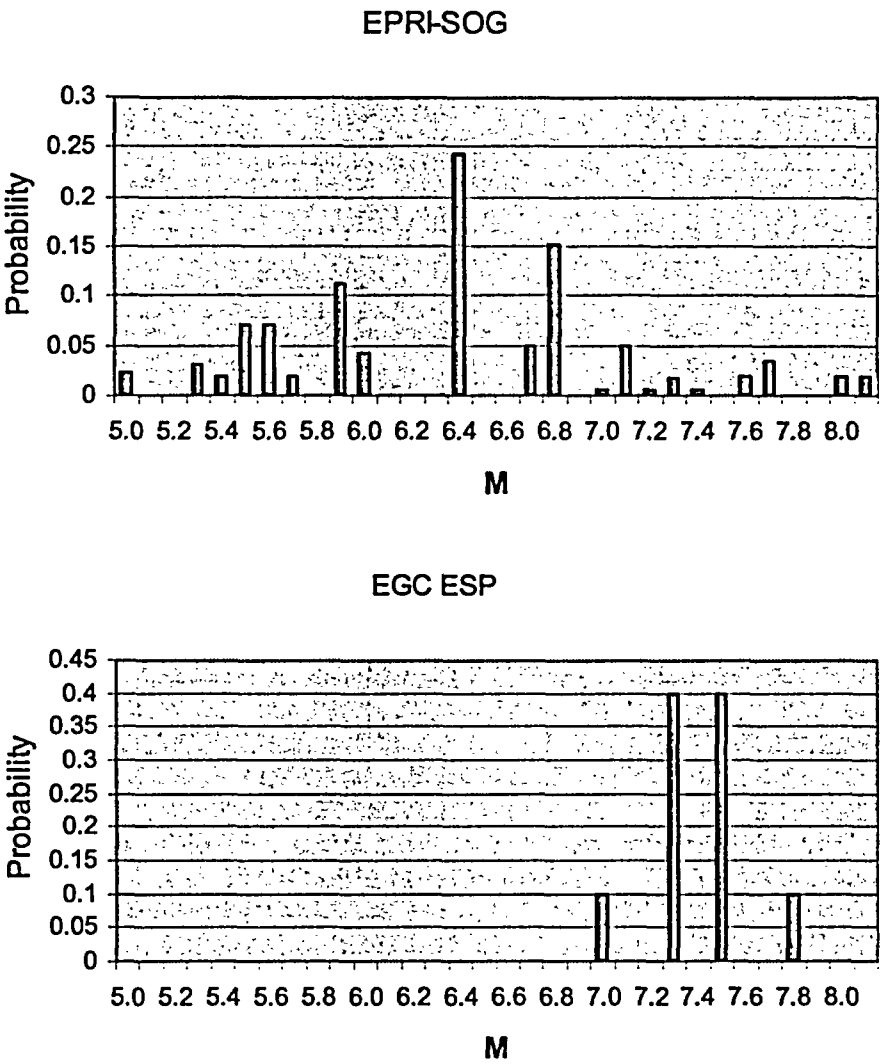

Modified from SSAR Appendix B, Figure 3.1-8

Figure 2.5.2-4-5: Maximum magnitude distributions for southern Illinois/southern Indiana sources. (Top) EPRI-SOG (1988) magnitude distributions converted from m_b to M. (Bottom) Updated distribution used in PSHA for EGC ESP site.

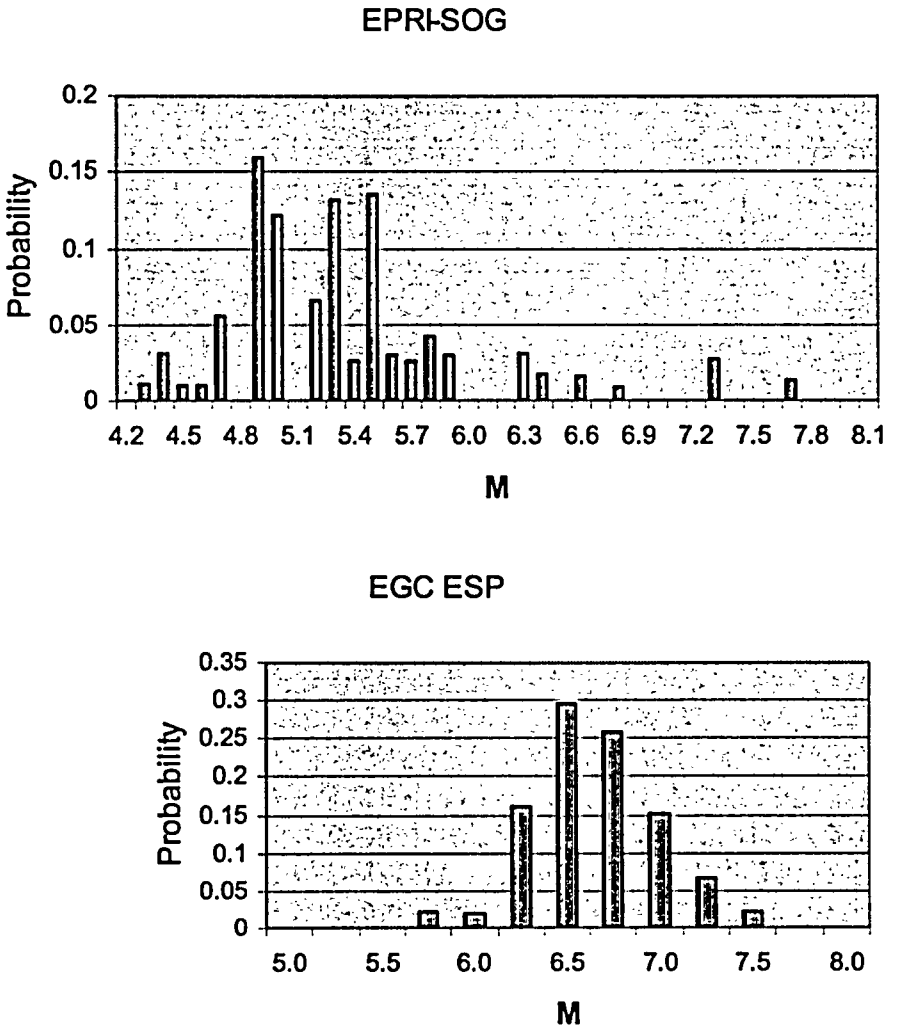

Modified from SSAR Appendix B, Figures 3.1-9 and 4.1-5

Figure 2.5.2-4-6: Maximum magnitude distributions for central Illinois sources. (Top) EPRI-SOG (1988) magnitude distributions converted from m_b to M. (Bottom) Updated distribution used in PSHA for EGC ESP site.

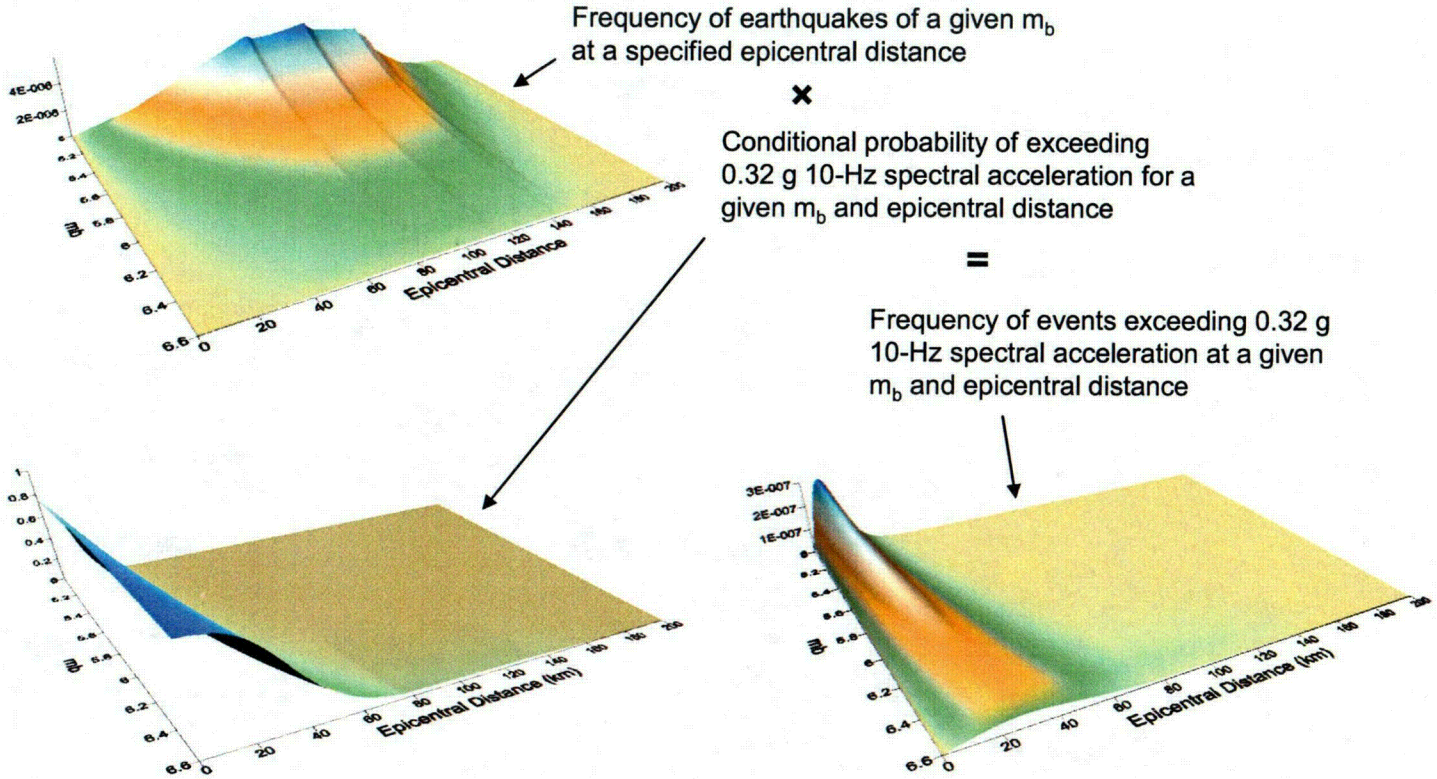

Figure 2.5.2-4-7: Example de-aggregation of the hazard from the central Illinois seismic source shown on Figure 2.5.2-4-3.

C14

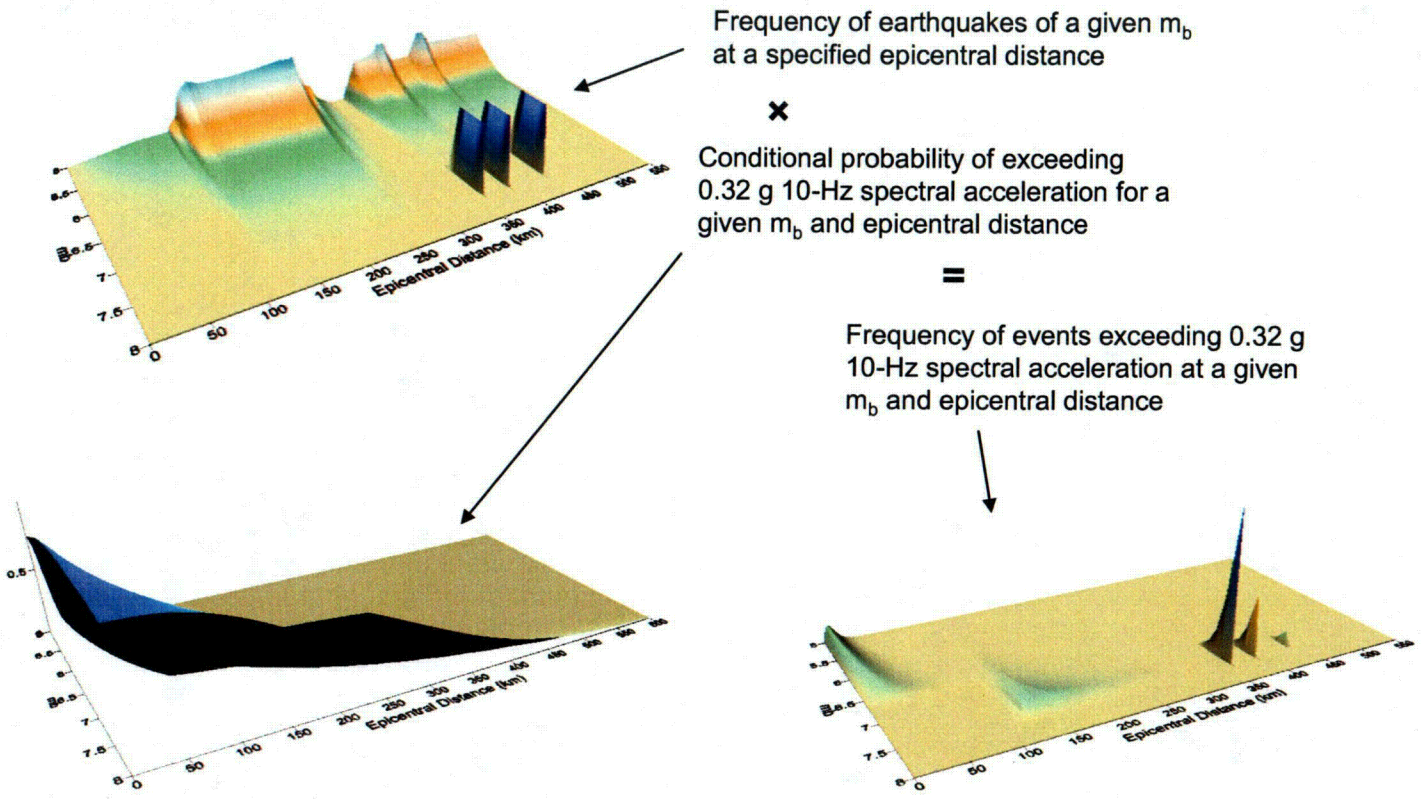

Figure 2.5.2-4-8: Example de-aggregation of the composite hazard from the three example seismic sources shown on Figure 2.5.2-4-3.

Percent Contribution to 10^{-4} Mean Hazard
(Average for 5 and 10 Hz Spectral Acceleration

Distance Interval (km)	Magnitude Interval, m_b					
	5-5.5	5.5-6	6-6.5	6.5-7	7-7.5	>7.5
0-15	9.4	4.8	2.0	0.3	0.0	0.0
15-25	3.7	3.5	2.3	0.5	0.0	0.0
25-50	2.2	3.6	4.1	1.3	0.0	0.0
50-100	0.4	1.2	2.6	2.2	0.3	0.0
100-200	0.2	0.9	3.7	10.1	3.6	0.0
200-300	0.0	0.1	0.9	4.6	2.4	0.0
300-400	0.0	0.0	0.1	2.9	16.8	1.1
400-500	0.0	0.0	0.0	0.5	6.1	1.0
>500	0.0	0.0	0.0	0.0	0.1	0.0

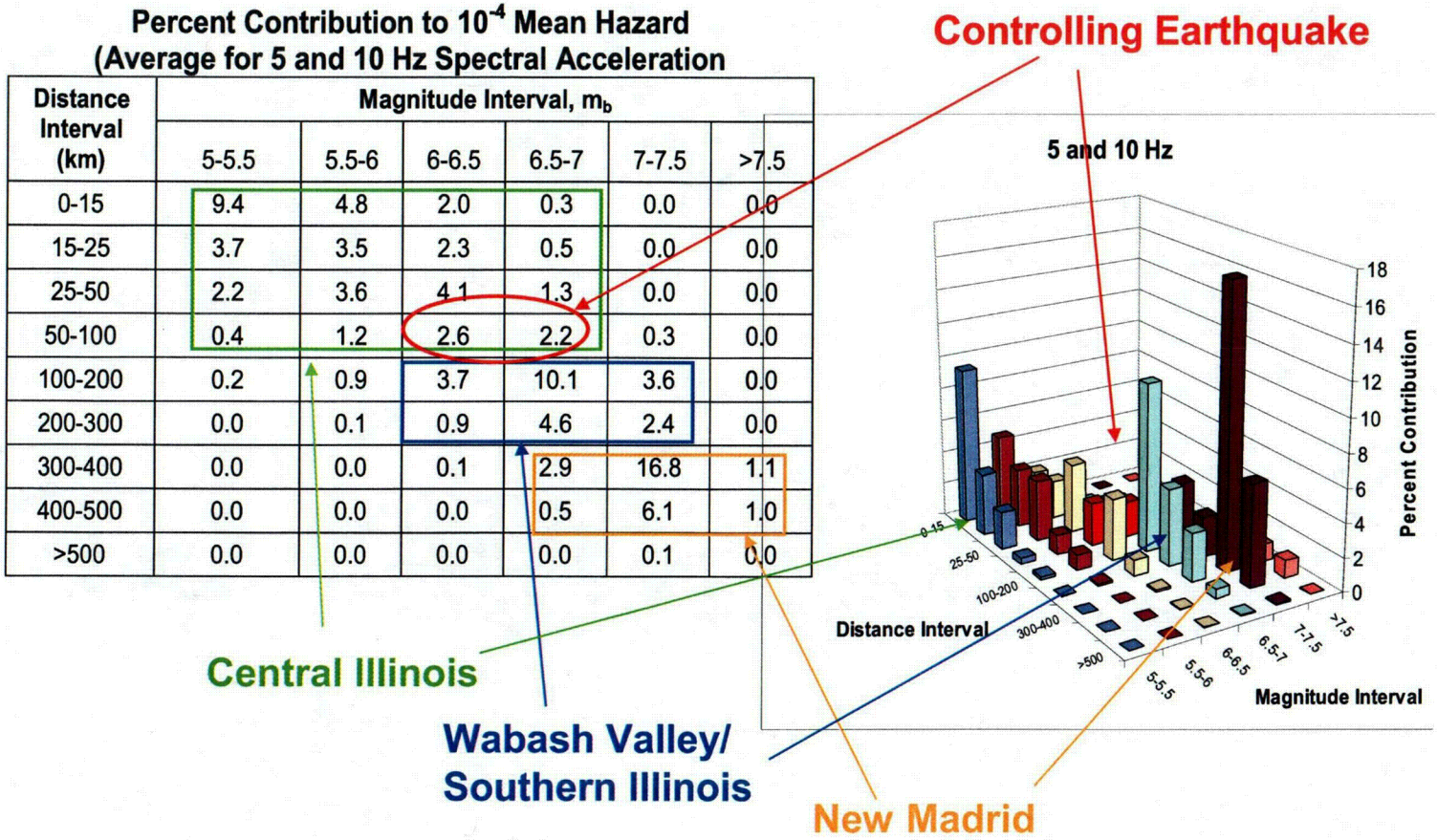

Modified from SSAR Appendix B, Figure 4.1-20

Figure 2.5.2-4-9: Computation of controlling earthquake for the 10^{-4} mean hazard (average of 5 and 10 Hz).

C16

Percent Contribution to 10^{-5} Mean Hazard
(Average for 5 and 10 Hz Spectral Acceleration

Distance Interval (km)	Magnitude Interval, m_b				
	5-5.5	5.5-6	6-6.5	6.5-7	7-7.5
0-15	20.0	16.2	10.6	2.3	0.0
15-25	2.2	4.6	6.3	2.2	0.0
25-50	0.6	1.9	4.7	3.1	0.1
50-100	0.0	0.2	1.0	1.7	0.5
100-200	0.0	0.1	0.8	4.4	2.9
200-300	0.0	0.0	0.1	1.3	1.1
300-400	0.0	0.0	0.0	0.6	5.5
400-500	0.0	0.0	0.0	0.1	2.0
>500	0.0	0.0	0.0	0.0	0.0

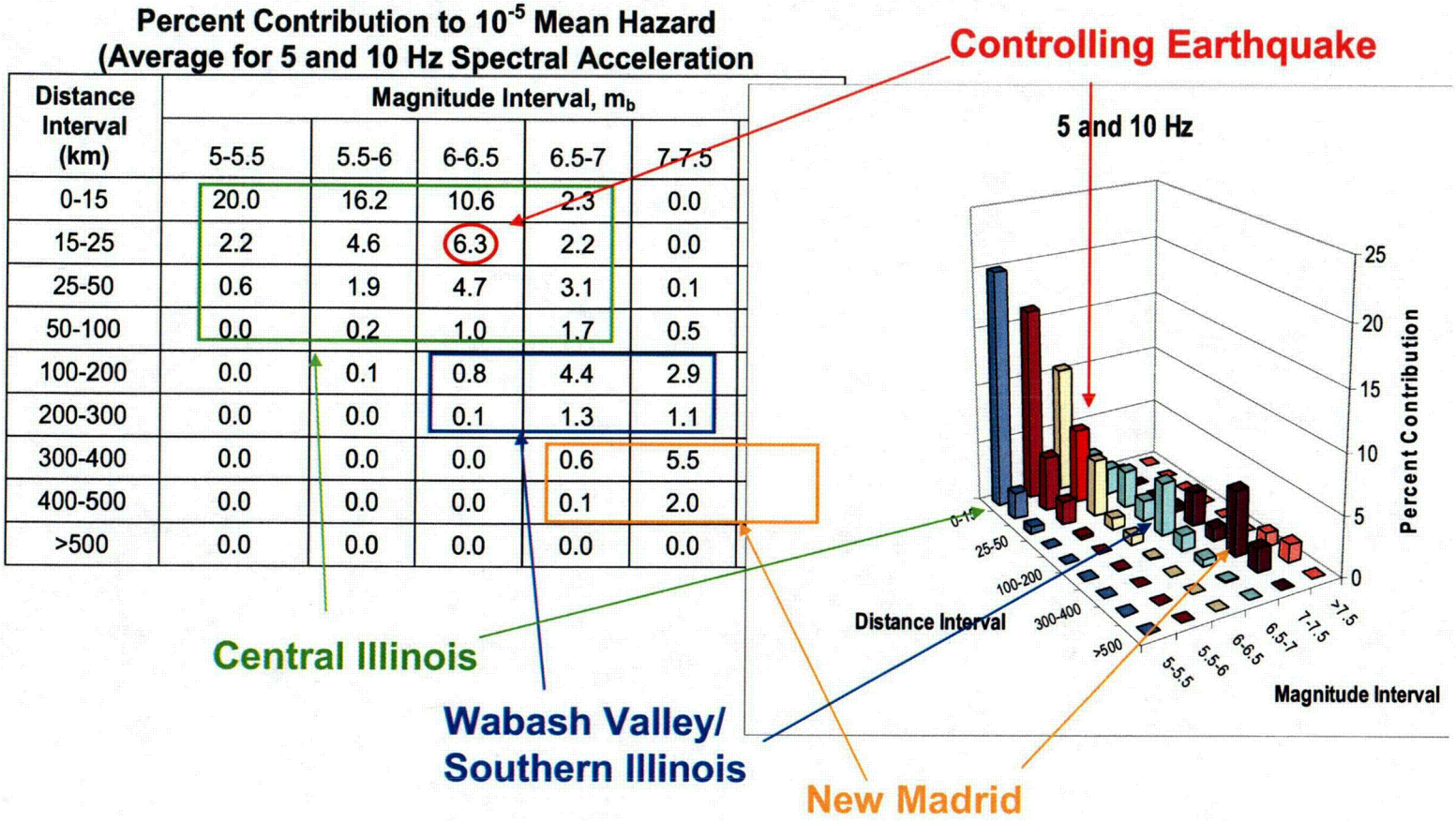

Modified from SSAR Appendix B, Figure 4.1-21

Figure 2.5.2-4-10: Computation of controlling earthquake for the 10^{-5} mean hazard (average of 5 and 10 Hz).

C17

(a)

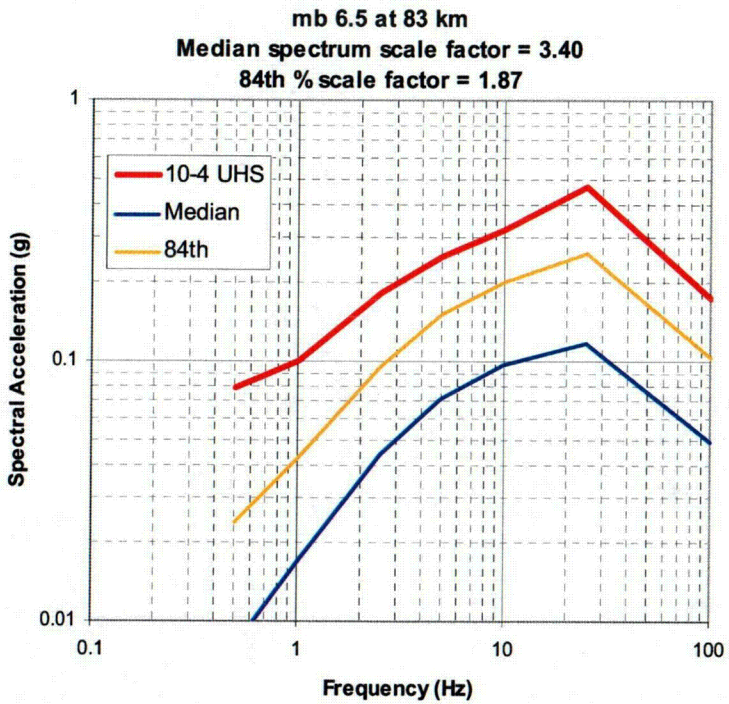

(b)

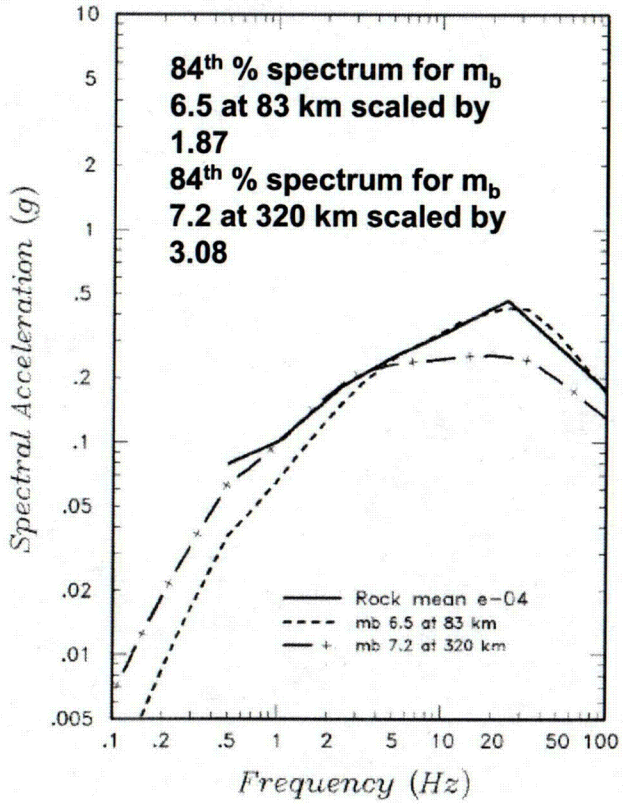

Modified from SSAR Appendix B, Figure 4.2-19

Figure 2.5.2-4-11: Scaling of response spectral shapes for controlling earthquakes to match Uniform Hazard Spectrum.

C18

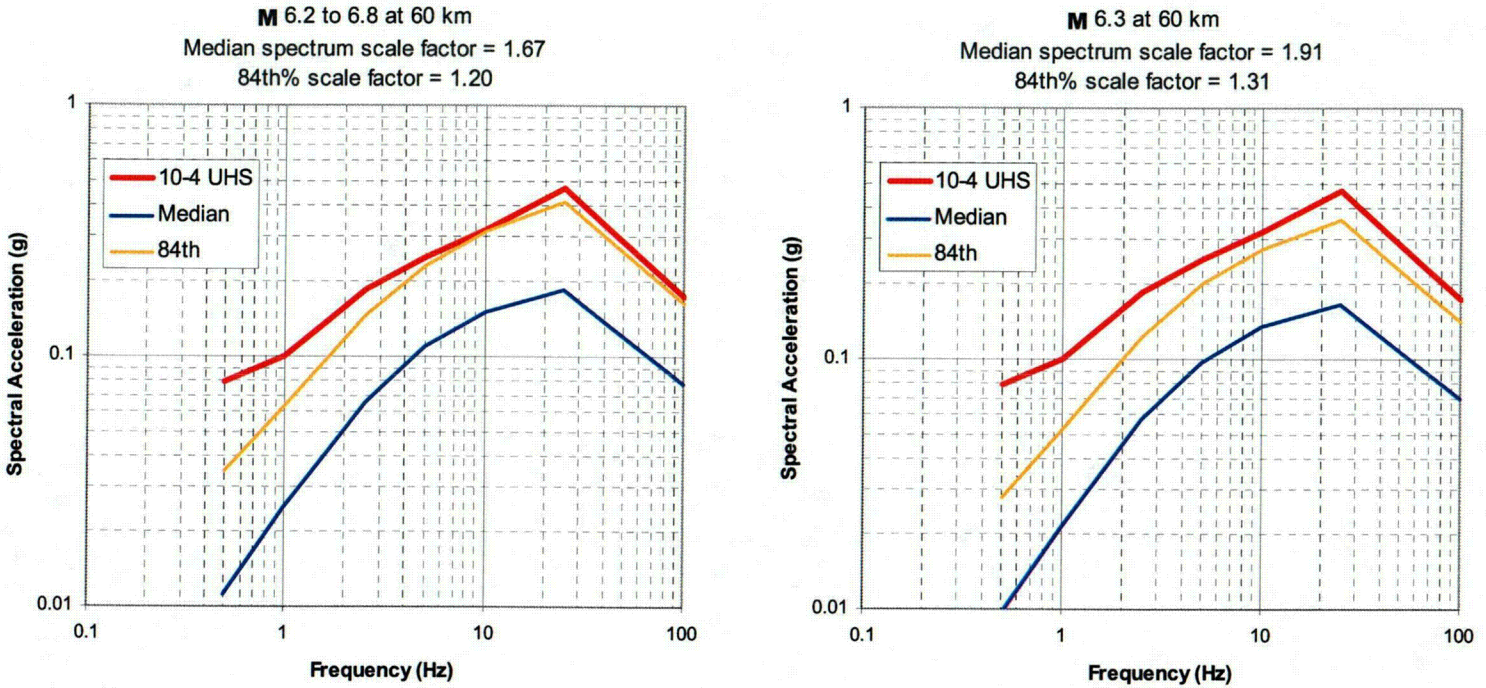

Figure 2.5.2-4-12: Comparison of 10^{-4} UHS with estimated ground motion response spectra for the Springfield earthquake.

Attachment to Response to DSER Open Item 2.5.2-4

Oct 20-05

To: Bob Youngs and Kathryn Hanson
Geomatrix Consultants
Oakland, CA

From: Stephen Obermeier
Rockport, IN

Subject: Update and critique of recent papers about paleoseismicity in Illinios

Below I discuss the following issues: (1) interpretations in two papers of prehistoric values of M in Illinois using the magnitude-bound method, where with one paper was written by Street, Bauer, and Woolery (2004, Short note: Magnitude scaling of prehistorical earthquakes in the Wabash Valley seismic zone of the central United States, Seism. Research Letters, p. 637-641), and the other was written by Olson, Green, and Obermeier (in press, Revised magnitude bound relation for the Wabash Valley seismic zone of the central United States, Seism. Research Letters; (2) the relevance of interpretations using the magnitude-bound method to interpretations of M using other techniques; and (3) the recent paper by Hough, Bilham, Mueller, Stephenson, Williams, and Odum (2005, Wagon loads of sand blows in White County, Illinois, Seism. Research Letters, p. 373-386), where they strongly suggest that the epicenter for one of the large 1811-12 earthquakes was centered in southeastern Illinois, which is about 200 km from the closest epicenter that is commonly accepted, in Missouri.

I discuss those issues below in the same numbered order.

1.The paper by Street at al. (2004) developed a new magnitude-bound curves for use in Illinois, one being their "lower-bound" curve (which would yield the lowest plausible value of M for a paleoearthquake), and the other was designated as their "preferred-bound (which I presume to be their best-estimate, although that is not so-stated in their paper). Street at al. gave no reason for their preferred bound solution. It is to be noted that their preferred solution is the same as the lower-bound solution using world-wise data, by Ambraseys (1988, Engineering seismology: Earthquake engineering and structural dynamics, Journal of the international Association of Earthquake engineering, vol. 17, p. 1-105), and the reason why that solution applies to the area of Illinois is not explained by Street et al.

The lower-bound solution by Street at al (2004) was based largely on more recent interpretations of the values of M for historic earthquakes in the New Madrid seismic zone and in Illinois, plus interpretations of Street et al. regarding occurrences of liquefaction in Illinois, as well as liquefaction-related data in papers written by others.

A followup to the paper by Street at al. (2004) was written by Olson et al. (in press), in which they also used more recent interpretations of M for historic earthquakes in the central US for developing their magnitude-bound solution. The paper by Olson et al., in addition, discussed in detail some major points of contention (listed below) with the paper by Street et al.

Major points of contention with the Street et al. paper, for their lower-bound solution, are the following:

a. They use a value of M 3.7 as the threshold for forming liquefaction features in Illinois. However, the smallest historic earthquake that has ever been observed to produce liquefaction, worldwide, is M 4.7 or 4.8. The smallest earthquake that has been observed to produce liquefaction throughout the central US is M 5.5, and there are extensive regions of susceptible sediments where many of the historic earthquakes have struck. Thus the use of a value of M 3.7 is unfounded.

b. They mis-state that Obermeier et al (1993, USGS Prof. Paper 1636) reported that the liquefaction susceptibility in Illinois is "high," at least regarding paleoliquefaction data for a magnitude-bound curve. However, no such statement was ever made in any Obermeier-related publications. (See for example hundreds of detailed boring logs in Obermeier (1989, USGS Prof. Paper 1336-B) as well as comments in Obermeier and Pond (1999, Seism. Research Letters, v. 70, p. 34-58).

c. Even more in error, Street et al. use a liquefaction susceptibility for their curve that is "very high." That susceptibility is clearly not supported by real data, as illustrated in the Obermeier reports.

d. Street et al. use data from historic earthquakes in eastern Canada for developing a curve for Illinois. However, the sites they cite in eastern Canada as showing effects of liquefaction probably were located above Leda Clay - which is a sediment having very high water content, and therefore there is a high likelihood that those sites experienced very high ground motion amplification (much like Mexico City). No such high-water content sediments occur in the area of Illinois-Indiana.

e. Street et al. accept the epicenter of the 31 October 1895 earthquake as being some 100 km north of Cairo, Illinois, as suggested by Bakun et al. (2003, BSSA, v. 93, p. 190-202). However, that scenario is shown by Olson et al. (in press) to be highly implausible, for multiple reasons discussed by Olson et al.

It should be noted that each of the items a-e listed above cause the magnitude-bound curve of Street et al to yield lower values for prehistoric earthquakes, when using paleoliquefaction effects for estimating magnitude. Again, all these items a-e (plus more) are discussed in detail in Olson et al (in press).

Finally, I point out again that the preferred solution by Street et al. is based on world-wide data, without any explanation. The solution in Olson et al. is based on data that are unique to the study region if Illinois-Indiana.

2. For what I have designated as the Springfield Earthquake of central Illinois (Obermeier, 1998, Engineering Geology, v. 50, p. 227-254; McNulty and Obermeier, 1999, Environ. & Engineering Geoscience, v. V, no. 2, p. 133-146), the value of M using the revised curve by Olson et al. (in press) is 6.3. The preferred solution of Street et al. (2004) is essentially the same as that of Olson et al., being 6.3-6.4. Previously the value of M using the magnitude-bound curve of Obermeier et al (1993, USGS Prof. Paper 1536) and of Pond (1996, Ph. D. thesis, Virginia Tech., Civil Engineering Dept. Blacksburg) ranged from 6.2 to 6.8.

On a related matter, the value of M using the revised value of Olson et al. (in press) for the paleoearthquake centered near Vincennes, Indiana, (the "Vincennes Earthquake"

that struck at about 6100 yr BP) is 7.1 – 7.3. Using the analytical method for analyzing the regional pattern of strength of shaking at the paleoliquefaction sites, presented in Green et al. (2005, Engineering Geology, v. 76, p. 263-293), the value is 7.5. (The ground motion amplifications in the Green et al. paper were calculated using the procedure recommended by the USGS.) The point of relevance is that the value of M using the analytical solution is a little higher (a few tenths) than the value of M using the revised curve of Olson et al. for the magnitude-bound method. As a result, I suspect that using the analytical method for the Springfield Earthquake might well yield a value of M a few tenths higher than the magnitude-bound method.

3. The paper by Hough et al. (2005) strongly contends that the epicenter of a large earthquake of the 1811-12 series (the 23 Jan 1812 event) may have been centered in southeastern Illinois, near the Indiana border. Their basis for that interpretation is mainly from features they interpret to be seismically induced sand blows, as well as a feature interpreted to be a fault scarp. Both the sand blows and a faulting event were first reported in a paper written some 100 years after the 1811-12 series of earthquakes (Berry, 1908, The Illinois earthquake of 1811 and 1812, Illinois State Historical Society Transactions, v. 68, p. 74-78). The basis for Berry's paper was oral accounts passed on through time.

Hough et al. conducted field work at the site described by Berry, and concluded that there are numerous sand blows there. However, about 15 years ago, when I first began paleoliquefaction searches in southern Illinois and Indiana, I also visited exactly the same site and looked for the features described by Berry. I observed then that there are many sand dunes in that region (with many being active) that are indistinguishable from seismic sand blows, unless one finds a feeder dike for the suspected feature. I never conducted an effort to look for feeder dikes (because that would have required a back-hoe), nor did Hough et al. Thus, attributing a seismic origin to those sand bodies is unconfirmed in my opinion.

Field searches for paleoliquefaction features have been conducted by several highly competent parties in the general vicinity of the site investigated by Hough et al. Results of these searches are shown and discussed in Munson et al. (1997, Liquefaction evidence for Holocene and latest Pleistocene in the southern halves of Indiana and Illinois, Seism. Research Letters, v. 68, p. 521-536). Shortly after the paper by Munson et al. was published, I wrote an overview paper presenting my interpretations of the ages of the features that were discovered in the area, with my reasons for interpretations. This was published as Obermeier, 1998 (Engineering Geology, v. 50, p. 227-254). All field searches reported in Munson et al. and in Obermeier were conducted by examining banks of major rivers in the region, such as Wabash and Little Wabash Rivers, plus more streams. (I also conducted airphoto searches in that region, looking for seismic sand blows, but the presence of numerous sand dunes in the area made the airphoto study of little use.) Some few, small liquefaction features of very young age were found at scattered locales, all in river banks, and some or all these features may well have been caused by the 1811-12 earthquakes. No large- or moderate-sized young features were discovered. However, quite a few liquefaction features were discovered at widespread sites, all probably being mid-Holocene or older in age. Partly on this basis of the discovery of the older features, and also because of the fact that the field setting of liquefiable sediments is one of great regional extent where the water table should have remained relatively shallow at many places, even during dry periods, I believe that it is very highly probable that field conditions throughout the region of southeastern Illinois

have been good for forming liquefaction features at many places, through most of Holocene time as well as in 1811-12.

Hough et al. also conducted seismic profiling along the supposed fault reported in the Berry (1908) paper. Hough et al. reported that their finding was inconsistent with descriptions by Berry, but Hough et al. did find some possible offsets in young sediments.

In summary, I believe that it is entirely plausible that seismic liquefaction features did form in 1811-12 in the area investigated by Hough et al., but that is unconfirmed. And, I believe that the paleoliquefaction studies reported by others than Hough et al. (i.e., Munson et al., and Obermeier) show that the regional extent of any strong shaking in southeastern Illinois must have been quite localized in 1811-12, and that an earthquake of large M was not centered there at that time.

NRC Letter Dated: 08/26/2005

NRC DSER Open Item 2.5.2-5

Section 2.5.2.3.6 - The staff asked the applicant to provide the following information with regard to the above concerns and comments resulting from the staff's review of RAI 2.5.2-7:

- Justify the assumption of a linear hazard curve in logarithmic space and the appropriateness of solely using the 10^{-4} to 10^{-5} interval to determine the amplitude ratio *AR*.
- Justify why a β value of 0.4 was used and show how the DF varies with different β values over the range of amplitude ratios.
- Clarify the meaning of "onset of significant inelastic deformation" (OSID), specifically the words "onset" and "significant," OSID with regard to the failure of SSCs and core damage, and the relationship of OSID to "essentially elastic" behavior.
- Justify the long-term stability of the target performance goal 10^{-5} in comparison to the hazard-based approach (reference probability) in RG 1.165, as both values require the use of PSHAs for several CEUS nuclear sites.
- Since the target performance goal 10^{-5} is based on seismic PRAs for current LWRs, justify the use of this value for advanced reactor designs, which may differ considerably from current LWRs.
- Since SSCs for nuclear power plants are designed using the seismic criteria in the SRP, clarify how the design criteria in ASCE/SEI Standard 43-05 are similar enough that SSCs designed following the SRP would also achieve a 1 percent or lower probability of unacceptable performance.

Without further elaboration by the applicant concerning the above issues, the staff is unable to determine the acceptability of the assumptions and equations underlying the performance-based approach. This is Open Item 2.5.2-5.

EGC RAI ID: SOI2-6

EGC RESPONSE:

Introduction

The EGC ESP application for the Clinton site established the Safe Shutdown Earthquake (SSE) Design Response Spectrum (DRS) following the Risk (Performance-Goal) Based Approach defined in ASCE Standard 43-05 (Ref. 1) for the most stringent Seismic Design Category SDC-5D. For SDC-5D, the quantitative target acceptable annual probability of unacceptable performance P_{FT} is[1]:

$$P_{FT} = \text{mean } 1\text{x}10^{-5}/\text{yr} \qquad (1.1)$$

[1] The term "mean" in front of the probability here and elsewhere indicates that the *mean* estimate of this probability should be used.

The qualitative description of acceptable performance for SDC-5D is to not exceed Limit State D which is defined in the ASCE Standard as "Essentially Elastic Behavior." Thus, the definition of unacceptable performance for SDC-5D is the "onset of significant inelastic deformation" and P_{FT} represents the target frequency for onset of significant inelastic deformation (FOSID).

In order to achieve the above defined target performance goal for SDC-5D, the ASCE Standard defines DRS by:

$$DRS = DF * UHRS \quad (1.2)$$

where the reference UHRS is defined at a reference seismic hazard exceedance frequency H of:

$$H = \text{mean } 1x10^{-4}/yr \quad (1.3)$$

and the required Design Factor DF is computed as follows. First, at each spectral frequency at which the UHRS is defined, an Amplitude Ratio A_R is computed from:

$$A_R = (SA_{0.1H})/(SA_H) \quad (1.4)$$

where SA_H is the spectral acceleration at the mean exceedance frequency H and $SA_{0.1H}$ is the spectral acceleration at 0.1H (i.e., the spectral accelerations at $1x10^{-4}$/yr and $1x10^{-5}$/yr). Then the Design Factor, DF, at each spectral frequency is given by

$$DF = \text{Maximum } (DF_1, DF_2) \quad (1.5)$$

where

$$DF_1 = 1.0 \quad (1.6)$$

and

$$DF_2 = 0.6(A_R)^{0.80} \quad (1.7)$$

Furthermore, for SDC-5D, the ASCE Standard specifies a lower bound on the DRS peak ground acceleration (PGA) of 0.10g. For nuclear power plant applications, the lower bound on the DRS should be a Regulatory Guide 1.60 response spectrum anchored to a PGA of 0.10g.

After this brief introduction, the following discussions respond to each of the six bulleted items in Open Item 2.5.2-5 concerning the above described Performance Based Approach for defining the SSE Design Response Spectrum (DRS). These responses draw heavily from Refs. 2 and 3 which have been previously submitted and can provide further background.

1st bullet:

• Justify the assumption of a linear hazard curve in logarithmic space and the appropriateness of solely using the 10-4 to 10-5 interval to determine the amplitude ratio *AR*.

Response to 1st bullet:

For the sensitivity studies conducted to develop Eqns. (1.5), (1.6), and (1.7) to define the Design Factor DF, seismic hazard curves were approximated by a power law:

$$H(a) = K_1 a^{-K_H} \quad (2.1)$$

where H(*a*) is the annual frequency of exceedance of ground motion level *a*, K_I is an appropriate constant, and K_H is a slope parameter defined by:

$$K_H = 1/\log(A_R) \quad (2.2)$$

in which A_R is the ratio of ground motions corresponding to a ten-fold reduction in exceedance frequency as given by Eqn. (1.4).

So long as the fragility curve $P_F(a)$ is lognormally distributed and the hazard curve is defined by Eqn. (2.1), a rigorous closed-form solution exists for the Design Factor DF required to achieve the target performance goal P_{FT}. This closed-form solution is derived in Refs. 1, 2, or 3 to be:

$$DF = \frac{\left[R_P e^{-f}\right]^{1/K_H}}{F_{1\%}} \quad (2.3)$$

$$f = 2.326K_H\beta - \tfrac{1}{2}(K_H\beta)^2 \quad (2.4)$$

where the Probability Ratio R_P is defined by:

$$R_P = H/P_{FT} = 1x10^{-4} / 1x10^{-5} = 10 \quad (2.5)$$

and the seismic fragility curve is lognormally distributed with a 1% failure probability capacity factor $F_{1\%}$ and logarithmic standard β.

Next, the Design Factor DF was computed from Eqn. (2.3) for the condition that the seismic demand and structural capacity evaluation criteria have sufficient conservatism to reasonably achieve *both* of the following:

1. Less Than About a 1% Probability of Unacceptable Performance for the Design Basis Earthquake Ground Motion, and
2. Less Than About a 10% Probability of Unacceptable Performance for a Ground Motion equal to 150% of the Design Basis Earthquake Ground Motion

Based on this condition, the values of $F_{1\%}$ and $F_{70\%}$ for β of 0.3, 0.4, 0.5, and 0.6 are:

β	0.3	0.4	0.5	0.6
$F_{1\%}$	1.10	1.0	1.0	1.0
$F_{70\%}$	2.58	3.13	4.16	5.53

The resulting Design Factors, DF, computed from Eqn. (2.3) for a range of A_R from 1.5 to 6.0 and β from 0.3 to 0.6 are shown in Table 2.5.2-5-1. Also shown in Table 2.5.2-5-1 is the DF from Eqn. (1.5) which is used to obtain the SSE DRS from Eqn. (1.2). The comparison of the DF from Eqn. (1.5) with those DF computed from Eqn. (2.3) will be discussed in the next section.

In developing Table 2.5.2-5-1, the seismic hazard curve was approximated by a power law which results in a linear hazard curve when plotted on a log-log plot. Seismic hazard curves are close to linear when plotted on a log-log plot (for example see Figure 2.5.2-5-1). However, they are not perfectly linear. They always curve downward with decreasing hazard exceedance frequency. Thus A_R reduces as the hazard exceedance frequency is reduced. In other words, an A_R computed over the range of the hazard exceedance frequency from $1x10^{-4}$/yr to $1x10^{-5}$/yr will be larger than that

computed over the $1x10^{-5}$/yr to $1x10^{-6}$/yr range. Furthermore, note in Table 2.5.2-5-1 that the required Design Factor DF increases with increasing A_R. Therefore, one must guard against selecting too low of an A_R value.

In order to rigorously determine the mean annual probability P_F of unacceptable performance, one must numerically convolve the mean seismic hazard curve and mean fragility curve by either of two analytically equivalent equations:

$$P_F = -\int_0^{+\infty} P_F(a)\left(\frac{dH(a)}{da}\right) da \qquad (2.6)$$

$$P_F = \int_0^{+\infty} H(a)\left(\frac{dP_F(a)}{da}\right) da \qquad (2.7)$$

where $P_F(a)$ is the conditional probability of failure given the ground motion level *a*, which, by definition, is the mean fragility curve, and $H(a)$ is the mean hazard exceedance frequency corresponding to ground motion level *a*. Based upon several hundred rigorous convolutions of hazard and fragility curves, it has been found that P_F is dominated by the portion of the fragility curve between about the 1% failure probability capacity $C_{1\%}$ and the 70% failure probability capacity $C_{70\%}$. The 1% failure probability capacity equals or exceeds the DRS. In turn, the DRS is given by Eqn. (1.2) with DF being always equal or greater than 1.0. Therefore, $C_{1\%}$ will always exceed the $1x10^{-4}$ UHRS.

Similarly, given the capacity conditions defined earlier for β=0.30, the $C_{70\%}$ will be at least:

$$C_{70\%} = 2.58(DF)(UHRS) \qquad (2.8)$$

where DF is given by Eqn. (1.5). For higher β, the $C_{70\%}$ will be even higher. Since the $1x10^{-5}$/yr ground motion is given by A_R (UHRS), it can be seen from Table 2.5.2-5-1 that $C_{70\%}$ will always exceed the $1x10^{-5}$/yr ground motion.

Therefore, defining A_R over the range of $1x10^{-4}$/yr to $1x10^{-5}$/yr slightly overestimates A_R for the range of ground motions that dominate P_F. Thus, establishing DF by approximating the hazard curve by a power law with A_R defined by Eqn. (1.4) introduces a slight conservative bias.

This slight conservative bias is illustrated by the following example taken from either Refs. 2 or 3. Many other cases have also been run to ensure that defining A_R by Eqn. (1.4) introduces a slight conservative bias to the computed DF and resulting P_F.

Figure 2.5.2-5-1 shows some representative normalized hazard curves taken from Figures 7.7 and 7.8 of NUREG/CR-6728 (Ref. 4). These hazard curves are all normalized to unity spectral acceleration at the reference hazard exceedance frequency H = mean $1x10^{-4}$/yr for ease of visualizing the differences in hazard curve slopes. Table 2.5.2-5-2 presents the tabulated normalized spectral acceleration values SA at 1 Hz and 10 Hz for one Eastern U.S. hazard curve and for the California hazard curve.

The approximate power-law hazard curves are defined by Equations (2.1) and (2.2) with A_R defined by Equation (1.4). These approximate hazard curves would appear as a straight line on the log-log plots of Figure 2.5.2-5-1 with the amplitude and slope defined by the spectral accelerations at $1x10^{-4}$/yr and $1x10^{-5}$/yr hazard exceedance frequencies. However, all actual seismic hazard curves have a downward curvature similar to those

shown in Figure 2.5.2-5-1 when plotted on log-log plots. The intent of this example is to study the effect of this downward curvature on the P_{FC} computed by rigorous numerical convolution versus the P_{FC} computed using the approximate power law hazard curve.

For each of the four normalized hazard curves tabulated in Table 2.5.2-5-2, Table 2.5.2-5-3 shows the Amplitude Factor A_R computed by Equation (1.4), the ASCE Standard Design Factor DF computed by Equation (1.5), and the resulting DRS spectral accelerations computed by Equation (1.2). The SSC fragility curves are defined by the conservatism factors given earlier in this section times the normalized DRS for each case considered. The actually achieved P_{FC} values computed by rigorous numerical convolution are also shown in Table 2.5.2-5-3.

Alternately, with a power law hazard curve approximated by Eqns. (2.1) and (2.2), both Refs. 2 and 3 show that the computed mean unacceptable performance annual probability P_{FC} can be directly obtained from:

$$(P_{FC}/H) = e^{-f}\left[DF * F_{1\%}\right]^{-K_H} \qquad (2.9)$$

where f is obtained from Equation (2.4). Table 2.5.2-5-4 compares the P_{FC} computed for the example hazard curves by rigorous numerical convolution versus computed using the approximate power law hazard curve with A_R defined by Eqn. (1.4). One can see that the use of the approximate power law hazard curve introduces a slight, but generally negligible, conservative bias for the computed P_{FC} so long as A_R is defined by Eqn. (1.4). Many other comparative examples using other hazard curves have shown similar results.

In summary, it has been shown that using a power law hazard curve with A_R defined by the ratio of the $1x10^{-5}$ to $1x10^{-4}$ spectral accelerations provides a very close (slightly conservative) estimate of P_{FC} as compared to rigorous numerical convolution. Therefore, the use of A_R defined by Eqn. (1.4) is justified for defining the Design Factor DF.

2nd bullet:

• Justify why a β value of 0.4 was used and show how the DF varies with different β values over the range of amplitude ratios.

Response to 2nd bullet:

The sensitivity studies performed to assess how the Design Factor DF varied as a function of A_R and fragility logarithmic standard deviation β values considered β values in the range of 0.3 to 0.6 as has been stated in Refs 1, 2, and 3. Based upon the power law approximation of the hazard curve, Table 2.5.2-5-1 (from Ref. 2 or 3) shows the computed DF versus A_R and β. The DF used in Eqn. (1.2) to define the SSE DRS is given by Eqn. (1.5). This Eqn. (1.5) was chosen to provide a generally conservatively biased DF over the range of A_R and β values considered in Table 2.5.2-5-1. The results for β of 0.4 and 0.5 were weighted more heavily than those for β of 0.3 and 0.6 because the fragility β values are most likely to lie in the 0.4 to 0.5 range and β of 0.3 and 0.6 are considered to be extreme low and high values, respectively. Even so, the entire range of β values was considered. Similarly, A_R values between 1.5 and 4.5 were considered most heavily when developing Eqn. (1.5) for DF. Hazard curves with A_R values less than 1.5 have not been seen for the $1x10^{-4}$ to $1x10^{-5}$ range. Also, over this exceedance frequency range, A_R values greater than 4.5 are very unlikely. As shown in Table AA.2

of Appendix A to Attachment 1, the EGC ESP values of A_R lie in the range of 2.0 to 2.6 so that they are well within the A_R range studied.

Again, based on the power law approximation of the seismic hazard curve, Refs. 2 and 3 have reported the achieved seismic risk P_{FC} results computed from Eqn. (2.9) when the ASCE Standard DF values defined by Eqn. (1.5) and $F_{1\%}$ defined in Section 2 are used. Table 2.5.2-5-5 (taken from Refs. 2 or 3) shows these results.

The conclusion is that with the ASCE Standard DRS defined as described above, the annual frequency of onset of significant inelastic deformation (FOSID) for an SSC that barely meets the acceptance criteria with no additional margin lies in the range of:

$$\text{FOSID} = \text{mean } 1.2\text{x}10^{-5}/\text{yr to } 0.5\text{x}10^{-5}/\text{yr} \qquad (3.1)$$

which on average is safely less than the target performance goal and never is higher than 120% of the target goal.

This conclusion has been verified in Ref. 3 by the rigorous numerical convolution of fragility and hazard curves for 28 Central and Eastern US (CEUS) nuclear power plant sites. Modern Probabilistic Seismic Hazard Assessments (PSHA) were performed for each of these sites in accordance with the EPRI ground motion model (Ref. 5). SSE DRS were computed for each site in accordance with the ASCE Performance Based criteria for Seismic Design Category SDC-5D as defined in Section 1 by Eqns. (1.2) through (1.7). The minimum individual Structure, System or Component (SSC) fragility curves were defined using the minimum "onset of significant inelastic deformation" seismic margin factors defined in Section 2 and logarithmic standard deviations β of 0.3, 0.4, 0.5, and 0.6. The annual frequency P_{FC} of "onset of significant inelastic deformation" (FOSID) was computed by numerical convolution of the PSHA hazard curves and minimum fragility curves for spectral accelerations at 5 and 10 Hz. The average of the 5 and 10 Hz results for P_{FC} (FOSID) are reported in Ref. 3. Figure 2.5.2-5-2, taken from Ref. 3, shows these results. Also shown in Figure 2.5.2-5-2 for comparison are the Seismic Core Damage Frequencies (SCCDF) reported in NUREG-1742 (Ref. 6) for 25 existing nuclear power plants which performed Seismic Probabilistic Risk Assessments (SPRA).

The results shown in Figure 2.5.2-5-2 are summarized as follows:

	ASCE Method FOSID *1x10^{-5}/yr				Existing Plant SCDF *1x10^{-5}/yr
β	0.3	0.4	0.5	0.6	
Range	0.71-1.17	0.66-0.99	0.51-0.75	0.41-0.58	0.019-23.0
Median	1.07	0.93	0.69	0.54	1.20

The FOSID values computed by rigorous numerical convolution for the 28 sites lie within the FOSID range defined in Eqn. (3.1). The highest source of variability is due to the logarithmic standard deviation β of the fragility with results for β=0.3 and 0.4 being close to the target P_{FT}=mean 1x10^{-5}/yr for FOSID and the β=0.6 results being between about 40 to 60% of the target. Thus, overall, a conservative bias is introduced. The EGC ESP

specific FOSID values are shown in Table AA.4 of Appendix A of Attachment 1 and are either close to or less than the median values shown in the above table.

For a given β, very little scatter exists in the computed FOSID. For 26 of the 28 sites, the computed FOSID for a given β are within 10% of the median value. For the other two sites, the computed FOSID are more than 10% less than the median value for a given β. Thus, the ASCE Method DRS achieves its goal of a nearly constant FOSID for an SSC at all sites.

Lastly, note that the FOSID for all 28 sites (and all β values) is less than the median SCDF reported for the 25 existing nuclear power plants. Furthermore, the "onset of significant inelastic behavior" of an SSC is generally far short of failure. In addition, the SCDF is typically less than the highest SSC failure frequency because of redundancy. Thus, the SCDF of a plant designed using a DRS obtained as defined above is expected to be significantly less than mean $1x10^{-5}$/yr. This topic will be amplified upon in the following sections.

3rd & 5th bullets:

• Clarify the meaning of "onset of significant inelastic deformation" (OSID), specifically the words "onset" and "significant," OSID with regard to the failure of SSCs and core damage, and the relationship of OSID to "essentially elastic" behavior.

• Since the target performance goal 10-5 is based on seismic PRAs for current LWRs, justify the use of this value for advanced reactor designs, which may differ considerably from current LWRs.

Combined Response to 3rd & 5th bullets:

In ASCE Standard 43-05 (Ref. 1), the qualitative performance goal for Seismic Design Category SDC-5D is for all SSCs in this category to remain within "Essentially Elastic Behavior." This goal is achieved by specifying linear elastic Demand analyses using sufficiently conservative parameter variation or parameter selection to envelope reasonable uncertainties. The computed Demand is then compared to conservative Code specified allowable Capacities. Generally, these Code specified allowable Capacities are defined sufficiently conservatively that there is less than a 2% probability of large inelastic SSC deformation if the actual Demand reaches the Code Capacity (see Commentary of Ref. 1 or Attachment I of Ref. 2 for further discussion). Lastly, the linear elastic computed Demand must be less than the Code Capacity. In particular, no "inelastic factor" (such as the factor F_μ permitted by ASCE 43-05 for Limit States A, B, and C) by which the linear computed seismic Demand can exceed the Code Capacity can be used for Limit State D, the limit state used for the EGC ESP.

The acceptance criteria for Limit State D in ASCE Standard 43-05 is very similar to the seismic capacity, seismic demand, and seismic design criteria laid out by the U.S. NRC for nuclear power plants in NUREG-0800 (Ref. 7) and Regulatory Guides, and professional design codes and standards referenced therein. This similarity topic will be further discussed in a subsequent section. Both ASCE Standard 43-05 and NRC seismic design criteria conservatively provide adequate seismic margin against the "onset of significant inelastic deformation." What this means is that localized inelasticity might occur at stress concentrations. However, the overall seismic response (deformations) will be essentially the same as those computed by the linear elastic seismic demand analysis. The "onset of significant inelastic deformation" and

"essentially elastic behavior" are qualitative descriptions of the seismic behavior of an SSC. No more precise definition of these terms is possible.

However, the "onset of significant inelastic deformation" of an SSC does not correspond to Seismic-Induced Core Damage particularly for an advanced reactor design with redundant safety features.

For the new Standard Plant designs, the U.S. NRC staff has required (SECY-98-0087) that a study be performed to show that the Seismic Core Damage HCLPF[2] margin factor is at least 1.67 times the DRS. The HCLPF point on the fragility curve computed in accordance with Ref. 8 corresponds to the mean 1% conditional probability of failure point on the Seismic Core Damage fragility curve. Thus, for Seismic Core Damage:

$$F_{1\%} = 1.67 \qquad (4.1)$$

For the above reason, NUREG/CR-6728 (Ref. 4) used the value of $F_{1\%}$=1.67, which is more liberal than the values of 1.0 and 1.1 implied by ASCE 43-05 criteria (see table in response to bullet 1).

With the DRS defined by the ASCE Standard for SDC-5D SSCs, it was shown above that the FOSID will lie within the range of $0.5x10^{-5}$/yr and $1.2x10^{-5}$/yr. The Seismic Core Damage Frequency (SCDF) will be much less assuming a HCLPF seismic margin $F_{1\%}$=1.67. Table 2.5.2-5-6 shows the SCDF obtained from numerically convolving the four normalized hazard curves defined in Table 2.5.2-5-2 and lognormal fragility curves. The fragility curves have HCLPF seismic margin $F_{1\%}$=1.67 and logarithmic standard deviations β in the range of 0.3 to 0.6.

Under these same assumptions, SCDF were also computed in Ref. 3 for the 28 CEUS sites considered therein. The SCDF results for these 28 sites are shown in Figure 2.5.2-5-3 taken from Ref. 3. The results shown in Figure 2.5.2-5-3 are summarized as follows:

	ASCE Method SCDF $F_{1\%}$=1.67 *$1x10^{-5}$/yr				Existing Plant SCDF *$1x10^{-5}$/yr
β	0.3	0.4	0.5	0.6	
Range	0.075-0.54	0.060-0.40	0.058-0.29	0.058-0.22	0.019-23.0
Median	0.38	0.26	0.19	0.15	1.20

The ASCE Standard 43-05 method for defining the DRS summarized above was developed to produce a nearly constant FOSID for a given β independent of the slope of the hazard curve. This ASCE Method does not produce a SCDF that is independent of the slope of the hazard curve for plants with a Seismic Core Damage HCLPF seismic margin of 1.67. The resulting SCDF will be higher for sites with high A_R ratios than for sites with low A_R ratios. For sites with A_R ratios of about 2.0 or less such as the EGC

[2] HCLPF is short for "High Confidence of a Low Probability of Failure".

ESP site, the SCDF will be in the range of 0.6×10^{-6}/yr to 2×10^{-6}/yr. However, with a HCLPF seismic margin of 1.67, the SCDF is less than 6×10^{-6}/yr for all 28 sites considered, which is less than 50% of the median SCDF reported for existing nuclear power plants (see Attachment 1 for further discussion). Thus, the EGC ESP site is in the low end of the SCDF range for the sites considered. The EGC ESP specific SCDF values are shown in Table AA.5 of Appendix A of Attachment 1. At 1 Hz the EGC ESP SCDF values are essentially the same as the median values shown in the above table. However, for natural frequencies of 2.5 Hz and higher, the EGC ESP SCDF values are less than the median values shown in the above table. The EGC ESP average 5 and 10 Hz SCDF values are only 50% of the median values shown above.

The goal of a lower SCDF than the median SCDF reported for existing LWRs is achieved for advanced reactor designs with a HCLPF seismic margin of at least 1.67. On average, the reduction is at least a factor of three.

It should be further noted that both the ASCE Standard criteria for SDC-5D and NRC criteria specify a lower bound for the SSE DRS of a Regulatory Guide 1.60 response spectrum anchored to a peak ground acceleration (PGA) of 0.10g. For the results shown in Figures 2.5.2-5-2 and 2.5.2-5-3, this lower bound requirement on the DRS was conservatively ignored because the purpose of the study was to demonstrate the effect of the slope ratio A_R and β on the FOSID and SCDF results. For 13 of the 28 sites studied in Ref. 3, the seismic hazard was very low so that the DRS spectral accelerations in the 5 to 10 Hz range were less than a 0.10g Regulatory Guide 1.60 spectrum would require. If the DRS for these 13 sites had been increased to the 0.10g Regulatory Guide 1.60 values, the FOSID and SCDF would have been less for these sites than shown in Figures 2.5.2-5-2 and 2.5.2-5-3, respectively. Thus, the comparisons shown in these figures for the ASCE Method are conservatively biased because this lower bound DRS correction was not made.

4th bullet:

• Justify the long-term stability of the target performance goal 10-5 in comparison to the hazard-based approach (reference probability) in RG 1.165, as both values require the use of PSHAs for several CEUS nuclear sites.

Response to 4th bullet:

The long-term stability of regulatory requirements and procedures is generally understood and accepted to be essential. A general distinction is made between stable regulatory requirements and procedures, which are essential, and technological implementation procedures that are used to demonstrate compliance with regulatory requirements and procedures. Implementation methods necessarily evolve with scientific and engineering technology advances and must be updated. Indeed, the recognition that the old seismic and geologic siting regulation, 10 CFR Part 100, Appendix A, lacked adequate stability in implementation motivated the Commission to issue the revised regulation Part 100.23, which contains seismic and geologic siting requirements that remain stable with time, and to place technical guidance for implementation of the regulatory requirements in Regulatory Guide 1.165 where it could be updated to incorporate advances in understanding.

Although Regulatory Guide 1.165 was officially issued in early 1997, the guidance is based on late 1980s to early 1990s technologies. EGC recognized that the guidance

required updating for the development of the ESP application for the Clinton site. Updating included the input parameters, seismic source assessments and an updated generic ground motion model for the site region (Ref. 5), the use of updated procedures contained in NUREG/CR-6728 (Ref. 4) for deriving hazard-consistent, site-specific ground motion transfer functions, and the use of the performance-based method described in ASCE 43-05 Standard (Ref. 1) as the basis for deriving site-specific safe shutdown earthquake (SSE) ground motion for the site.

EGC used the ASCE 43-05 Standard performance-based approach for the determination of the site-specific SSE ground motion because it is based on a risk informed criterion, making it a stable method for implementing the requirements of Part 100.23 with respect to determination of SSE ground motion. EGC recognized that the reference probability approach of Regulatory Guide 1.165 does not provide the regulatory stability that was originally intended and expected, as it is inherently unstable with the updating of the input parameters for PSHAs for CEUS sites. Updating the PSHAs at CEUS sites changes the basis upon which the reference probability was established and a new reference probability must be established. The performance-based criterion on the other hand, remains unchanged by updating the PSHAs, even though the site-specific SSE ground motion will reflect the updated PSHA results. The method provides uniform performance across sites and thus provides performance consistency and regulatory stability.

5th bullet:

• Since the target performance goal 10-5 is based on seismic PRAs for current LWRs, justify the use of this value for advanced reactor designs, which may differ considerably from current LWRs.

Response to 5th bullet:

See combined response to 3rd and 5th bullets.

6th bullet:

• Since SSCs for nuclear power plants are designed using the seismic criteria in the SRP, clarify how the design criteria in ASCE/SEI Standard 43-05 are similar enough that SSCs designed following the SRP would also achieve a 1 percent or lower probability of unacceptable performance.

Response to 6th bullet:

In most aspects, the seismic design criteria in ASCE Standard 43-05 for Seismic Design Category SDC-5D are identical to the NRC Standard Review Plan (SRP) seismic design criteria given in the latest edition of Ref. 7, Regulatory Guides, and professional design codes and standards referenced therein. A few exceptions exist and these will be discussed herein.

In several aspects, the Seismic Demand analysis criteria given in ASCE Standard 43-05 are more liberal than that specified by the NRC. One of these aspects is that some of the damping levels permitted in Table 3-2 of ASCE Standard 43-05 are more liberal than those specified in Regulatory Guide 1.61. The differences are not large. However, due to differences in permissible damping levels to be used in the Demand analyses, the

computed Demands might be as much as 20% less by ASCE Standard 43-05 than by the SRP.

A second difference is in the development of in-structure response spectra (ISRS). For seismic analysis criteria, ASCE Standard 43-05 refers to ASCE 4 (Ref. 9). In turn ASCE 4 does not require the ISRS from the Upper Bound Soil-Structure-Interaction (SSI) analysis to be broadened on the stiff side nor the Lower Bound SSI analysis to be broadened on the soft side. In addition, ISRS narrow frequency peaks are allowed to be reduced 15%. These differences from the SRP might reduce ISRS up to another 20% below those computed in accordance with the SRP.

No Seismic Demand criterion was found where ASCE Standard 43-05 is more conservative than the SRP. The net result is that the Seismic Demands computed by ASCE Standard 43-05 will never be higher than those computed by the SRP and might be as much as a factor of 1.4 less. Thus, the SRP requirements can increase the seismic demand margin by as much as a factor of 1.4 above that defined in the Commentary of ASCE Standard 43-05.

Nearly all of the Seismic Capacities determined in accordance with ASCE Standard 43-05 will be identical to those determined in accordance with the SRP. Two important exceptions exist.

ASCE Standard 43-05 permits higher capacities for low-rise shear walls than are permitted by ACI 349 referenced in the SRP. In this regard, the SRP is more conservative.

The only place found where ASCE Standard 43-05 is more conservative than the SRP is for components qualified by test. ASCE Standard 43-05 requires that the Test Response Spectrum (TRS) for components qualified by test to be a factor of 1.4 times the ISRS. No similar requirement exists in the SRP. However, this additional requirement is partially compensated by the ISRS being as much as a factor of 1.4 less by ASCE 43-05 than by the SRP.

The above summarizes all of the important differences found between the ASCE Standard 43-05 seismic criteria for SDC-5D and the SRP seismic criteria. Thus, the differences in criteria can be judged to be sufficiently small that the SRP is considered to also reasonably achieve both of the following for the "onset of significant inelastic deformation":

1. Less Than About a 1% Probability of Unacceptable Performance for the Design Basis Earthquake Ground Motion, and
2. Less Than About a 10% Probability of Unacceptable Performance for a Ground Motion equal to 150% of the Design Basis Earthquake Ground Motion

References

1. ASCE Standard 43-05, *Seismic Design Criteria for Structures, Systems, and Components in Nuclear Facilities,* ASCE/SEI 43-05 American Society of Civil Engineers (ASCE), 2005

2. Kennedy, R.P. *Risk (Performance-Goal) Based Approach Used in Exelon Generation Company Early Site Permit Application for Establishing the SSE Design Responses Spectrum,* Rev. 1, prepared for Exelon Generation Company, December 2004 (provided to NRC via EGC correspondence dated January 14, 2005)
3. *Performance-Based Seismic Design Spectra,* Program on Technology Innovation: Assessment of a Performance-Based Approach for Determining Seismic Ground Motions for New Plant Sites, Vol. 1, TR-1012045, Electric Power Research Institute (EPRI), September 2005
4. *Technical Basis for Revision of Regulatory Guidance on Design Ground Motions: Hazard-and Risk-consistent Ground Motion Spectra Guidelines,* NUREG/CR-6728, U.S. Nuclear Regulatory Commission (NRC), Oct. 2001
5. *CEUS Ground Motion Project Final Report,* 1009684, Electric Power Research Institute (EPRI), December 2004
6. *Perspective Gained From the Individual Plant Examination of External Events (IPEEE) Program,* NUREG-1742, Volumes 1 and 2, U.S. Nuclear Regulatory Commission (NRC), Sept. 2001
7. *Standard Review Plan,* NUREG-0800, U.S. Nuclear Regulatory Commission (NRC)
8. *A Methodology for Assessment of Nuclear Power Plant Seismic Margin,* EPRI NP-6041-SL, Revision 1, Electric Power Research Institute (EPRI), August 1991
9. ASCE Standard 4-98, *Seismic Analysis of Safety-Related Nuclear Structures and Commentary,* American Society of Civil Engineers (ASCE), 2000

ASSOCIATED EGC ESP APPLICATION REVISIONS:

None

ATTACHMENTS:

Tables 2.5.2-5-1 through 2.5.2-5-6

Figures 2.5.2-5-1 through 2.5.2-5-3

1) Further Discussion of Slope Ratios (A_R), Design Factors (DF), Exceedance Frequency for ASCE Standard 43-05 (Ref. 1) Design Response Spectra, and Resulting Maximum Seismic Core Damage Frequencies (SCDF) for 28 Central and Eastern U.S. (CEUS) Sites

   Appendix A to Attachment 1: Computation of FOSID and SCDF for EGC ESP Site Specific Hazard Curves When Design Response Spectrum is Defined by ASCE Standard 43-05

2) Reference 3, EPRI TR-1012045, Volumes 1 & 2, is attached.

Table 2.5.2-5-1

Design Factor DF Values Required To Achieve A Probability Ratio $R_P = 10$
(from Table 7.1 of Ref. 2 or Table A-4 of Ref. 3)

A_R	DF				DF
	$F_{1\%}$=1.1 β = .3	$F_{1\%}$=1.0 β = .4	$F_{1\%}$=1.0 β = .5	$F_{1\%}$=1.0 β = .6	Eqn (1.5)
1.5	0.88	0.93	0.95	1.03	1.0
1.75	0.96	0.96	0.91	0.91	1.0
2	1.05	1.03	0.95	0.9	1.04
2.25	1.16	1.11	1	0.93	1.15
2.5	1.27	1.21	1.07	0.97	1.25
2.75	1.38	1.3	1.14	1.03	1.35
3	1.50	1.4	1.22	1.08	1.44
3.25	1.61	1.5	1.3	1.14	1.54
3.5	1.73	1.6	1.38	1.21	1.63
3.75	1.84	1.7	1.46	1.27	1.73
4	1.96	1.8	1.54	1.34	1.82
4.25	2.07	1.9	1.62	1.4	1.91
4.5	2.19	2.01	1.7	1.47	2.0
4.75	2.30	2.11	1.79	1.54	2.09
5	2.42	2.21	1.87	1.6	2.17
5.25	2.54	2.31	1.95	1.67	2.26
5.5	2.65	2.42	2.04	1.74	2.35
5.75	2.77	2.52	2.12	1.8	2.43
6	2.88	2.62	2.2	1.87	2.52

Recommended Eqn. (1.5) DF Factors Are Conservatively Biased on Average

Table 2.5.2-5-2

Typical Normalized Spectral Acceleration Hazard Curve Values

Hazard Exceedance Frequency $H_{(SA)}$	Eastern U.S.		California	
	1 Hz SA	10 Hz SA	1Hz SA	10 Hz SA
5×10^{-2}	0.014	0.018	0.087	0.046
2×10^{-2}	0.027	0.034	0.13	0.072
1×10^{-2}	0.045	0.055	0.175	0.100
5×10^{-3}	0.07	0.089	0.236	0.139
2×10^{-3}	0.143	0.169	0.351	0.215
1×10^{-3}	0.235	0.275	0.474	0.334
5×10^{-4}	0.383	0.424	0.629	0.511
2×10^{-4}	0.681	0.709	0.814	0.762
1×10^{-4}	1.00	1.0	1.0	1.0
5×10^{-5}	1.46	1.41	1.23	1.22
2×10^{-5}	2.35	2.13	1.61	1.51
1×10^{-5}	3.27	2.88	1.89	1.76
5×10^{-6}	4.38	3.65	2.2	2.05
2×10^{-6}	6.44	4.62	2.68	2.42
1×10^{-6}	8.59	5.43	3.1	2.72
5×10^{-7}	10.34	6.38	3.58	3.06
2×10^{-7}	13.21	7.9	4.24	3.56
1×10^{-7}	15.9	9.28	4.67	3.84

Table 2.5.2-5-3

Individual SSC Seismic Risks P_{FC} (FOSID) Achieved for Representative Hazard Curves

Hazard Curve	UHRS			DRS	SSC Seismic Risk P_{FC} ($*10^{-5}$)			
	SA_{UHRS}	A_R	DF	SA_{DRS}	$F_{1\%}$=1.1 β = 0.30	$F_{1\%}$=1.0 β = 0.40	$F_{1\%}$=1.0 β = 0.50	$F_{1\%}$=1.0 β = 0.60
EUS 1Hz	1.00	3.27	1.55	1.55	1.09	0.93	0.69	0.52
EUS 10 Hz	1.00	2.88	1.40	1.40	1.03	0.87	0.62	0.46
Calif 1 Hz	1.00	1.89	1.00	1.00	1.04	0.96	0.73	0.61
Calif 10 Hz	1.00	1.76	1.00	1.00	0.84	0.78	0.58	0.48

Table 2.5.2-5-4

Comparison of Seismic Risk P_{FC} Computed By Rigorous Numerical Convolution of Hazard and Fragility Curves Versus Power Law Approximation of Hazard Curve

(Power Law Approximation Shown In Parenthesis)

Hazard Curve	SSC Seismic Risk P_{FC} ($*10^{-5}$)			
	$F_{1\%}$=1.1 β=0.30	$F_{1\%}$=1.0 β=0.40	$F_{1\%}$=1.0 β=0.50	$F_{1\%}$=1.0 β=0.60
EUS 1Hz	1.09 (1.09)	0.93 (0.95)	0.69 (0.71)	0.52 (0.56)
EUS 10 Hz	1.03 (1.06)	0.87 (0.93)	0.62 (0.69)	0.46 (0.54)
Calif 1 Hz	1.04 (1.03)	0.96 (0.98)	0.73 (0.76)	0.61 (0.68)
Calif 10 Hz	0.84 (0.84)	0.78 (0.85)	0.58 (0.70)	0.48 (0.67)

Table 2.5.2-5-5

Individual SSC Seismic Risk P_{FC} (FOSID) Obtained Using Eqn. (1.5) Design Factors
(P_{FC} values shown should be multiplied times $1x10^{-5}$/yr)

A_R	P_{FC}			
	$F_{1\%}$=1.1 β = .3	$F_{1\%}$=1.0 β = .4	$F_{1\%}$=1.0 β = .5	$F_{1\%}$=1.0 β = .6
1.5	0.47	0.67	0.76	1.2
1.75	0.82	0.84	0.69	0.68
2	1.03	0.95	0.72	0.61
2.25	1.03	0.92	0.68	0.55
2.5	1.04	0.92	0.68	0.53
2.75	1.06	0.92	0.69	0.54
3	1.08	0.93	0.7	0.55
3.25	1.09	0.95	0.71	0.56
3.5	1.1	0.96	0.73	0.57
3.75	1.12	0.97	0.74	0.59
4	1.13	0.98	0.76	0.6
4.25	1.14	1	0.77	0.61
4.5	1.15	1.01	0.78	0.62
4.75	1.16	1.02	0.79	0.64
5	1.17	1.02	0.81	0.65
5.25	1.17	1.03	0.82	0.66
5.5	1.18	1.04	0.83	0.67
5.75	1.19	1.05	0.83	0.68
6	1.19	1.05	0.84	0.68

Table 2.5.2-5-6

Seismic Core Damage Frequency (SCDF) for DRS Defined by ASCE Standard 43-5 Method and HCLPF Seismic Margin of 1.67

Hazard Curve	A_R	DRS SA_{DRS}	SCDF ($*10^{-6}$)			
			β=0.30	β=0.40	β=0.50	β=0.60
EUS 1Hz	3.27	1.55	4.3	2.9	2.1	1.6
EUS 10 Hz	2.88	1.40	3.1	2.0	1.4	1.1
Calif 1 Hz	1.89	1.00	1.8	1.2	1.0	0.9
Calif 10 Hz	1.76	1.00	1.1	0.8	0.7	0.6

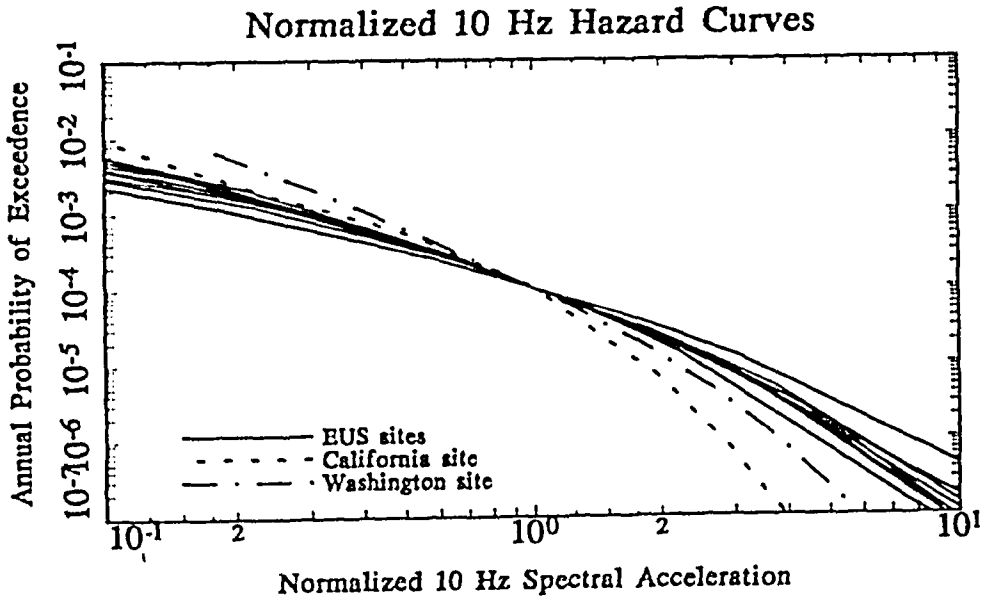

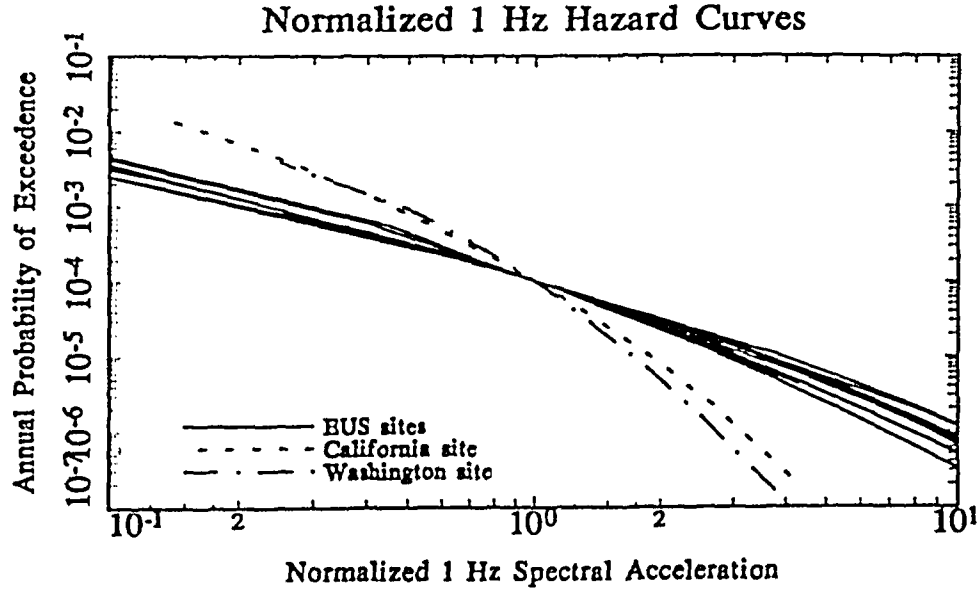

Figure 2.5.2-5-1: SA (10 Hz) and SA (1 Hz) hazard curves for the eleven sites normalized by the acceleration value corresponding to mean 10^{-4} annual probability (From Figs. 7.7 and 7.8 of Ref. 4)

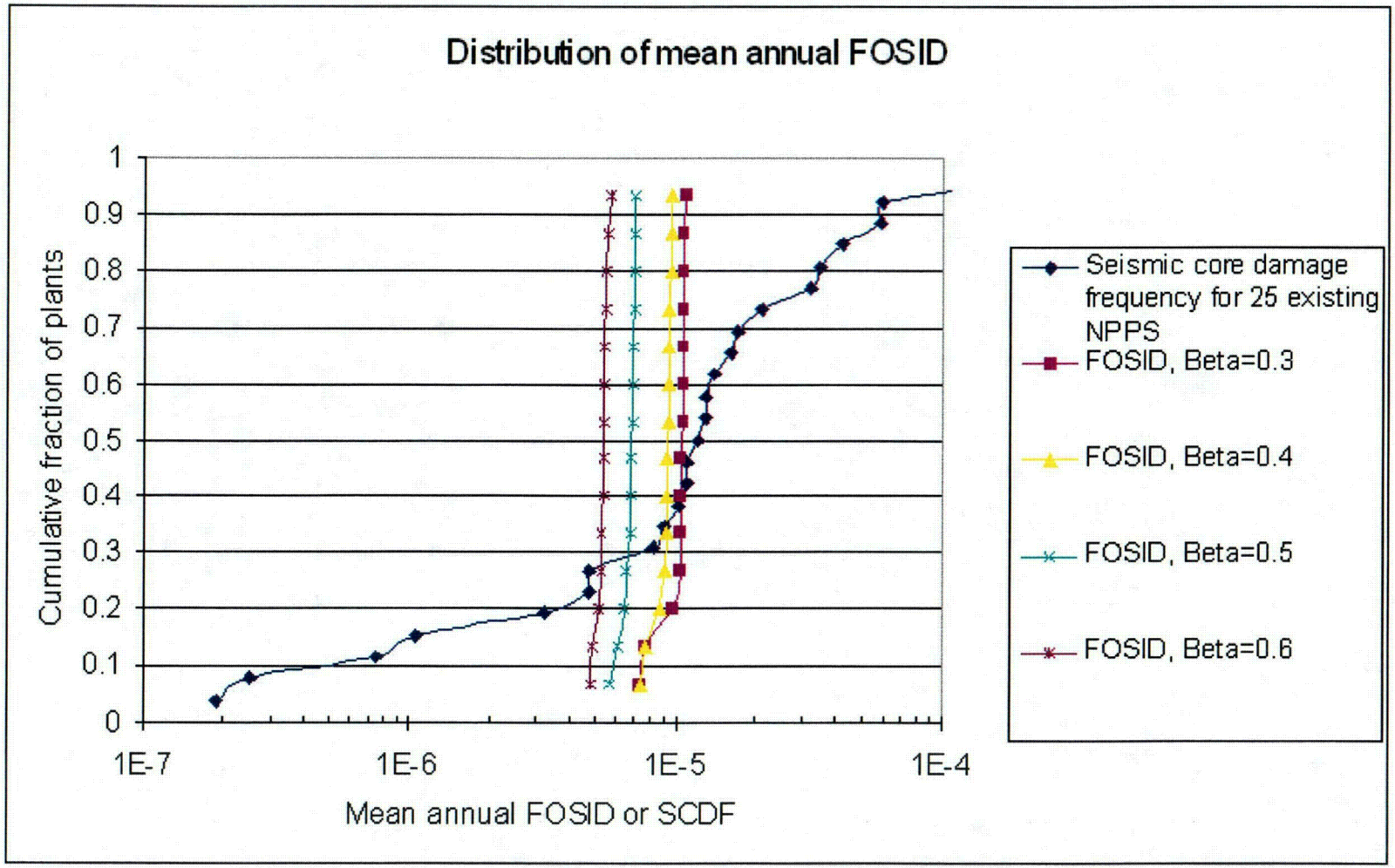

Figure 2.5.2-5-2: Cumulative distribution of ASCE Method FOSIDs for components, compared to Existing Plant SCDF (From Ref. 3)

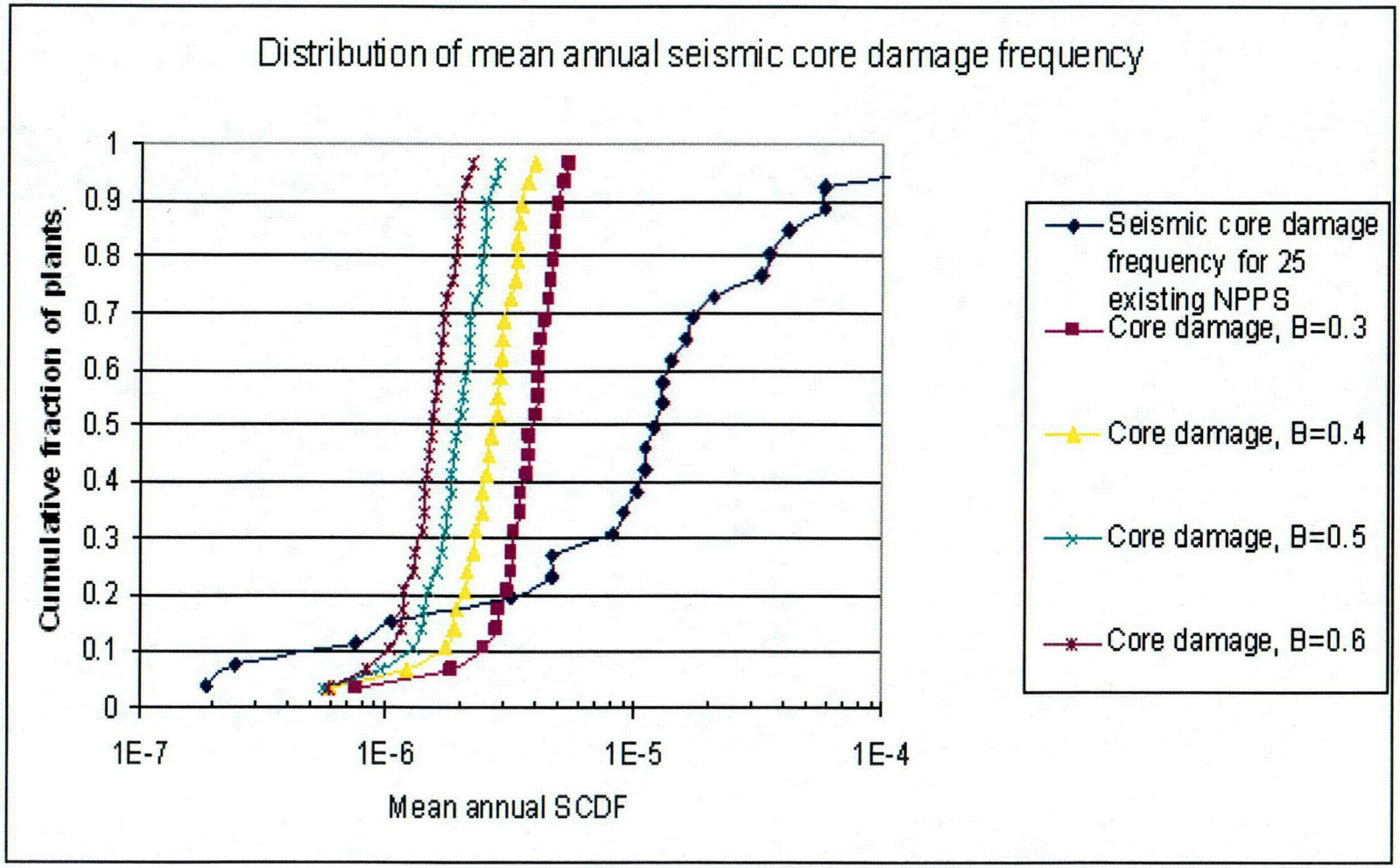

Figure 2.5.2-5-3: Cumulative distribution of ASCE Method SCDF, compared to Existing Plant SCDF (From Ref. 3)

C21

ATTACHMENT 1 to Response to DSER OI 2.5.2-5

Further Discussion of Slope Ratios (A_R), Design Factors (DF), Exceedance Frequency for ASCE Standard 43-05 (Ref. 1) Design Response Spectra, and Resulting Maximum Seismic Core Damage Frequencies (SCDF) for 28 Central and Eastern U.S. (CEUS) Sites

Ref. 2 presents study results associated with defining the SSE Design Response Spectrum (DRS) by the ASCE Standard 43-05 (Ref. 1) approach utilized for the EGC ESP site. These study results are presented for 28 Central and Eastern U.S. sites. This attachment presents additional information (Ref. 3) developed in the Ref. 2 study and compares this information with that developed for the EGC ESP site.

Table A1.1 (from Ref. 3) presents statistical information on the slope ratio (A_R), design factor (DF) and the DRS mean exceedance frequency (PE) in the 1.0 to 10.0 Hz range for the 28 CEUS sites studied in Ref. 2. Table A1.1 also shows the EGC ESP site values for comparison.

For these 28 sites and natural frequency ranges, the total range on slope ratios (A_R) is from 1.50 to 4.36 which results in a range of DF from 1.0 to 1.95. A_R values of 1.89 and less result in DF of 1.0 and DRS exceedance frequency (PE) of mean $1x10^{-4}$/yr. Conversely, the high A_R of 4.36 results in DF of 1.95 and PE of $0.37x10^{-4}$/yr.

For the middle 70% of the sites (20 of 28), the range is smaller. For these middle 70%, the A_R range is about 2.25 to about 3.5 which results in DF of about 1.15 to 1.65 with PE ranging from about $0.7x10^{-4}$/yr to about $0.4x10^{-4}$/yr.

Two sites have A_R values (in the frequency range of 2.5 Hz and higher) of less than 2.1 resulting in DF of less than 1.09 and PE between $0.8x10^{-4}$/yr and $1.0x10^{-4}$/yr. These two sites have relatively high rock response spectra at mean $1.0x10^{-4}$/yr and are soil sites. The rock response spectra are amplified by the soil. However, the soil amplification factors are less for the mean $1.0x10^{-5}$/yr rock motion than they are for the mean $1.0x10^{-4}$/yr rock motions. As a result, the A_R ratios at 2.5 Hz and higher frequencies are less than 2.1 for the soil response spectra. The EGC ESP site is one of these two sites.

Ref. 2 presents Frequency of Onset of Significant Inelastic Deformation (FOSID) results averaged for 5 and 10 Hz for the 28 sites when the SSE DRS is defined by the ASCE Standard 43-05 Method. These results are summarized in Table A1.2. The FOSID values computed by rigorous numerical convolution for the 28 sites lie within a FOSID range of mean $1.2x10^{-5}$/yr and $0.4x10^{-5}$/yr. The highest source of variability is due to the logarithmic standard deviation, β, of the fragility with results for β=0.3 and 0.4 being close to the target P_{FT}=mean $1x10^{-5}$/yr for FOSID and the β=0.6 results being between about 40 to 60% of the target. Thus, overall, a conservative bias is introduced.

For a given β, very little scatter exists in the computed FOSID. For 26 of the 28 sites, the computed FOSID for a given β are within 10% of the median value. For the other 2 sites, the computed FOSID are more than 10% less than the median value for a given β. Thus, the ASCE Method DRS achieves its goal of a nearly constant FOSID for an SSC at all sites.

The EGC ESP site has computed FOSID values within the lowest 16% of the FOSID values computed for the 28 sites. The other site with A_R less than 2.1 (and thus DF less than 1.09) is also in the lowest 16% of computed FOSID values. Therefore, if an exceedance frequency (PE) of mean $0.5x10^{-4}$/yr is appropriate for the DRS for the median CEUS site, then it is also appropriate for sites with low A_R less than 2.1 to have DRS mean exceedance frequencies in the range of $0.8x10^{-4}$/yr to $1.0x10^{-4}$/yr. Only in this way can a nearly constant FOSID be achieved.

Ref. 2 also presents Seismic Core Damage Frequency (SCDF) results averaged for 5 and 10 Hz for the 28 sites when the SSE DRS is defined by the ASCE Standard 43-05 Method. These results are summarized in Table A1.3.

The highest SCDF results are obtained for the logarithmic standard deviation β=0.3 case. For β=0.3, 26 of the 28 sites have computed maximum SCDF between about $0.3x10^{-5}$/yr and about $0.5x10^{-5}$/yr. However, the two sites with A_R less than 2.1 produce SCDF results less than $0.2x10^{-5}$/yr even though the exceedance frequency of the DRS lies in the mean $0.8x10^{-4}$/yr to mean $1.0x10^{-4}$/yr range. If the DRS is defined by the ASCE Method, sites with low A_R ratios and thus low DF will have the lowest SCDF.

The FOSID and SCDF results shown in Tables A1.2 and A1.3 for the EGC ESP site are from the 28 site study presented in Ref. 2. The reported FOSID and SCDF results shown are the average of the 5 and 10 Hz results. Appendix A to this attachment presents the FOSID and SCDF results obtained using the EGC ESP site specific hazard curves. In Appendix A, results are shown individually for the 1, 2.5, 5, and 10 Hz hazard curves. The average of the 5 and 10 Hz FOSID and SCDF results obtained using the EGC ESP site specific hazard curves are nearly identical (within 5%) with the EGC ESP site FOSID and SCDF results reported in Tables A1.2 and A1.3.

The conclusion is that when the SSE DRS is defined by the ASCE Method, the maximum FOSID for plants at all sites will be nearly constant and less than about $1x10^{-5}$/yr. The maximum SCDF will reliably be less than $0.6x10^{-5}$/yr for Standard Plant designs with HCLPF seismic margins of at least 1.67. Furthermore, plants located at sites with low A_R ratios such as the EGC ESP site will have the lowest maximum SCDF.

References

1. ASCE Standard 43-05, *Seismic Design Criteria for Structures, Systems, and Components in Nuclear Facilities,* ASCE/SEI 43-05, American Society of Civil Engineers (ASCE), 2005

2. *Performance-Based Seismic Design Spectra,* Program on Technology Innovation: Assessment of a Performance-Based Approach for Determining Seismic Ground Motions for New Plant Sites, Vol. 1, TR-1012045, Electric Power Research Institute (EPRI), September 2005

3. Personal Communication between R.K. McGuire (author of Ref. 2) and R.P. Kennedy, October 2005

Table A1.1

Statistics on A_R, DF (ratio of DRS/1E-4 amplitude), and DRS Mean Exceedance Frequency PE/1E-4 for 28 Sites in Ref. 2 Study Compared with EGC ESP Site

	Min	16th	50th	84th	Max	EGC ESP Site
10 Hz, AR	1.50	2.26	3.01	3.67	4.36	2.08
10 Hz, DF	1	1.15	1.45	1.70	1.95	1.08
10 Hz, PE/1E-4	0.37	0.40	0.48	0.68	1	0.79
5 Hz, AR	1.64	2.17	2.63	3.33	4.05	2.00
5 Hz, DF	1	1.11	1.30	1.57	1.84	1.04
5 Hz, PE/1E-4	0.38	0.43	0.54	0.75	1	0.87
2.5 Hz, AR	1.54	2.19	2.42	3.23	3.81	2.02
2.5 Hz, DF	1	1.13	1.22	1.53	1.75	1.05
2.5 Hz, PE/1E-4	0.4	0.45	0.62	0.76	1	0.84
1 Hz, AR	1.58	2.24	2.49	3.40	3.77	2.63
1 Hz, DF	1	1.14	1.24	1.60	1.74	1.30
1 Hz, PE/1E-4	0.39	0.44	0.61	0.73	1	0.53

Table A1.2

Range of Frequency of Onset of Significant Inelastic Deformation (FOSID) Results for 28 Sites

	ASCE Method FOSID *$1x10^{-5}$/yr			
β	0.3	0.4	0.5	0.6
Range	0.71-1.17	0.66-0.99	0.51-0.75	0.41-0.58
16%-84%	1.03-1.12	0.91-0.96	0.66-0.72	0.52-0.56
Median	1.07	0.93	0.69	0.54
EGC ESP Site	0.98	0.87	0.64	0.51

Table A1.3

Range of Seismic Core Damage Frequency (SCDF) Results for 28 CEUS Sites (from Ref. 2)

	ASCE Method SCDF $F_{1\%}$=1.67 *1x10^{-5}/yr			
β	0.3	0.4	0.5	0.6
Range	0.075-0.54	0.060-0.40	0.058-0.29	0.058-0.22
16%-18%	0.28-0.48	0.19-0.34	0.14-0.25	0.12-0.20
Median	0.38	0.26	0.19	0.15
EGC ESP Site	0.19	0.12	0.095	0.084

Appendix A to Attachment 1 to Response to DSER OI 2.5.2-5

Computation of FOSID and SCDF for EGC ESP Site Specific Hazard Curves When Design Response Spectrum is Defined by ASCE Standard 43-05

The EGC ESP site specific hazard curves for 1, 2.5, 5 and 10 Hz are shown in Table AA.1. This table reports Spectral Acceleration (SA) in terms of mean exceedance frequency (H). Using these hazard curves, the mean Frequency of Onset of Significant Inelastic Deformation (FOSID) and mean Seismic Core Damage Frequency (SCDF) are determined by numerically convolving the mean seismic hazard curve and mean fragility curve using:

$$P_F = -\int_0^{+\infty} P_F(a)\left(\frac{dH(a)}{da}\right) da \qquad \text{(AA.1)}$$

where $P_F(a)$ is the conditional probability of FOSID or SCDF given the ground motion level a, which, by definition, is the mean fragility curve, and $H(a)$ is the mean hazard exceedance frequency corresponding to ground motion level a.

Given the seismic hazard curves shown in Table AA.1, the Design Response Spectrum (DRS) is defined by the ASCE Standard 43-05 (Ref. 1) approach utilized for the EGC ESP site. The resulting slope ratios (A_R), design factors (DF) and DRS values at 1, 2.5, 5, and 10 Hz are shown in Table AA.2.

The lognormal fragility curve is defined in terms of the 1% non-exceedance probability capacity $C_{1\%}$, and the logarithmic standard deviation β. In turn:

$$C_{1\%} = F_{1\%} \cdot DRS \qquad \text{(AA.2)}$$

where $F_{1\%}$ is the 1% non-exceedance probability seismic margin factor. For SCDF:

SCDF

$$F_{1\%} = 1.67 \quad \text{all } \beta \qquad \text{(AA.3)}$$

and for FOSID:

FOSID

$$F_{1\%} = 1.10 \quad \text{for } \beta = 0.30$$
$$F_{1\%} = 1.00 \quad \text{for } \beta \geq 0.40 \qquad \text{(AA.4)}$$

Given this description of the fragility curve and the properties of the lognormal distribution the conditional probability $P_{F(a)}$ for FOSID or SCDF is defined for any ground motion level a. Thus, the total FOSID or SCDF can be determined from Eqn. (AA.1).

An example numerical convolution of hazard and fragility using Eqn. (AA.1) is shown in Table AA.3 for SCDF using the 5 Hz hazard curve and $\beta = 0.30$. For this example, the $C_{1\%}$ and median capacity $C_{50\%}$ are:

$\beta = 0.30$

$C_{1\%} = 1.67(0.6125) = 1.023g$

$C_{50\%} = C_{1\%}\, e^{2.326\beta} = 2.0553g$

In this example, the SA values are defined at 0.1g increments from 0.6g to 3.2 g which is the SA region that is needed for computing P_F. For each SA value, the exceedance frequency H is defined by interpolation of the H values shown in Table AA.1 for the 5 Hz hazard curve. Next ΔH is found by differencing adjacent values of H. The conditional $P_{F(a)}$ is determined from the lognormal fragility curve at the midpoint value of SA for each interval. For each interval, the product of $\Delta H * P_{F(a)}$ is obtained and summed over all intervals to obtain P_F. For this example case $P_F = 2.235 \times 10^{-6}$/yr.

Table AA.4 presents the Frequency of Onset of Significant Inelastic Deformation (FOSID) results computed using the EGC ESP site specific soil hazard curves for 1, 2.5, 5, and 10 Hz coupled with the FOSID seismic margins defined by Eqn. AA.4. Despite the variation of A_R, the computed FOSID are nearly constant over all natural frequencies for a given fragility β. The range of FOSID are from 0.5×10^{-5}/yr to 1.06×10^{-5}/yr. Therefore, the target FOSID goal is achieved.

Table AA.5 presents the Seismic Core Damage Frequency SCDF consistent with a minimum core damage HCLPF seismic margin $F_{1\%}$ of 1.67. The computed SCDF range from 3.9×10^{-6}/yr to 0.8×10^{-6}/yr. These SCDF are consistent with the SCDF values presented in Ref. 2. Again, hazard curves with low A_R values and thus lower DF values produce the lowest SCDF results.

Table AA.1
EGC ESP Site Specific Soil Hazard Curves

1 Hz		2.5 Hz		5 Hz		10 Hz	
SA (g)	H	SA (g)	H	SA (g)	H	SA (g)	H
0.00128	5.306E-02	0.00270	1.284E-01	0.00324	9.160E-02	0.00260	8.228E-02
0.00200	3.854E-02	0.00402	1.025E-01	0.00463	7.859E-02	0.00374	7.130E-02
0.00314	2.747E-02	0.00600	7.758E-02	0.00661	6.511E-02	0.00538	5.981E-02
0.00493	1.912E-02	0.00894	5.605E-02	0.00945	5.195E-02	0.00774	4.877E-02
0.00773	1.289E-02	0.01333	3.901E-02	0.01351	3.972E-02	0.01114	3.808E-02
0.01211	8.718E-03	0.01986	2.662E-02	0.01931	2.952E-02	0.01604	2.907E-02
0.01899	5.784E-03	0.02961	1.782E-02	0.02759	2.100E-02	0.02308	2.119E-02
0.02977	3.703E-03	0.04413	1.180E-02	0.03944	1.454E-02	0.03321	1.494E-02
0.04668	2.244E-03	0.06578	7.554E-03	0.05637	9.903E-03	0.04778	1.020E-02
0.07319	1.228E-03	0.09806	4.493E-03	0.08057	6.500E-03	0.06876	6.593E-03
0.11475	5.691E-04	0.14616	2.501E-03	0.11515	3.973E-03	0.09894	3.938E-03
0.17991	2.389E-04	0.21786	1.208E-03	0.16458	2.255E-03	0.14236	2.152E-03
0.28207	8.601E-05	0.32473	5.178E-04	0.23523	1.148E-03	0.20486	1.074E-03
0.44224	2.931E-05	0.48404	1.510E-04	0.33621	5.127E-04	0.29478	4.823E-04
0.69336	1.007E-05	0.72149	4.098E-05	0.48054	1.932E-04	0.42417	1.930E-04
1.08709	3.540E-06	1.07543	1.106E-05	0.68682	5.986E-05	0.61037	6.745E-05
1.70439	1.082E-06	1.60301	3.194E-06	0.98165	1.785E-05	0.87829	2.237E-05
2.67223	3.160E-07	2.38940	7.276E-07	1.40304	5.554E-06	1.26383	6.367E-06
4.18966	8.337E-08	3.56157	4.326E-08	2.00532	1.432E-06	1.81859	3.517E-07
6.56876	1.379E-08	5.30876	7.029E-09	2.86615	8.066E-08	2.61688	1.257E-07
10.29882	1.858E-09	7.91308	1.302E-09	4.09650	1.246E-08	3.76557	4.136E-08
16.14700	3.244E-10	11.79500	2.824E-10	5.85500	2.343E-09	5.41850	1.285E-08

Table AA.2
Computation of DRS Spectral Acceleration (SA)

	1 Hz	2.5 Hz	5 Hz	10 Hz
$1x10^{-4}$ SA	0.2640	0.5491	0.5874	0.5326
$1x10^{-5}$ SA	0.6934	1.1110	1.1720	1.1089
A_R	2.626	2.023	1.995	2.0821
DF	1.299	1.054	1.043	1.079
DRS SA	0.3430	0.5790	0.6125	0.5746

Table AA.3:
Determination of SCDF (P_F) Using 5 Hz Hazard Curve and Logarithmic Standard Deviation β of 0.30

SA (g)	H $*10^{-6}$	ΔH $*10^{-6}$	$P_F(a)$	$P_F(a) \cdot \Delta H$ $*10^{-6}$
0.6	93.271			
		37.15	0	0.002
0.7	56.121			
		20.423	0	0.008
0.8	35.698			
		11.746	0.002	0.019
0.9	23.952			
		7.153	0.005	0.036
1.0	16.799			
		4.496	0.013	0.057
1.1	12.302			
		3.045	0.026	0.081
1.2	9.257			
		2.131	0.049	0.104
1.3	7.126			
		1.533	0.081	0.124
1.4	5.593			
		1.283	0.122	0.157
1.5	4.310			
		0.936	0.173	0.162
1.6	3.373			
		0.693	0.232	0.161
1.7	2.680			
		0.523	0.296	0.155
1.8	2.157			
		0.400	0.363	0.145
1.9	1.757			
		0.311	0.430	0.134
2.0	1.446			
		0.459	0.497	0.228
2.1	0.988			
		0.309	0.560	0.173
2.2	0.679			
		0.204	0.619	0.126
2.3	0.475			
		0.138	0.672	0.093
2.4	0.337			
		0.094	0.721	0.068
2.5	0.243			
		0.066	0.764	0.050
2.6	0.177			
		0.046	0.802	0.037
2.7	0.130			
		0.033	0.834	0.028
2.8	0.097			
		0.021	0.862	0.019
2.9	0.076			
		0.012	0.886	0.011
3.0	0.064			
		0.010	0.906	0.009
3.1	0.054			
		0.054	0.930	0.050

$$\overline{P_F = \Sigma = 2.235 * 10^{-6}}$$

Table AA.4
Frequency of Onset of Significant Inelastic Deformation
FOSID for EGC ESP Hazard Curves

β	ASCE Method FOSID *1x10^{-5}/yr				
	1 Hz	2.5 Hz	5 Hz	10 Hz	Average 5 & 10 Hz
0.3	1.06	1.03	1.02	0.97	0.99
0.4	0.93	0.95	0.94	0.87	0.90
0.5	0.69	0.71	0.69	0.62	0.66
0.6	0.54	0.58	0.57	0.50	0.53

Table AA.5
Seismic Core Damage Frequency SCDF for
EGC ESP Hazard Curves

β	ASCE Method SCDF $F_{1\%}$ = 1.67 *1x10^{-5}/yr				
	1 Hz	2.5 Hz	5 Hz	10 Hz	Average 5 & 10 Hz
0.3	0.39	0.26	0.22	0.16	0.19
0.4	0.27	0.17	0.14	0.11	0.12
0.5	0.20	0.12	0.11	0.086	0.096
0.6	0.15	0.10	0.087	0.078	0.082

NRC Letter Dated: 08/26/2005

NRC DSER Open Item 2.5.4-1

Section 2.5.4.3.2 - The staff reviewed the applicant's comparison of the soil properties between the two sites in Section 5.2 of SSAR Appendix A. The staff's review included a comparison between SPT blowcount values, in situ dry density, moisture content, Atterberg limits, compressibility and strength characteristics, P- and S-wave velocities, and modulus and damping properties. In addition, the staff also reviewed the tabulated statistical summaries of the geotechnical test results that the applicant provided in response to RAI 2.5.4-1. Figures 5-7 through 5-18 in SSAR Appendix A provide an excellent visual comparison of the engineering properties between the CPS and ESP sites. While there are some outliers, for the most part the staff concurs with the applicant's conclusion that the subsurface conditions are similar between the two sites. As such, the staff concludes that the applicant has sufficiently sampled the ESP site subsurface in order to establish the similarity between the CPS and ESP sites. The staff notes that 76 locations were drilled and sampled by the licensee for the CPS site investigation and that some of these locations (10) overlapped with the ESP site area. Regarding future subsurface investigations for the ESP site, the applicant stated the following:

> The work being carried out for the EGC ESP was being done before reactor plant design had been selected. Therefore, some of the spacing and depth requirements given in Appendix C of Regulatory Guide 1.132 could not be established. Once a reactor plant design is selected, then the requirements in Appendix C of Regulatory Guide 1.132 will be reviewed again during the COL stage, along with the design requirements of the reactor plant design, to determine whether additional drilling and sampling is needed.

Concerning the appropriate spacing of borings or soundings, RG 1.132 states that for favorable uniform geologic conditions, at least one boring should be made at the location of every safety-related structure. Where variable conditions occur, RG 1.132 states that the spacing between borings should be smaller. For larger, heavier structures, such as the containment and auxiliary buildings, RG 1.132 recommends a boring spacing of at least 100 ft with a number of additional borings along the periphery, at corners, and other selected locations. Regarding the appropriate depth for borings, RG 1.132 states that all borings should extend at least 33 ft below the lowest part of the foundation. With regard to these recommendations in RG 1.132, the staff cannot accept the applicant's concluding statement to review RG 1.132 at the COL stage to "determine whether additional drilling and sampling is needed" as sufficient. While the staff's review of the applicant's geotechnical field and laboratory test results confirmed the similarity between the CPS and ESP subsurface soil layers and properties, this similarity does not eliminate the need for further soil borings during the COL stage. There are enough variations in the soil properties within the ESP site itself to necessitate further exploration at the COL stage. Examples include variations in SPT blowcount values, S-wave velocities, and other static and dynamic properties, which may indicate localized areas of variable subsurface material. This is Open Item 2.5.4-1.

EGC RAI ID: SOI2-7

EGC RESPONSE:

This Open Issue deals with the need for additional field drilling and sampling of soil at the EGC ESP Site during the COL stage of the project. Wording in the EGC ESP indicates that the need for additional explorations will be determined during the COL stage. This wording will be revised to indicate that additional exploration work is expected consistent with the following information.

If this site is selected in the future for a COL application, additional explorations will be conducted by the COL contractor for the final design of the selected reactor system. This additional exploration work will include a sufficient amount of drilling and sampling to characterize soil conditions and collect soil samples for laboratory testing necessary for the final design of the foundations for the structures. The numbers and locations of the additional explorations will depend on the depth and plan view area of the foundation for the selected reactor system, the net weight of the various components of the reactor system, and the sensitivity of the selected system to settlement. These explorations would be required to meet the standard of practice for foundation design of a large structure. Additional explorations will also be required for the new intake alignment, and could be required to assess construction methods. Examples of exploration carried out for construction evaluations could include groundwater pump tests for dewatering evaluations or collections of samples from selected areas for material re-use studies.

The COL application will consider and address Regulatory Guide 1.132 when determining the number, location, depth, and type of explorations. The specific scope of final design explorations will also consider the design requirements of the structure and the uniformity of conditions encountered during the COL explorations relative to previous information and relative to design requirements such that appropriate and sufficient information is available for final design of the selected reactor system.

ASSOCIATED EGC ESP APPLICATION REVISIONS:

1) Revise SSAR Appendix A, Section 1.1.3, third paragraph, last two sentences, from:

Whether additional explorations and laboratory testing will be required for the COL stage depends on the foundation design requirements for the selected system. This decision will consider the importance of soil-property variation to system performance and the apparent margin in performance for the selected system in light of the potential soil-property variation.

To read:

Additional explorations and laboratory testing required for the COL stage to meet final design requirements depends on the foundation design requirements. The COL applicant will utilize the guidance provided in Regulatory Guide 1.132 when planning the locations, depths, and types of explorations for the final design. The scope of future final design explorations will also consider the importance of soil-property variation to system performance and the apparent margin in performance for the selected system in light of the potential soil-property variation.

2) Revise SSAR Appendix A, Section 3.1.1, third paragraph, second bullet, last sentence, from:

Once a reactor plant design is selected, then the requirements in Appendix C of Regulatory Guide 1.132 will be reviewed again during the COL stage, along with the design requirements of the reactor plant design, to determine whether additional drilling and sampling is needed.

To read:

Once a reactor plant design is selected (during the COL stage), the guidance of Appendix C of Regulatory Guide 1.132 will be utilized, along with the design requirements of the reactor plant design, to determine the locations, depths and types of additional drilling and sampling needed for the final design of the foundation system.

3) Revise SSAR Appendix A, Section 7, first paragraph, last sentence, from:

However, additional geotechnical work could be required at the COL stage to address reactor plant design-specific geotechnical design criteria.

To read:

However, additional geotechnical work will be required at the COL stage to address reactor plant design-specific geotechnical design criteria.

4) Revise SSAR Appendix A, Section 7.2, first paragraph, from:

The geotechnical work completed for the EGC ESP Site is not necessarily sufficient for final design of the selected reactor plant design. Additional field explorations, laboratory testing, and engineering studies may be required depending on the specific characteristics of the selected system. The extent of any additional explorations, laboratory testing, and engineering studies, if any are required, cannot be determined at this time. They will depend on the footprint and depth of the structures, the net weight, and the sensitivity of their performance to variations in soil properties. Nothing was identified during the geotechnical work described in this Geotechnical Report that would make any of these future investigations or studies particularly risky or difficult.

To read:

The geotechnical work completed for the EGC ESP Site is not considered sufficient for final design of the selected reactor plant design. Additional field explorations, laboratory testing, and engineering studies will be required. The extent of any additional explorations, laboratory testing, and engineering studies, if any are required, cannot be determined at this time. They will depend on the footprint and depth of the structures, the net weight, and the sensitivity of their performance to variations in soil properties. Regulatory Guide 1.132 will be utilized, together with foundation design requirements, to determine the locations, depths, and types of additional explorations. Nothing was identified during the geotechnical work described in this Geotechnical Report that would make any of these future investigations or studies particularly risky or difficult.

ATTACHMENTS:

None

NRC Letter Dated: 08/26/2005

NRC DSER Permit Condition 2.5-1

Sections 2.5.4.3.8 & 2.5.4.3.12 - Based on its review of SSAR Section 2.5.4.8 and the applicant's response to RAI 2.5.4-6, described above, the staff concludes that the applicant has employed an acceptable methodology to determine the liquefaction potential of the soil underlying the ESP site. Because portions of the upper 60 ft of soil are susceptible to liquefaction, the applicant stated that these soils would be either removed or replaced or improved to reduce any liquefaction potential. This is Permit Condition 2.5-1.

EGC RAI ID: SPC2-1

EGC RESPONSE:

This action is consistent with COL expectations as expressed in EGC ESP SSAR Section 2.5.4.12. Therefore, EGC has no comment on this proposed ESP Permit Condition.

ASSOCIATED EGC ESP APPLICATION REVISIONS:

None

ATTACHMENTS:

None

NRC Letter Dated: 08/26/2005

NRC DSER COL Action Item 2.5.4-1

Section 2.5.4.3.3 - Section 2.5.4.3 of RS-002 directs the staff to compare the applicant's plot plans and the profiles of all seismic Category I facilities with the subsurface profile and material properties. Based on this comparison, the staff can determine if (1) the applicant performed sufficient exploration of the subsurface and (2) the applicant's foundation design assumptions contain adequate margins of safety. The applicant decided to provide this information as part of its COL submittal. Submission of the applicant's plot plans and the profiles of all seismic Category I facilities for comparison with the subsurface profile and material properties is COL Action Item 2.5.4-1.

EGC RAI ID: SAI2-1

EGC RESPONSE:

This action is consistent with COL expectations as expressed in EGC ESP SSAR Sections 2.5.4.5, 2.5.4.12, and 2.5.4.14. Therefore, EGC has no comment on this proposed COL Action Item.

ASSOCIATED EGC ESP APPLICATION REVISIONS:

None

ATTACHMENTS:

None

NRC Letter Dated: 08/26/2005

NRC DSER COL Action Item 2.5.4-2

Section 2.5.4.3.5 - Since the applicant has not selected a reactor design or location within the ESP site, it did not provide detailed excavation and backfill plans or plot plans and profiles as outlined in Section 2.5.4 of RS-002. Therefore, the staff could not adequately evaluate the applicant's excavation and backfill plans and will await future submittal of these plans as part of the COL or CP application. This is COL Action Item 2.5.4-2.

EGC RAI ID: SAI2-2

EGC RESPONSE:

This action is consistent with COL expectations as expressed in EGC ESP SSAR Sections 2.5.4.5, 2.5.4.12, and 2.5.4.14. Therefore, EGC has no comment on this proposed COL Action Item.

ASSOCIATED EGC ESP APPLICATION REVISIONS:

None

ATTACHMENTS:

None

NRC Letter Dated: 08/26/2005

NRC DSER COL Action Item 2.5.4-3

Section 2.5.4.3.5 - SSAR Section 2.5.4.14 states that the applicant will map any future excavation associated with the construction of a new nuclear power plant to confirm that the soil types and consistency are in agreement with the conditions identified and interpreted from the ESP field explorations. The applicant stated that this field mapping will involve inspecting excavated slopes for the presence of previously unknown fault offsets. The applicant also committed to inform the NRC staff (1) if it encounters previously unknown geologic features that could represent a hazard to the plant and (2) when site excavations are open for examination and evaluation. These commitments comprise COL Action Item 2.5.4-3.

EGC RAI ID: SAI2-3

EGC RESPONSE:

This action is consistent with commitments in EGC ESP SSAR Section 2.5.4.14. Therefore, EGC has no comment on this proposed COL Action Item.

ASSOCIATED EGC ESP APPLICATION REVISIONS:

None

ATTACHMENTS:

None

NRC Letter Dated: 08/26/2005

NRC DSER COL Action Item 2.5.4-4

Section 2.5.4.3.6 - Since the applicant has not selected a reactor design or location within the ESP site, it did not provide an evaluation of ground water conditions as they affect foundation stability or detailed dewatering plans as outlined in Section 2.5.4 of RS-002. Therefore, the staff could not evaluate the ground water conditions as they affect the loading and stability of foundation materials or the applicant's dewatering plans during construction as well as ground water control throughout the life of the plant. As such, the staff will await the future submittal of these evaluations and plans as part of the COL or CP application. The need to evaluate ground water conditions as they affect foundation stability or detailed dewatering plans is COL Action Item 2.5.4-4.

EGC RAI ID: SAI2-4

EGC RESPONSE:

This action is consistent with dewatering commitments in EGC ESP SSAR Appendix A Section 6.5 and with general expectations for foundation design requirements. Therefore, EGC has no comment on this proposed COL Action Item.

ASSOCIATED EGC ESP APPLICATION REVISIONS:

None

ATTACHMENTS:

None

NRC Letter Dated: 08/26/2005

NRC DSER COL Action Item 2.5.4-5

Section 2.5.4.3.10 - Since, as the applicant points out, the minimum bearing capacity value established by the applicant provides an FOS greater than 1.5 compared to the minimum calculated bearing capacity for the CPS Category I structures, the staff finds that this value is appropriate as a PPE for the ESP site. This finding is based on the applicant's commitment to excavate approximately 55 ft below the ground surface and to backfill with highly compacted granular fill. In addition, the average undrained shear strength of the Illinoian till must be similar to that underlying the CPS site. The applicant stated that the actual foundation depth, size, and shape, structure locations, and settlement limits "will be considered to confirm the final ultimate bearing capacity at COL." The need for the COL or CP applicant to perform a complete static stability assessment (including bearing capacities, settlement analyses, and lateral load assessment) and to ensure that the bearing capacities meet the minimum value of 25 tsf comprises COL Action Item 2.5.4-5.

EGC RAI ID: SAI2-5

EGC RESPONSE:

This action is consistent with commitments in EGC ESP SSAR Section 2.5.4.10. Therefore, EGC has no comment on this proposed COL Action Item.

ASSOCIATED EGC ESP APPLICATION REVISIONS:

None

ATTACHMENTS:

None

NRC Letter Dated: 08/26/2005

NRC DSER COL Action Item 2.5.4-6

Section 2.5.4.3.11 - SSAR Section 2.5.4.11 states that the design criteria for the ESP site Category I structures will be established during the COL stage. Since the applicant has not selected a reactor design or location within the ESP site, its deferral of a description of the design criteria to the COL stage is acceptable to the staff. The need for the COL or CP applicant to describe the design criteria and methods, including the FOSs from the design analyses, is COL Action Item 2.5.4-6.

EGC RAI ID: SAI2-6

EGC RESPONSE:

This action is consistent with commitments in EGC ESP SSAR Section 2.5.4.11. Therefore, EGC has no comment on this proposed COL Action Item.

ASSOCIATED EGC ESP APPLICATION REVISIONS:

None

ATTACHMENTS:

None

NRC Letter Dated: 08/26/2005

NRC DSER COL Action Item 2.5.5-1

Section 2.5.5.3 - In SSAR Section 2.5.5, the applicant provided a general description of its plan for future slope stability analyses at the COL stage. Although the general description was useful to the staff in performing a complete review, the COL or CP applicant will need to provide detailed slope stability analyses. This is COL Action Item 2.5.5-1.

EGC RAI ID: SAI2-7

EGC RESPONSE:

This action is consistent with commitments in EGC ESP SSAR Section 2.5.5. Therefore, EGC has no comment on this proposed COL Action Item.

ASSOCIATED EGC ESP APPLICATION REVISIONS:

None

ATTACHMENTS:

None

NRC Letter Dated: 08/26/2005

NRC DSER COL Action Item 2.5.6-1

Section 2.5.6.3 - SSAR Section 2.5.6 states that the ESP facility will use cooling towers for cooling, with Clinton Lake being used to provide makeup water to the cooling towers. Since the ESP facility will use the CPS UHS to supply makeup water to the cooling towers, the applicant stated that it would perform evaluations (if appropriate) at the COL stage to assess the performance of the submerged dam forming the UHS under the ESP SSE ground motion. The applicant's decision to delay this evaluation until the COL stage is acceptable to the staff. This is COL Action Item 2.5.6-1.

EGC RAI ID: SAI2-8

EGC RESPONSE:

With the recognition that such an assessment would not be appropriate or necessary unless the ESP facility design utilizes the CPS UHS for water supply makeup to an ESP water-cooled UHS, this action is consistent with commitments in EGC ESP SSAR Section 2.5.6. Therefore, EGC has no comment on this proposed COL Action Item.

ASSOCIATED EGC ESP APPLICATION REVISIONS:

None

ATTACHMENTS:

None

EPRI | ELECTRIC POWER RESEARCH INSTITUTE

Program on Technology Innovation: Assessment of a Performance-Based Approach for Determining Seismic Ground Motions for New Plant Sites, V2

Volume 2: Seismic Hazard Results at 28 Sites

Technical Report

Program on Technology Innovation: Assessment of a Performance-Based Approach for Determining Seismic Ground Motions for New Plant Sites, V2

Volume 2: Seismic Hazard Results at 28 Sites

1012045

Final Report, August 2005

Cosponsor
U.S. Department of Energy
Office of Nuclear Energy
Science & Technology
19901 Germantown Road, NE-20
Germantown, MD 20874-1290

EPRI Project Manager
R. Kassawara and L. Sandell

Electric Power Research Institute • 3420 Hillview Avenue, Palo Alto, California 94304 • PO Box 10412, Palo Alto, California 94303 • USA
800.313.3774 • 650.855.2121 • askepri@epri.com • www.epri.com

DISCLAIMER OF WARRANTIES AND LIMITATION OF LIABILITIES

ORGANIZATION(S) THAT PREPARED THIS DOCUMENT

Risk Engineering, Inc.

Pacific Engineering & Analysis

ORDERING INFORMATION

Requests for copies of this report should be directed to EPRI Orders and Conferences, 1355 Willow Way, Suite 278, Concord, CA 94520, (800) 313-3774, press 2 or internally x5379, (925) 609-9169, (925) 609-1310 (fax).

CITATIONS

This report was prepared by

Risk Engineering, Inc.
4155 Darley Avenue, Suite A
Boulder, CO 80305

Principal Investigator
R. McGuire

Pacific Engineering & Analysis
311 Pomona Avenue
El Cerrito, CA 94530

Principal Investigator
W. Silva

This report describes research sponsored by the Electric Power Research Institute (EPRI) and U.S. Department of Energy.

The report is a corporate document that should be cited in the literature in the following manner:

Program on Technology Innovation: Assessment of a Performance-Based Approach for Determining Seismic Ground Motions for New Plant Sites, V2: Volume 2: Seismic Hazard Results at 28 Sites. EPRI, Palo Alto, CA and U.S. Department of Energy, Germantown, MD: 2005. 1012045.

PRODUCT DESCRIPTION

Interest in recent years in early site permits (ESPs) for new nuclear plants has prompted a reevaluation of seismic design criteria and a reexamination of the basis for current criteria. Currently, Regulatory Guide 1.165 bases seismic design requirements on probabilistic seismic hazard analyses (PSHAs) at 29 nuclear plant sites using results that were published in 1989 and 1994. Much new work has been undertaken since to better understand earthquakes in the Central and Eastern United States (CEUS) and associated strong ground motions. This study recalculates seismic hazard at 28 of the original 29 nuclear plant sites, accounting for new information as a basis for further work to redefine seismic criteria for new nuclear plants in the CEUS.

Results & Findings

This work calculates probabilistic seismic hazard at 28 nuclear plant sites in the CEUS for ground motions between the peak ground acceleration (PGA, at 100 Hz) and 1 Hz. New information on seismic sources in the CEUS has been incorporated in the probabilistic estimates, and a new comprehensive model of ground motion (quantifying both aleatory and epistemic uncertainty) has been used. The seismic hazard results define means and fractiles of spectral accelerations with annual frequencies of exceedance between 10^{-3} and 10^{-7}.

Challenges & Objective(s)

This report will be useful in establishing the basis for seismic design of new nuclear plants in the CEUS. Current regulations (Regulatory Guide 1.165) lead to overly conservative requirements for seismic design, and the current study will allow further analyses to show that performance-based methods for establishing seismic criteria (such as that proposed by a committee of the American Society of Civil Engineers) are reasonable and result in seismically safe plants.

Applications, Values & Use

These results can be used in several ways. First, the seismic design values recommended by performance-based procedures can be calculated for the 28 nuclear plants and can be compared to current design levels to evaluate consistency with current practice. Second, simple models of nuclear plant seismic behavior can be used with the seismic hazard calculated here to compare to calculated annual frequencies of seismically induced core melt from detailed probabilistic risk assessments done for existing nuclear plants. This comparison also will allow evaluations of consistency between seismic designs determined with performance-based procedures and estimates of current nuclear plant safety.

EPRI Perspective

This study could only be undertaken by an industry group such as EPRI that has a broad perspective on nuclear plant policy and that can make a substantial independent contribution to solving design issues. The current seismic design requirements of Regulatory Guide 1.165 are

based on seismic hazard estimates that are approaching 20 years, and applying for exemptions on a site-by-site basis would likely be time-consuming and perhaps unsuccessful.

Approach

The approach taken here was to use new information on earthquake sources in the CEUS and on earthquake ground motion estimation and to modify earlier work published by EPRI in 1989. The three 2003 ESP applications for nuclear plants in the CEUS contain substantial, detailed, new information on seismic sources, and a large study published by EPRI in 2004 contains a comprehensive model for estimating seismic ground motions. This information leads to a comprehensive, justifiable set of assumptions for calculating probabilistic seismic hazard. For some sites, a study of dynamic site response was undertaken. Information on site properties for these sites was taken from existing final safety analysis reports (FSARs) for these sites and from the three ESP applications.

Keywords

Probabilistic seismic hazard analysis (PSHA)
Seismic design criteria
New nuclear plant deployment

ABSTRACT

Probabilistic seismic hazard analyses are calculated at 28 nuclear plant sites in the Central and Eastern United States for ground motions with spectral frequencies between 100 Hz and 1 Hz. New information on seismic sources in the region is incorporated in the probabilistic estimates, and a new comprehensive model of ground motion (quantifying both aleatory and epistemic uncertainty) is used. These seismic hazard results quantify the means and fractiles of spectral accelerations with annual frequencies of exceedance between 10^{-3} and 10^{-7}. Results also are calculated as uniform hazard spectra. These hazard results can be used to determine appropriate seismic design criteria for new plants.

ACKNOWLEDGMENTS

This material is based upon work supported by the U.S. Department of Energy under Award No. DE-FC07-04ID14533. EPRI would also like to recognize the support provided by Adrian Heymer and Cedric Jobe of the Nuclear Energy Institute.

CONTENTS

LIST OF FIGURES

LIST OF TABLES

1
INTRODUCTION

This report examines seismic hazard at 28 nuclear plant sites in the Central and Eastern United States (CEUS). It builds upon seismic hazard results reported by EPRI (1989), updating those results to account for new information regarding earthquake occurrences and the associated ground motions.

The 28 sites investigated here constitute a majority of the 29 sites used to establish a reference probability in Regulatory Guide 1.165 (USNRC, 1997). (The Callaway site is not included in this study.) Plants are founded on hard rock, soft rock, and soil of varying thickness and stiffness. Descriptions of site foundation materials are given in Section 3, and site-response calculations are described in Section 5.

In a separate study, these seismic hazard calculations are used to examine the seismic design recommendations for nuclear plants made by ASCE (2005).

2
SEISMIC HAZARD INPUTS

2.1 EPRI Seismic Sources

The seismic hazard calculations conducted here build on the calculations made for the EPRI-Seismicity Owners Group (SOG) study of seismic hazard at nuclear sites in the CEUS (EPRI, 1989). Those calculations used seismic source inputs specified by six Earth Science Teams (ESTs), and used three ground motion equations to calculate the mean and fractiles of seismic hazard at 57 nuclear plant sites. Site-specific reports for each of the 57 nuclear plant sites specify the seismic sources and source combinations used to calculate seismic hazard in the 1989 study. An additional resource used to replicate the assumptions of the 1989 study was the documentation by Risk Engineering, Inc (1989).

2.2 Changes and Additional Seismic Sources

For seismic sources, significant new information has become available on the occurrence of large earthquakes in the CEUS. Three Early Site Permit (ESP) applications (Dominion, 2003; Entergy, 2003; Exelon, 2003) have been submitted to the US Nuclear Regulatory Commission in recent years. All three studies used the EPRI-SOG study as a basis and examined seismicity in the CEUS and determined how the EPRI-SOG sources should be updated to reflect more recent information.

Changes to seismic sources developed in the EPRI-SOG study are concentrated in five regions:

1. Charleston seismic zone. This source of a large historical earthquake on the East Coast in 1886 was modeled with exponential magnitude distributions by the six EPRI-SOG ESTs, with large earthquakes (M~6.8 to 7.3) having a recurrence interval of several thousand years. More recent information indicates a mean recurrence interval of about 550 years for the same magnitude event. Further, an East Coast fault system has been hypothesized for the Charleston region and farther north into North Carolina, although this structure is given a low probability of existence and a low probability of activity if it exists outside of South Carolina (Dominion, 2003). This fault system is modeled with two additional East Coast faults, following Dominion (2003). The shorter recurrence interval for large earthquakes in the Charleston seismic zone is modeled with an additional East Coast fault, in addition to the Charleston sources defined by the EPRI-SOG teams, following the Dominion (2003) ESP application.

2. New Madrid seismic zone. This source of three large historical earthquakes in the Central US during 1811-1812 was modeled by the six EPRI-SOG ESTs using exponential magnitude

distributions with activity rates estimated from lower-level seismicity. The recurrence interval of the largest earthquakes (M~7.5 to 8.2) was estimated to be several thousand years. More recent evidence indicates a mean recurrence interval of about 500 years for these large earthquakes. They were modeled with additional faults in the New Madrid seismic zone: the Blytheville Arch fault, the East Prairie fault, and the Reelfoot rift fault. A cluster model was used to represent the occurrence of multiple earthquakes on separate faults, as happened over a period of three months in 1811-1812. The cluster model represented the possibility of two or three events occurring within a short period of time, with a mean recurrence (of the cluster) of about 500 years. These three faults were used in addition to the New Madrid seismic zone specified by each of the six EPRI-SOG ESTs, following the model described in Exelon (2003, Appendix B, Section 4.1.1).

3. Wabash Valley and Illinois regions. The seismicity north of the New Madrid seismic zone was modeled by each of the EPRI-SOG ESTs, using a variety of seismic sources. Studies of paleo-earthquake evidence indicate that moderate-to-large earthquakes have occurred in this region in prehistoric times; therefore, the maximum magnitudes of EPRI-SOG team sources were revised upward to reflect this new evidence. In sources representing the Wabash Valley-Southern Illinois region, maximum magnitudes in the range M~7.3 to 7.5 were used. For the Central Illinois region, maximum magnitudes in the range M~6.3 to 7 were used. For both regions, the maximum magnitude distributions described in Exelon (2003, Appendix B, Sections 4.1.2 and 4.1.3) were adopted.

4. Saline River source. Several lineaments in Southern Arkansas prompted Entergy (2003) to define a seismic source southwest of the New Madrid seismic zone that may have the potential to produce M=6 to 7 earthquakes, based on paleoliquefaction and other evidence. Mean recurrence intervals for these earthquakes are estimated to be between 1000 years and 125,000 years, depending on the earthquake magnitude. This source was modeled as an area source.

5. Gulf Coast region. Many seismic sources in the Gulf Coast had maximum magnitude distributions assigned by EPRI-SOG teams that extended below m_b=5.0. The Entergy (2003) study reviewed these sources and revised the maximum magnitude distributions, using a minimum M_{max} value of 5.0 (corresponding to $m_{b,\,max}$~5.4) (Entergy, 2003, Section 2.5.2, page 2.5-49).

Several inconsistencies among assumptions in the three ESP applications were addressed. Two of the three ESP applications used a minimum magnitude for seismic hazard calculations of m_b=5.0 (following EPRI, 1989), and the third used a minimum magnitude of M=5.0 (which corresponds to m_b~5.4). For this study we followed the assumption of two of the three ESP applications and adopted a minimum magnitude of m_b=5.0. The Exelon (2003) study used the cluster model to describe earthquake occurrences on the New Madrid faults; the Entergy (2003) study assumed that earthquake occurrences on each fault were independent. This study adopted the cluster model as being more representative of the current understanding of earthquake occurrences in the New Madrid seismic zone.

2.3 Ground Motion Equations

The ground motion equations used in this study are the ones developed by the Electric Power Research Institute (EPRI, 2004) specifically for the CEUS. These consist of estimates of mean log spectral acceleration for 7 structural frequencies (100, 25, 10, 5, 2.5, 1, and 0.5 Hz) and estimates of logarithmic standard deviation. Epistemic uncertainties in both the mean log spectral acceleration and in the logarithmic standard deviation are represented with alternative models, each with an assigned weight. Different models are recommended based on whether the source of earthquakes is in the Mid-Continent region or the Gulf Coast region, whether the source is a general-area source or a non-general-area source, whether the source represents a rifted or non-rifted tectonic feature, and whether the source is modeled with a point or an extended rupture.

3
SITES STUDIED

3.1 Overview

Twenty-eight sites were studied in this project, those being the majority of sites examined in Reg. Guide 1.165 (USNRC, 1997). (A twenty-ninth site studied in USNRC, 1997, the Callaway site, was not studied here because it was not included in the 1989 EPRI study results.) Table 3-1 lists the 28 sites studied in this project and the site category designated in the USNRC (1997) study and in the EPRI (1989) study.

Twelve of the 28 sites were designated as rock sites by both the USNRC (1997) and EPRI (1989) studies, so these were treated as rock sites here, with no site-specific calculations. Sixteen of the 28 sites were designated as some category of soil by either the USNRC (1997) study, the EPRI (1989) study, or both. For some sites, the USNRC (1997) study indicated rock plus a soil category at sites where critical facilities are founded on both. Soil categories used in the USNRC (1997) study are as follows:

- Sand-S1 increasing V_s with depth 25 to 80 feet
- Sand-S2 increasing V_s with depth 80 to 180 feet
- Sand-S3 increasing V_s with depth 180 to 300 feet
- Till-S1 constant V_s with depth 25 to 80 feet
- Till-S2 constant V_s with depth 80 to 180 feet
- Till-S3 constant V_s with depth 180 to 300 feet
- Deep soil all soils >300 feet

where V_s is shear-wave velocity. Soil categories used in the EPRI (1989) study are as follows:

- I 10-30 feet
- II 30-80 feet
- III 80-180 feet
- IV 180-400 feet
- V >400 feet

Table 3-1
28 Plant Sites and Assigned Site Categories

Plant site	EPRI site category	NRC site category	Comments
Beaver Valley	Soil-III	Sand-S1	Site-specific calculation, see Section 4
Bellefonte	Rock	Rock	Treated as rock site
Braidwood	Rock	Rock	Treated as rock site
Brunswick	Soil-III	Sand-S1	Site-specific calculation, see Section 4
Byron	Rock	Rock	Treated as rock site
Catawba	Rock	Rock/Sand-S1	Site-specific calculation, see Section 4
Clinton	Soil-IV	Till-T3	Site-specific calculation, see Section 4
Comanche Peak	Rock	Rock	Treated as rock site
Davis Besse	Rock	Rock	Treated as rock site
Grand Gulf	N/A*	Deep soil	Site-specific calculation, see Section 4
Hope Creek	Soil-V	Deep soil	Site-specific calculation, see Section 4
LaSalle	Soil-III	Till-T2	Site-specific calculation, see Section 4
Limerick	Rock	Rock	Treated as rock site
McGuire	Rock	Rock	Treated as rock site
Millstone	Rock	Rock	Treated as rock site
Nine Mile Point	Rock	Rock/Sand-S1	Site-specific calculation, see Section 4
North Anna	Rock	Rock/Sand-S1	Site-specific calculation, see Section 4
Perry	Rock	Rock	Treated as rock site
River Bend	Site-specific soil	Deep soil	Site-specific calculation, see Section 4
Seabrook	Rock	Rock	Treated as rock site
Shearon Harris	Rock	Sand-S1	Site-specific calculation, see Section 4
South Texas	Site-specific soil	Deep soil	Site-specific calculation, see Section 4
Summer	Rock	Rock/Sand-S1	Site-specific calculation, see Section 4
Three Mile Island	Rock	Rock/Sand-S1	Site-specific calculation, see Section 4
Vogtle	Soil-V	Deep soil	Site-specific calculation, see Section 4
Waterford	Site-specific soil	Deep soil	Site-specific calculation, see Section 4
Watts Bar	Rock	Rock	Treated as rock site
Wolf Creek	Rock	Rock	Treated as rock site

* Grand Gulf not included in published EPRI (1989) results, site studied later.

Figure 3-1 shows a map with the 28 sites, with a key that designates how each site was treated (rock site or site-specific calculation)

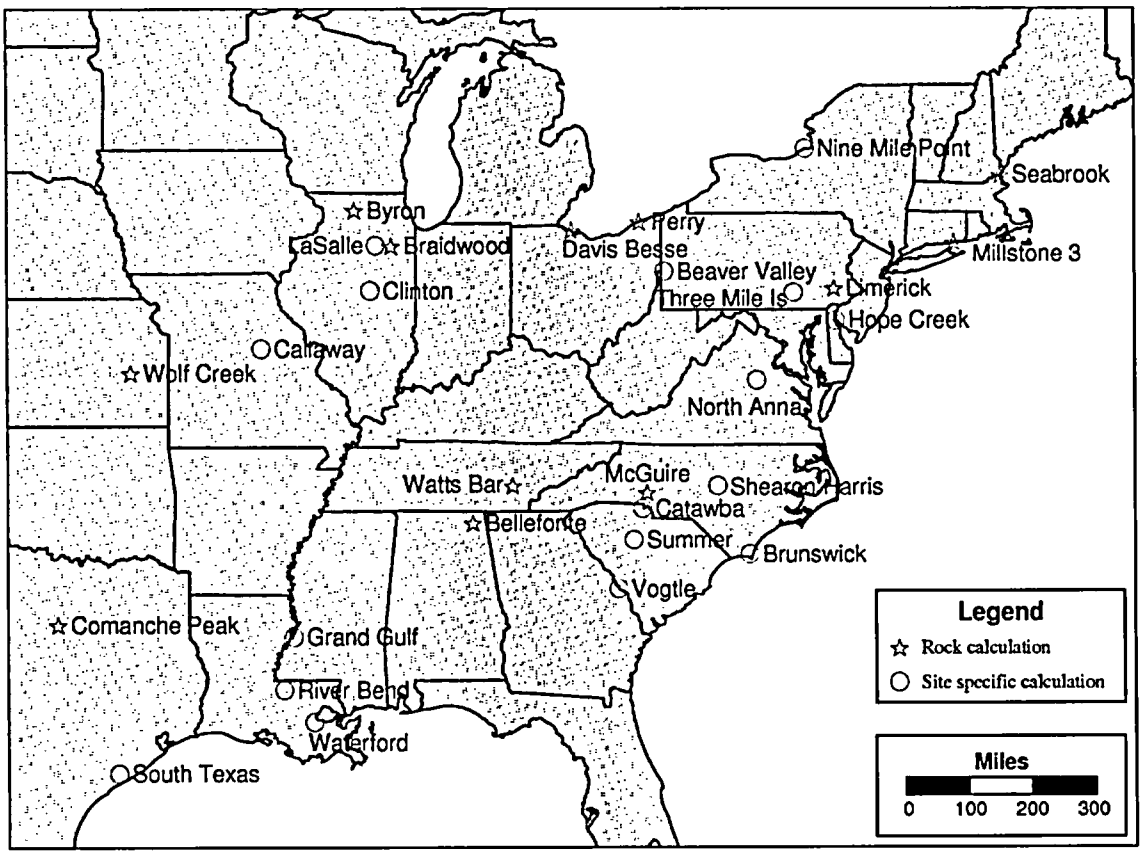

Figure 3-1
Map Showing 28 Plant Sites In the CEUS

4
ROCK HAZARD CALCULATIONS

4.1 Seismic Sources Used for Each Site

Seismic hazard calculations were done for rock conditions at each site. The EPRI-SOG seismic sources were used to calculate rock seismic hazard, as explained in Section 2 above. Some sites had additional sources added to reflect the current understanding of earthquake sources, also described in Section 2 above.

Appendix A documents the seismic sources used in the calculation of seismic hazard at each site.

4.2 Verification Studies at Four Sites with EPRI Results

Verification studies were conducted at four sites to verify that the computer code used in this project (FRISK88) accurately replicates the results obtained in the EPRI (1989) study given the same inputs. For these calculations, the original EPRI (1989) sources and ground motion equations were used without modification. The four sites were selected in four parts of the CEUS to replicate seismic hazard for four different regions. These sites were as follows:

- Northeast site
- Mid-Atlantic site
- Southeast site
- Midwest site

Tables 4-1 through 4-4 compare the seismic hazard (annual frequency of exceedence) for four peak ground acceleration (PGA) levels for the results published in the EPRI (1989) study, the replicated results in this study, and the percent difference (difference in the replicated results, compared to the original results).

Table 4-1
Northeast Site: Verification of 1989 Rock Hazard Results

PGA	Percent Difference		
(g)	Mean	Median	85th
0.05	0.08%	-3.06%	14.55%
0.10	0.18%	0.48%	2.51%
0.25	1.04%	2.00%	-1.85%
0.50	2.41%	0.84%	-8.00%

Table 4-2
Mid-Atlantic Site: Verification of 1989 Rock Hazard Results

PGA	Percent Difference		
(g)	Mean	Median	85th
0.05	-1.61%	0.05%	3.70%
0.10	-1.18%	-2.08%	4.35%
0.25	2.69%	2.07%	3.30%
0.50	6.50%	9.53%	-6.57%

Table 4-3
Southeast Site: Verification of 1989 Rock Hazard Results

PGA	Percent Difference		
(g)	Mean	Median	85th
0.05	0.94%	-1.61%	-8.39%
0.10	1.48%	1.05%	-11.71%
0.25	2.22%	4.97%	-3.51%
0.50	3.69%	3.95%	2.15%

Table 4-4
Midwest Site: Verification of 1989 Rock Hazard Results

PGA	Percent Difference		
(g)	Mean	Median	85th
0.05	-0.24%	-4.56%	-2.56%
0.10	-1.39%	-11.94%	-8.67%
0.25	1.17%	0.92%	-11.07%
0.50	6.12%	-5.11%	3.44%

Generally the results in Tables 4-1 through 4-4 show replication of the original results to within several percent, with a few results (generally the 85%) showing a difference of 12% to 15%. A 3% difference in the annual frequency of exceedence corresponds to approximately a 1% difference in ground motion for a given annual frequency of exceedence. Results were compared to PGA levels only, because the EPRI (1989) study reports mean results only for PGA, not for spectral amplitude. Results are available from EPRI (1989) only to two significant figures, which itself implies a precision of $\pm$5% (e.g. an annual frequency of 1.049E-5 would be reported as 1.0E-5, and an annual frequency of 1.050E-5 would be reported as 1.1E-5). One site used for verification is a deep soil site, and rock hazard results were obtained for verification purposes from archived electronic files rather than from EPRI (1989), which only reported soil hazard results.

4.3 Verification Studies at Three Sites with ESP Application Results

At three sites (Clinton, Grand Gulf, and North Anna), owners have submitted ESP applications for new plant construction, and these applications include seismic hazard results. Comparisons were made to published results for these three sites to verify that the current study replicates the seismic hazard obtained in those three site applications. Site-specific calculations of ground motion were made for all three sites, and comparisons were made for rock conditions using available rock results reported for each of the three sites.

Figures 4-1 and 4-2 show rock results reported for the Clinton site (Exelon, 2003), compared to results calculated in this study for rock conditions. The comparisons in Figures 4-1 and 4-2 check the EPRI-SOG seismic sources, the changes to those sources (see Section 2 above), the additional sources used for the New Madrid seismic zone (see Section 2 above), and the EPRI (2004) rock ground motion equations. Figure 4-1 replicates the median, 5%, and 95% seismic hazard for PGA, 5 Hz spectral acceleration (SA), and 1 Hz SA. There is some mismatch for the 5% fractile at annual frequencies of exceedence below 10^{-5} (the current study's results are low compared to the published results), but for the median and 95% hazard the current study accurately replicates the published Clinton results. Figure 4-2 shows that the current study accurately replicates the mean uniform hazard spectra for 10^{-4} and 10^{-5} annual frequencies of exceedence.

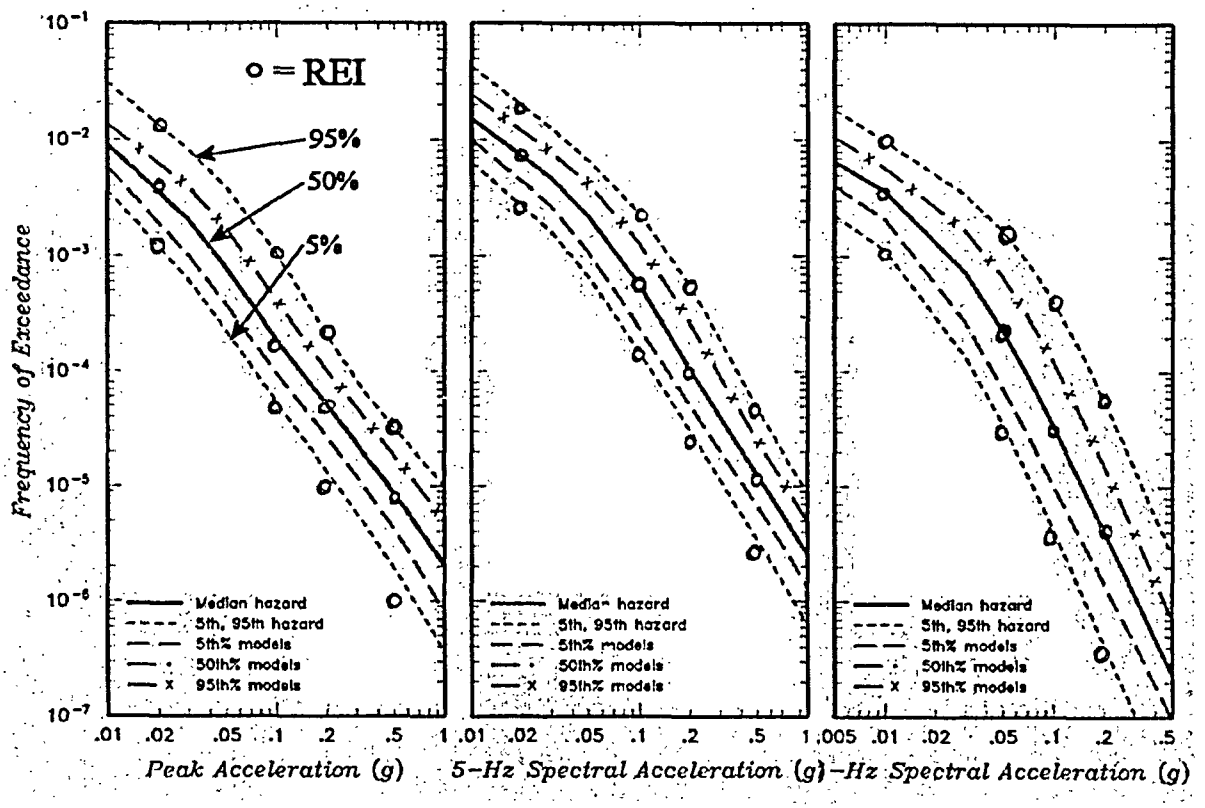

Figure 4-1
Verification of PGA, 5 Hz, and 1 Hz Rock Hazard Results for the Clinton Site (Published Results from Exelon (2003) Site Safety Analysis Report, Appendix B, Figure 4.1-12a)

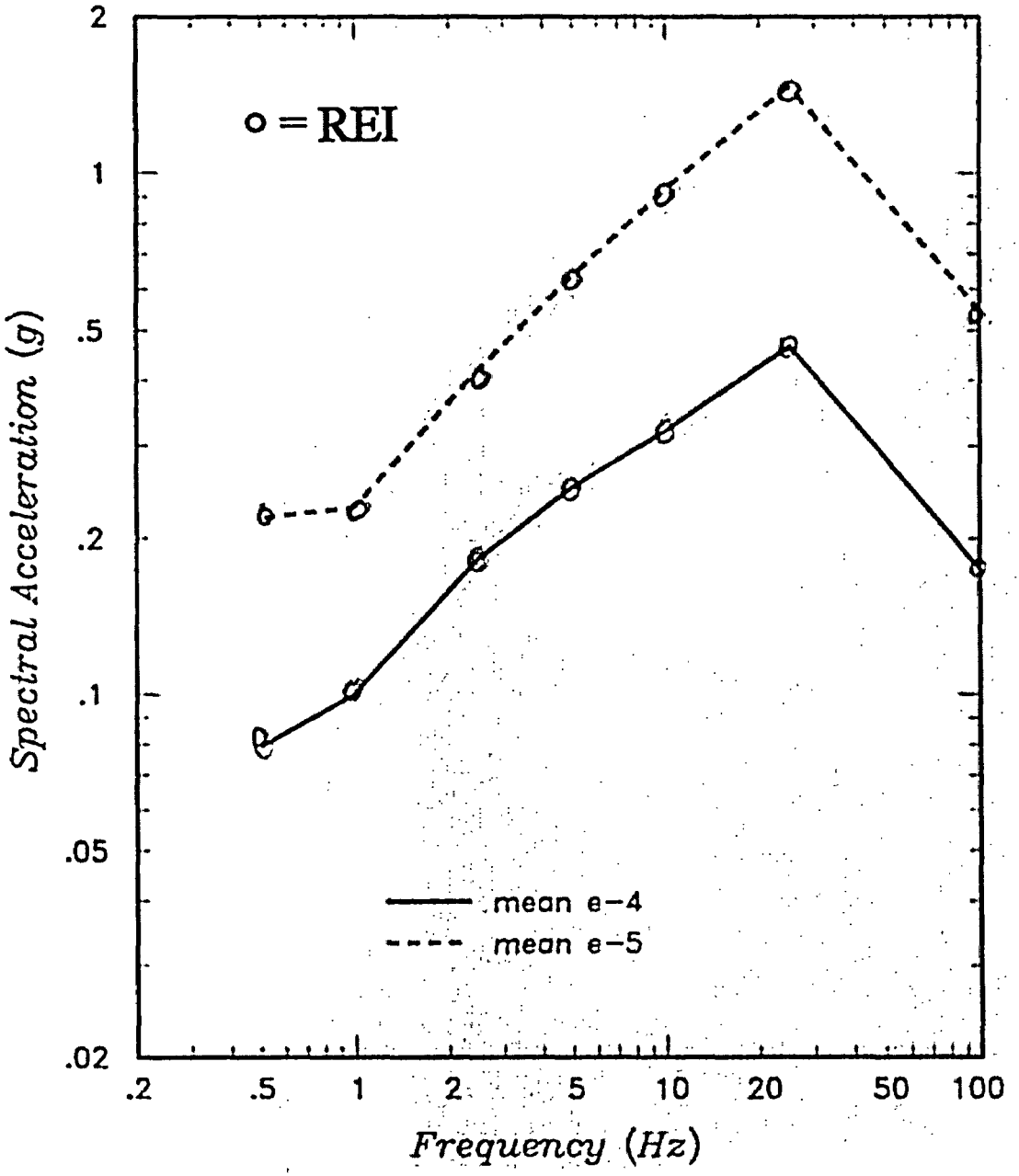

Figure 4-2
Verification of UHS Rock Results for the Clinton Site (Published Results from Exelon (2003) Site Safety Analysis Report, Appendix B, Figure 4.1-19)

Figures 4-3 and 4-4 show rock results reported for the Grand Gulf site (Entergy, 2003), compared to results calculated in this study for rock conditions. Figure 4-3 shows mean, median, 15%, and 85% seismic hazard results for 10 Hz SA, and Figure 4-4 shows a similar comparison for 1 Hz SA. Overall the comparison is excellent, with some mismatch between reported results for the 15% seismic hazard for 10 Hz SA and annual frequencies below 10^{-6} (the current study's results are high compared to the published results). For this comparison the seismic sources were modeled as reported in the Entergy (2003) report; i.e. a minimum magnitude of M=5 was used, maximum magnitudes in Gulf Coast sources were modified, and seismic sources representing the New Madrid and Saline River seismic zones were modeled as area sources at the closest approach to the Grand Gulf site.

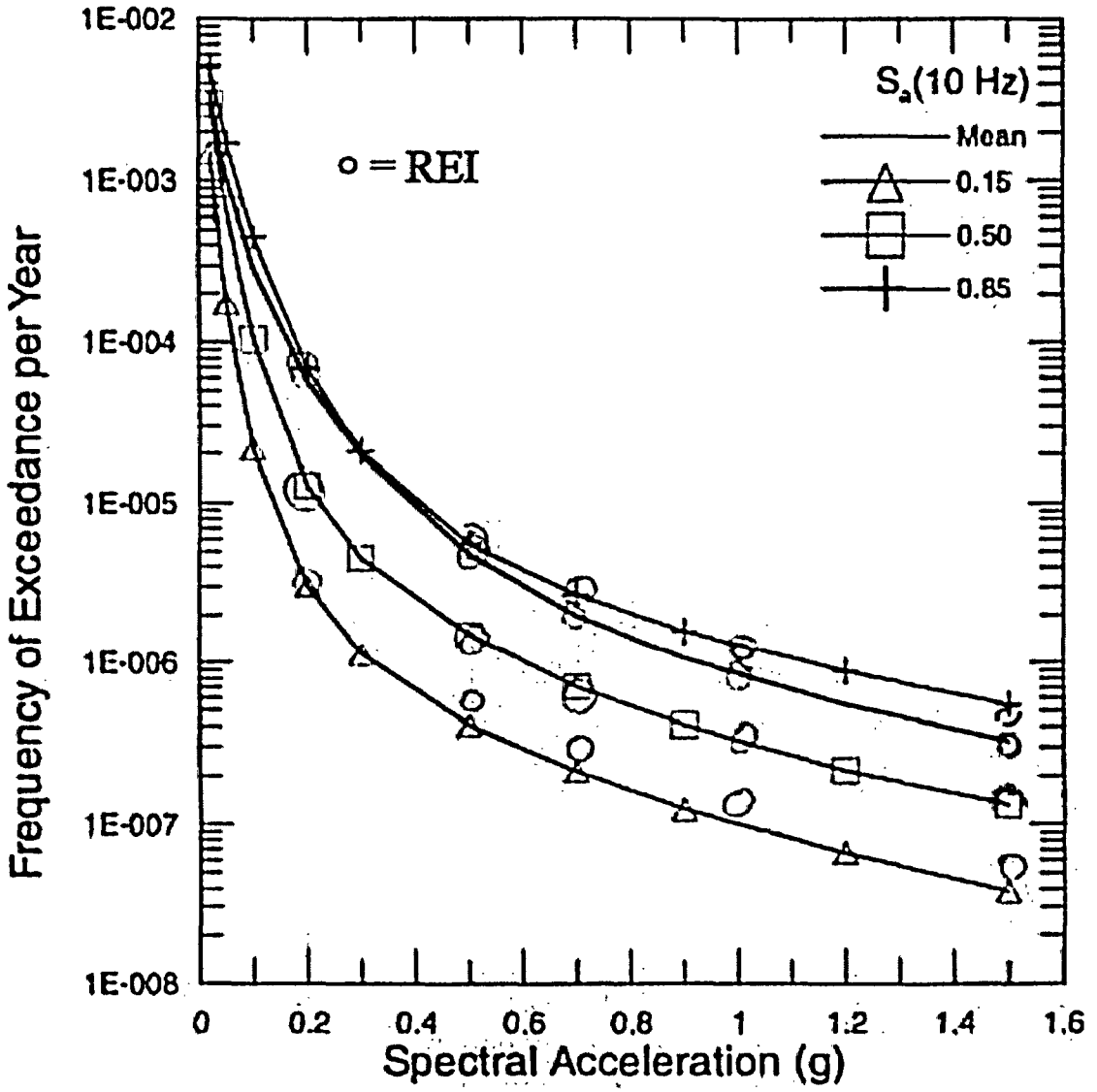

Figure 4-3
Verification of 10 Hz Rock Hazard Results for the Grand Gulf Site (Published Results from Figure 2.5-52 of Entergy, 2003)

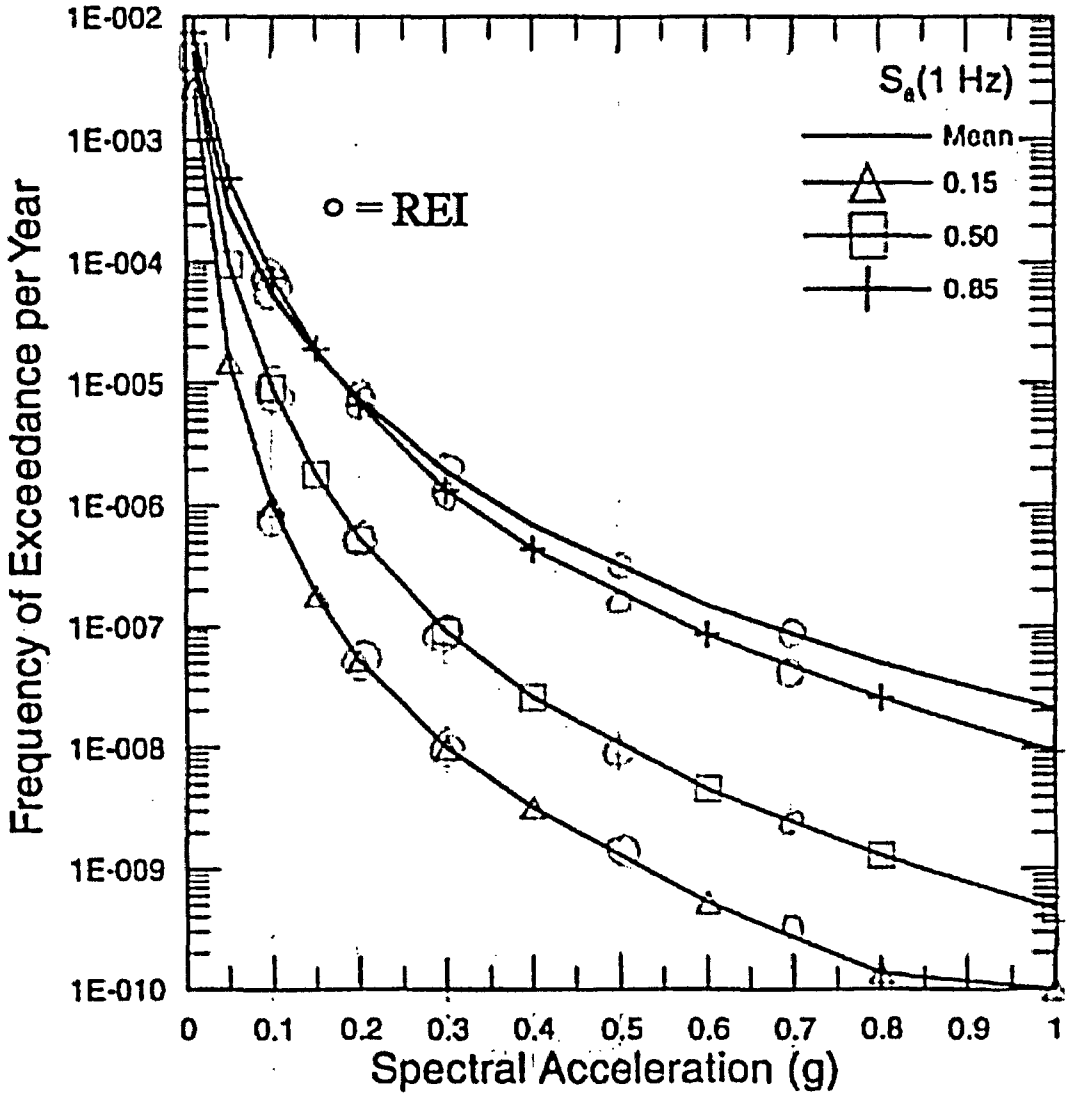

Figure 4-4
Verification of 1 Hz Rock Hazard Results for the Grand Gulf Site (Published Results from Figure 2.5-49 of Entergy, 2003)

Table 4-5 compares ground motions reported for hard rock conditions for the North Anna site (Dominion, 2003) with those calculated in this study, for spectral frequencies from 0.5 Hz to PGA and for annual frequencies of 10^{-4} and 10^{-5}. The same models and seismic hazard software (FRISK88) were used for both studies, so the results are identical. This conclusion applies also to fractiles of seismic hazard for the North Anna site.

Table 4-5
Replication of North Anna Hard Rock Hazard Results

	2003 Reported results*		Replicated results			
Frequency, Hz	mean 10^{-4} SA, g	mean 10^{-5} SA, g	mean 10^{-4} SA, g	mean 10^{-5} SA, g	% difference	% difference
0.5	0.0298	0.0944	0.0298	0.0944	0	0
1	0.0463	0.134	0.0463	0.134	0	0
2.5	0.120	0.364	0.120	0.364	0	0
5	0.235	0.735	0.235	0.735	0	0
10	0.373	1.216	0.373	1.216	0	0
25	0.569	1.99	0.569	1.99	0	0
100 (PGA)	0.214	0.753	0.214	0.753	0	0

*Results taken from Table 2.5-26 of Dominion (2003)

4.4 Rock Hazard Results for 28 Sites

Seismic hazard results were calculated for hard rock conditions for the 28 sites studied under this project. These calculations included the following:

- Seismic hazard curves (mean, 15%, median, and 85%) from 10^{-3} to 10^{-7} annual frequency of exceedence, for six structural frequencies.
- UHS amplitudes (mean, 15%, median, and 85%) for 10^{-4} and 10^{-5} annual frequencies of exceedence.
- Mean SA for 5 Hz and 10 Hz for ten annual frequencies of exceedence, ranging from $5x10^{-4}$ to $5x10^{-7}$.

5
DEVELOPMENT OF SITE SPECIFIC AMPLIFICATION FACTORS

Site specific equivalent-linear site response analyses were performed for each of the 16 sites listed in Table 3-1 as having a site-specific calculation. The foundation levels of the reactor buildings were used to assess the thickness of surficial materials at the sites. For all the sites considered, where soils extended to depths exceeding 500 ft or the shear-wave velocity exceeded about 3,500 ft/sec (1,067m/sec), linear response was assumed (Silva et al.; 1997, 1998a, 1998b, 1999, 2000).

To develop the amplification factors, control motions were specified at the surface of the Mid-continent crustal model (EPRI, 1993) with a shear-wave velocity of 2.83 km/sec, a defined shallow crustal damping parameter (kappa; Anderson and Hough, 1984) of 0.006 sec, and a frequency-dependent deep-crustal damping Q model of 670 $f^{0.33}$ (EPRI, 1993). These values are consistent with the EPRI attenuation models (EPRI, 2004). Distances were then determined to generate a suite of motions with expected peak acceleration values which cover the range of spectral accelerations (0.5, 1.0, 2.5, 5.0, 10.0, 25.0, 100.0 Hz) anticipated at the sites analyzed. To cover the range of motions, 18 expected (median) peak acceleration values were run from 0.01g to 5.00g (Table 5-1). A single moment magnitude M 6.5 was used with the stochastic point source model (Silva et al.; 1999, 2000). This magnitude reflects a reasonable average over the sites, structural frequencies, and hazard levels considered. Amplification factors were then developed by placing the site profile on the Mid-Continent crustal model at each distance, generating soil motions, and taking the ratios of soil response spectra to rock response spectra (both at 5% damping). For the higher levels of rock motions, above about 1 to 2g for the softer profiles, the high-frequency amplification factors were significantly less than 1, which may be exaggerated. To adjust the factors for these cases a heuristic lower bound of 0.5 was implemented (EPRI, 1993; Abrahamson and Silva, 1997).

Table 5-1
Distances and Depths Used to Generate Hard Rock Peak Accelerations

Expected Peak Acceleration (%g)	Epicentral Distance (km)	Depth (km)
1	235.0	8.0
5	80.0	8.0
10	47.0	8.0
20	26.0	8.0
30	18.0	8.0
40	13.0	8.0
50	9.5	8.0
75	3.0	8.0
100	0.0	6.5
125	0.0	5.3
150	0.0	4.5
200	0.0	3.3
250	0.0	2.7
300	0.0	2.3
350	0.0	1.9
400	0.0	1.7
450	0.0	1.5
500	0.0	1.4

To accommodate aleatory variability in dynamic material properties expected to occur across each site (footprint), shear-wave velocity profiles, G/G_{max}, and hysteretic damping curves were randomized. Since depth to basement material (defined as shear-wave velocity of 2.83 km/sec (9,285 ft/sec)) is poorly known at many deep soil sites, it was taken at a large enough depth to easily accommodate maximum soil amplification to the lowest frequency of interest, 0.5 Hz (Silva et al., 1999, 2000). For these cases, basement depth was randomized over a large range as well, to smooth over potential low-frequency resonances. For sites where depth to basement is relatively well known, a more restrictive range was used. In all cases, the basement depth randomization assumed a uniform distribution (EPRI, 1993).

For these deep soil and sedimentary rock sites, shear-wave velocities are poorly known for depths below those characterized by the site investigations. The approach taken here was to assume a deep base-case profile based on shear-wave velocity measurements made in similar materials and depths (analog profiles). Epistemic variability in the deep velocities was

accommodated by considering higher and lower mean deep-velocity profiles, all with the same shallow profile, based on site investigations. As is well known in site response analyses, alternative reasonable assumptions regarding deep velocities beneath soil sites has little impact on computed amplification, provided the site total kappa value (Anderson and Hough, 1984) remains fixed. Kappa, at low strain, controls the high frequency ($\geq$ 5 Hz) amplification and an effort has been made to provide reasonably conservative yet realistic estimates of base-case values for each site, based on experience with similar sites that have measured values (Anderson and Hough, 1984; Silva and Darragh, 1995; Silva et al., 1997). Epistemic variability in kappa is accommodated by considering higher and lower values, generally with about a 50% variation on the base-case values. Naturally, as loading levels increase and non-linearity becomes more pronounced, the potential impacts of the assumed kappa values decreases.

The profile randomization scheme, which varies both layer velocity and thickness, was based on a correlation model developed from an analysis of variance of about 500 measured shear-wave velocity profiles (EPRI, 1993; Silva et al., 1997). This model used variability in velocity that was appropriate for a large structural footprint. The parametric variation includes profile velocity layer thickness, depth to basement material (2.83 km/sec), G/G_{max}, and hysteretic damping curves.

To accommodate variability in the modulus reduction and damping curves on a generic basis, the curves were independently randomized about the base case values. A lognormal distribution was assumed with a logarithmic Φ of 0.30 at a cyclic shear strain of 3×10^{-2}% with upper and lower bounds of 2Φ (EPRI, 1993). The distribution was based on an analysis of variance of measured G/G_{max} and hysteretic damping curves and was considered appropriate for applications to generic (material type specific) nonlinear properties. The truncation was necessary to prevent modulus reduction or damping models that were not physically realizable. The random curves were generated by sampling the transformed normal distribution with a logarithmic Φ of 0.35, computing the change in normalized modulus reduction or percent damping at 3×10^{-2}% shear strain, and applying this factor at all strains. The random perturbation factor was reduced or tapered near the ends of the strain range to preserve the general shape of the median curves (Silva, 1992; EPRI, 1993).

To accommodate epistemic variability in dynamic material properties, multiple base case (mean) models were considered, each with associated aleatory variability captured by the randomization process. Amplification factors were then expressed as median and $\pm 1\sigma$ estimates based on 100 realizations at each distance (Silva et al., 1999; 2000). Median amplification factors reflecting the site epistemic variability were then used to develop soil hazard curves from the rock hazard curves using the analytical approximation recommended in NUREG/CR-6769 (Equation A-16 from REI, 2002) and Bazzurro and Cornell (Equation 17 from Bazzurro and Cornell, 2004). The epistemic variability in the rock hazard was preserved by using a distribution of rock hazard reflected in twenty fractiles evenly distributed from the 2.5 to 97.5 percentiles. Site epistemic variability was captured through multiple soil hazard curves corresponding to each rock hazard fractile. For cases where the analytical estimate of the soil hazard was invalid, the more accurate approach of conditioning the rock hazard with the probability distribution of the site-specific amplification factors was used (Bazzurro and Cornell, 2004)

6
CONCLUSIONS

This study applies state-of-the-art seismic hazard software to calculate seismic hazard at 28 nuclear plant sites in the CEUS. The basis for the seismic sources used in these hazard calculations is the set of sources developed and documented during the EPRI (1989) study. These sources are updated using interpretations published in more recent applications. The ground motion equations used here are those developed and published by EPRI (2004).

Verification of calculations made here with results published by EPRI (1989), using the same inputs, show that similar results are obtained (generally within several percent, in terms of annual frequency of exceedence for a given ground motion). This verifies that the software used in this study (the FRISK88 package) accurately calculates seismic hazard. Additional verification is made by comparing the FRISK88 results with rock hazard results documented in three ESP applications submitted by utilities in 2003. This verification shows that the updates to the seismic sources, and the EPRI (2004) ground motion equations, are accurately represented and calculated.

Quantitative comparisons between the current results and those published for the 28 sites in the EPRI (1989) study have not been made. Nevertheless, qualitative conclusions can be drawn regarding the effects of new information.

The interpretations of seismic sources in the New Madrid and Charleston regions indicates that current estimates of the possible sizes of large earthquakes in those regions are similar to those made in 1989. However, current estimates of recurrence intervals are shorter than those used in 1989, and this leads to higher seismic hazard at sites affected by those sources, particularly for lower-frequency ground motions. Recent studies in Southern and Central Illinois indicate that moderate-to-large earthquakes might be possible for sources located there, and these moderate-to-large earthquakes were not modeled in the 1989 study. The result is that estimates of seismic hazard are higher for sites in Illinois. In the Gulf Coast, seismic activity rates are low and the possible range of magnitudes is limited to small and moderate earthquakes, but estimates of possible earthquake size have increased somewhat. This increases seismic hazard slightly for sites located in the Gulf Coast, but estimates of ground motion hazard remain low.

7
REFERENCES

Abrahamson, N.A. and Silva, W.J. (1997). "Empirical response spectral attenuation relations for shallow crustal earthquakes." *Seism. Res. Lett.*, 68(1), 94-127.

Anderson, J. G. and S. E. Hough (1984). "A Model for the Shape of the Fourier Amplitude Spectrum of Acceleration at High Frequencies." *Bull. Seism. Soc. Am.*, 74(5), 1969-1993.

ASCE (2005). *Seismic Design Criteria for Structures, Systems, and Components in Nuclear Facilities*, Amer. Soc. Civil Engrs, Rept. ASCE/SEI 43-05.

Bazzurro, Paolo and C.A. Cornell (2004). "Nonlinear soil-site effects in probabilistic seismic-hazard analysis." *Bull. Seism. Soc. Am.*, 94(6), 2110-2123.

Dominion (2003). *North Anna Early Site Permit Application*, Dominion Nuclear North Anna LLC, Docket No. 52-008, Sept. 25.

EPRI (1989). *Probabilistic Seismic Hazard Evaluations at Nuclear Plant Sites in the Central and Eastern United States: Resolution of the Charleston Earthquake Issue*, Elec. Power Res. Inst., Rept. NP-6395-D, Palo Alto, CA, Apr.

EPRI (1993). "Guidelines for determining design basis ground motions." Palo Alto, Calif: Electric Power Research Institute, vol. 1-5, EPRI TR-102293.

vol. 1: Methodology and guidelines for estimating earthquake ground motion in eastern North America.

vol. 2: Appendices for ground motion estimation.

vol. 3: Appendices for field investigations.

vol. 4: Appendices for laboratory investigations.

vol. 5: Quantification of seismic source effects.

EPRI (2004). *CEUS Ground Motion Project Final Report*, Elec. Power Res. Inst., Rept. 1009684, Palo Alto, CA, Dec.

Entergy (2003). *Early Site Permit Application, Grand Gulf site*, Intergy Corp, Docket No. 52-009, Oct. 16.

Exelon (2003). *Early Site Permit Application, Clinton site*, Exelon Generation Co. LLC, ESP Application for Clinton site, Docket No. 52-007, Sept. 25.

Risk Engineering, Inc. (REI). (1989) *EQHAZARD Primer*, Elec. Power Res. Inst., Report NP-6452-D, Palo Alto, CA, June.

Risk Engineering, Inc. (REI) (2002). "Technical basis for revision of regulatory guidance on design ground motions: development of hazard- and risk-consistent seismic spectra for two sites." U.S. Nuclear Regulatory Commission, Rept. NUREG/CR-6769, Washington, DC 20555-0001.

Silva, W.J. (1992). "Factors controlling strong ground motions and their associated uncertainties." *Seismic and Dynamic Analysis and Design Considerations for High Level Nuclear Waste Repositories, ASCE* 132-161.

Silva, W.J., and R. Darragh, (1995). "Engineering characterization of earthquake strong ground motion recorded at rock sites." Palo Alto, Calif.: Electric Power Research Institute, Final Report RP 2556-48.

Silva, W.J., R.B.Darragh, and I. Wong (1998a). "Engineering characterization of earthquake strong ground motions with applications to the Pacific Northwest." In Assessing and Reducing Earthquake Hazards in the Pacific Northwest. *U.S. Geological Survey Professional Paper 15601.*

Silva, W.J., N. Abrahamson, G. Toro and C. Costantino. (1997). "Description and validation of the stochastic ground motion model." Report Submitted to Brookhaven National Laboratory, Associated Universities, Inc. Upton, New York 11973, Contract No. 770573.

Silva, W.J. Costantino, C. Li, Sylvia (1998b). "Quantification of nonlinear soil response for the Loma Prieta, Northridge, and Imperial Valley California earthquakes.@ Proceedings of The Second International Symposium on The effects of Surface Geology on Seismic Motion Seismic Motion/Yokohama/Japan/1-3 December 1998, Irikura, Kudo, Okada & Sasatani (eds.), 1137—1143.

Silva, W. J.,S. Li, B. Darragh, and N. Gregor (1999). "Surface geology based strong motion amplification factors for the San Francisco Bay and Los Angeles Areas." A PEARL report to PG&E/CEC/Caltrans, Award No. SA2120-59652.

Silva, W.J., R. Darragh, N. Gregor, G. Martin, C. Kircher, N. Abrahamson (2000). "Reassessment of site coefficients and near-fault factors for building code provisions.@ Final Report *USGS Grant award* #98-HQ-GR-1010.

USNRC (1997). *Identification and Characterization of seismic sources and determination of safe shutdown earthquake ground motion*, US Nuc. Reg. Comm., Reg. Guide 1.165, March.

A
SEISMIC SOURCES USED IN THE CALCULATIONS FOR EACH OF THE 28 SITES

Table A-1
Seismic Sources used for the Beaver Valley Site

TEAM	SEISMIC SOURCES
BECHTEL	24 25A BZ5 BZ6
DAMES & MOORE	04 4C 07 08 73
LAW ENGINEERING	17 112
RONDOUT	12 C02
WESTON GEOPHYSICAL	101 102 C12 C13 C14 C15 C16 C19
WOODWARD-CLYDE	35 61 63 B69

Table A-2
Seismic Sources used for the Bellefonte Site

TEAM	SEISMIC SOURCES
BECHTEL	25 25A 30 BZ0 BZ3 BZ5 BZ6
DAMES & MOORE	08 21 41 54 71
LAW ENGINEERING	17 18 115
RONDOUT	1 9 13 25 26 C02
WESTON GEOPHYSICAL	24 31 32 C11 C17 C19
WOODWARD-CLYDE	29 29A 31A 40 B39
(ADDITIONAL)	3 NEW MADRID FAULTS
(ADDITIONAL)	EAST COAST FAULT SYSTEM - SOUTH

Table A-3
Seismic Sources used for the Braidwood Site

TEAM	SEISMIC SOURCES
BECHTEL	30 BZ3
DAMES & MOORE	15A 16B 18A 21 70 71
LAW ENGINEERING	18 116
RONDOUT	1 4 15 52
WESTON GEOPHYSICAL	30 31 33 105 C29
WOODWARD-CLYDE	36 36A 44 56 B62
(ADDITIONAL)	3 NEW MADRID FAULTS

Table A-4
Seismic Sources used for the Brunswick Site

TEAM	SEISMIC SOURCES
BECHTEL	H N3 BZ4 BZ5 C07
DAMES & MOORE	53 54
LAW ENGINEERING	22 35 107 108 C09 C10 C11 M35
RONDOUT	24 26 C01
WESTON GEOPHYSICAL	25 26 104 C20 C21 C23 C24 C26 C27 C33 C35
WOODWARD-CLYDE	29 29A 29B 30 B23
(ADDITIONAL)	3 EAST COAST FAULTS

Table A-5
Seismic Sources used for the Byron Site

TEAM	SEISMIC SOURCES
BECHTEL	BZ3
DAMES & MOORE	15A 16B 17 18A 70 71
LAW ENGINEERING	116
RONDOUT	15
WESTON GEOPHYSICAL	30 100 105 C29
WOODWARD-CLYDE	55 56 B61
(ADDITIONAL)	3 NEW MADRID FAULTS

Table A-6
Seismic Sources used for the Catawba Site

TEAM	SEISMIC SOURCES
BECHTEL	F G H N3 BZ4 BZ5
DAMES & MOORE	04 4B 41 53 54
LAW ENGINEERING	17 22 107 108 C09 C10 C11 M31 M32 M33 M34 M35 M36 M37
RONDOUT	24 25 26 27 28
WESTON GEOPHYSICAL	24 25 26 104 C17 C19 C20 C21 C23 C24 C26 C27 C33 C35
WOODWARD-CLYDE	29 29A 29B 30 31A B28
(ADDITIONAL)	3 EAST COAST FAULTS

Table A-7
Seismic Sources used for the Clinton Site

TEAM	SEISMIC SOURCES
BECHTEL	30 BZ0 BZ3 K
DAMES & MOORE	18 18A 19 21 70 71
LAW ENGINEERING	06 07 18 116
RONDOUT	1 2 4 15 52
WESTON GEOPHYSICAL	31 32 33 34 105 C11 C29
WOODWARD-CLYDE	40 42 43 44 B47
(ADDITIONAL)	3 NEW MADRID FAULTS

Table A-8
Seismic Sources used for the Comanche Peak Site

TEAM	SEISMIC SOURCES
BECHTEL	38 39 BZ2 BZ3 C04
DAMES & MOORE	20 25 25A 28 28B 67
LAW ENGINEERING	26 124
RONDOUT	16 C02
WESTON GEOPHYSICAL	36 109 C31
WOODWARD-CLYDE	46 46A B44
(ADDITIONAL)	3 NEW MADRID FAULTS

Table A-9
Seismic Sources used for the David Besse Site

TEAM	SEISMIC SOURCES
BECHTEL	N1 BZ3 BZ6 C10
DAMES & MOORE	07 08 12 14 14B 15 70 73
LAW ENGINEERING	111 112 115
RONDOUT	7 8 10 11 12 C02
WESTON GEOPHYSICAL	29 101 105 C13 C14 C16
WOODWARD-CLYDE	35 36 37 38 39 B68

Table A-10
Seismic Sources used for the Grand Gulf Site

TEAM	SEISMIC SOURCES
BECHTEL	30 BZ1 BZ3
DAMES & MOORE	20 21 25 C15
LAW ENGINEERING	18 126
RONDOUT	1 16 51
WESTON GEOPHYSICAL	31 32 36 107 C11
WOODWARD-CLYDE	40 44 B40
(ADDITIONAL)	3 NEW MADRID FAULTS
(ADDITIONAL)	SALINE RIVER SOURCE

Table A-11
Seismic Sources used for the Hope Creek Site

TEAM	SEISMIC SOURCES
BECHTEL	BZ4 BZ5
DAMES & MOORE	04 4D 41 42 47 53
LAW ENGINEERING	17 22 107 C09 C10 C11 C13 M16 M17 M18 M19 M20 M21
RONDOUT	30 31
WESTON GEOPHYSICAL	28A C08 C09 C22 C23 C28 C34
WOODWARD-CLYDE	21 21A 22 23 24 53 63 B09

Table A-12
Seismic Sources used for the LaSalle Site

TEAM	SEISMIC SOURCES
BECHTEL	30 BZ3
DAMES & MOORE	15A 16B 18A 21 70 71
LAW ENGINEERING	18 116
RONDOUT	1 4 15
WESTON GEOPHYSICAL	30 31 105 C29
WOODWARD-CLYDE	44 56 B60
(ADDITIONAL)	3 NEW MADRID FAULTS

Table A-13
Seismic Sources used for the Limerick Site

TEAM	SEISMIC SOURCES
BECHTEL	13 BZ4 BZ5
DAMES & MOORE	04 4D 08 41 42 47 53
LAW ENGINEERING	17 22 217 C09 C10 M14 M15 M16 M17 M18 M19
RONDOUT	30 31
WESTON GEOPHYSICAL	28A 28B C07 C10 C19 C22 C23 C28 C34
WOODWARD-CLYDE	21 21A 22 23 24 53 63 B18

Table A-14
Seismic Sources used for the McGuire Site

TEAM	SEISMIC SOURCES
BECHTEL	F G H N3 BZ4 BZ5
DAMES & MOORE	04 4B 41 53 54
LAW ENGINEERING	17 22 35 107 217 C10 C11 M31 M32 M33 M34 M35 M36
RONDOUT	24 25 26 27 28 C02
WESTON GEOPHYSICAL	23 24 25 26 C17 C18 C19 C20 C21 C23 C24 C27 C33
WOODWARD-CLYDE	29 29A 29B 30 31 31A B26
(ADDITIONAL)	3 EAST COAST FAULTS

Table A-15
Seismic Sources used for the Millstone Site

TEAM	SEISMIC SOURCES							
BECHTEL	08	B	BZ4	BZ5	BZ8			
DAMES & MOORE	2	4	4A	41	47	53	63	C14
LAW ENGINEERING	17	22	102	103	C09	M10	M11	M12
	M13	M14	M15					
RONDOUT	31	40	41	44				
WESTON GEOPHYSICAL	06	10	13	16	17	19	20	28A
	39	C06	C07	C10				
WOODWARD-CLYDE	08	10	11	23	57	59	B07	

Table A-16
Seismic Sources used for the Nine Mile Point Site

TEAM	SEISMIC SOURCES							
BECHTEL	07	11	C	D	BZ5	BZ6	BZ7	C05
DAMES & MOORE	03	09	38	39B	C02	C09	C10	C11
LAW ENGINEERING	11	17	111					
RONDOUT	33	34	35	47	C02			
WESTON GEOPHYSICAL	04	05	07	08	C12	C13	C14	C16
WOODWARD-CLYDE	15	18	19	33	34	C10	B14	

Table A-17
Seismic Sources used for the North Anna Site

TEAM	SEISMIC SOURCES
BECHTEL	24 E BZ4 BZ5
DAMES & MOORE	04 4B 40 41 42 47 53
LAW ENGINEERING	17 22 107 217 C09 C10 C11 M19 M20 M21 M22 M23 M24 M27
RONDOUT	28 29 30
WESTON GEOPHYSICAL	22 C19 C21 C22 C23 C34 C35
WOODWARD-CLYDE	26 27 29 29A B22
(ADDITIONAL)	EAST COAST FAULT SYSTEM - SOUTH

Table A-18
Seismic Sources used for the Perry Site

TEAM	SEISMIC SOURCES
BECHTEL	27 D N1 BZ6 C06
DAMES & MOORE	07 08 14 14B 15 70 73
LAW ENGINEERING	111 112
RONDOUT	10 11 12 33 C02
WESTON GEOPHYSICAL	07 101 C12 C14 C15 C16 C32
WOODWARD-CLYDE	33 35 61 63 B70

Table A-19
Seismic Sources used for the River Bend Site

TEAM	SEISMIC SOURCES
BECHTEL	30 BZ1
DAMES & MOORE	20 21 25 C15
LAW ENGINEERING	18 126
RONDOUT	1 51
WESTON GEOPHYSICAL	31 107
WOODWARD-CLYDE	40 B42
(ADDITIONAL)	3 NEW MADRID FAULTS
(ADDITIONAL)	SALINE RIVER SOURCE

Table A-20
Seismic Sources used for the Seabrook Site

TEAM	SEISMIC SOURCES
BECHTEL	03 08 09 B BZ4 BZ7 BZ8
DAMES & MOORE	02 53 56 59 61 63
LAW ENGINEERING	12 21 22 24 102 103 C09 C12 M08 M09 M10
RONDOUT	31 37 40 41 43
WESTON GEOPHYSICAL	01 13 14 16 17 C03 C04 C05
WOODWARD-CLYDE	06 08 09 12 58 59 B02

Table A-21
Seismic Sources used for the Shearon Harris Site

TEAM	SEISMIC SOURCES
BECHTEL	13 F H N3 BZ4 BZ5
DAMES & MOORE	40 41 53 54
LAW ENGINEERING	17 35 107 C09 C10 C11 M27 M28 M31 M32 M33 M34 M35
RONDOUT	24 26 28 29 C01
WESTON GEOPHYSICAL	22 25 26 28D 104 C19 C20 C21 C22 C24 C25 C26 C28 C33 C35
WOODWARD-CLYDE	26 27 29 29A 29B 30 B24
(ADDITIONAL)	3 EAST COAST FAULTS

Table A-22
Seismic Sources used for the South Texas Site

TEAM	SEISMIC SOURCES
BECHTEL	BZ1 BZ2
DAMES & MOORE	20 25
LAW ENGINEERING	124 126
RONDOUT	51
WESTON GEOPHYSICAL	107
WOODWARD-CLYDE	B43
(ADDITIONAL)	3 NEW MADRID FAULTS
(ADDITIONAL)	SALINE RIVER SOURCE

Table A-23
Seismic Sources used for the Summer Site

TEAM	SEISMIC SOURCES
BECHTEL	F G H N3 BZ4 BZ5
DAMES & MOORE	41 53 54
LAW ENGINEERING	17 22 107 108 C09 C10 C11 M31 M32 M33 M34 M36 M37 M38 M39
RONDOUT	24 26
WESTON GEOPHYSICAL	25 26 104 C19 C20 C21 C23 C24 C26 C27 C33 C35
WOODWARD-CLYDE	29 29A 29B 30 31A B31
(ADDITIONAL)	3 EAST COAST FAULTS

Table A-24
Seismic Sources used for the Three Mile Island Site

TEAM	SEISMIC SOURCES
BECHTEL	13 24 BZ4 BZ5
DAMES & MOORE	04 4C 08 41 42 47
LAW ENGINEERING	17 22 217 C09 C10 C11 M16 M17 M18 M19 N20 M21
RONDOUT	30 31
WESTON GEOPHYSICAL	28A 28B 102 C08 C09 C17 C18 C22 C23 C28 C34
WOODWARD-CLYDE	21 21A 22 23 53 61 63 B17

Table A-25
Seismic Sources used for the Vogtle Site

TEAM	SEISMIC SOURCES
BECHTEL	F G H N3 BZ4 BZ5
DAMES & MOORE	20 41 52 53 54
LAW ENGINEERING	17 22 35 108 C09 C10 C11 M33 M36 M37 M38 M39 M40 M41 M42
RONDOUT	24 26
WESTON GEOPHYSICAL	25 26 104 C19 C20 C21 C23 C24 C26 C27 C33 C35
WOODWARD-CLYDE	29 29A 29B 30 B32
(ADDITIONAL)	3 EAST COAST FAULTS

Table A-26
Seismic Sources used for the Waterford Site

TEAM	SEISMIC SOURCES
BECHTEL	30 BZ1
DAMES & MOORE	21 20
LAW ENGINEERING	18 126
RONDOUT	1 51
WESTON GEOPHYSICAL	31 32 107 C11
WOODWARD-CLYDE	40 B41
(ADDITIONAL)	3 NEW MADRID FAULTS
(ADDITIONAL)	SALINE RIVER SOURCE

Table A-27
Seismic Sources used for the Watts Bar Site

TEAM	SEISMIC SOURCES
BECHTEL	24 25 25A 30 F H BZ0 BZ5 BZ6
DAMES & MOORE	04 4A 05 21 41 54
LAW ENGINEERING	01 17 18 115 217
RONDOUT	1 5 9 25 26 27
WESTON GEOPHYSICAL	24 31 C17 C19
WOODWARD-CLYDE	29 29A 29B 31 31A 40 B29
(ADDITIONAL)	3 NEW MADRID FAULTS
(ADDITIONAL)	EAST COAST FAULT SYSTEM - SOUTH

Table A-28
Seismic Sources used for the Wolf Creek Site

TEAM	SEISMIC SOURCES
BECHTEL	41 42 BZ3 C01 C02 C03
DAMES & MOORE	35B 36 37 37B 68A 68B 69
LAW ENGINEERING	30 118 119 C04 C05
RONDOUT	18 21
WESTON GEOPHYSICAL	35 108 C30
WOODWARD-CLYDE	45 47 54 60 B48
(ADDITIONAL)	3 NEW MADRID FAULTS

B
SITE DESCRIPTIONS FOR SITE-SPECIFIC ANALYSES

This Appendix contains descriptions of site conditions for the 16 sites that were handled with site-specific calculations. Several sites use the following empirical relation between kappa and the average shear-wave velocity at rock sites (Silva et al., 1997).

$$\log(\text{kappa}) = 2.2189 - 1.0930 * \log(V_S), \qquad \text{Eq. B-1}$$

Multiple models are used to capture epistemic uncertainty in site response, and these models (and their weights) are described in the subsection for each of the 16 sites.

B.1 BEAVER VALLEY SITE

The Beaver Valley Power Station is located along the Ohio River a few miles (several km) east of the Pennsylvania-Ohio border. The site is within the Appalachian Plateau physiographic province.

The site is underlain by older Pleistocene (?) terrace deposits (sand and gravel, containing variable amounts of cobbles and rock fragments) within an erosional bedrock valley of the Ohio River. The terrace has a maximum thickness of about 100 ft (30.5m) and rests directly upon bedrock of Pennsylvanian age. The bedrock underlying the site consists primarily of Paleozoic sandstone and shale with inter-bedded coal units. Below the Paleozoic sandstones and coal seams lie shales, sandstones, and siltstones as well as the Salina Group which contains salt beds. The uppermost salt bed occurs at a depth of about 4,700 ft (1,432m) below the plant site. Precambrian crystalline basement rock was estimated to be at a depth of about 10,500 ft (3,200m) (EPRI, 1989).

B.1.1 Soil Profile Information

The reactor containment building is founded on the terrace deposits with an embedment depth of 54 ft (16.5m). The terrace deposits are about 46 ft (14.0m) thick beneath this structure. Bedrock of Paleozoic age underlies the terrace deposits. Basement rock is estimated to be at a depth of 5,000 ft (1,524m) (rock hazard defined as basement material with a Vs of 2.83 km/sec).

Weston Geophysical made seismic wave velocity measurements into the bedrock at 100 ft (30.5m). In the terrace deposits the shear wave velocity ranged from 600 to 1,200 f/sec (182.9 to 365.7 m/sec) above the water table and 1,300 ft/sec (396.2 m/sec) below the water table. The depth to the water table was measured between 66 and 69 ft (20 and 21m). The measured shear-wave velocity at the top of the bedrock (shale) is 6,000 ft/sec (1,828.7 m/sec).

Site-specific measurements of modulus reduction and damping curves were not available in REI (1989).

B.1.2 Description of Base Case Profiles

Discussed below are the base case site dynamic material properties intended to capture site epistemic variability (uncertainty). Aleatory variability (randomness) is accommodated through randomization about the base case properties. Multiple median (logarithmic mean) amplification factors (over aleatory variability) are then weighted to accommodate site epistemic variability in the site-specific soil hazard curves.

B.1.2.1 Shear-Wave Velocity Profiles

Measured shear-wave velocities extend to a depth of about 50 ft below the reactor containment structure in Figure B-1 and are estimated from velocities in similar material beyond this depth. The stair-stepped profile (M1P1 in Figure B-1) is considered the base-case profile and is continued to a depth of 5,000 ft (1,524m) (randomized $\pm$ 2,000 ft) (610m). Lower and higher velocity alternatives (M1P2 and M1P3 respectively) are considered as well, with M1P3 reaching hard rock shear-wave velocities (9,285 ft/sec, 2.83 km/sec) at a depth of about 2,000 ft (610m) (randomized $\pm$ 500 ft (152m)).

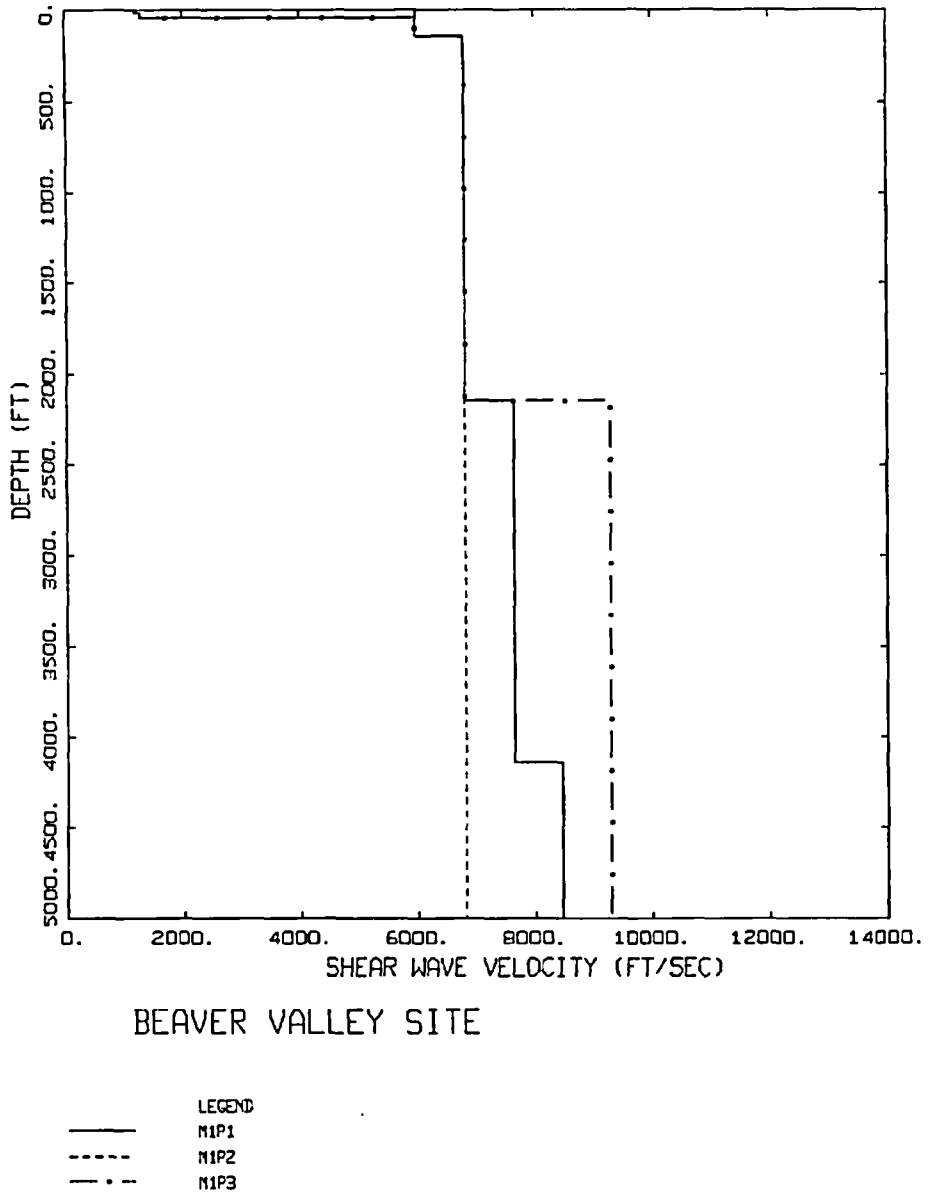

Figure B-1
Shear-Wave Velocity Profiles for the Beaver Valley Site

Profile M1P1 is considered the base case profile with M1P2 and M1P3 to accommodate lower and higher at-depth velocities. All three profiles are estimates below a depth of about 50 ft (15m).

B.1.2.2 Modulus Reduction and Hysteretic Damping Curves

For the terrace sands and gravels in the top 50 ft (15m) of the profile, the EPRI (1993) cohesionless soil curves are considered appropriate. The materials with shear-wave velocities of 6,000 ft/sec (1,829 m/sec) and greater are considered linear.

B.1.2.3 Regional Crustal Damping (kappa)

Based on Equation B-1, the kappa value for 6,000 ft/sec (1,828.7 m/sec) material is 0.0123 sec, Adding the low strain damping from the EPRI (1993) curves for the approximately 50 ft of gravely soil below the reactor containment vessel, a kappa value of about 0.0013 sec, the total base-case kappa at the soil surface is about 0.0136 sec. This value is assumed appropriate for the base-case profile (M1P1) as well as the low and high velocity profiles (M1P2 and M1P3, Figure B-1). To consider alternative mean kappa values for the base case profile, a high total kappa (M1P1.KH) of 0.04 sec, a typical value for soft rock in Western North America was assumed. For a low kappa (M1P1.KL) a rock (6,000 ft/sec, 1,828.71 m/sec) value of 0.01 sec was assumed for a low kappa total site value of 0.0113 sec.

B.1.2.4 Profile Weights

Table B-1
Beaver Valley Weights

Properties*	Category Weights
M1P1	0.5
M1P1.KH	0.2
M1P1.KL	0.3
M1P1	0.6
M1P2	0.2
M1P3	0.2
	Combined Weights
M1P1	0.30
M1P1.KH	0.12
M1P1.KL	0.18
M1P2	0.20
M1P3	0.20

*M1P1; base-case profile, kappa = 0.0136 sec

M1P1.KH; base-case profile, kappa = 0.04 sec

M1P1.KL; base-case profile, kappa = 0.0113 sec

M1P2; low gradient profile, kappa = 0.0136 sec

M1P3; high gradient profile, kappa = 0.0136 sec

B.2 BRUNSWICK SITE

The Brunswick Steam Electric Plant is located in the southeastern portion of North Carolina. The site is located on the Atlantic seaboard within 5 miles (8.0 km) of the Atlantic Ocean and is within the Atlantic Coastal Plain physiographic province. Its location is about 90 miles (145 km) southeast of the Fall Line, the boundary between the flat lying deposits of the Coastal Plain and the folded formations of the Piedmont and Appalachian regions.

The site is underlain by the Miocene Yorktown Formation (alternating clay and sand), Oligocene sediments (limestone over lenses of clay and sand), Eocene Castle Hayne Limestone (shell limestone over sandstone with some clay) and the Cretaceous Peedee Formation (calcareous clay and sand). Crystalline basement rock was estimated to be at a depth of about 1,500 ft (457.2m) (EPRI, 1989).

B.2.1 Soil Profile Information

The reactor buildings are founded on very dense sand of the Yorktown formation at a depth of about 48 ft (14.6m). Prior to construction, this sand was overlain by loose sands (Pamlico Terrace Formation) and soft silty clays and clay silts (top of Yorktown Formation). The engineered fill of the plant island was placed on the lower 30 ft (9.1m) of the Yorktown formation, which is composed of medium to coarse grained and well-compacted sand with minor lenses of clay near the top. The dense sand is underlain by 80 ft (24.4m) of limestone that is underlain by 70 ft (21.3m) of sandstone over 270 ft of silty clay and clayey silt to a depth of 600 ft (182.9m). The bottom silty clay unit (Peedee) is well consolidated, soft to medium hard using a rock hardness classification (EPRI, 1989). Basement rock is estimated to be at a depth of 1,500 ft (457.2m) (rock hazard defined as basement material with a Vs of 2.83 km/sec).

Weston Geophysical made seismic wave velocity measurements to a depth of 600 ft (182.9m). In the stiff sand of the Yorktown formation, assumed foundation material, the shear-wave velocity was measured as 1,400 ft/sec (426.7 m/sec). The measured shear-wave velocity at the top of the limestone is 5,500 ft/sec (1,676.3 m/sec). Below the limestone the measured shear-wave velocity decreases to 4,500 ft/sec (1,371.5 m/sec) in sandstone and to 3,000 ft/sec (914.4 m/sec) in the Peedee formation with 600 ft (183m) reflecting the deepest measurements.

Site-specific laboratory dynamic material testing for modulus reduction and hysteretic damping strain dependencies reflecting recent procedures were not available for this site (EPRI, 1989).

B.2.2 Description of Base Case Profiles

B.2.2.1 Shear Wave Velocity Profiles

Figure B-2 shows the measured shear-wave velocity (to a depth of about 600 ft (182.9m)) with the deepest measurements extrapolated to crystalline basement at an estimated depth of 1,500 ft (randomized + 500 ft) (457 + 152m). This is considered the base case profile (M1P1, Figure B-

2) and profile M1P2 (Figure B-2) is intended to accommodate the potential for a velocity gradient in the stiff silty clay. The reactor building is founded at a depth of 48 ft (14.6m), which was removed from the measured shear-wave velocities.

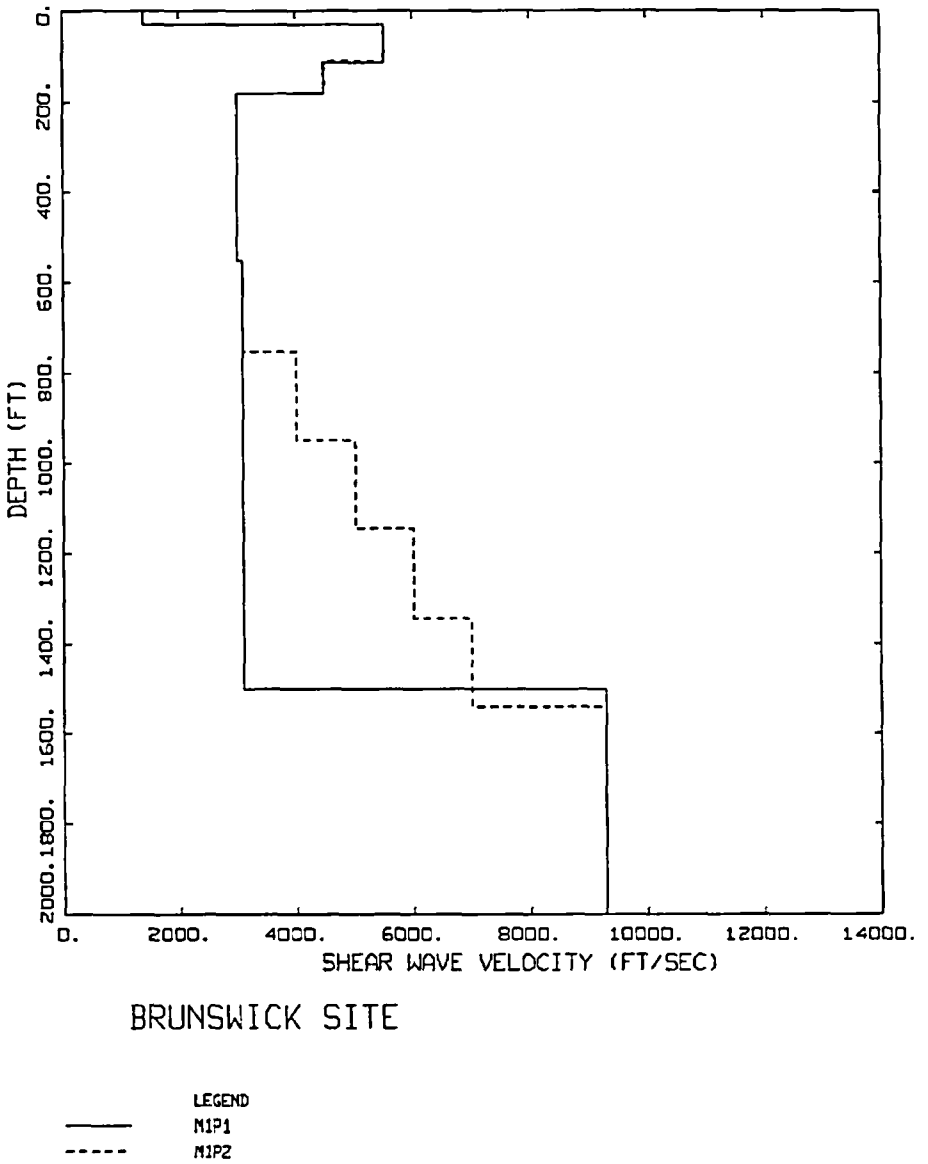

Figure B-2
Shear-Wave Velocity Profiles for the Brunswick Site

Profile M1P1 is considered the base case profile with M1P2 to accommodate a gradient in the deep stiff silty clay. Both profiles are estimates below a depth of about 600 ft (183m).

B.2.2.2 Modulus Reduction and Hysteretic Damping Curves

For the units which have similar soil types and depth ranges, G/G_{max} and hysteretic damping curves from the well characterized Savannah River Site, located within the Atlantic Coastal Plain along the Georgia and South Carolina border, were used. The Dry Branch curves from Savannah River Site (SRS, 1996) were used for the stiff sands of the Miocene Yorktown Formation in the top 30 ft (9.1 m) of the profile. Peninsular Range rock curves (Silva et al., 1997) were used for the limestone and sandstone. For the silty clays of the Peedee formation, the deep clay curves from the Savannah River Site (SRS, 1996) were selected. The materials are considered to behave linearly below a depth of 500 ft (152.4 m; Silva et al.; 1997, 1998b).

B.2.2.3 Regional Crustal Damping (kappa)

A kappa of 0.02 sec was assumed as the base case value for this site based on the similarity of the profile to the 1,000 ft (304.8m) soil profile of the Savannah River Site, where a value for kappa of 0.02 sec has been measured. To accommodate the possibility of a higher kappa value due to the additional 500 ft of soil, relative to the Savannah River profile, amplification factors were also developed for a kappa value of 0.03 sec. The high gradient profile (M1P2, Figure B-2) was assumed to reflect the base case kappa value of 0.02 sec.

B.2.2.4 Profile Weights

The profile weights for the amplification factors are listed below in Table B-2.

Table B-2
Brunswick Weights

Properties*	Category Weights
M1P1	0.6
M1P1.KH	0.4
M1P1	0.8
M1P2	0.2
	Combined Weights
M1P1	0.48
M1P1.KH	0.32
M1P2	0.20

*M1P1; base case profile, kappa = 0.02 sec

M1P1.KH; base case profile, kappa = 0.03 sec

M1P2; high gradient profile, kappa = 0.02 sec

B.3 CATAWBA SITE

The Catawba Nuclear Station is located adjacent to Lake Wylie in York County, in the north central portion of South Carolina. The site is located in the Charlotte Belt of the Piedmont physiographic province; a deeply eroded plateau-like segment of the Appalachian Mountain System. The Charlotte Belt is characterized by an extensive complex of intrusive; and with the exception of a few broad folds is dominated by plutonic contacts.

The site is located on a Paleozoic basement rock consisting of adamellite (predominant rock underlying the site), amphibolite, diorite, porphyritic diorite, aplite and pegmatite. A thin soil and a zone of weathered bedrock (saprolite) overlie fresh unweathered crystalline bedrock, which is encountered at depths of 25 to 75 ft (7.6 to 22.9 m) across the plant area (EPRI, 1989).

B.3.1 Soil Profile Information

The reactor buildings are founded crystalline bedrock at a depth of about 50 ft (15.2 m) below finished grade (0 to 30 ft (0 to 9.1 m) below the original surface) with the central core about 77 ft (23.5m) deep. The foundation excavation required the removal of the overlying soil and weathered rock. Basement rock is estimated to be at a depth of 119 ft (36.3m) (rock hazard defined as basement material with a Vs of 2.83 km/sec).

Geophysical measurements included seismic refraction, uphole, and cross-hole. During the uphole survey, measurements of shear wave velocity were made to a depth of 120 ft (36.6m). Measured shear-wave velocities in the bedrock ranged from 3,000 ft/sec (914.4 m/sec) to 9,000 ft/sec (2,743 m/sec).

Site-specific laboratory dynamic material testing for modulus reduction and hysteretic damping strain dependencies reflecting recent procedures were not available for this site (EPRI, 1989).

B.3.2 Description of Base Case Profiles

B.3.2.1 Shear Wave Velocity Profiles

The base-case shear-wave velocity profile is shown in Figure B-3 (M1P1) and is based on geophysical surveys at the site. It shows a gradient over the top 100 ft (30.47m) increasing from about 3,000 ft/sec (914.36 m/sec) at the surface (average embedment depth) to the reference rock velocity of 9,285 ft/sec (2.83 km/sec) at about 100 ft (30.47m). This softer rock zone is likely an artifact of partial weathering and fracturing and was not completely stripped from the site. To accommodate portions of embedment in contact with hard rock, profile M1P2 (Figure B-3) considers reference rock conditions at the surface (50 to 80 ft, 15 to 24m below actual grade).

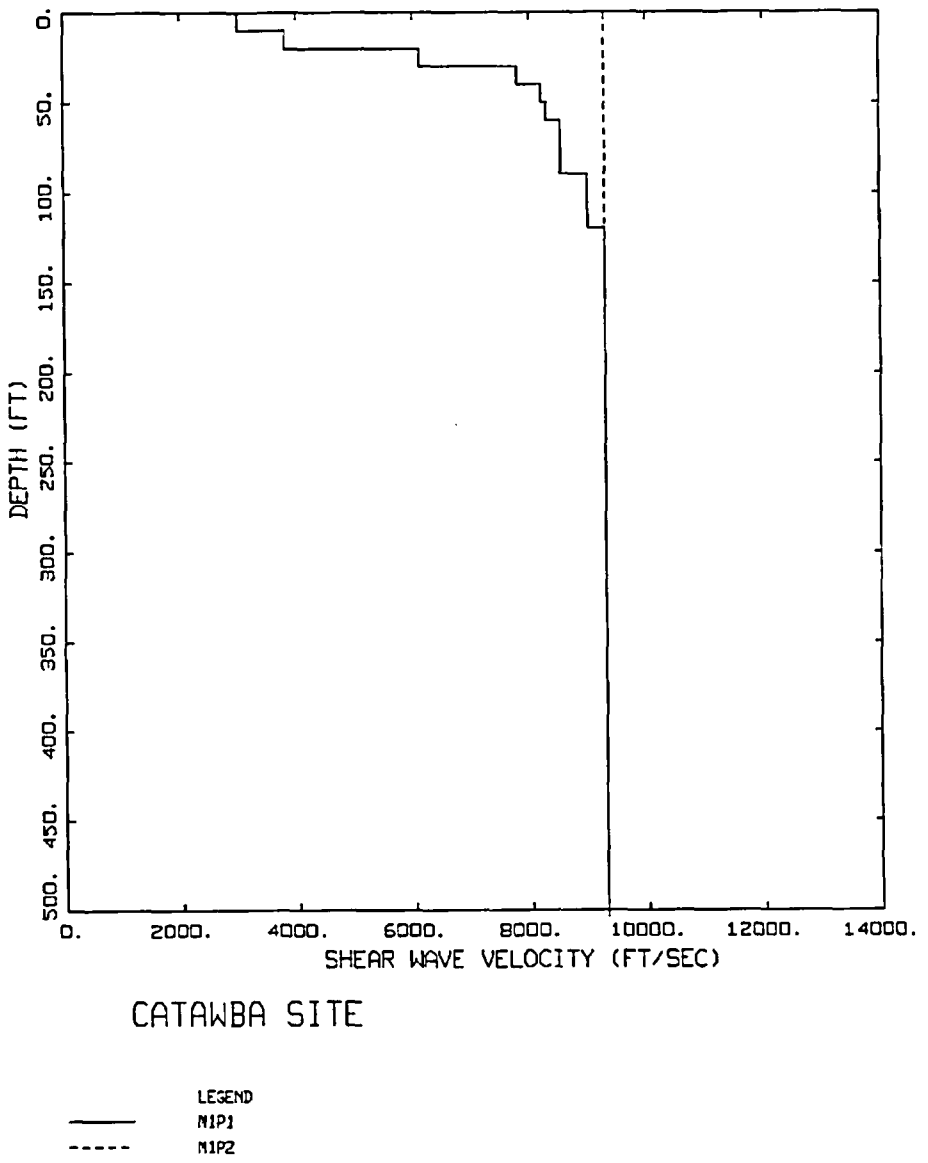

Figure B-3
Shear-Wave Velocity Profiles for the Catawba Site

Profile M1P1 is considered the base case profile and is based on measured velocities to a depth of about 70 ft (21m). Profile M1P2 accommodates the high range of shear-wave velocities of the bedrock and reflects the hard rock reference velocity of 9,285 ft/sec (2.83 km/sec).

B.3.2.2 Modulus Reduction and Hysteretic Damping Curves

For the base case profile (M1P1), Peninsular Range cohesion-less soil curves (Silva et al., 1997) were used for the top 10 ft (3.0m). Peninsular Range rock curves (Silva et al., 1997) were used from 10 ft (3.0m) to 70 ft (21.3m).

B.3.2.3 Regional Crustal Damping (kappa)

For the hard rock below a depth of about 70 ft (21.3m), the CEUS standard value of 0.006 sec was assumed. The kappa contributed by the low strain material in profile M1P1 damping at shallower depths is about 0.001 sec, for a total site kappa value of 0.007 sec. The reference rock profile kappa value is assumed to be 0.006 sec, reflecting hard rock outcrop hazard.

B.3.2.4 Profile Weights

The profile weights for the amplification factors are listed below in Table B-3.

Table B-3
Catawba Weights

Properties*	Category Weights
M1P1	0.6
M1P2	0.4
	Combined Weights
M1P1	0.6
M1P2	0.4

*M1P1; base-case profile, kappa = 0.007 sec

M1P2; low gradient profile, kappa = 0.007 sec

B.4 CLINTON SITE

The Clinton Power Station is located in the Illinois Basin, slightly west of the La Salle Anticlinal Belt about 6 miles (9.7 km) east of the city of Clinton, Illinois. The site is within the Till Plains section of the Central Lowland physiographic province.

Strata underlying the site consist of an estimated 170 to 360 ft (51.8 to 109.7m) of Quaternary overburden, largely Wisconsinan, Illinoian, and pre-Illinoian aged glacial deposits resting on essentially flat-lying Pennsylvanian-aged shales, sandstones and thin coal beds. Precambrian

crystalline basement rock was estimated to be at a depth of about 4,000 ft (1,219m) (Exelon, 2003).

B.4.1 Soil Profile Information

Major power block structures are founded on compacted fill resting on stiff Illinoian till at an embedment depth of about 56 ft (17.1m). Basement rock is estimated to be at a depth of 4,000 ft (1,219m) (rock hazard defined as basement material with a Vs of 2.83 km/sec).

Recent suspension shear-wave velocity measurements (1 hole) were made into the bedrock at a depth about 300 ft (91m) (Exelon, 2003). In the top 42 ft (1.3m) of loess and weathered Wisconsinian glacial till deposits, the shear-wave velocity is 975 ft/sec (297 m/sec). In the next 17 ft (5.2m) of overburden the velocity is 1,343 ft/sec (409 m/sec). In the Illinoian and pre-Illinoian glacial till above the bedrock the shear-wave velocity is about 2,000 ft/sec (609 m/sec). The measured shear-wave velocity at the top of the bedrock (limestone, shale, and sandstone) is about 4,000 ft/sec (1,219 m/sec) at a depth of about 300 ft (91m) (Exelon, 2003).

CH2M Hill performed laboratory testing. Resonant column and torsional shear dynamic tests were performed to estimate site-specific modulus reduction and hysteretic damping curves (Exelon, 2003).

B.4.2 Description of Base Case Profiles

B.4.2.1 Shear Wave Velocity Profiles

The base-case shear-wave velocity profile (M1P1) is shown in Figure B-4 with the top 300 ft (91m) based on a smoothed suspension log survey (Exelon, 2003) which penetrated local bedrock of shales, sandstones and coal beds. Precambrian basement lies at an estimated depth of 4,000 ft (1,219m). For depths below about 300 ft (91m), several regional (within about 10 miles, 16 km) oil well compressional-wave surveys were available with at least one extending to a depth of about 5,000 ft (1,524m). Based on assumptions of values for Poisson's ratios for these materials (0.25 to 0.35), the base-case profile was extended to a depth of 4,000 ft (1,219m) and randomized $\pm$ 2,000 ft (610m). To consider alternative deep velocities, profile M1P2 provides for a shear-wave velocity of nearly 6,000 ft/sec (1,288 m/sec) to Precambrian basement while profile M1P3 considers Precambrian basement velocities occur locally at a depth of 1,200 ft (366m) (randomized $\pm$ 400 ft, $\pm$ 122m).

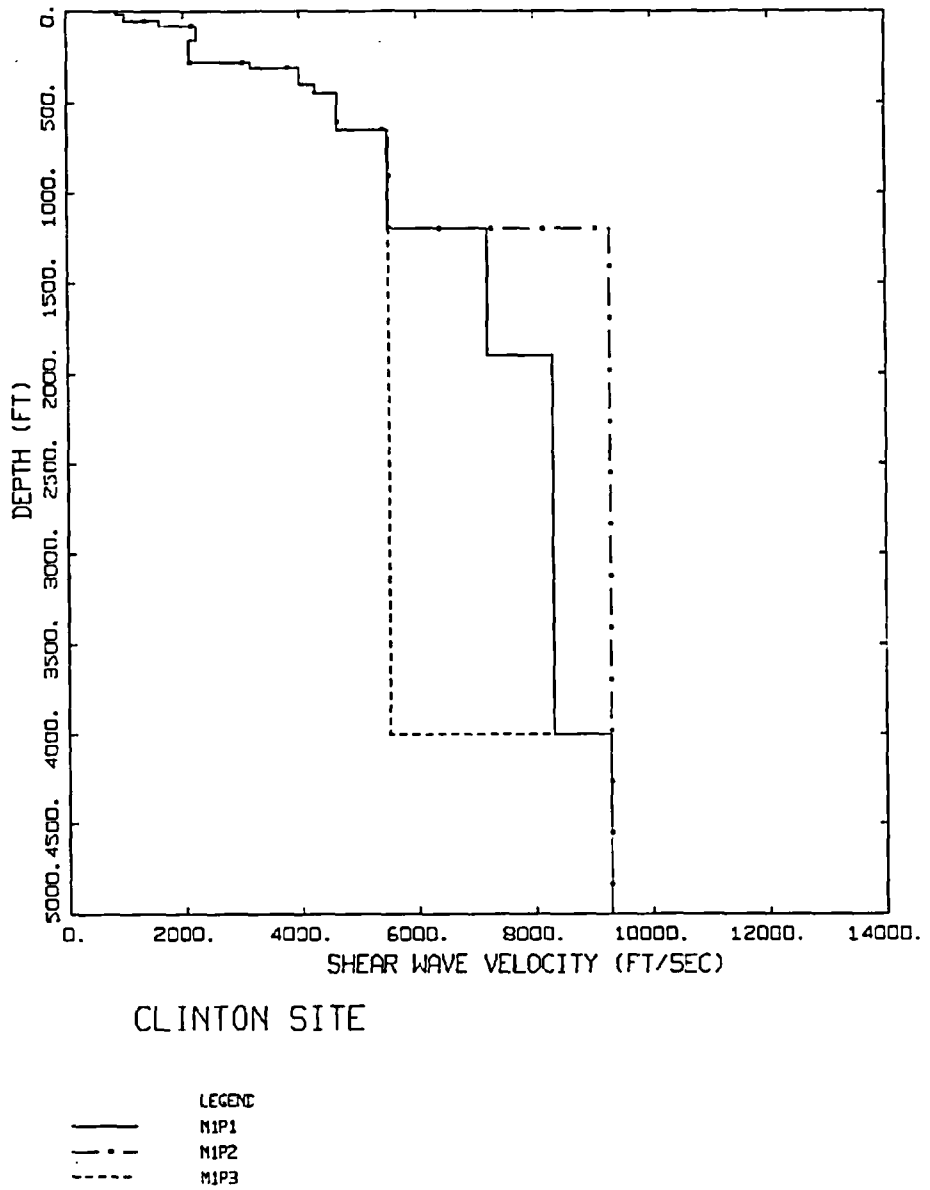

Figure B-4
Shear-Wave Velocity Profiles for the Clinton Site

Profile M1P1 is considered the base case profile with M1P2 and M1P3 to accommodate higher and lower at-depth velocities. All three profiles are estimates below a depth of about 300 ft (91m).

B.4.2.2 Modulus Reduction and Hysteretic Damping Curves

Based on comparison of recent resonant column and torsional shear test results with the EPRI (1993) cohesion-less soil curves, the EPRI curves were adopted for the glacial deposits overlying the shale and sandstone bedrock (Exelon, 2003).

B.4.2.3 Regional Crustal Damping (kappa)

To assess an appropriate kappa value for the site (shallow soil over sedimentary rock), the empirical rock site relation between kappa and the average shear-wave velocity over the top 100 ft (31m) (Equation B-1) was applied to the rock beneath the soil. For a shear-wave velocity of 4,000 ft/sec (1,219 m/sec) (Figure B-4), the estimated kappa value is 0.019 sec. Adding the low strain damping in the soil section, with a kappa value of 0.0034 sec, results in a total site kappa value of 0.0224 sec. To accommodate the possibility that the 300 ft (91m) of soil and nearly 4,000 ft (1,219m) of sedimentary rock may have a kappa value similar to Western North America soft rock, a total kappa value of 0.04 sec (Silva and Darragh, 1995; Silva et al., 1997) was also used. For the deep low (profile M1P2) and high (profile M1P3) velocity profiles (Figure B-4), the base-case total kappa value of 0.0224 sec was used.

B.4.2.4 Profile Weights

The profile weights for the amplification factors are listed below in Table B-4.

Table B-4
Clinton Weights

Properties*	Category Weights
M1P1	0.6
M1P1.KH	0.4
M1P1	0.6
M1P2	0.2
M1P3	0.2
	Combined Weights
M1P1	0.36
M1P1.KH	0.40
M1P2	0.12
M1P3	0.12

*M1P1; base case profile, kappa = 0.0224 sec

M1P1.KH; base case profile, kappa = 0.04 sec

M1P2; low gradient profile, kappa = 0.0224 sec

M1P2; high gradient profile, kappa = 0.0224 sec

B.5 GRAND GULF SITE

The Grand Gulf Nuclear Station is located in west-central Mississippi about 25 miles (40 km) south of Vicksburg. The site is within the Loess Hills (Uplands) sub province at the western margin bordering the Mississippi Alluvial Valley (Lowlands) sub province of the Gulf Coastal Plain.

The site is underlain by a sequence of late Pliocene to Quaternary eolian and alluvial deposits overlying the Miocene Catahoula Formation that consists of non-marine and littoral bedrock. The Catahoula bedrock underlying the site consists of weakly cemented claystone that extends to the bottom of the deepest boring (447 ft, 136m). The strata underlying the site consist of a thick

and stratigraphically complex sequence of relatively flat lying sediments that are part of the Gulf Coast geosyncline. These sediments are about 20,000 ft (6,000m) thick and unconformably overlie a sequence or rocks composed mainly of Mesozoic limestone. Precambrian crystalline basement rock was estimated to be at a depth of about 27,000 ft (8,200m) (Entergy, 2003).

B.5.1 Soil Profile Information

The Loess deposits were removed at the site and the reactor is founded on alluvium of the Upland Complex. Precambrian basement rock is estimated to be at a depth of 27,000 ft (8,200m) (rock hazard defined as basement material with a Vs of 2.83 km/sec).

Geophysical refraction and crosshole seismic surveys were performed in 1971 to 1972 (Entergy (1994)). Recently, the shear-wave velocity profile at the site was based on three P-S suspension velocity log surveys, with the deepest extending to a depth of about 225 ft (Entergy, 2003). The shallow materials consist of about 75 ft (23m) of loess, 85 ft (26m) of young alluvium, with old alluvium to a depth of about 200 ft (61m) where claystones of the Upland Catahoula formation were encountered. Both the old and young alluvium comprise the terrace deposits of the Uplands. The maximum depth of the suspension log surveys was about 225 ft (69m).

William Lettis and Associates also performed laboratory testing. Resonant column and torsional shear dynamic tests were performed to estimate site-specific modulus reduction and hysteretic damping curves (Entergy, 2003).

B.5.2 Description of Base Case Profiles

B.5.2.1 Shear Wave Velocity Profiles

To extend the measured profile to a depth of about 3,000 ft (914m), a generic Mississippi embayment shear-wave velocity profile was used. This generic profile was developed for ground shaking studies in the embayment by Professor Glenn Rix of the MAE Center (personal communication, 2002). The profile is based on a large number of shallow and several deep velocity surveys and extends to a depth of 3,600 (1,100m). For the site base case profile, the shallow velocities to a depth of about 225 ft replaced those of the generic Mississippi embayment upland profile, which had similar velocities (about 2,000 ft/sec) at these depths. The complete base case profile is shown in Figure B-5 (profile M1P1) to a depth of about 3,200 ft (975m) where shear-wave velocity is set to 2.83 km/sec, appropriate for hard rock conditions. To consider alternative deep shear-wave velocities, profile M1P2 provides for a low sediment velocity to Precambrian basement while profile M1P3 considers the possibility of a rapidly increasing shear-wave velocity with depth. All three profiles have basement depth randomized $\pm$ 500 ft (152m).

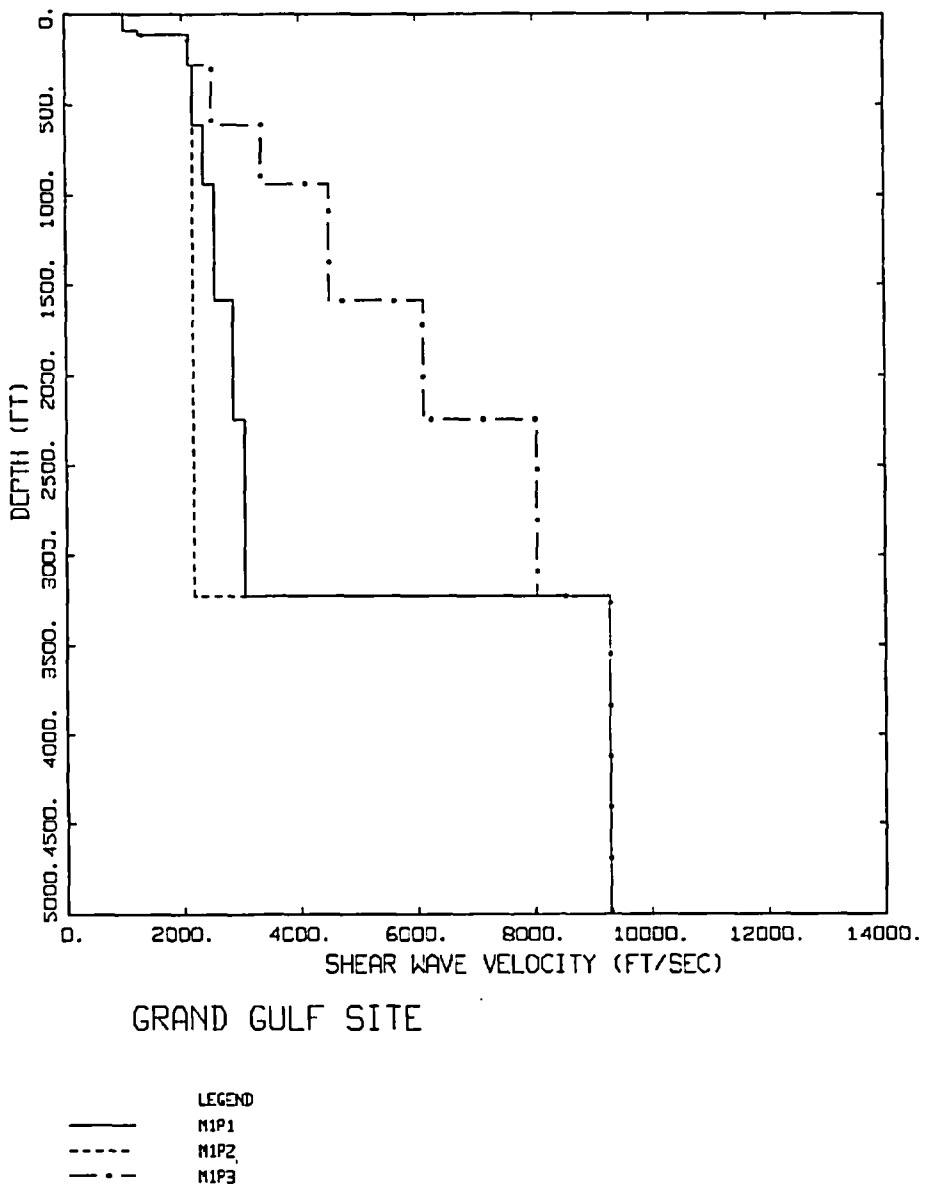

Figure B-5
Shear-Wave Velocity Profiles for the Grand Gulf Site

Profile M1P1 is considered the base case profile with M1P2 and M1P3 to accommodate lower and higher at-depth velocities. All three profiles are estimates below a depth of about 200 ft (61m).

B.5.2.2 Modulus Reduction and Hysteretic Damping Curves

Based on comparison of recent resonant column and torsional shear test results with the EPRI (1993) cohesion-less soil curves, the EPRI curves were adopted for the deposits with a site-specific assignment (Entergy, 2003). For the claystones at depths below the site characterization, the Peninsular Range curves were used, to a depth of 500 ft (152 m) with linear response below (Entergy, 2003).

B.5.2.3 Regional Crustal Damping (kappa)

For the deep sedimentary basin, 27,000 ft (8,200m) to Precambrian basement, a total base-case site kappa value of 0.046 sec was assumed. This is considered a conservative (low) value for this region of the embayment (Professor R. Herrmann personal communication, 2001) and based on deep soils/sediments in the Western United States (Anderson and Hough, 1984; Silva et al., 1997). Alternative considerations for a lower total kappa value of 0.028 sec (M1P1.KH) and a higher total kappa value of 0.066 sec were also used for the base-case profile (M1P1) and are based on subtracting and adding a kappa of about 0.02 sec to the base case value of 0.046 sec.

B.5.2.4 Profile Weights

The profile weights for the amplification factors are listed below in Table B-5.

Table B-5
Grand Gulf Weights

Properties*	Category Weights
M1P1	0.6
M1P1.KH	0.2
M1P1.KL	0.2
M1P1	0.8
M1P2	0.1
M1P3	0.1
	Combined Weights
M1P1	0.48
M1P1.KH	0.16
M1P1.KL	0.16
M1P2	0.10
M1P3	0.10

*M1P1; base case profile, kappa = 0.046 sec

M1P1.KH; base case profile, kappa = 0.066 sec

M1P1.KL; base case profile, kappa = 0.028 sec

M1P2; low gradient profile, kappa = 0.046 sec

M1P2; high gradient profile, kappa = 0.046 sec

B.6 HOPE CREEK SITE

The Hope Creek Generating Station is located on an artificial island, a man-made promontory on the east bank of the Delaware River in New Jersey. The site is within the Atlantic Coastal Plain physiographic province about 18 miles (29 km) southeast of the Fall Line.

The site is underlain by three Quaternary units including 30 to 45 ft (9 to14m) of hydraulic fill, 2 to 12 ft (0.6 to 3.7m) of coarse sand and gravel and 5 to 20 ft (1.5 to 6.1m) of non-organic clay. These strata are deposited on the Miocene Kirkwood Formation, a 2 to 6 foot (0.6 to 1.8m) thick basal sand overlying a silty organic clay. The Kirkwood unconformably overlies the Eocene Vincentown Formation that consists of basal sandstone and two overlying sand units. The soils above and into the Vincentown were removed to a depth of approximately that 72 ft (22m) at the location of the power block (EPRI, 1989).

The Vincentown conformably overlies 14 to 20 ft (4.3 to 6.1m) of fine-to-medium sand and silt of the Paleocene Hornerstown Formation. The Mesozoic strata are primarily sands with clay and gravel. Precambrian and Early Paleozoic crystalline basement rock was estimated to be at a depth of about 1,800 ft (550m).

B.6.1 Soil Profile Information

The Quaternary units including the fill as well as the Miocene Kirkwood Formation were removed during the construction of the power block. The power block is founded on the sands of the Vincentown Formation. Basement rock is estimated to be at a depth of 1,800 ft (550m) (rock hazard defined as basement material with a Vs of 2.83 km/sec).

Geophysical refraction and up-hole seismic studies were performed to measure seismic velocities at the site to a depth of 400 ft (122m). The average shear-wave velocity is 1,850 ft/sec (564 m/sec) in the Vincentown and Hornerstown Formations and the underlying strata.

Site-specific laboratory dynamic material testing for modulus reduction and hysteretic damping strain dependencies reflecting recent procedures were not available for this site (EPRI, 1989).

B.6.2 Description of Base Case Profiles

B.6.2.1 Shear Wave Velocity Profiles

Figure B-6 shows the base-case shear-wave velocity profile (M1P1) with an assumed increase in velocity from depth of 400 ft (122m) to 800 ft (244m) where the shear-wave velocity is taken to reach 3,000 ft/sec (914 m/sec), due to age and confinement. Alternatively, the velocity at a depth of about 400 ft (122m) (1,850 ft/sec, 564 m/sec), based on up-hole measurements, is continued to Precambrian basement at a depth of 1,800 ft (550m) (profile M1P2, Figure B-6). Both profiles are randomized in depth $\pm$500 ft (152m).

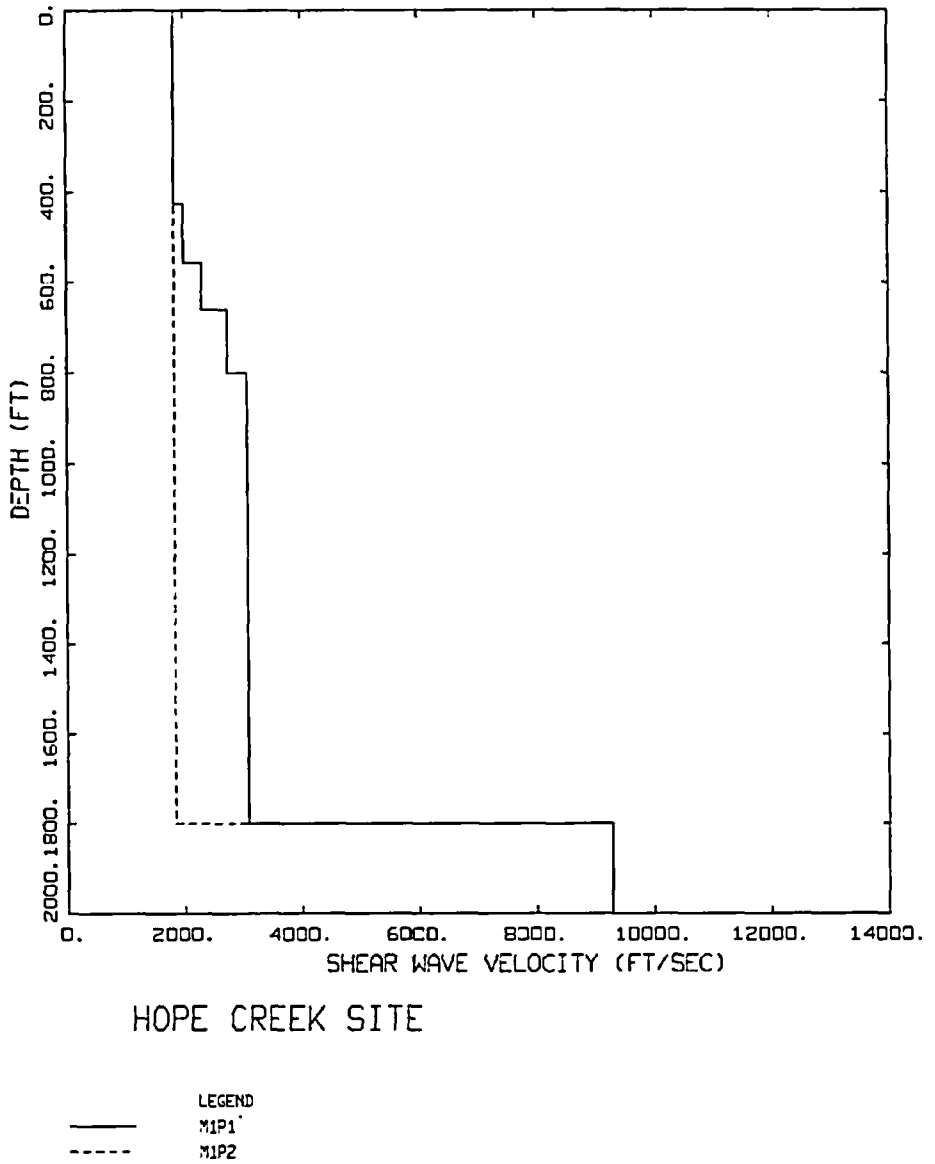

Figure B-6
Shear-Wave Velocity Profiles for the Hope Creek Site

Profile M1P1 is considered the base case profile with M1P2 to accommodate a continued low velocity in the deep sands, clays, and gravels. Both profiles are estimates below a depth of about 400 ft (122m).

B.6.2.2 Modulus Reduction and Hysteretic Damping Curves

Since little recent information was available for site-specific nonlinear dynamic material properties, Peninsular Range modulus reduction and damping curves were taken as base-case properties (Silva et al., 1997; 1998b). These curves are based on modeling recorded strong ground motions in Southern California, are more linear than the EPRI (1993) cures, and are considered to reflect expected non-linearity of the Pleistocene (and earlier) soil (sands and clays) beneath the power block. To consider the potential influence of gravels on the soil non-linearity, the more nonlinear EPRI (1993) curves are considered as well (M2P1).

B.6.2.3 Regional Crustal Damping (kappa)

Based on location within the same physiographic province as the Savannah River Site and similar thickness of soils (about 1,000 ft, 305m for the Savannah River Site), the measured Savannah River kappa value of 0.02 sec (Fletcher, 1995) was adopted as the base-case value. A 50% increase, due to the deeper depth to Precambrian basement of about 1,800 ft (550m), was also considered (M1P1.KH).

B.6.2.4 Profile Weights

The profile weights for the amplification factors are listed below in Table B-6.

Table B-6
Hope Creek Weights

Properties*	Category Weights
M1P1	0.7
M1P1.KH	0.3
P1	0.7
P2	0.3
M1	0.7
M2	0.3
	Combined Weights
M1P1	0.343
M1P1.KH	0.210
M1P2	0.210
M2P1	0.147
M2P2	0.090

*M1P1; base case profile, Peninsular Range Curves, kappa = 0.02 sec

M1P1.KH; base case profile, Peninsular Range Curves, kappa = 0.03 sec

M1P2; low gradient profile, Peninsular Range Curves, kappa = 0.02 sec

M2P2; low gradient profile, EPRI Curves, kappa = 0.02 sec

M2P1; base case profile, EPRI Curves, kappa = 0.02 sec

B.7 LA SALLE SITE

The La Salle County Nuclear Generating Station is located in Northeastern Illinois at the northern end of the Illinois Basin.

The site is underlain by Pleistocene Wisconsinan Wedron silty clay glacial till with some localized sand and gravel deposits. The thickness of the till in the area of the plant structures is about 170 ft (52m). The glacially derived Pleistocene deposits unconformably overlie a complex series of Paleozoic shales, sandstones, siltstones, clays, coals, and limestones with a total thickness of about 4,000 ft (1,220m). Precambrian crystalline basement rock was estimated to be at a depth of about 4,200 ft (1,280m) (EPRI, 1989).

B.7.1 Soil Profile Information

The top 44 ft (13.4m) of the Pleistocene Wedron Formation was removed during construction of the reactor building. The thickness of the remaining till underneath the reactor building is about 126 ft (38.4m). The Paleozoic strata consist of the Pennsylvanian Carbondale (151 ft (46m) thick) and Spoon Formations (25 ft (7.6m) thick). Drilling penetrated both of these formations during the site investigation. The remaining Paleozoic strata include about 600 ft (180m) of interbedded limestones, dolomites, sandstone and shale overlying about 3,300 ft (1,000m) of Cambrian sandstone, shale, and dolomite. Basement rock is estimated to be at a depth of 4,200 ft (1,280m) (rock hazard defined as basement material with a Vs of 2.83 km/sec).

Geophysical refraction studies measured compressional seismic velocities into the top of the Paleozoic shales and siltstones at a depth of 170 ft (52m). The estimated (from Vp and estimate of Poisson's ratio) shear-wave velocities are 400 ft/sec (122 m/sec), 1,640 ft/sec (500 m/sec) and 4,800 ft/sec (1,463 m/sec) in the upper till, lower Till and Paleozoic Formations, respectively (EPRI, 1989).

Site-specific laboratory dynamic material testing for modulus reduction and hysteretic damping strain dependencies reflecting recent procedures were not available for this site (EPRI, 1989).

B.7.2 Description of Base Case Profiles

B.7.2.1 Shear Wave Velocity Profiles

Figure B-7 shows the base-case profile (M1P1) to a depth of 4,200 ft (1,280m) (randomized + 1,000 ft (305m) where it encounters Precambrian basement. To consider the likelihood of a gradient in the deep sandstones, shales, and dolomites, profile M1P2 (Figure B-7) has shear-wave velocity increasing with depth.

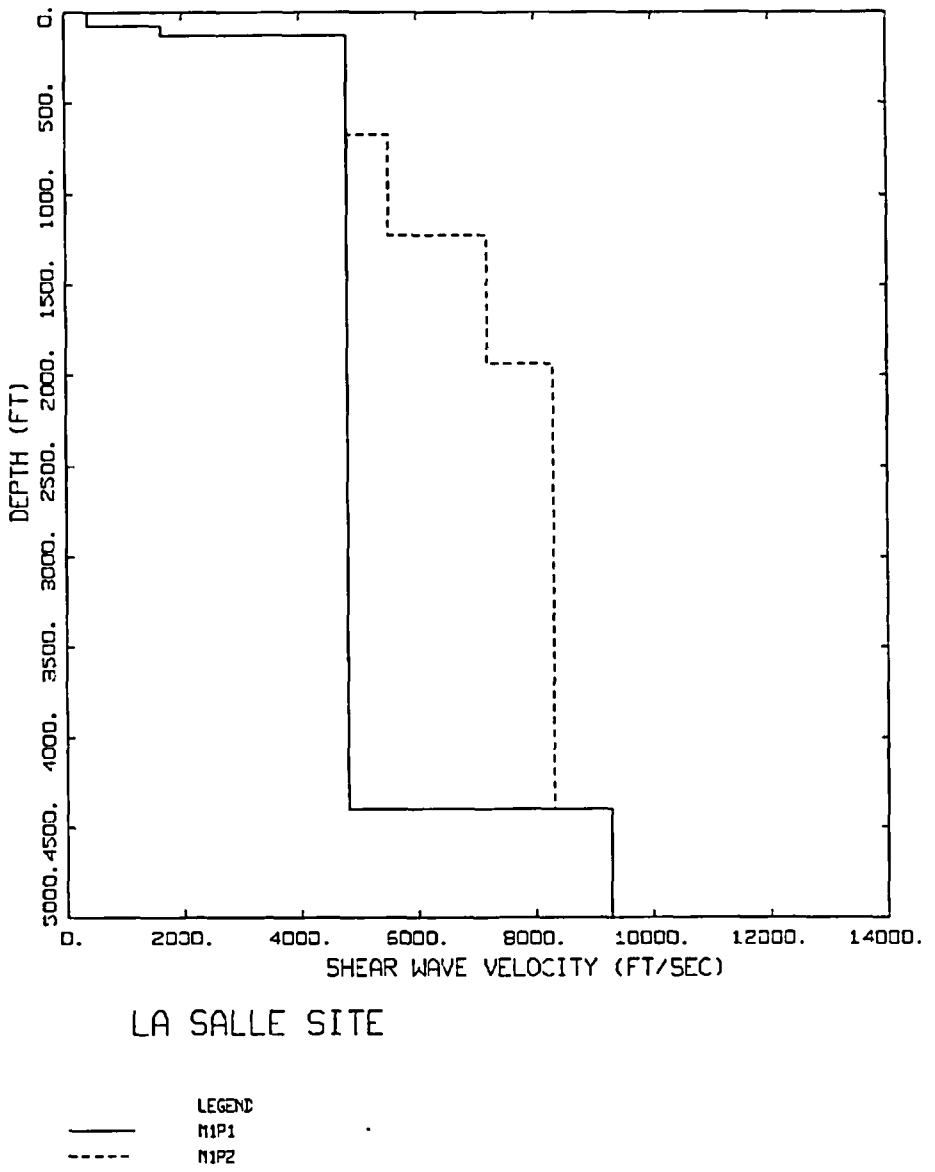

Figure B-7
Shear-Wave Velocity Profiles for the La Salle Site

Profile M1P1 is considered the base case profile with M1P2 to accommodate a gradient in the deep sandstone and dolomite. Both profiles reflect estimates below a depth of about 600 ft (183m).

B.7.2.2 Modulus Reduction and Hysteretic Damping Curves

For the till section of the profile, approximately the top 126 ft (38.4), EPRI Till curves (EPRI, 1993) were used (M1 in Table B-7). To consider the possibility that the upper and lower Till behaves at high strain in a manner similar to typical cohesion-less soil, the EPRI (1993) curves for sands, gravels, and low PI clays were also used (M2 in Table B-7).

B.7.2.3 Regional Crustal Damping (kappa)

Using Equation B-1 and considering the Carbondale shale and siltstone as outcropping with an average shear-wave velocity over the top 100 ft (31m) at 4,800 ft/sec (1,463 m/sec), the estimated kappa value is 0.0157 sec. For the overlying Till section, the low-strain damping in the EPRI (1993) Till curves contribute a kappa of 0.007 sec while the EPRI (1993) soil curves contribute 0.005 sec, resulting in a total site kappa of 0.0223 sec and 0.0207 sec respectively.

To consider alternative mean kappa values, the rock outcrop was considered to have a kappa value of 0.01 sec, resulting in a total site kappa of 0.0166 (M1P1.KL in Table B-7). For a high kappa value, the total kappa was taken as 0.04 sec, an overall conservative average value for western North America rock and soil sites (Silva et al., 1997).

B.7.2.4 Profile Weights

The profile weights for the amplification factors are listed below in Table B-7.

Table B-7
La Salle Weights

Properties*	Category Weights
M1P1	0.4
M1P1.KH	0.2
M1P1.KL	0.4
P1	0.5
P2	0.5
M1	0.5
M2	0.5
	Combined Weights
M1P1	0.1
M1P1.KH	0.1
M1P1.KL	0.2
M1P2	0.5
M2P1	0.1

*M1P1; base case profile, Till Curves, kappa = 0.0223 sec

M1P1.KH; base case profile, Till Curves, kappa = 0.04 sec

M1P1.KL; base case profile, Till Curves, kappa = 0.0166 sec

M1P2; low gradient profile, Till Curves, kappa = 0.0223 sec

M2P1; base case profile, EPRI Curves, kappa = 0.0207 sec

B.8 NINE MILE POINT SITE

The Nine Mile Point Nuclear Station is located on the south shore of Lake Ontario in Oswego County, New York. The site is located in the Erie-Ontario Lowlands physiographic province.

The site is located on 10 to 15 ft (3 to 4.5m) of Pleistocene glacial deposits, a sandy till. Moderately hard Oswego sandstone of Ordovician age lies beneath the till. Thinly bedded silty and clayey lenses are common in the Oswego Formation that is about 175 ft (53m) thick at the site. This formation grades down in to the Lorraine group that consists of shale and siltstone. This group was estimated to be 665 ft (200m) thick. Below these strata are the Ordovician Trenton limestone and Cambrian Potsdam sandstone groups of about 820 ft (250m) and 30 ft (9m) thick, respectively. Crystalline basement rock was estimated to be at a depth of about 1,700 ft (520m) (EPRI, 1989).

B.8.1 Soil Profile Information

The surficial glacial till was removed during construction. The Unit 1 and Unit 2 plant structures are founded on firm bedrock consisting of Oswego sandstone or Lorraine shale, respectively. Basement rock is estimated to be at a depth of 1,700 ft (520m) (rock hazard defined as basement material with a Vs of 2.83 km/sec).

Geophysical measurements including seismic refraction, uphole, and cross-hole were performed from 1964 to 1978. During the cross-hole survey, measurements of shear-wave velocity were made to a depth of 350 ft (106.7m). The measured shear-wave velocity in the Oswego sandstone at depth was about 8,000 ft/sec (2,438 m/sec). Inferred shear-wave velocities based on compression-wave velocities range from about 5,000 ft/sec (1,524 m/sec) to about 8,000 ft/sec (2,438 m/sec) over the shallow portion of the sandstones below the surficial till. A 3D geophysical survey showed a range in shear-wave velocities from 3,600 ft/sec (1,097 m/sec) to about 7,000 ft/sec (2,133 m/sec) (EPRI, 1989).

Site-specific laboratory dynamic material testing for modulus reduction and hysteretic damping strain dependencies reflecting recent procedures were not available for this site.

B.8.2 Description of Base Case Profiles

B.8.2.1 Shear Wave Velocity Profiles

Figure B-8 shows the base-case profile (M1P1) with a steep gradient in the shallow sandstone reaching hard rock velocities (9,285 ft/sec, 2.83 km/sec) at a depth of about 60 ft (18m) (randomized + 40 ft, 12m). To accommodate the range in inferred and measured shear-wave velocities, profile M1P2 (Figure B-8) considers hard rock as foundation material and profile M1P3 (Figure B-8) assumes a low near surface velocity of 5,000 ft/sec (1,524 m/sec) extends to basement material at a depth of 1,700 ft (518m) (randomized + 500 ft, 152m).

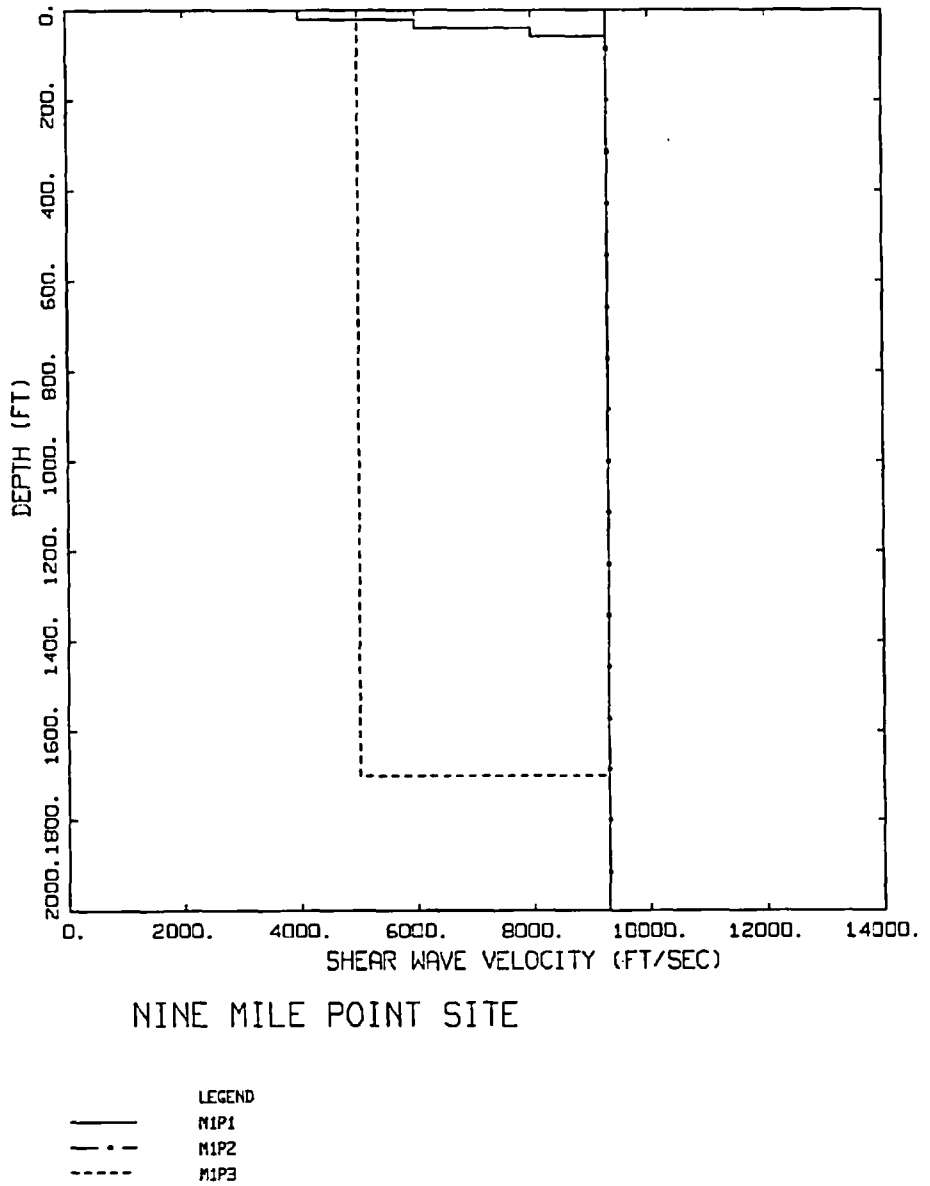

Figure B-8
Shear-Wave Velocity Profiles for the Nine Mile Point Site

Profile M1P1 is considered the base case profile with M1P2 and M1P3 to accommodate higher and lower velocities at the surface and with depth. The range in profiles is intended to capture the range in inferred (from shallow compressional-wave refraction) and measured (crosshole) shear-wave velocities.

B.8.2.2 Modulus Reduction and Hysteretic Damping Curves

For the all three profiles (Figure B-8) the Peninsular Range rock curves (Silva et al., 1997) are used for the very shallow materials (approximately 60 ft, 18m).

B.8.2.3 Regional Crustal Damping (kappa)

For the base-case profile (M1P1, Figure B-8), the average shear-wave velocity over the top 100 ft (31m) is nearly 7,000 ft/sec (2,133 m/sec) resulting in an estimated kappa value of 0.01 sec using Equation B-1. The high velocity profile (M1P2) has the defined central and eastern North America hard rock kappa value of 0.006 sec (amplification of 1.0). For the low-velocity profile, with a shear-wave velocity of 5,000 ft/sec (1,524 m/sec), Equation B-1 gives an expected kappa value of 0.015 sec (M1P3).

To consider alternatives for the base case profile M1P1.KL and M1P1.KH have kappa values of 0.006 and 0.020 sec, respectively.

B.8.2.4 Profile Weights

Profile weighs used for the amplification factors are listed below in Table B-8.

Table B-8
Nine Mile Point Weights

Properties*	Category Weights
M1P1	0.6
M1P1.KH	0.2
M1P1.KL	0.2
M1P1	0.5
M1P2	0.3
M1P3	0.2
	Combined Weights
M1P1	0.3
M1P1.KH	0.1
M1P1.KL	0.1
M1P2	0.3
M1P3	0.2

*M1P1; base case profile, kappa = 0.01 sec

M1P1.KH; base case profile, kappa = 0.02 sec

M1P1.KL; base case profile, kappa = 0.006 sec

M1P2; high velocity profile, kappa = 0.006 sec

M1P3; low velocity profile, kappa = 0.015 sec

B.9 NORTH ANNA SITE

The North Anna Power Station is located on the southern shore of Lake Anna in Northeastern Virginia. The site is located in the central part of the Piedmont physiographic province.

The site is located on a Paleozoic basement rocks consisting of granitic gneiss. A thin soil and a zone of weathered bedrock (saprolite) overlie slightly weathered to fresh un-weathered crystalline bedrock, which is encountered at depths of about 40 ft (12.2m) across the plant area (EPRI, 1989).

B.9.1 Soil Profile Information

The reactor buildings are founded crystalline bedrock at a depth of about 68 ft (20.7m) below finished grade. Basement rock is estimated to be at a depth of 100 ft (30.5m) (rock hazard defined as basement material with a Vs of 2.83 km/sec).

Geophysical measurements included seismic refraction, in-hole (Birdwell 3D logs), and cross-hole were performed (EPRI, 1989). For the deepest hole, shear-wave velocities around 8,000 ft/sec (1,838 m/sec) are measured at depths of 130 ft (40m). The range in measured shear-wave velocities was from about 4,000 ft/sec (1,219 m/sec) to about 8,000 ft/sec (1,838 m/sec). Dominion (2003) completed a downhole seismic test that determined shear-wave velocities to a depth of 67.5 ft (20.6m) for the North Anna site. The velocity at this depth was 6,030 ft/sec (1,838 m/sec).

Site-specific laboratory dynamic material testing for modulus reduction and hysteretic damping strain dependencies reflecting recent procedures were not available for this site.

B.9.2 Description of Base Case Profiles

B.9.2.1 Shear Wave Velocity Profiles

Figure B-9 shows the base-case profile (M1P1). The surface shear-wave velocity is 6,030 ft/sec (1,838 m/sec) and is based on a recent suspension log survey with this velocity encountered at a depth of about 60 ft (18m), the reactor building foundation depth. The increase in velocities below reflects application of a gradient taken from crosshole seismic tests in similar Piedmont physiographic province materials (Catawba Site, Section B-3). To accommodate higher outcrop velocities, profile M1P2 has hard rock outcropping at the surface (reactor containment depth) with a shear-wave velocity of 9,285 ft/sec (2.83 km/sec). To consider a low surficial velocity and high velocity gradient, profile M1P3 (Figure B-9) is based on the low range of crosshole seismic tests (EPRI, 1989). Profile M1P1, the base-case, is assumed to encounter hard rock conditions at a depth of 119 ft (36m) (randomized + 33 ft (10m)). For the high gradient profile (M1P3) hard rock is at a depth of 139 ft (42m), randomized + 50 ft (15m).

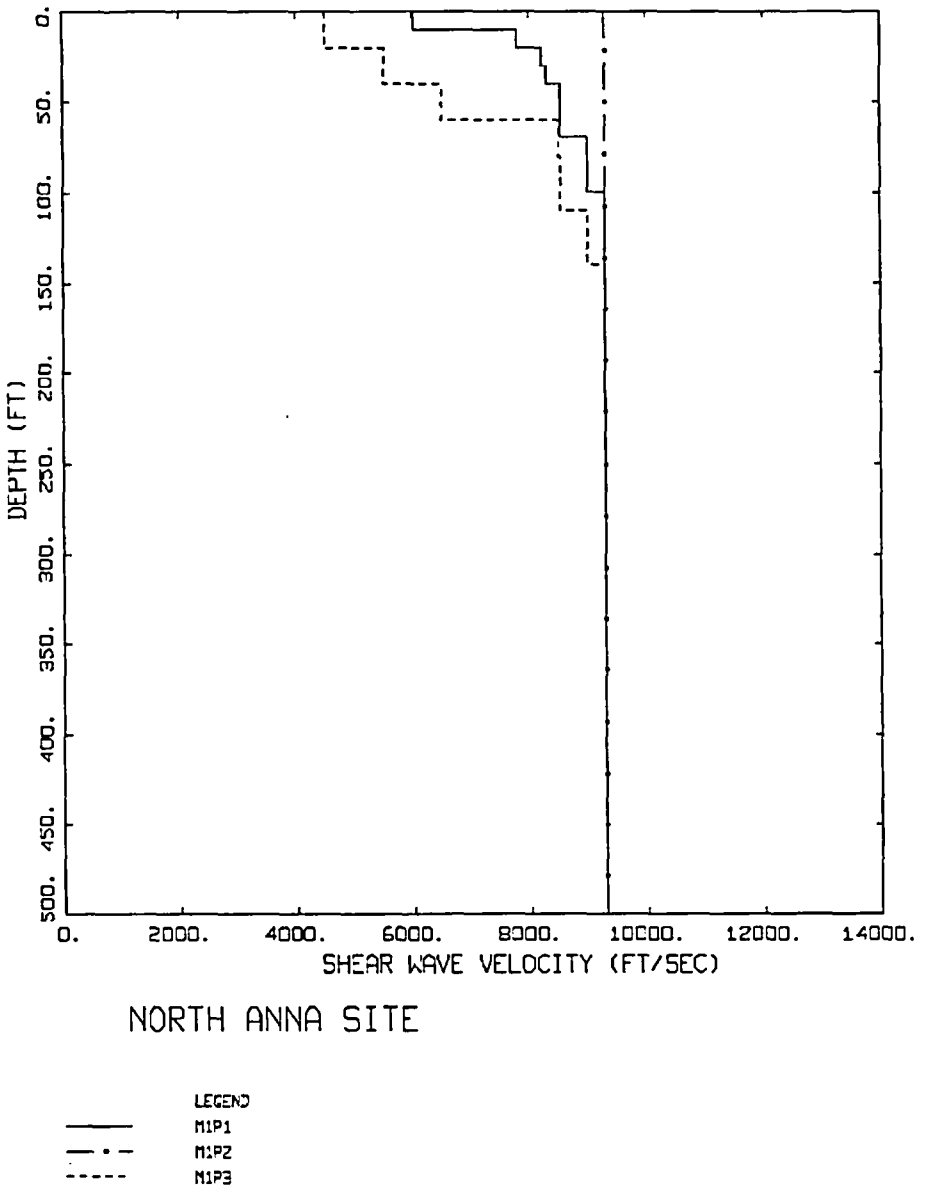

Figure B-9
Shear-Wave Velocity Profiles for the North Anna Site

Profile M1P1 is considered the base case profile with M1P2 and M1P3 to accommodate higher and lower velocities. All three profiles are estimates below a depth of about 50 ft (15m).

B.9.2.2 Modulus Reduction and Hysteretic Damping Curves

In the shallow potion of the profiles, approximately top 100 ft (31m) the Peninsular Range rock curves (Silva et al., 1997) are used.

B.9.2.3 Regional Crustal Damping (kappa)

The kappa value for the base-case profile was taken as the hard rock value of 0.006 sec plus that contributed by the low-strain damping from the Peninsular Range rock curves (Silva et al., 1997), a value of 0.0008 sec, for a total kappa of about 0.007 sec. With an average shear-wave velocity over the top 100 ft (31m) of just over 8,000 ft/sec (2,438 m/sec), Equation B-1 gives a similar value of 0.0087 sec. High velocity profile M1P2 (Figure B-9) has the reference kappa of 0.006 sec (amplification of 1.0) while the low velocity (high gradient) profile (M1P3) was given a total kappa value of 0.012 sec, based on Equation B-1 with an average shear-wave velocity (100 ft, 31m) of 6,384 ft/sec (1946 m/sec).

B.9.2.4 Profile Weights

The B-9 lists profile weights used for the amplification factors.

Table B-9
North Anna Weights

Properties*	Category Weights
M1P1	0.5
M1P2	0.1
M1P3	0.4
	Combined Weights
M1P1	0.5
M1P2	0.1
M1P3	0.4

*M1P1; base case profile, kappa = 0.007 sec

M1P2; high velocity profile, kappa = 0.006 sec

M1P3; low gradient profile, kappa = 0.012 sec

B.10 RIVER BEND SITE

The River Bend Station about 24 miles (39 km) northwest of Baton Rouge, Louisiana on the Uplands complex adjacent to the Mississippi alluvial valley. The site is in the Southern Hills physiographic section of the Gulf Coastal Plain physiographic province. The plant area is situated 1.9 mi (3.3 km) northeast of the east bank of the Mississippi River adjacent to the Deltaic physiographic province. In the site vicinity the Uplands are composed of Plio-Pleistocene fluvial deposits with an overlying blanket of loess.

The near surface stratigraphy is consists of about 8 ft (2.4m) of loess over the Pleistocene Port Hickey Top Stratum and terrace deposits 60 ft (18m) thick. Beneath these strata are silty sands, sands, clays, and gravels of the Pliocene Citronelle Formation and the hard clay of the Pascagoula Formation. The Pascagoula Formation was the oldest formation encountered by borings in the site area. It is a part of the Grand Gulf – Fleming Group that is about 6,500 ft (2,000m) thick at the site. The strata underlying the site consist of a thick and stratigraphically complex sequence of relatively flat lying sediments that are part of the Gulf Coast geosyncline. These sediments are about 20,000 ft (6,000m) thick and unconformably overlie a sequence or rocks composed mainly of Mesozoic limestone. Precambrian crystalline basement rock was estimated to be at a depth of about 27,000 ft (8,200m) (EPRI, 1989).

B.10.1 Soil Profile Information

The Loess, Port Hickey, and top 20 ft (6m) of the Citronelle deposits were removed at the site to a depth of 88 ft (27m). The reactor building is founded on 40 ft (12m) of compacted fill on top 60 ft (18m) of fine to medium sand and gravel (Citronelle Buried Channel Deposits). Underlying the Citronelle is several thousand feet of hard clay (Pascagoula Formation). Rock hazard defined as basement material with a Vs of 2.83 km/sec is taken at a depth of 5,000 ft (1,524m) which is deep enough to accommodate soil amplification at the lowest frequency of interest, 0.5 Hz (Silva et al., 1999, 2000).

Geophysical measurements included seismic refraction, downhole, uphole and cross-hole were performed. In the deepest boring shear-wave velocities around 1,200 ft/sec (365 m/sec) are measured at depths of 210 ft (64m) in the Pascagoula clay. Shear-wave velocity for the compacted fill is calculated from estimates of shear moduli and density at about 700 ft/sec (213 m/sec).

Site-specific laboratory dynamic material testing for modulus reduction and hysteretic damping strain dependencies reflecting recent procedures were not available for this site.

B.10.2 Description of Base Case Profiles

B.10.2.1 Shear Wave Velocity Profiles

Shown in Figure B-10 are the base-case (M1P1), low deep velocity (M1P2), and high deep gradient (M1P3) profile with all three reflecting measured shear-wave velocities in the top

roughly 120 ft (37m) (top 90 ft (27m) removed for embedment of reactor building). The top 40 ft (12m) reflecting compacted fill underlying the reactor building. Below the deepest measured velocity (1,200 ft/sec) (365 m/sec) the base-case velocities were assumed to increase to about 2,000 ft/sec (610 m/sec) at a depth of about 500 ft (152m), based on profiles in the Uplands province in the northern portion of the embayment (Entergy, 2003). The low-velocity profile (M1P2, Figure B-10) reflects the assumption of a continued Uplands 500 ft (112m) depth velocity to a depth of 3,281 ft (1 km), taken as a fictitious depth to basement to allow amplification to the lowest frequency of interest, 0.5 Hz. The high gradient profile (M1P3) accommodates the possibility of a rapidly increasing velocity with depth, reaching firm rock conditions around 1,000 ft to 2,000 ft (305m to 610m). All three profiles had depth to basement material at 3,281 ft (1 km) and randomized $\pm$ 500 ft (152m).

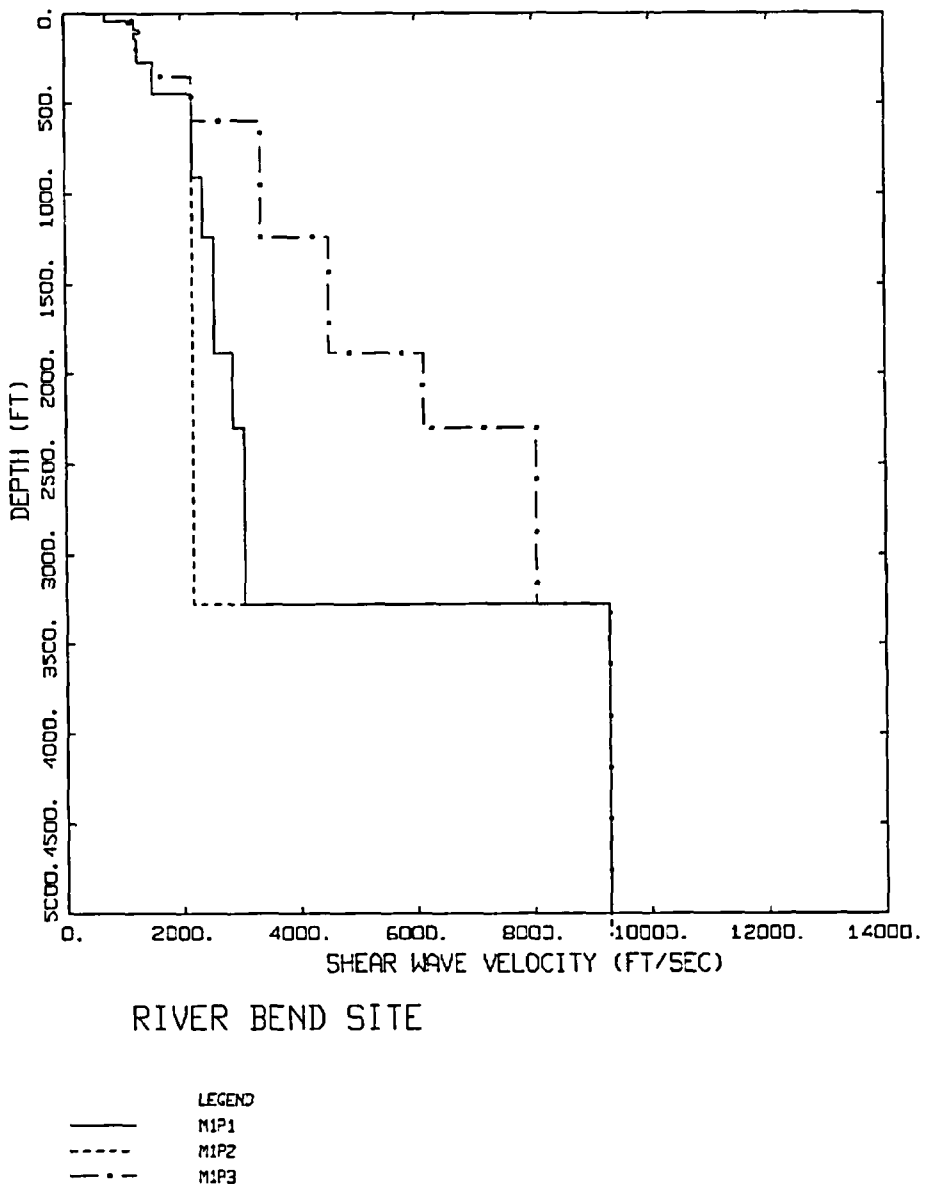

Figure B-10
Shear-Wave Velocity Profiles for the River Bend Site

Profile M1P1 is considered the base case profile with M1P2 and M1P3 to accommodate lower and higher velocities at depth. Profiles reflect estimates below measured velocities depth of about 100 ft (31m).

B.10.2.2 Modulus Reduction and Hysteretic Damping Curves

For the compacted fill and Pleistocene terrace deposits of the Citronelle sands, clays, and gravels over the top approximately 98 ft (30m), the EPRI (1993) 250 ft to 500 ft (76m to 152m) were used. For the Pascagoula clays, index properties suggested a PI of about 20% (EPRI, 1989) and resonant column tests showed modulus reduction curves consistent with Vucetic and Dobry (1991) cohesive soil curves reflecting a PI closer to 50% (EPRI, 1989). As a result the Vucetic and Dobry (1991) curves for a PI of 50% were used for depths between 98 ft (30m) and 272 ft (83m). For the clays below this depth the Vucetic and Dobry curves for a PI of 100% were used, to accommodate the potential effects of confining pressure. Below a depth of about 450 ft (137m), the EPRI (1993) 500 ft to 1,000 ft (152m to 304m) curves were used, consistent with the deep clays at the Savannah River Site (SRS, 1996).

B.10.2.3 Regional Crustal Damping (kappa)

As with the Grand Gulf Site (Section B.5), located in the Uplands complex of the Mississippi embayment, the base-case total site kappa value was taken as 0.046 sec. Higher and lower kappa values based on a 50% variation of the base-case value giving 0.069 sec (M1P1.KH in Table B-10) and 0.031 sec (M1P1.KL in Table B-10) were used as well.

B.10.2.4 Profile Weights

Table B-10 lists the weights used for the amplification factors.

Table B-10
River Bend Weights

Properties*	Category Weights
M1P1	0.6
M1P1.KH	0.2
M1P1.KL	0.2
M1P1	0.8
M1P2	0.1
M1P3	0.1
	Combined Weights
M1P1	0.48
M1P1.KH	0.16
M1P1.KL	0.16
M1P2	0.10
M1P3	0.10

*M1P1; base case profile, kappa = 0.046 sec

M1P1.KH; base case profile, kappa = 0.069 sec

M1P1.KL; base case profile, kappa = 0.031 sec

M1P2; high velocity profile, kappa = 0.046 sec

M1P3; low velocity profile, kappa = 0.046 sec

B.11 SHEARON HARRIS SITE

The Shearon Harris Nuclear Power Plant is located near the northern end of a reservoir on Buckhorn Creek in the extreme southwest corner of Wake County and the southeast corner of Chatman County in North Carolina. The site is located in the Triassic belt subdivision of the Piedmont Plateau physiographic province, a deeply eroded plateau-like segment of the Appalachian Mountain System. The site is located in the south central part of the Durham Basin that is about 52 miles (84 km) long with a maximum width of 20 miles (43 km) which is the northern most of three basins within the Deep River Triassic Basin.

The main plant structures are located on Triassic-age Sanford Formation consisting of gently dipping, well-consolidated sandstone, siltstone, and shaly siltstone. A thin residual soil and a zone of weathered bedrock overlie dense, massive sedimentary bedrock, which is encountered at depths of 16 ft (4.9m) across the plant area. Crystalline basement rock was estimated to be at a depth of at least 6,000 ft (1,829m) (EPRI, 1989).

B.11.1 Soil Profile Information

The reactor buildings are founded on siltstone and sandstone bedrock at an embedment depth of about 26 ft to 81 ft (8m to 25m) below finished grade. The bedrock at the site was originally overlain by about 8 ft (2.4m) of residual soils and about 8 ft (2.4m) of weathered and fractured rock. Basement rock is estimated to be at a depth over 6,000 ft (1,829m) (rock hazard defined as basement material with a Vs of 2.83 km/sec).

Geophysical measurements included seismic refraction, shear-wave velocity, and up-hole compressional-wave velocity measurements. Shear-wave velocity measurements at the top of the Sanford Formation (reactor buildings foundation material) are 5,600 ft/sec (1,707 m/sec) (EPRI, 1989).

Site-specific laboratory dynamic material testing for modulus reduction and hysteretic damping strain dependencies reflecting recent procedures were not available for this site.

B.11.2 Description of Base Case Profiles

B.11.2.1 Shear Wave Velocity Profiles

Figure B-11 shows the base-case profile (M1P1) with an embedment depth shear-wave velocity for the sandstones and siltstones of 5,600 ft/sec (1,707 m/sec) extending to crystalline basement, taken at a depth 6,000 ft (1,829m) and randomized $\pm$ 2,000 ft (610m). To consider the effects of an increase in velocities with depth, profile M1P2 (Figure B-11) considers reaching hard rock conditions, with a shear-wave velocity of 9,285 ft/sec (2.83 km/sec), at a depth of 500 ft (152m) (randomized $\pm$ 300 ft, 91m).

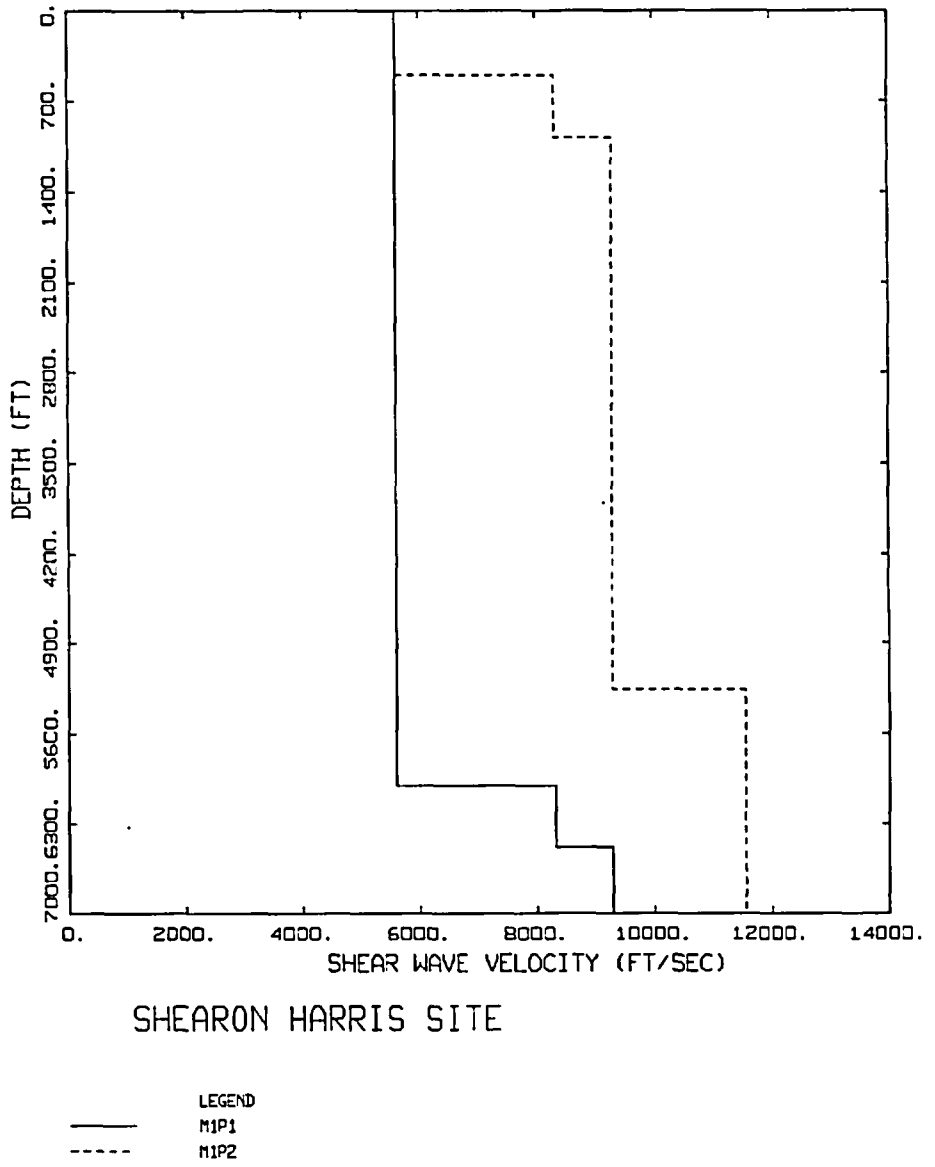

Figure B-11
Shear-Wave Velocity Profiles for the Shearon Harris Site

Profile M1P1 is considered the base case profile with M1P2 to accommodate a gradient in the deep sandstone and dolomite. Both profiles reflect estimates below a depth of about 50 ft (15m).

B.11.2.2 Modulus Reduction and Hysteretic Damping Curves

To accommodate possible nonlinear effects in the shallow portions of the profiles, the Peninsular Range rock curves (Silva et al., 1997) were used over the top 100 ft (31m).

B.11.2.3 Regional Crustal Damping (kappa)

For the outcropping sandstones and siltstones, the average shear-wave velocity over the top 100 ft (31m) is 5,600 ft/sec (1,707 m/sec) resulting in a kappa value of 0.0132 sec (Equation B-1). High and low kappa values considering a $\pm$ 50% variation in the base-case value were also considered. These values were 0.0198 sec (M1P1.KH in Table B-11) and 0.0088 sec (M1P1.KL in Table B-11) respectively.

B.11.2.4 Profile Weights

The profile weights for the amplification factors are listed below in Table B-11.

Table B-11
Shearon Harris Weights

Properties*	Category Weights
M1P1	0.6
M1P1.KH	0.2
M1P1.KL	0.2
M1P1	0.7
M1P2	0.3
	Combined Weights
M1P1	0.42
M1P1.KH	0.14
M1P1.KL	0.14
M1P2	0.30

*M1P1; base case profile, kappa = 0.0132 sec

M1P1.KH; base case profile, kappa = 0.0198sec

M1P1.KL; base case profile, kappa = 0.0088 sec

M1P2; high gradient profile, kappa = 0.0132 sec

B.12 SOUTH TEXAS SITE

The South Texas Project is located along the west bank of the Colorado River about 15 miles (24 km) from the Gulf of Mexico near Bay City, Texas. The site is in the Texas Gulf Plain physiographic province that is dominated by a thick sedimentary prism known as the Gulf Coast Geosyncline.

The near surface stratigraphy consists of about 700 ft to 800 ft (200m to 250m) of Pleistocene Beaumont and Lissie Formations. The upper 300 ft (90m) consists of layers of silty sand and clay with some sandy silt and fine sand. Quaternary sediments are present to at least 2620 ft (800m) beneath the site. The base of the Miocene Oakville sandstone is at about 6,200 ft

(1,900m). Pre-Cretaceous basement rock was estimated to be at a depth of about 34,500 ft (10,500m) (EPRI, 1989).

The strata above the pre-Cretaceous basement rock include 26,000 ft (7,900m) of Cenozoic sediments underlain by 8,500 ft (2,600m) of Cretaceous rocks. Basement rocks consists of 17,000 ft (5,200m) of pre-Cretaceous units that rest on rocks with high seismic velocities that have been termed "lower continental or oceanic crust" (EPRI, 1989).

B.12.1 Soil Profile Information

The top 60 ft (18m) of soil deposits (Layers A, B, C and D; EPRI, 1989) were removed at the site for construction of the reactor containment building. The reactor building foundations are supported by a dense to very dense, slightly silty sand of the Beaumont Formation. The upper 300 ft (91m) of soil generally consists of alternating layers of stiff to hard silty clay and dense to very dense silty sand. Hard rock hazard is defined at basement material with a Vs of 2.83 km/sec.

Shear-wave velocities were measured during cross-hole tests. The reactor building foundations are supported by sand with a shear-wave velocity of 1,150 ft/sec (350 m/sec). In the deepest boring shear-wave velocities around 1,585 ft/sec (483 m/sec) are measured at depths of 341 ft (104m) in the Pleistocene soils.

Dynamic testing of representative soils samples were performed on the natural soils and compacted backfill to estimate modulus reduction and damping curves EPRI (1989). Site-specific laboratory dynamic material testing for modulus reduction and hysteretic damping strain dependencies reflecting recent procedures were not available for this site.

B.12.2 Description of Base Case Profiles

B.12.2.1 Shear Wave Velocity Profiles

Figure B-12 shows the base-case shear-wave velocity profile (M1P1) based on crosshole measurements over approximately the top 250 ft (76m). Below that depth the Mississippi embayment lowlands profile, which had similar velocities at this depth, was used to extrapolate the base-case profile to a depth of 2,500 ft (762m), to capture potential low-frequency (0.5 Hz) amplification. This generic profile was developed for ground shaking studies in the embayment by Professor Glenn Rix of the MAE Center (personal communication, 2002). The profile is based on a large number of shallow and several deep velocity surveys and extends to a depth of 3,600 ft (1,100m). To accommodate amplification from lower shear-wave velocities beneath 250 ft (76m) (M1P2 in Figure B-12), the deepest measured velocity (1,585 ft/sec (483 m/sec)) was extended to a depth of 1,000 ft (305m), where it was merged to the base-case profile. To consider a steeper velocity gradient, the EPRI (1993) 1,000 ft (305m) stiff sand profile was added to the base of the measured velocities and increased, with a similar gradient, to a depth of 2,500 ft (762m). All three profiles are randomized in depth to 9,285 ft/sec (2.83 km/sec) velocities occurring at a depth of 2,500 ft (726m) and randomized $\pm$ 500 ft (152m).

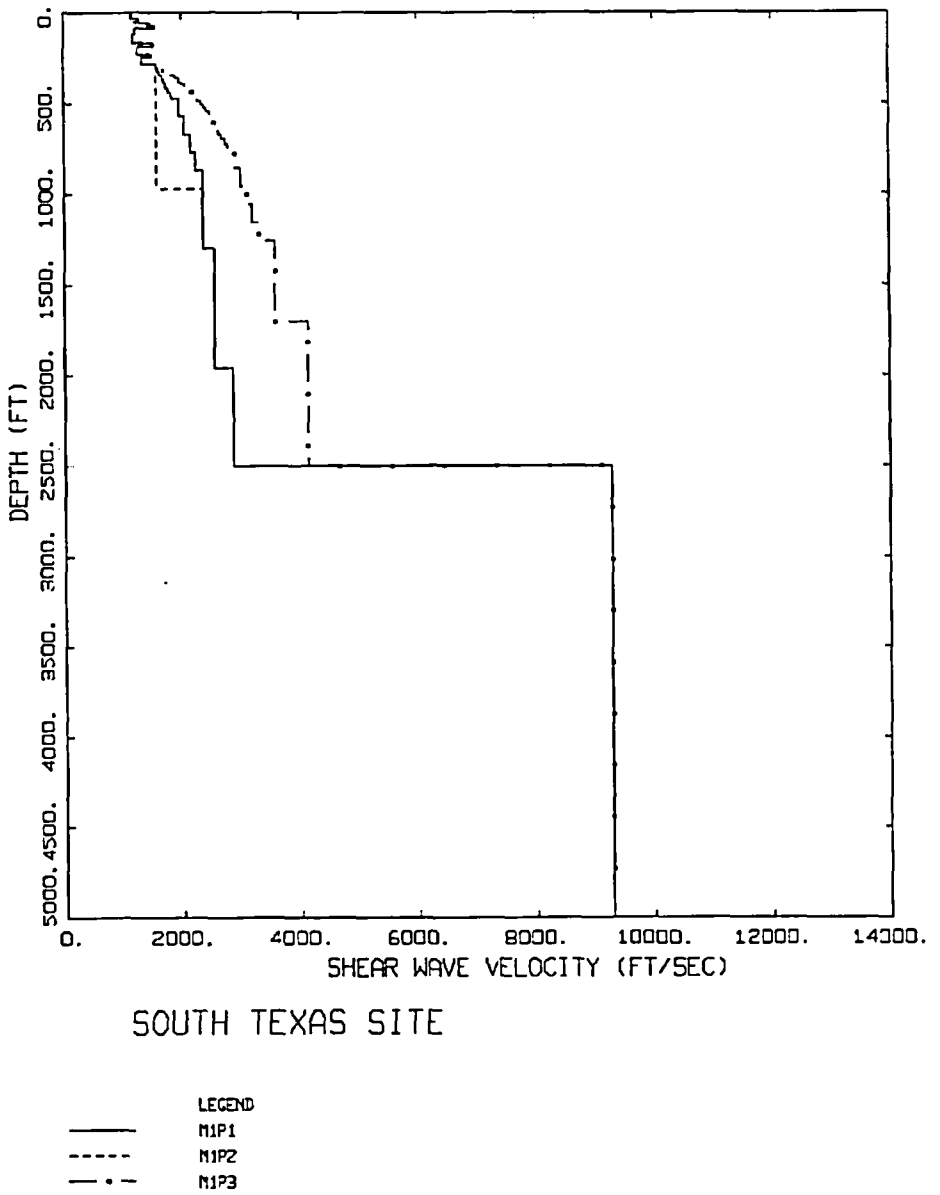

Figure B-12
Shear-Wave Velocity Profiles for the South Texas Site

Profile M1P1 is considered the base case profile with M1P2 and M1P3 to accommodate lower and higher velocities at depth. Profiles reflect estimates below measured velocities depth of about 250 ft (76m).

B.12.2.2 Modulus Reduction and Hysteretic Damping Curves

For the Holocene cohesion-less soils, laboratory dynamic material property testing showed G/G_{max} curves similar to those of EPRI (1993). As a result the EPRI (1993) curves were selected to reflect the base-case dynamic material (M1P1) properties as they are based on more recent testing procedures and have been extensively validated by modeling recorded strong ground motions (Silva et al., 1997; 1998b).

To consider the possibility of more linear response, the Peninsular Range curves (M2P1) were considered as well.

B.12.2.3 Regional Crustal Damping (kappa)

The base-case kappa value was taken as 0.046 sec, as with the other sites located on the deep soils of the Mississippi embayment. High and low kappa values based on a $\pm$ 50% variation about the base-case value were also considered. These alternative values were 0.069 sec and 0.031 sec respectively.

B.12.2.4 Profile Weights

The profile weights for the amplification factors are listed below in Table B-12.

Table B-12
South Texas Weights

Properties*	Category Weights
M1P1	0.6
M1P1.KH	0.2
M1P1.KL	0.2
M1P1	0.8
M1P2	0.1
M1P3	0.1
M1	0.6
M2	0.4
	Combined Weights
M1P1	0.288
M1P1.KH	0.160
M1P1.KL	0.160
M1P2	0.100
M1P3	0.100
M2P1	0.192

*M1P1; base case profile, EPRI curves, kappa = 0.046 sec

M1P1.KH; base case profile, EPRI curves, kappa = 0.069sec

M1P1.KL; base case profile, EPRI curves, kappa = 0.031 sec

M1P2; low gradient profile, EPRI curves, kappa = 0.046 sec

M1P3; high gradient profile, EPRI curves, kappa = 0.046 sec

M2P1; base case profile, Peninsular Range curves, kappa = 0.046 sec

B.13 SUMMER SITE

The Virgil C. Summer Nuclear Station is located approximately 1 mile (1.6 km) east of Broad River in Fairfield County in South Carolina. The site is located within the Piedmont physiographic province

The site is located on Paleozoic basement rocks of the Carolina Slate Belt consisting of granodiorite and migmatite. An 80 ft (24m) thick layer of residual soil (saprolite) and a 10 ft (3m) thick zone of weathered and jointed bedrock overlie sound crystalline bedrock, which is encountered at depths of 90 ft (27.4m) across the plant area EPRI (1989).

B.13.1 Soil Profile Information

The reactor buildings are founded on fill concrete overlying weathered rock overlying crystalline bedrock at a depth of about 39 ft (11.9m) below finished grade. Basement rock is estimated to be at a depth of 129 ft (39m) (rock hazard defined as basement material with a Vs of 2.83 km/sec).

Geophysical measurements included seismic refraction and surface wave testing. Shear-wave velocities for the weathered rock ranged from 1,500 ft/sec to 2,300 ft/sec (460 ft/sec to 700 m/sec) and in the basement rock from 7,400 to 8,000 ft/sec (2,250 to 2,440 m/sec) (EPRI, 1989).

Site-specific laboratory dynamic material testing for modulus reduction and hysteretic damping strain dependencies reflecting recent procedures were not available for this site.

B.13.2 Description of Base Case Profiles

B.13.2.1 Shear Wave Velocity Profiles

The base-case profile (M1P1), shown in Figure B-13 has relatively low shear-wave velocities at the surface, about 2,000 ft/sec (610 m/sec). This profile, along with an alternative shallow velocity gradient, having a surface shear-wave velocity of 4,000 ft/sec (1,219 m/sec) (M1P2), are intended to capture portions of the foundations not excavated into firm rock. The criteria used for excavation was a minimum compressional-wave velocity of 8,000 ft/sec (2,438 km/sec) (EPRI, 1989) which, for Poisson's ratios in the 0.35 to 0.4 range in weathered rock, would likely result in a near-surface low shear-wave velocity. Both of the gradient models in Figure B-13 were taken from crosshole measurements at the Catawba site (Section B.3), taken above the reactor containment embedment depth. Both sites are located within the Piedmont physiographic province typified by residual soil (saprolite) overlying weathered and joined bedrock which grades into firm to hard basement material. To consider reactor buildings founded on hard rock, profile M1P3 in Figure B-13 treats the hard rock shear-wave velocity (9,285 ft/sec (2.83 km/sec)) as outcropping at the free surface (embedment depth). Basement depth for profile M1P1 is randomized at 129 $\pm$ 50 ft (39.3 $\pm$ 15.2m). Basement depth for profile M1P2 is randomized at 119 $\pm$ 50 ft (36.3 $\pm$ 15.2m).

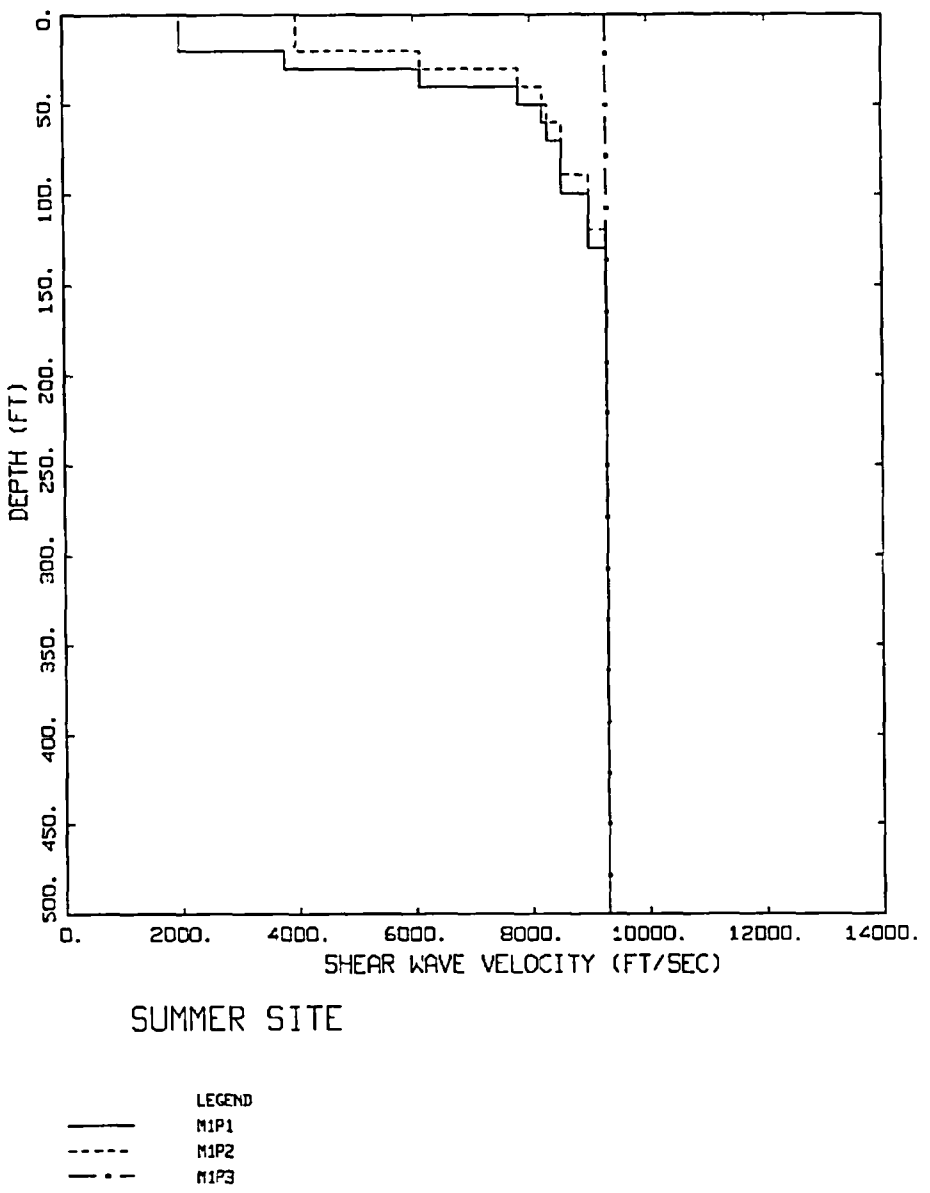

Figure B-13
Shear-Wave Velocity Profiles for the Summer Site

Profile M1P1 is considered the base case profile with M1P2 and M1P3 to accommodate higher near surface velocities. All three profiles are estimates below a depth of about 10 ft (3m).

B.13.2.2 Modulus Reduction and Hysteretic Damping Curves

For the softer profiles, M1P1 and M1P2 in Figure B-13, the Peninsular Range cohesion-less soil G/G_{max} and hysteretic damping curves (Silva et al., 1997) are used to a depth of 20 ft (6m) with the Peninsular Range rock curved to a depth of about 100 ft (31m). Linear response is assumed at greater depths.

B.13.2.3 Regional Crustal Damping (kappa)

For both gradient profiles, M1P1 and M1P2 in Figure B-13, the kappa contributed by the low-strain damping in the nonlinear portions of the profiles (approximately 100 ft (31m)) is 0.001 sec. Adding the hard rock value of 0.006 sec results in a total site kappa value of 0.007 sec. For the hard rock outcropping, the hard rock kappa value of 0.006 sec was used (amplification of 1).

B.13.2.4 Profile Weights

The profile weights for the amplification factors are listed below in Table B-13.

Table B-13
Summer Weights

Properties*	Category Weights
M1P1	0.3
M1P2	0.3
M1P3	0.4
	Combined Weights
M1P1	0.3
M1P2	0.3
M1P3	0.4

*M1P1; base case profile, kappa = 0.007 sec

M1P2; high gradient profile, kappa = 0.007 sec

M1P3; high velocity profile, kappa = 0.006 sec

B.14 THREE MILE ISLAND SITE

The Three Mile Island Nuclear Station is located on Three Mile Island in the Susquehanna River in Dauphin County, Pennsylvania. The site is located in the Gettysburg Basin section of the

Piedmont physiographic province. Three Mile Island was formed as a result of fluvial deposition by the Susquehanna River.

The main plant structures are located on Triassic-age Gettysburg Shale Formation consisting of sandstone, siltstone, and claystone. Surficial materials consist of loose to medium fine silty sand and gravel overlying a layer of medium dense to very dense coarse sand and gravel with numerous boulders and cobbles. Soil depths are 20 ft (6m) in the plant vicinity. There is about 1 to 3 ft (0.3 to 0.9m) of weathered shale beneath the soils. Underlying the Gettysburg Shale is a sequence of lower Paleozoic clastic and carbonate deposits. These strata overlie Precambrian crystalline basement rock estimated to be at a depth of about 16,000 ft (4,800m) (EPRI, 1989).

B.14.1 Soil Profile Information

The reactor buildings are founded on medium hard to hard shale, sandstone, and siltstone bedrock at an embedment depth of about 31 (9.4m) below finished grade. The sound bedrock at the site was originally overlain by about 20 ft (6.2m) of fluvial deposits. Basement rock is at an approximate depth of 16,000 ft (4,800m) (rock hazard defined as basement material with a Vs of 2.83 km/sec).

The compressional-wave velocities at the site were measured by a seismic refraction survey. Compressional-wave velocity measurements at the top of the Gettysburg Shale range from 8,500 ft/sec to 11,000 ft/sec (2,600 m/sec to 3,350 m/sec) (EPRI, 1989). Shear-wave velocities were calculated from compressional-wave velocities with the assumption of Poisson's ratio.

Site-specific laboratory dynamic material testing for modulus reduction and hysteretic damping strain dependencies reflecting recent procedures were not available for this site.

B.14.2 Description of Base Case Profiles

B.14.2.1 Shear Wave Velocity Profiles

Based on a shallow compressional-wave refraction survey giving velocities about 10,000 ft/sec (3,048 m/sec) and assuming a range in Poisson's ratio of 0.3 to 0.4, shear-wave velocities are in the range of 4,000 ft/sec (1,219 m/sec) to 5,000 ft/sec (1,524 m/sec). To accommodate these variabilities, a shear-wave velocity of 4,000 ft/sec (1,219 m/sec) was assumed for the surface and to a depth of 100 ft (31m) where the velocity was increased to 6,000 ft/sec (1,229 m/sec). This base-case profile (M1P1) is shown in Figure B-14. At a depth of about 2,000 ft (610m), the sedimentary rocks, sandstone, shale, and siltstone are taken to reflect an increase in velocity with depth, reaching hard rock velocities (9,285 ft/sec (2.83 km/sec)) at a depth of 5,000 ft (1,524m), deep enough to capture amplification to a frequency of 0.5 Hz. This depth is randomized $\pm$ 2,000 ft (610m) to smooth potential resonances. Profile M1P2, Figure B-14 assumes a constant sedimentary rock velocity with depth (to 5,000 ft $\pm$ 2,000 ft (1,524m $\pm$ 610m)). Profile M1P3 considers the case of encountering hard rock velocity at a depth of about 2,000 ft (610m), randomized $\pm$ 500 ft (152m).

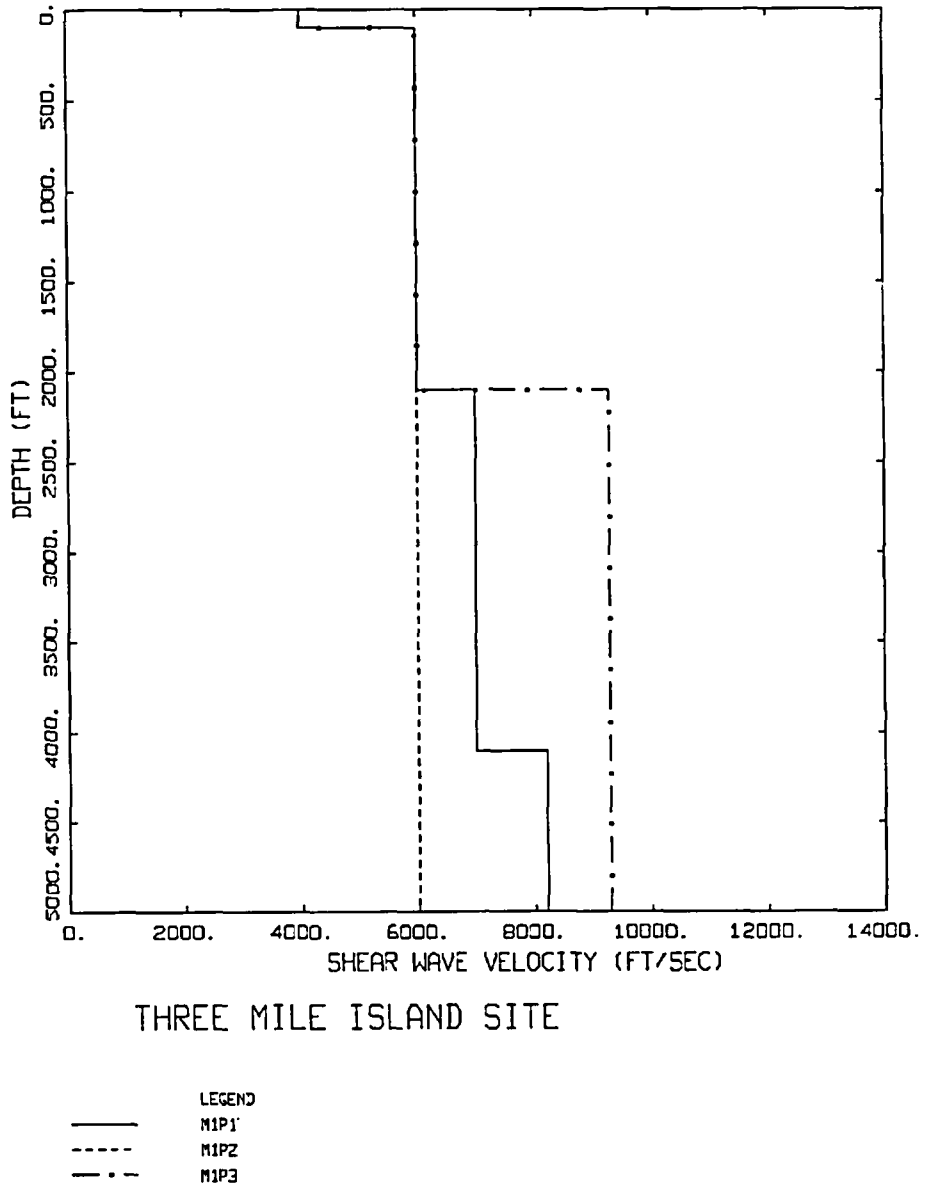

Figure B-14
Shear-Wave Velocity Profiles for the Three Mile Island Site

Profile M1P1 is considered the base case profile with M1P2 and M1P3 to accommodate lower and higher velocities at depth. All three profiles are estimates below a depth of about 50 ft (15m).

B.14.2.2 Modulus Reduction and Hysteretic Damping Curves

Peninsular Range rock curves (Silva et al., 1997) are used over the top 100 ft (31m) in all three profiles (Figure B-14).

B.14.2.3 Regional Crustal Damping (kappa)

For a shear-wave velocity of 4,000 ft/sec over the top 100 ft, Equation B-1 gives a kappa value of about 0.02 sec, which was adopted as the base-case value (Table B-14). To accommodate higher and lower kappa values, 0.04 sec and 0.01 sec were considered as well. The higher kappa value, 0.04 sec considers the site as having typical western North America soft rock conditions (Anderson and Hough 1984; Silva et al., 1997) while the low kappa (0.01 sec) reflects an assumption of firm to hard rock conditions (Silva and Darragh, 1995).

B.14.2.4 Profile Weights

The profile weights for the amplification factors are listed below in Table B-14.

Table B-14
Three Mile Island Weights

Properties*	Category Weights
M1P1	0.5
M1P1.KH	0.2
M1P1.KL	0.3
M1P1	0.6
M1P2	0.2
M1P3	0.2
	Combined Weights
M1P1	0.3
M1P1.KH	0.2
M1P1.KL	0.3
M1P2	0.1
M1P3	0.1

*M1P1; base case profile, kappa = 0.02 sec

M1P1.KH; base case profile, kappa = 0.04 sec

M1P1.KL; base case profile, kappa = 0.01 sec

M1P2; low deep velocity profile, kappa = 0.02 sec

M1P3; high deep velocity profile, kappa = 0.02 sec

B.15 VOGTLE SITE

The Vogtle Nuclear Plant is located on the southwest side of the Savannah River in Burke County, Georgia across the river from Barnwell County, South Carolina. The site is in the Tifton Upland of the Atlantic Coastal Plain physiographic province.

The near surface deposits are Quaternary alluvial deposits from the Savannah River and its tributaries. The Blue Bluff Member of the middle Eocene Lisbon formation forms the foundation for critical plant structures. This moderately hard calcareous siltstone or marl is underlain by quartz sand. The total thickness of the Blue Bluff member at the plant site is about 70 ft (21m). The quartz sand is about 100 ft (30m) thick and overlies an approximately 50 ft (15m) thick unit composed of interbedded clay, silty sand, and lignitic beds representing the Huber and Ellenton Formations of Paleocene age (EPRI, 1989).

The pre-Tertiary units include approximately 600 ft (180m) of Cretaceous sediments including the Tuscaloosa Formation that consists of fluvial and estuarine deposits of sand and minor gravel intercalated with silt and clay. The contact between the Cretaceous and the basement complex is at a depth exceeding 1,000 ft (305m) below the surface. The basement complex includes sediments of the buried Triassic Dunbarton Basin that mainly consist of breccias in a matrix of claystone and siltstone, alternating layers of sandstone, mudstone, siltstone, and claystone. The Precambrian crystalline basement rocks exposed northwest of the site include gneiss, granite, phyllite and greenstone (EPRI, 1989).

B.15.1 Soil Profile Information

The containment buildings are founded on compacted select sand backfill 61 ft (18.6m) below plant grade with the base of the reactor cavity mat at a depth of 85 ft (26m). The fill was placed in an excavation 90 ft (27m) below finished grade resulting in about 28.5 ft (8.7m) of fill below the containment building foundation. The excavation was made because the original soil consisted of very loose to dense sands that were potentially liquefiable and due to the presence of the thin shelly Utley limestone. A very hard calcareous clay marl (Blue Bluff Member of the Lisbon Formation) about 70 ft (21m) thick underlies the fill. A thick (750 ft (229m)) dense, coarse sand with minor interbedded silty clay and clayey silts underlies the marl. Basement rock is estimated to be at a depth of about 1,500 ft (457m) (rock hazard defined as basement material with a Vs of 2.83 km/sec).

Compressional- and shear-wave velocity measurements were made from cross-hole tests to a depth of 290 ft (88m). At this depth the shear-wave velocity of the clay marl was 1,700 ft/sec (520 m/sec). The shear-wave velocity for the compacted fill is calculated from shear moduli and density to be about 767 ft/sec (234 m/sec) in the top 10 ft (3m) and 1258 ft/sec (384 m/sec) below 10 ft (3m).

Site-specific laboratory dynamic material testing for modulus reduction and hysteretic damping strain dependencies reflecting recent procedures were not available for this site.

B.15.2 Description of Base Case Profiles

B.15.2.1 Shear Wave Velocity Profiles

The base-case shear-wave velocity profile reflecting reactor embedment conditions consists of about 30 ft (9m) of compacted fill overlying about 210 ft (64m) of measured (crosshole) velocities. Below that depth (about 240 ft (73m)), the nearby Savannah River Site profile (SRS, 1996) was adopted to a depth of 1,000 ft (305m). At this depth the Triassic Dumbarton basin was assumed to overly Precambrian basement, taken at a depth of about 1,500 ft (457m). Depth to the Dumbarton Basin sedimentary material was randomized $\pm$ 400 ft (122m).

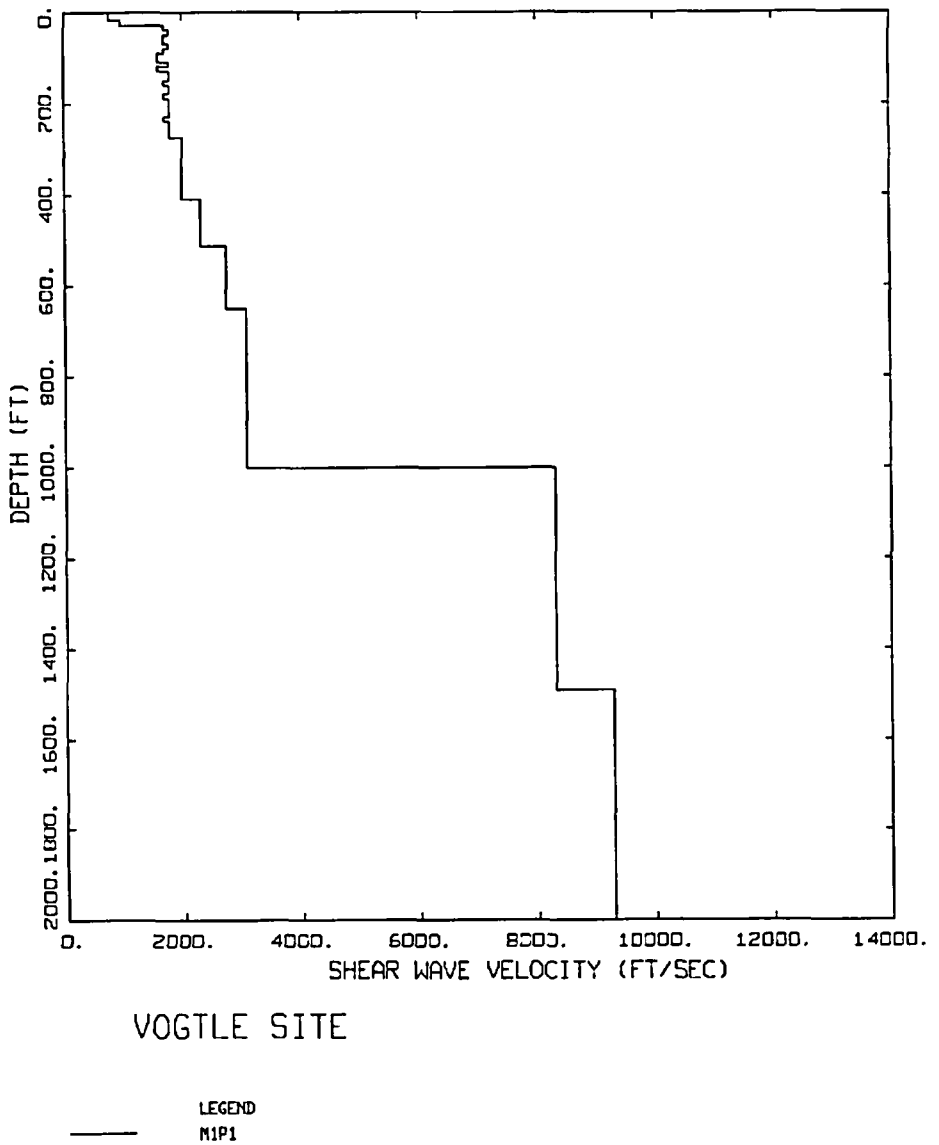

Figure B-15
Shear-Wave Velocity Profiles for the Vogtle Site

B.15.2.2 Modulus Reduction and Hysteretic Damping Curves

For the fill material (top 30 ft (9m)), the EPRI (1993) curves were used throughout. To accommodate epistemic variability in appropriate suites of curves for the profile below the fill, three sets of G/G_{max} and hysteretic damping curves were used: EPRI (1993), Peninsular Range (Silva et al., 1997; 1998b), and Savannah River (SRS, 1996). For the base-case profile (M1P1)

the Savannah River curves were used over the top 500 ft (152m), beginning with the Savannah River shallow clay curves (SRS, 1996), taken to occur below the fill at the Vogtle site. Below a depth of 500 ft, the soil is assumed to behave in a linear manner (Silva et al., 1997; 1998b). Profile M2P1 considers the same shear-wave velocities with the EPRI (1993) curves replacing Savannah River curves below the fill and to the depth where the Savannah River profile was added below the Vogtle measured velocities (about 240 ft (73m) in Figure B.15).

Profile M3P1 replaces the EPRI (1993) curves below the fill material with Peninsular Range curves while profile M4P1 has Savannah River curves below the fill and EPRI (1993) below the portion of the Vogtle profile with measured shear-wave velocities. For the Savannah River curves, the Savannah River shallow clay was used for the Vogtle marls. The entire suite of dynamic material model combinations is listed in Table B-15.

B.15.2.3 Regional Crustal Damping (kappa)

Based on a measured kappa value at the nearby Savannah River Site of 0.02 sec (Fletcher, 1995), the base-case total site kappa value was assumed to be 0.02 sec. A 50% increase to 0.03 sec was taken as the high value (M1P1.KH). For a low kappa (M1P1.KL), the base-case profile (M1P1), with a low-strain damping contributing a kappa value of 0.0064 sec, was added to the hard rock kappa of 0.006 sec and rounded up to total 0.013 sec, to accommodate 426 ft (130m) of Triassic Basin sedimentary rock overlying hard rock conditions.

B.15.2.4 Profile Weights

The profile weights for the amplification factors are listed below in Table B-15.

Table B-15
Vogtle Weights

Properties*	Category Weights
M1P1	0.6
M1P1.KH	0.2
M1P1.KL	0.2
M1	0.7
M2, M3, M4, M5	0.3
	Combined Weights
M1P1	0.420
M1P1.KH	0.140
M1P1.KL	0.140
M2P1	0.075
M3P1	0.075
M4P1	0.075
M5P1	0.075

*M1P1; base case profile, kappa = 0.02 sec

M1P1.KH; base case profile, kappa = 0.03 sec

M1P1.KL; base case profile, kappa = 0.013 sec

M2P1; base case profile, kappa = 0.02 sec

M3P1; base case profile, kappa = 0.02 sec

M4P1; base case profile, kappa = 0.02 sec

M5P1; base case profile, kappa = 0.02 sec

Table B-16
Vogtle G/G_{max} and Hysteretic Damping Curves

Profiles					
Depth	M1P1	M2P1	M3P1	M4P1	M5P1
0 ft – 30 ft (9m)	EPRI	EPRI	EPRI	EPRI	EPRI
30 ft – 240 ft (9m – 73m)	SR	EPRI	PR	SR	SR
240 ft – 500 FT (73m – 152m)	SR	SR	SR	EPRI	PR

where

- EPRI represents EPRI (1993) curves
- SR represents Savannah River curves (SRS, 1996)
- PR represents Peninsular Range curves (Silva et al., 1997, 1998b)

B.16 WATERFORD SITE

The Waterford Steam Electric Station is located in southern Louisiana within the Mississippi River deltaic plain physiographic province. Since early Jurassic time, nearly continuous marine deposition has resulted in strata in excess of 40,000 ft (12,200m) beneath the site.

The upper 500 ft (152m) of the site has been characterized by drilling as flat lying sediments. The top 53 ft (16m) consists of recent clays and silty clay with silt and sand lenses. The Pleistocene Prairie Formation consists of interbedded sands and clays with varying amounts of silt and extends to a depth of about 1,100 ft (335m). The Pliocene – Pleistocene deposits consist of the Citronelle Formation of interbedded sands and clays that extend to about 1,900 ft (580m). Beneath these strata are about 3,000 ft (915m) of Pliocene clays with relatively thin sand layers. Between 7,500 and 10,500 ft (2,285 to 3,200m) is a sequence of shale alternating with thin sandstone layers. This unit overlies a continuous sequence of shale ranging in age from middle to upper Jurassic. The lower Jurassic Louann salt beds are the deepest sediments known to occur above crystalline bedrock. Precambrian crystalline basement rock was estimated to be at a depth greater than 40,000 ft (12,200m) (EPRI, 1989).

B.16.1 Soil Profile Information

The reactor building is founded upon Pleistocene stiff, tan, gray, and fissured clay at a depth of about 60 ft (18m) below natural grade. The thickness of this stratum is approximately 37 ft (11m) (30 ft (9m) below reactor foundation). This layer is underlain by a 15 ft (4.6m) thick soil of very dense silty sand and then by over 100 ft (30m) of clay layers with various stiffnesses. Hard rock hazard is defined as basement material with a Vs of 2.83 km/sec.

Geophysical measurements, including seismic uphole and cross-hole, were performed. In the deepest boring, shear-wave velocities around 1,075 ft/sec (330 m/sec) are measured at depths of about 220 ft (67m) in the Pleistocene soils. These measurements were projected into the lower

Pleistocene at depth of 400 ft (122m) with a shear-wave velocity of 1,625 ft/sec (495 m/sec) in EPRI (1989).

Site-specific laboratory dynamic material testing for modulus reduction and hysteretic damping strain dependencies reflecting recent procedures were not available for this site.

B.16.2 Description of Base Case Profiles

B.16.2.1 Shear Wave Velocity Profiles

The base-case shear-wave velocity profile (M1P1) is shown in Figure B-16 and is based on measured shear-wave velocities to a depth of about 250 ft (76m). The profile reflects embedment depths at the surface (top 60 ft (18m) removed from the site profile). Below that depth the measured velocity was extended 200 ft (61m) and the uplands profile (see Grand Gulf, Section B.5) developed for the upper Mississippi embayment was added to a depth of 2,500 ft (762m). This depth was considered sufficient to capture soil amplification to the lowest frequency of interest (0.5 Hz).

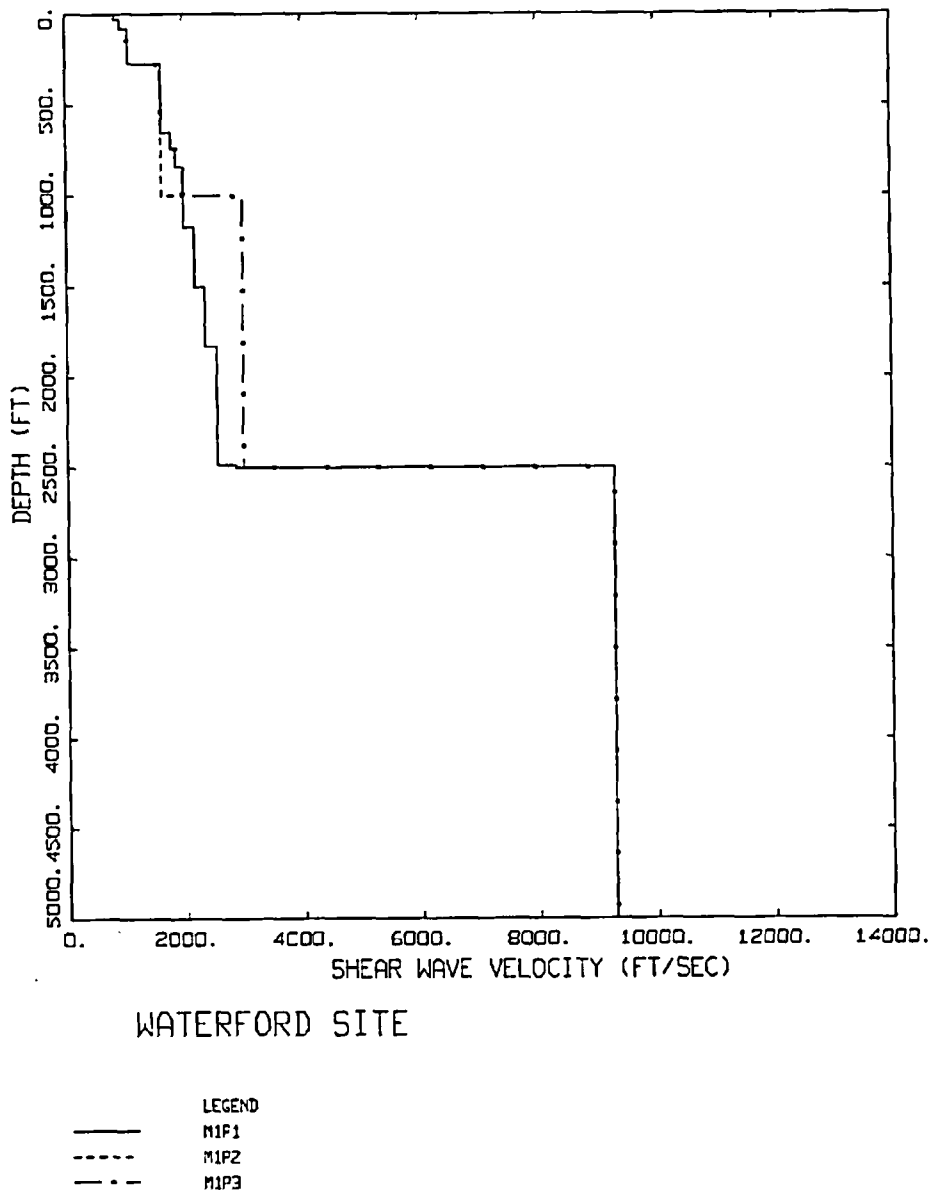

Figure B-16
Shear-Wave Velocity Profiles for the Waterford Site

Profile M1P1 is considered the base case profile with M1P2 and M1P3 to accommodate lower and higher velocities at depth. All three profiles are estimates below a depth of about 250 ft (76m).

Alternative profiles were considered as well with profile M1P2 extending the deepest measured shear-wave velocity (1,625 ft/sec (495 m/sec)) to a depth of 1,000 ft (305m) where it merges with the base-case profile (Mississippi embayment uplands generic profile). To consider higher

at-depth velocities, profile M1P3 (Figure B-16) has an increase in velocity to 3,000 ft/sec (914 m/sec) at a depth of 1,000 ft (305m). All three profiles have depth to hard rock randomized ± 1,000 ft (305m).

B.16.2.2 Modulus Reduction and Hysteretic Damping Curves

To provide alternative base-case dynamic material properties, both the EPRI (1993) (M1P1) and Peninsular Range (Silva et al., 1997, 1998b) (M2P1) curves were considered. EPRI (1989) shows G/G_{max} and hysteretic damping curves based on laboratory dynamic material testing. Although these curves do not reflect more recent procedures and are not considered reliable for direct use, they do suggest the EPRI (1993) curves may be more appropriate for these materials and the amplification weights (Table B-17) have been selected to reflect these considerations.

B.16.2.3 Regional Crustal Damping (kappa)

As with the other Mississippi embayment sites (Grand Gulf, Section B.5 and River Bend, Section B.10) the total site kappa value for the base-case was 0.046 sec. High and low kappa values based on a ± 50% variation result in 0.069 sec (M1P1.KH in Table B-17) and 0.031 sec (M1P1.KL in Table B-17) respectively.

B.16.2.4 Profile Weights

The profile weights for the amplification factors are listed below in Table B-17.

Table B-17
Waterford Weights

Properties*	Category Weights
M1P1	0.6
M1P1.KH	0.2
M1P1.KL	0.2
M1P1	0.8
M1P2	0.1
M1P3	0.1
M1	0.6
M2	0.4
	Combined Weights
M1P1	0.288
M1P1.KH	0.096
M1P1.KL	0.096
M1P2	0.060
M1P3	0.060
M2P1	0.400

*M1P1; base case profile, EPRI Curves, kappa = 0.046 sec

M1P1.KH; base case profile, EPRI Curves, kappa = 0.069 sec

M1P1.KL; base case profile, EPRI Curves, kappa = 0.031 sec

M1P2; low gradient profile, EPRI Curves, kappa = 0.046 sec

M1P3; high gradient profile, EPRI Curves, kappa = 0.046 sec

M2P1; base case profile, Peninsular Range Curves, kappa = 0.046 sec

B.17 References

Anderson, J. G. and S. E. Hough (1984). "A Model for the Shape of the Fourier Amplitude Spectrum of Acceleration at High Frequencies." *Bull. Seism. Soc. Am.*, 74(5), 1969-1993.

Dominion (2003). *North Anna Early Site Permit Application*, Dominion Nuclear North Anna LLC, Docket No. 52-008, Sept. 25.

Electric Power Research Institute (1989) *Probabilistic Seismic Hazard Evaluations at Nuclear Plant Sites in the Central and Eastern United States: Resolution of the Charleston Earthquake Issue*, Elec. Power Res. Inst., Report NP-6395-D, Palo Alto, CA, April.

Electric Power Research Institute (1993). "Guidelines for determining design basis ground motions." Palo Alto, Calif: Electric Power Research Institute, vol. 1-5, EPRI TR-102293.

vol. 1: Methodology and guidelines for estimating earthquake ground motion in eastern North America.

vol. 2: Appendices for ground motion estimation.

vol. 3: Appendices for field investigations.

vol. 4: Appendices for laboratory investigations.

vol. 5: Quantification of seismic source effects.

Entergy (1994). "Updated Final Safety Evaluation Report for the Grand Gulf Nuclear Station." (UFSAR), Rev. 8, Section 2.5, Geology, Seismology and Geotechnical Engineering, Docket No. 52-009.

Entergy (2003). *Early Site Permit Application, Grand Gulf site,* Intergy Corp, Docket No. 52-009, Oct. 16.

Exelon (2003). *Early Site Permit Application, Clinton site*, Exelon Generation Co. LLC, ESP Application for Clinton site, Docket No. 52-007, Sept. 25.

Fletcher, J.B. (1995). "Source parameters and crustal Q for four earthquakes in South Carolina." *Seism. Res. Lett.*, 66(4), 44-58.

Risk Engineering, Inc. (REI) (1989). "Probabilistic seismic hazard evaluations at nuclear plant sites in the central and eastern United States: resolution of the Charleston earthquake issue," Elec. Power Res. Inst, Rept. NP-6395-D, Palo Alto, CA, April, (CD ROM).

Silva, W.J., and R. Darragh, (1995). "Engineering characterization of earthquake strong ground motion recorded at rock sites." Palo Alto, Calif.: Electric Power Research Institute, Final Report RP 2556-48.

Silva, W.J., N. Abrahamson, G. Toro and C. Costantino. (1997). "Description and validation of the stochastic ground motion model." Report Submitted to Brookhaven National Laboratory, Associated Universities, Inc. Upton, New York 11973, Contract No. 770573.

Silva, W.J. Costantino, C. Li, Sylvia (1998b). "Quantification of nonlinear soil response for the Loma Prieta, Northridge, and Imperial Valley California earthquakes.@ Proceedings of The Second International Symposium on The effects of Surface Geology on Seismic Motion Seismic Motion/Yokohama/Japan/1-3 December 1998, Irikura, Kudo, Okada & Sasatani (eds.), 1137—1143.

Silva, W. J.,S. Li, B. Darragh, and N. Gregor (1999). "Surface geology based strong motion amplification factors for the San Francisco Bay and Los Angeles Areas." A PEARL report to PG&E/CEC/Caltrans, Award No. SA2120-59652.

Silva, W.J., R. Darragh, N. Gregor, G. Martin, C. Kircher, N. Abrahamson (2000). "Reassessment of site coefficients and near-fault factors for building code provisions.@ Final Report *USGS Grant award* #98-HQ-GR-1010.

SRS (1996). *Investigations of Nonlinear Dynamic Soil Properties at the Savannah River Site*, WSRC-TR-0062, Rev. 0, March 22, 1996.

Vucetic, M.; R. Dobry (1991). "Effects of Soil Plasticity on Cyclic Response." *Journal of Geotechnical Engineering, ASCE*, 117(1), 89-107.

Export Control Restrictions

Access to and use of EPRI Intellectual Property is granted with the specific understanding and requirement that responsibility for ensuring full compliance with all applicable U.S. and foreign export laws and regulations is being undertaken by you and your company. This includes an obligation to ensure that any individual receiving access hereunder who is not a U.S. citizen or permanent U.S. resident is permitted access under applicable U.S. and foreign export laws and regulations. In the event you are uncertain whether you or your company may lawfully obtain access to this EPRI Intellectual Property, you acknowledge that it is your obligation to consult with your company's legal counsel to determine whether this access is lawful. Although EPRI may make available on a case-by-case basis an informal assessment of the applicable U.S. export classification for specific EPRI Intellectual Property, you and your company acknowledge that this assessment is solely for informational purposes and not for reliance purposes. You and your company acknowledge that it is still the obligation of you and your company to make your own assessment of the applicable U.S. export classification and ensure compliance accordingly. You and your company understand and acknowledge your obligations to make a prompt report to EPRI and the appropriate authorities regarding any access to or use of EPRI Intellectual Property hereunder that may be in violation of applicable U.S. or foreign export laws or regulations.

Printed on recycled paper in the United States of America

The Electric Power Research Institute (EPRI)

The Electric Power Research Institute (EPRI), with major locations in Palo Alto, California, and Charlotte, North Carolina, was established in 1973 as an independent, nonprofit center for public interest energy and environmental research. EPRI brings together members, participants, the Institute's scientists and engineers, and other leading experts to work collaboratively on solutions to the challenges of electric power. These solutions span nearly every area of electricity generation, delivery, and use, including health, safety, and environment. EPRI's members represent over 90% of the electricity generated in the United States. International participation represents nearly 15% of EPRI's total research, development, and demonstration program.

Together...Shaping the Future of Electricity

Program:

Technology Innovation

1012045

ELECTRIC POWER RESEARCH INSTITUTE

3420 Hillview Avenue, Palo Alto, California 94304-1395 • PO Box 10412, Palo Alto, California 94303-0813 USA

800.313.3774 • 650.855.2121 • askepri@epri.com • www.epri.com

EPRI | ELECTRIC POWER RESEARCH INSTITUTE

Program on Technology Innovation: Assessment of a Performance-Based Approach for Determining Seismic Ground Motions for New Plant Sites, V1

Volume 1: Performance-Based Seismic Design Spectra

Technical Report

Program on Technology Innovation: Assessment of a Performance-Based Approach for Determining Seismic Ground Motions for New Plant Sites, V1

Volume 1: Performance-Based Seismic Design Spectra

1012044

Final Report, August 2005

Cosponsor
U.S. Department of Energy
Office of Nuclear Energy
Science & Technology
19901 Germantown Road, NE-20
Germantown, MD 20874-1290

EPRI Project Manager
R. Kassawara and L. Sandell

Electric Power Research Institute • 3420 Hillview Avenue, Palo Alto, California 94304 • PO Box 10412, Palo Alto, California 94303 • USA
800.313.3774 • 650.855.2121 • askepri@epri.com • www.epri.com

DISCLAIMER OF WARRANTIES AND LIMITATION OF LIABILITIES

ORGANIZATION(S) THAT PREPARED THIS DOCUMENT

Risk Engineering, Inc.

ORDERING INFORMATION

Requests for copies of this report should be directed to EPRI Orders and Conferences, 1355 Willow Way, Suite 278, Concord, CA 94520, (800) 313-3774, press 2 or internally x5379, (925) 609-9169, (925) 609-1310 (fax).

CITATIONS

This report was prepared by

Risk Engineering, Inc.
4155 Darley Avenue, Suite A
Boulder, CO 80305

Principal Investigator
R. McGuire

This report describes research sponsored by the Electric Power Research Institute (EPRI) and U.S. Department of Energy.

The report is a corporate document that should be cited in the literature in the following manner:

Program on Technology Innovation: Assessment of a Performance-Based Approach for Determining Seismic Ground Motions for New Plant Sites, V1: Volume 1: Performance-Based Seismic Design Spectra. EPRI, Palo Alto, CA and U.S. Department of Energy, Germantown, MD: 2005. 1012044.

PRODUCT DESCRIPTION

This study evaluates the method for calculating seismic design spectra recommended by the American Society of Civil Engineers (ASCE) in 2005. Design spectra calculated by this method are compared to existing seismic design spectra at 28 nuclear plant sites in the Central and Eastern United States. Hypothetical nuclear plant component performance is calculated based on these spectra, and these calculations are compared to performance goals that form the basis for the recommended design spectra. Finally, hypothetical plant-level seismic performance calculations based on these spectra are compared to estimates of seismic core damage at plants for which a probabilistic risk assessment has been published.

Results & Findings

The recommended method for calculating seismic design spectra results in spectra that are consistent with seismic designs at the 28 nuclear plants studied here. These are the majority of plants used in Regulatory Guide 1.165 to establish a "reference probability" for seismic design. Further, the recommended method results in component performance that is consistent with seismic performance goals for nuclear components and with plant-level performance calculations made for existing nuclear plants in the United States.

Challenges & Objective(s)

This study will benefit nuclear utilities who plan to license and construct new nuclear facilities in the Central and Eastern United States. The ASCE method leads to reasonable yet conservative seismic designs as compared to the current seismic design requirements contained in the United States Nuclear Regulatory Commission (USNRC) Regulatory Guide 1.165, which are based on seismic hazard interpretations made during the mid to late 1980s. Validating the ASCE method means that resources will not be used to meet overly conservative regulations based on outdated seismic hazard estimates.

Applications, Values & Use

These results can be used in several ways. First, the seismic design values can be calculated by performance-based procedures for the 28 nuclear plants to support the use of performance-based approaches as an alternative to that described in Regulatory Guide 1.165. Second, simple models of nuclear plant seismic behavior can be developed, assuming that new plants have been designed according to the performance-based procedures. Those simple models can be integrated with seismic ground motion hazard to calculate annual frequencies of seismically induced unacceptable plant performance. These annual frequencies can be compared to estimated core melt frequencies from detailed probabilistic risk assessments done for existing plants. This second comparison allows evaluation of the consistency between seismic designs determined with performance-based procedures and estimates of current nuclear plant safety.

EPRI Perspective

EPRI has an industrywide perspective and can address broad design-philosophy issues that cannot be addressed for individual sites. The comparisons presented here for 28 nuclear plant sites could only be accomplished with this broad perspective.

Approach

The approach taken here is to develop hypothetical seismic design spectra using the recommended method for 28 sites and make comparisons with available data and inferences at those sites. This approach gives insight into how consistent and conservative the recommended method is compared to previous methods and compared to other estimates of nuclear plant performance.

Keywords

Seismic design spectra
Probabilistic seismic hazard analysis
Seismic performance
New nuclear plant deployment

ABSTRACT

Up-to-date seismic hazard analyses at 28 nuclear plant sites in the Central and Eastern United States form the basis for recommended seismic design ground motions at these sites. The recommended motions follow a procedure published by the American Society of Civil Engineers (ASCE) in 2005. Dynamic site-response analyses were incorporated into the calculations to estimate surface motions at 16 of the 28 sites. The recommended motions at 5 and 10 Hz are equivalent to existing seismic design motions for the 28 sites. Further, inferred annual frequencies with which nuclear components experience unacceptable behavior are ~10^{-5} or less, which is the goal of the recommended approach. Finally, the recommended motions lead to generic estimates of plant-level behavior that indicate better performance (in terms of annual seismic core damage frequency) than published results for the majority of 25 existing U.S. nuclear plants. These comparisons show that the ASCE approach leads to conservative design levels that are consistent with past practice.

ACKNOWLEDGMENTS

This material is based upon work supported by the U.S. Department of Energy under Award No. DE-FC07-04ID14533. EPRI would also like to recognize the support provided by Adrian Heymer and Cedric Jobe of the Nuclear Energy Institute.

CONTENTS

LIST OF FIGURES

LIST OF TABLES

1
INTRODUCTION

This study uses the probabilistic seismic hazard analysis (PSHA) results calculated and documented in a separate report (REI, 2005) to compare proposed seismic design bases with experience from independent methods. The impetus for these comparisons is Regulatory Guide 1.165 (RG1.165) (USNRC, 1997), which establishes the basis for seismic design using available PSHA results. RG1.165 defines a reference probability by comparing PSHA results to actual design spectra at 29 existing nuclear plants in the Central and Eastern United States (CEUS).

Understanding of earthquake occurrences and the associated ground motions is constantly evolving in the CEUS, as elsewhere. New data are continuously being collected, and analysis methods are being improved. The earthquake problem in the CEUS is especially oriented toward analytical procedures because of the low rate of occurrence of moderate-to-large shocks in the region. This low rate implies that few high-quality empirical data on moderate-to-large shocks are available, and the hazard from earthquake shaking must be estimated from analysis and inference.

Two major studies, conducted by Lawrence Livermore National Laboratories (LLNL) (Bernreuter et al, 1989; Sobel, 1994) and the Electric Power Research Institute (EPRI, 1989), are endorsed by RG1.165. The seismological inferences on which these studies were based were made in the mid-to-late 1980s, so these studies were based on interpretations that are now approaching 20 years old. Appendix E of RG1.165 gives guidance on when PSHA results must be updated for a specific site, and when changes in seismic sources and ground motion models require a reexamination of the reference probability defined in Appendix B of RG1.165.

New information on seismic sources has been compiled in conjunction with three Early Site Permit (ESP) applications for new nuclear plants submitted by Dominion (2003), Entergy (2003), and Exelon (2003). The new information leads to new seismic sources in the Central US and in the Charleston, South Carolina area, and to revised parameters (principally, estimates of maximum magnitude) in other sources. Details of these changes are given in REI (2005). Also, new models of earthquake ground motion have been derived in a major study by EPRI (2004), which quantifies mean ground motion and the associated aleatory and epistemic uncertainties as a function of magnitude and distance.

The results reported in REI (2005) use this new information to calculate PSHA results at 28 nuclear plant sites. These are the same sites used in RG1.165 to establish the reference probability (see Table B.1 of RG1.165), except that the Callaway site was not included in REI (2005). (The Callaway site was not included in the EPRI [1989] study of seismic hazards.) Twelve of the 28 sites were treated as rock, and the remaining 16 were studied for site-specific response (soil or soft rock). This site-specific response was taken into account in deriving the

surface seismic hazard curves. Figure 1-1 shows the locations of the sites in the CEUS and the categorization of the site as rock calculation or as a site-specific calculation.

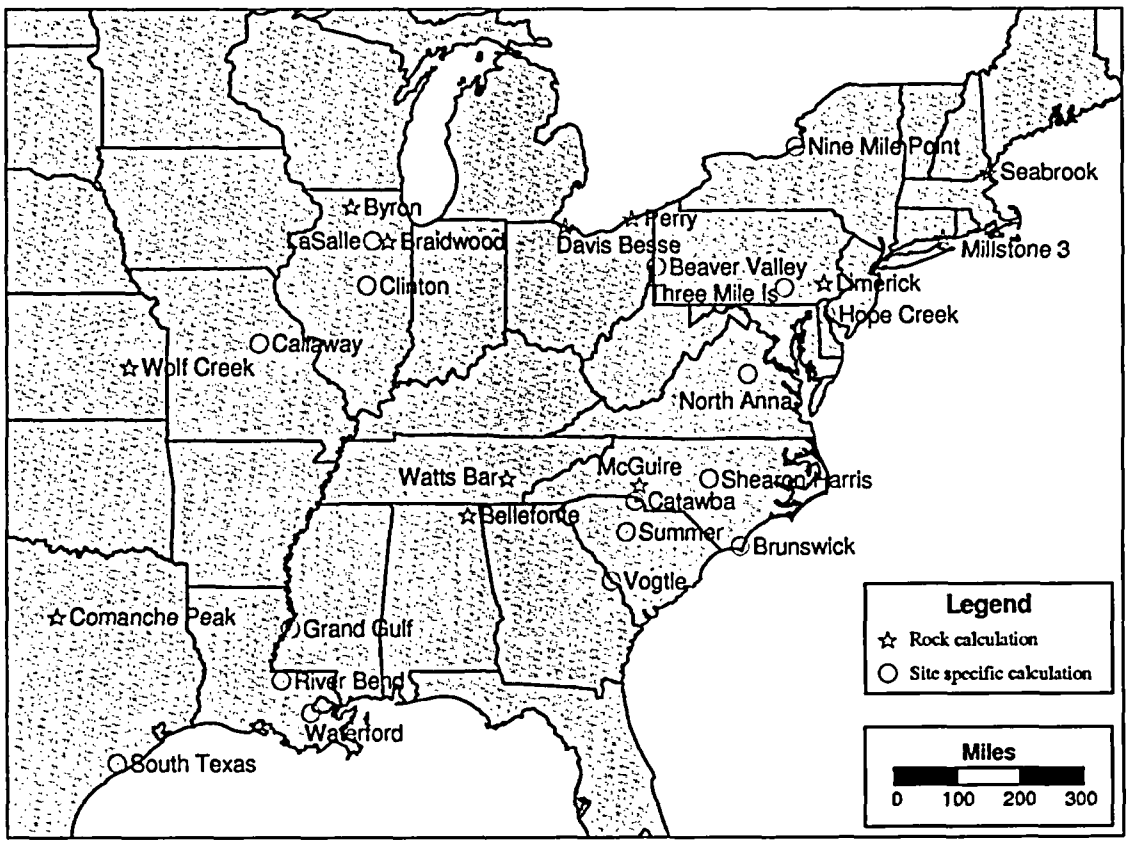

Figure 1-1
Map Showing 28 Plant Sites Where Hazard Curves were Calculated.

Concurrent with the changes in seismic hazard models has been an interest in establishing seismic design requirements using the seismic performance of generic models of structures and equipment. This method has a conceptual advantage over alternatives in that it explicitly includes estimates of the dynamic response of components (structures and equipment) that are being designed. The method convolves frequencies of occurrence of seismic ground motion with generic fragilities (probabilities of not achieving specific performance levels given ground motion amplitude) to estimate annual frequencies with which components exceed defined limit states. These frequencies can then be compared to calculated frequencies of damage and failure estimated in probabilistic risk assessments of existing nuclear plants, or to performance goals established by independent methods. The point is that the design can be evaluated in the context of the performance of the structure or equipment that is being designed, not in the abstract.

The performance-based ground motions developed in this report are derived using the performance-based method developed by ASCE (2005). Details of this method are given in Section 3.2. Performance-based ground motions at the 28 plant sites are based on the updated PSHA results, and these ground motions are used for two comparisons. First, they are compared to licensing basis SSE ground motions at the 28 plant sites. Second, the estimated annual frequencies with which generic component- or plant-models fail to achieve defined performance objectives are compared to calculated frequencies of seismically induced core damage from detailed Probabilistic Risk Assessment (PRA) studies for existing nuclear facilities. The results of these comparisons are presented in Section 3.2.

All of the comparisons in Section 3 focus on spectral response at 5 and 10 Hz. These are the structural frequencies used in RG1.165 to establish the reference probability, and it is appropriate to focus on seismic hazard at these structural frequencies to evaluate the ASCE (2005) recommended method for deriving performance-based design ground motions against the RG1.165 reference probability method.

2
SUMMARY OF APPROACH

2.1 Summary of ASCE Method

The seismic design basis investigated here is the method recommended by ASCE (2005) to develop a design response spectrum (DRS), herein referred to as the "ASCE DRS method". This was developed based on the calculated responses of a set of generic components of nuclear facilities subjected to ground shaking. A summary of the ASCE DRS method is given below. Further background on this method is contained in Appendix A and in the source reference itself (ASCE, 2005). The ASCE DRS method was applied to the seismic hazard results calculated at the 28 sites for surface conditions, either based on generic hard rock or based on site-specific calculations of site response. Two sets of comparisons were made, as described in the subsections below.

For seismic design category 5 (SDC 5) components (the most severe), the recommended DRS at each structural frequency f is given by:

$$DRS = DF * UHRS \qquad \text{Equation 2-1}$$

where $UHRS$ is the uniform hazard response spectrum amplitude at structural frequency f at a specified annual frequency of exceedence (which is 1×10^{-4} for SDC 5 components, see ASCE, 2005, Table C2.2-1), and

$$DF = max(DF_1, DF_2) \qquad \text{Equation 2-2}$$

where

$$DF_1 = 1.0 \qquad \text{Equation 2-3}$$

for SDC 5 components, and

$$DF_2 = 0.6 A_R^{\alpha} \qquad \text{Equation 2-4}$$

Parameter A_R is the ratio of ground motion corresponding to a change in hazard (annual frequency of exceedence) of a factor of 10, from 10^{-4} to 10^{-5}, and α=0.8 (see ASCE, 2005, Table C2.2-4).

Equation 2-1 specifies the nominal level of seismic design for each component at structural frequency *f*. Designing a component for this seismic motion requires assuring that both of two seismic margin factors F_N are achieved:

$F_{N1\%} \geq 1.0$ against a 1% conditional probability of unacceptable performance **Equation 2-5**

$F_{N10\%} \geq 1.5$ against a 10% conditional probability of unacceptable performance **Equation 2-6**

Equation 2-5 says that the component must be designed so that the DRS causes, at most, a 1% probability of unacceptable performance. Equation 2-6 says that the component must be designed so that 1.5 times the DRS causes, at most, a 10% probability of unacceptable performance. The component must be designed to have sufficient capacity to meet both criteria.

The seismic fragilities of components are conveniently specified by a nominal design level (with an associated conditional probability of unacceptable performance, which might be 1% or 10%, see Equations 2-5 and 2-6) and a logarithmic standard deviation β. For structures and equipment mounted at ground level, β will generally be in the range of 0.3 to 0.5. For equipment mounted high in structures, β will generally be in the range of 0.4 to 0.6. For comparison purposes it is useful to examine component fragilities for a range of β values.

2.2 Considerations for Comparing Seismic Designs

The most direct comparison that can be made is to compare seismic design levels recommended by Equation 2-1 with existing seismic design levels at the 28 nuclear plant sites examined in this study. This will give perspective on the use of Equation 2-1 compared to the practice in place at the time these 28 plants were licensed, designed and built. For this comparison the design levels at existing plants were taken from Sobel (1994). Six of the 29 nuclear plants listed in Appendix B of RG1.165 indicate that rock is the primary site condition, with "sand-S1" being a secondary site condition. For these plants, five of which are included in this study, only the primary site condition (rock) is used for comparison.

Structural frequencies *f* of 5 and 10 Hz are examined in order to develop a composite comparison of recommended design vs. existing design levels. These are the frequencies used in RG1.165 to determine a "reference probability" level based on existing plants' designs. An average composite ratio of recommended design level divided by existing design level at the two structural frequencies is used for comparison purposes.

Many of the plants are located in areas of low seismicity, where the calculated seismic hazard is low. When these plants were designed, a minimum level of seismic design was used, unrelated to the level of seismic hazard, because it was cost-effective to do so. Consistent with this experience, the ASCE-DRS method specifies that a minimum design corresponding to a peak ground acceleration (PGA) level of 0.1g should be used. This minimum seismic design level is applied here at each plant by anchoring a Regulatory Guide 1.60 (RG1.60) (USNRC, 1973) spectrum to 0.1g PGA.

Results of these comparisons are presented in Section 3.

2.3 Considerations for Comparing Estimated Failure Rates

The ASCE method is based on achieving a minimum level of seismic performance of generic plant components. It is useful to compare the estimated seismic performance with the calculated seismic performance of actual nuclear plants assessed using detailed, plant-specific PRAs.

As discussed in Section 2.1, the seismic fragilities of components are specified by a nominal design level (with an associated conditional probability of unacceptable performance, which might be 1% or 10%, see Equations 2-5 and 2-6) and a logarithmic standard deviation β. These two parameters define the lognormal distribution used to represent component performance as a function of ground motion amplitude. To investigate component performance, we assume that components have been designed according to the ASCE recommendations described in Section 2.1, and that the resulting component fragilities are lognormally distributed with respect to the onset of significant nonlinear performance. The annual seismic risk (P_F) is then calculated as a convolution of the hazard curve and the fragility curve:

$$P_F = \int_0^{\infty} H(a) \frac{dP_{Fla}}{da} da \qquad \textbf{Equation 2-7}$$

where $H(a)$ is the seismic hazard curve for the structural frequency f of the component and P_{Fla} is the probability of unacceptable performance (defined here as the onset of significant inelastic deformation) of the component given amplitude a. Thus P_F represents the *frequency* of seismically induced onset of significant inelastic deformation (FOSID). With additional assumptions on the shape of the hazard curve, a closed-form solution can be derived for Equation 2-7 (see, for example, REI, 2001 and Appendix B). For this project the integration of Equation 2-7 is performed numerically in order to account accurately for the shape of the seismic hazard curves.

Quite separately from the design criteria indicated in Section 2.1 for individual components, overall plant seismic behavior can be modeled with a lognormal distribution, based on the required seismic design level. For this application it is assumed that a factor of safety of 1.67 applies to the DRS to estimate the ground motion associated with a 1% probability of seismically induced core damage. With this factor of safety on the seismic design level and β values from 0.3 to 0.6 representing the uncertainty in overall plant seismic behavior, a lognormal distribution represents the probability of seismically induced core damage. These choices for the factor of safety and β values are based on extensive experience from published PRAs at existing nuclear power plants.

A summary of calculated annual frequencies of seismically induced core damage from published PRAs of existing plants is available in USNRC (2002). These calculated annual frequencies are used in the next section to compare to both estimated annual FOSIDs and estimated plant-level behavior.

3
RESULTS OF COMPARISONS

3.1 Seismic Design Basis

The first comparison is between seismic design levels determined by the ASCE DRS method described in Section 2 and existing seismic design levels at the 28 nuclear plant sites. For this comparison, the existing seismic design levels documented in Sobel (1994) were used. Further, for the sites indicated in Table B.1 of RG1.165 with two site conditions (a primary and a secondary), only the primary condition (rock) was used.

Figure 3-1 shows a cumulative distribution of the average ratio of DRS (from Equation 2-1) to the existing SSE for 5 and 10 Hz for the 28 plant sites. For determination of the DRS, a minimum design criterion is applied corresponding to a RG1.60 spectrum anchored to 0.1g PGA. This minimum is recommended in the ASCE DRS method (ASCE, 2005).

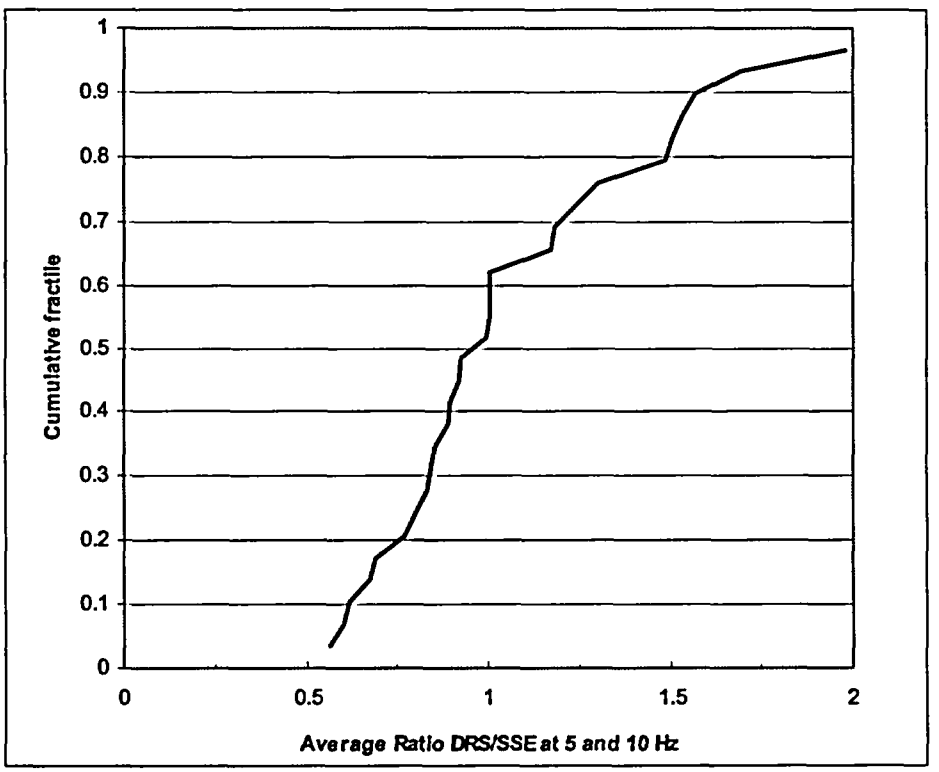

Figure 3-1
Cumulative Distribution of DRS/SSE Ratio at 5 and 10 Hz

Table 3-1 shows the cumulative distribution of the DRS/SSE ratio corresponding to Figure 3-1. As discussed in Section 2.2, the design at 5 and 10 Hz was used for the comparisons in Figure 3-1 and Table 3-1 because these response spectrum frequencies were used in RG1.165 to establish a reference probability for the purpose of deriving site-specific recommended seismic ground motions that are hazard-specific from site-to-site and consistent with the median hazard for 29 nuclear plants that have licensing basis SSE ground motions derived following the requirements of 10CFR Part 100, Appendix A, and spectral shapes defined by RG1.60.

Table 3-1
Cumulative Distribution of DRS/SSE Ratio

Cumulative Fractile	Average DRS/SSE ratio for 5 and 10 Hz
0.1	0.616
0.2	0.756
0.3	0.839
0.4	0.892
0.5	0.963
0.53	1.000
0.6	1.006
0.7	1.200
0.8	1.490
0.9	1.585

Figure 3-1 and Table 3-1 indicate that an average DRS/SSE ratio of unity is achieved at a cumulative fractile of 0.53. Stated another way, if the 28 plants had been designed using the ASCE DRS method, approximately one-half of the plants would have new designs exceeding existing designs (ratios of DRS/SSE >1) and approximately one-half would have new designs below existing designs (ratios of DRS/SSE<1). The plants where new designs would be below existing designs are plants where the calculated seismic hazard is low. For example, this would occur at a site where the hazard-based DRS PGA might be 0.11g, but the existing plant's SSE PGA was chosen (for conservatism) to be 0.15g.

The conclusion from Figure 3-1 and Table 3-1 is that the ASCE DRS method leads to seismic designs that are equivalent to seismic designs at existing nuclear plant sites.

3.2 Component-Level and Plant-Level Behavior

A second set of comparisons can be made based on component-level and plant-level behavior under seismic load, as described in Section 2.3. This component-level and plant-level behavior can be compared to calculated Seismic Core Damage Frequencies (SCDFs) from detailed PRAs of existing nuclear plants.

Table 2.2 of USNRC (2002) provides a summary of mean SCDFs from published PRAs of US nuclear plants. For comparison purposes we used results in Table 2.2 of USNRC (2002) that came from EPRI seismic hazard curves, or an update to those results if that is indicated in Table 2.2 of USNRC (2002). These results, reproduced in Table A-2 (this document), are most similar to the hazard results developed here, which have their basis in the EPRI (1989) seismic hazard study. Twenty-five plants have EPRI results available, and the distribution of these mean SCDFs form a benchmark against which other results can be compared.

As described in Section 2.3, two sets of comparisons are made here, based on the ASCE DRS method. First, the FOSID of components is calculated using distributions of component seismic fragility based on the ASCE DRS method. To be consistent with the results used in RG1.165 to establish the reference probability, structural frequencies of 5 and 10 Hz are examined, and the average FOSID for components with these two frequencies is calculated. Each component must meet the criteria regarding factor of safety against unacceptable performance described in Equations 2-5 and 2-6. We examine a range of logarithmic standard deviations β from 0.3 to 0.6 as noted in section A.5.1, for structures and equipment mounted at ground level, β will generally be in the range of 0.3 to 0.5. For equipment mounted high in structures, β will generally be in the range of 0.4 to 0.6.

Figure 3-2 compares the cumulative distribution of average FOSID of components with f=5 and 10 Hz to the cumulative distribution of SCDF from 25 existing nuclear power plants (from USNRC, 2002). Components with β=0.6 indicate the lowest FOSID, and components with β=0.3 indicate the highest FOSID. For the latter components, the factor of safety criterion indicated in Equation 2-6 governs, whereas for components with β=0.4, 0.5, and 0.6, the factor of safety criterion indicated in Equation 2-5 governs.

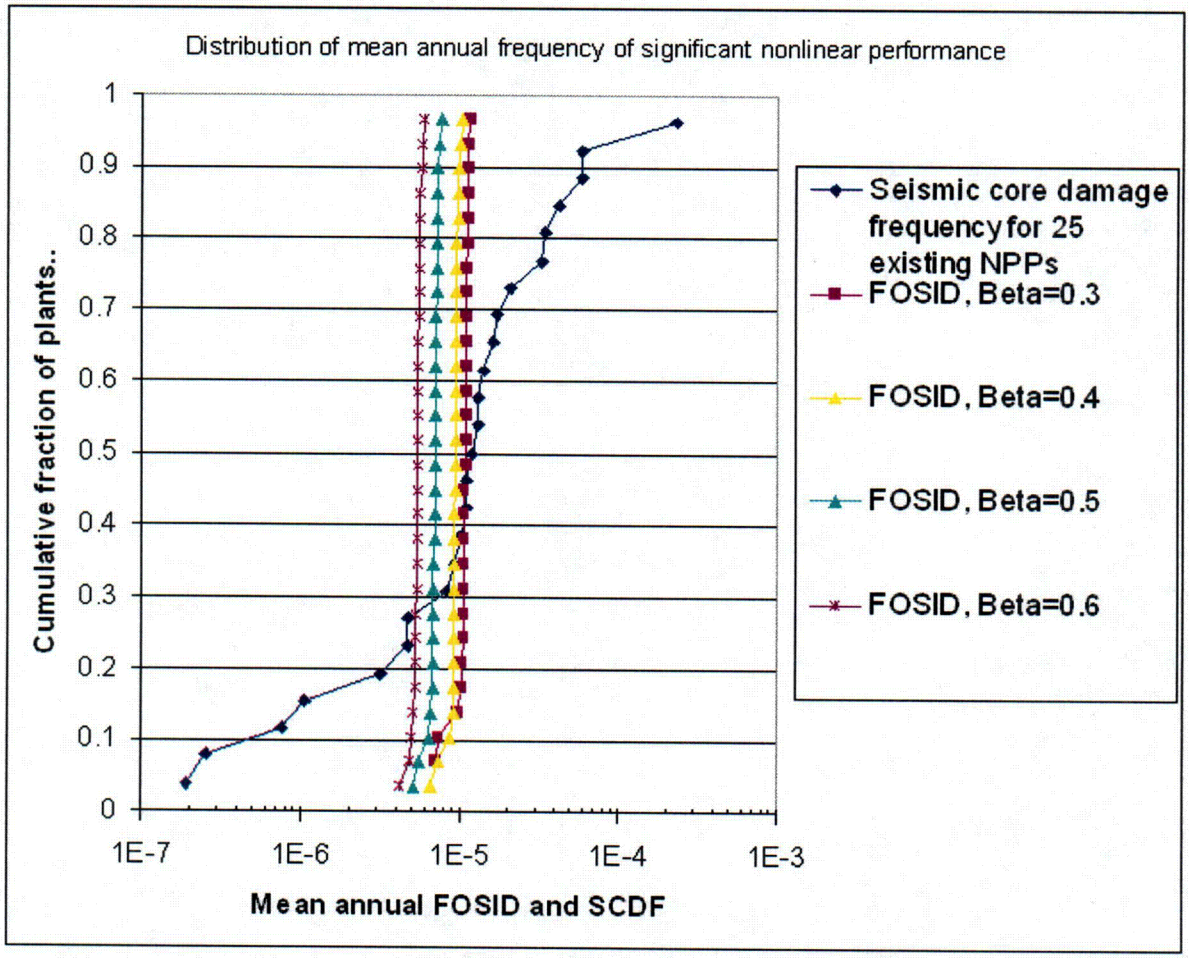

Figure 3-2
Distribution of FOSID for Components, Compared to Distribution of SCDF for 25 Existing Nuclear Power Plants

The median annual FOSIDs for the four β values are shown in Table 3-2, along with the median SCDF for the 25 existing NPPs.

CZZ

Table 3-2
Median SCDF and FOSID Values for Curves Shown in Figure 3-2

Measure of performance	Median
Annual SCDF of 25 existing plants	1.20×10^{-5}
Annual FOSID for β=0.3	1.07×10^{-5}
Annual FOSID for β=0.4	0.93×10^{-5}
Annual FOSID for β=0.5	0.69×10^{-5}
Annual FOSID for β=0.6	0.54×10^{-5}

Overall, the calculated FOSID distributions are very consistent across the 28 plant sites, with median values ranging from 1.07×10^{-5} for β=0.3 to 0.54×10^{-5} for β=0.6. This is not surprising, given that the goal of the ASCE DRS method is to achieve a reduction in frequency of a factor of 10 from the nominal seismic hazard level (1×10^{-4}) to the FOSID (see ASCE, 2005, Table C2.2-1). That is, the target performance goal for SDC 5 components is an annual frequency of occurrence of the limit state (represented here as the onset of significant nonlinear performance) of 1×10^{-5} (see ASCE, 2005, Table 1.2-1). Note for this comparison that no minimum design requirement was introduced, as was the case for the results presented in Figure 3-1. Note also in Figure 3-2 that several of the sites (at the lower end of the cumulative distribution) achieve a lower FOSID. These are sites with deep soils that do not amplify ground motions much above the amplitudes associated with annual frequencies of exceedence of 10^{-4} to 10^{-5}, so the ASCE DRS method (which assumes that the seismic hazard curve continues to increase) is conservative for these deep soil sites, compared to rock sites.

The behavior of individual components can be taken as a *very conservative* indicator of plant-level behavior, because it can be argued that a single component experiencing the onset of significant nonlinear behavior is very unlikely to lead to plant core damage. While there are multiple components that might affect plant operations during seismic events, there also are multiple redundant safety systems to protect plant performance in the case of failure of a single component. Therefore it is highly likely that plant-level performance (in terms of damage to plant systems or to the plant core) lies to the left of the FOSID curves in Figure 3-2. Nevertheless, the FOSID distributions indicate seismic safety that is consistent with, or better than, the seismic safety of existing nuclear plants. That is, even for components with β=0.3 (the most critical), the distribution of FOSID is lower than the mean SCDF for more than 50% of existing nuclear plants. This is a strong indicator that the ASCE DRS method leads to nuclear plant seismic designs that are safer than existing plants.

A second comparison can be made modeling overall plant-level seismic behavior with a lognormal distribution representing the probability of seismically induced core damage. As discussed in Section 2.3, a factor of safety on the DRS of 1.67 is assumed for this calculation, to estimate the ground motion associated with a 1% conditional probability of core damage. Also, β values from 0.3 to 0.6 are used. With these assumptions, Figure 3-3 shows the cumulative distribution of mean annual SCDF for the 28 plant sites studied here, compared to the cumulative distribution of mean annual SCDF for 25 existing nuclear power plants.

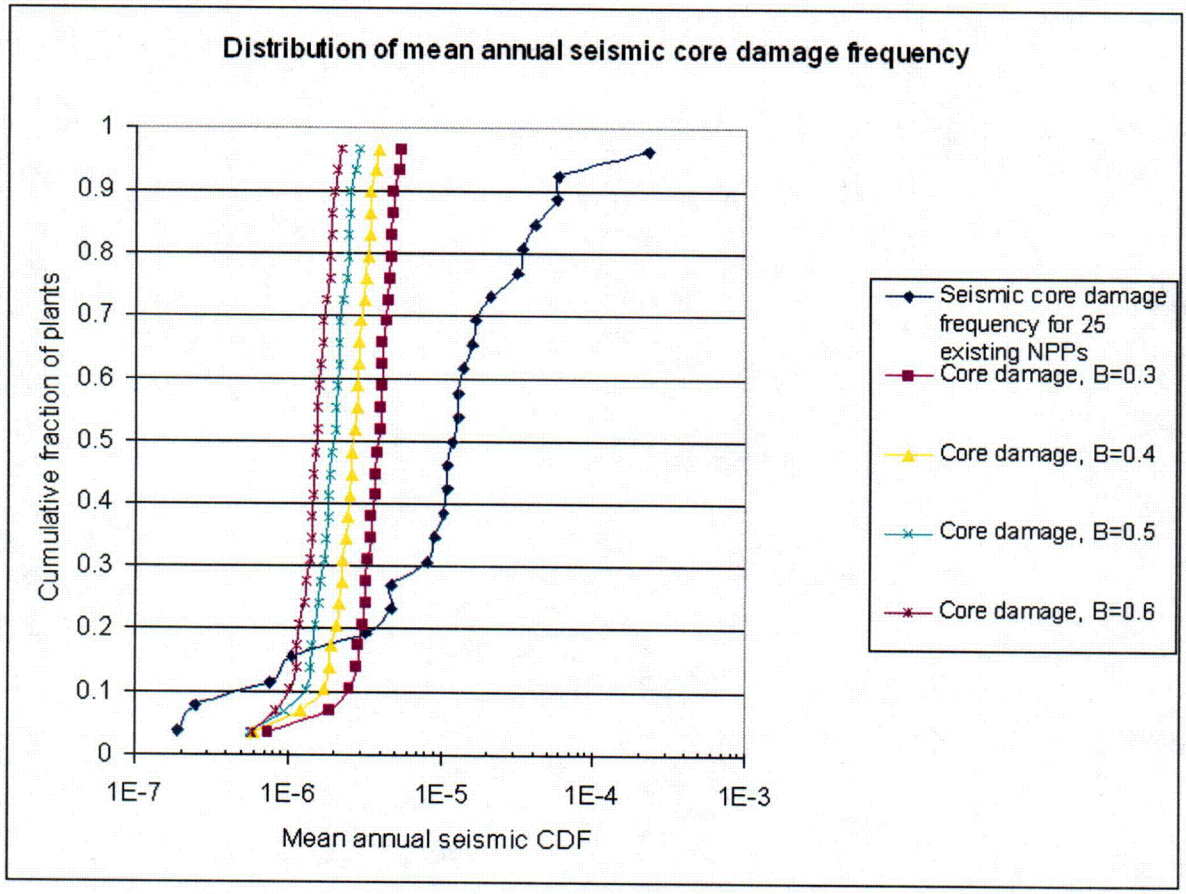

Figure 3-3
Distribution of Plant-Level Performance, Compared to Distribution of SCDF for 25 Existing Nuclear Power Plants

Figure 3-3 shows that, if plants are designed using the ASCE DRS method, simple models of plant-level seismic behavior indicate mean annual SCDFs lower than the majority of existing nuclear plants. The cumulative distribution of SCDF for plants designed to the ASCE DRS method crosses the cumulative distribution of SCDF for 25 existing nuclear plants at about the 0.2 fractile, meaning that newly designed plants would be safer seismically than about 80% of existing plants. Median SCDF estimates from the distributions shown in Figure 3-3 are tabulated in Table 3-3. For plant-level seismic performance using seismic designs based on the ASCE DRS, the estimated median SCDF ranges from 0.38×10^{-5} for β=0.3 to 0.15×10^{-5} for β=0.6. These estimates are well below the median SCDF of 25 existing plants reported in detailed plant PRAs of 1.20×10^{-5}.

C23

Table 3-3
Median SCDFs for Curves Shown in Figure 3-3

Measure of performance	Median
Annual SCDF of 25 existing plants	1.20×10^{-5}
Annual SCDF for β=0.3	0.38×10^{-5}
Annual SCDF for β=0.4	0.26×10^{-5}
Annual SCDF for β=0.5	0.19×10^{-5}
Annual SCDF for β=0.6	0.15×10^{-5}

4
CONCLUSIONS

The seismic hazard results calculated for 28 nuclear plant sites in the CEUS can be used to infer the seismic safety of plants designed according to the ASCE DRS method (ASCE, 2005), which is based on seismic hazard calculations. The goal of the ASCE DRS method is to achieve target performance goals for individual components, and thus to achieve conservative seismic safety of the plant as a whole.

Application of the ASCE DRS method allows comparisons to be made on several levels. Comparing the recommended seismic design levels to existing seismic design levels at the 28 plant sites shows that the ASCE DRS method, at structural frequencies of 5 and 10 Hz, leads to higher designs for about half the plants, and lower designs for the other half. A similar result is obtained in RG1.165 (see Figure B.2 of USNRC, 1997). Structural frequencies of 5 and 10 Hz are the focus because these frequencies were used in Appendix B of RG1.165 to establish a reference probability for seismic design based on existing nuclear plants.

Using the ASCE DRS method and modeling the fragilities of generic components allows us to estimate the FOSID. The stated aim of the ASCE DRS method is to achieve a performance goal for component non-performance of 1×10^{-5}/yr. Attainment of this goal is demonstrated here by calculating FOSIDs for generic components designed by the ASCE DRS method, for structural frequencies of 5 and 10 Hz. The distribution of FOSID for these components indicates lower median frequencies than the median SCDF reported for 25 existing nuclear plants.

A further comparison uses general models of plant seismic behavior to model SCDFs for plants designed using the ASCE DRS method, concentrating on structural frequencies of 5 and 10 Hz. This comparison indicates that such plants would be safer against seismic events than 80% of existing nuclear plants. This observation provides a strong validation for the ASCE DRS method.

Overall these comparisons support the ASCE DRS method and show that its application, using up-to-date seismic hazard curves, will lead to seismic designs and safety at nuclear plants that are as safe as or safer than existing plants.

5
REFERENCES

ASCE (2005). *Seismic Design Criteria for Structures, Systems, and Components in Nuclear Facilities*, Amer. Soc. Civil Engrs, Rept. ASCE/SEI 43-05.

Bernreuter, D.L., et al (1989). *Seismic Hazard Characterization of 69 Nuclear Plant Sites East of the Rocky Mountains*, US Nuc. Reg. Comm, Rept. NUREG/CR-5250, Jan.

Dominion (2003). *North Anna Early Site Permit Application*, Dominion Nuclear North Anna LLC, Docket No. 52-008, Sept. 25.

Entergy (2003). *Early Site Permit Application, Grand Gulf site*, Entergy Corp, Docket No. 52-009, Oct. 16.

EPRI (1989). *Probabilistic Seismic Hazard Evaluations at Nuclear Power Plant Sites in the Central and Eastern United States: Resolution of the Charleston Earthquake Issue*, Elec. Power Res. Inst. Rept. NP-6395-D, Palo Alto, CA, Apr.

EPRI (2004). *CEUS Ground Motion Project Final Report*, Elec. Power Res. Inst., Rept. 1009684, Palo Alto, CA, Dec.

Exelon (2003). *Early Site Permit Application*, Exelon Generation Co. LLC, Docket No. 52-007, Sept. 25.

Risk Engineering, Inc. (REI) (2001). *Technical Basis for Revision of Regulatory Guidance on Design Ground Motions: Hazard- and Risk-Consistent Ground Motion Spectra Guidelines*, Risk Engineering, Inc, rept. to US Nuc. Reg. Comm, NUREG/CR-6728, Oct.

Risk Engineering, Inc. (REI) (2005). *Assessment of a Performance-Based Approach for Determining Seismic Ground Motions for New Plant Sites: V2: Seismic Hazard Results at 28 Sites*, Elec. Power Res. Inst. Product ID. 1012045, Palo Alto, CA, Jul.

Sobel, P. (1994). *Revised Livermore Seismic Hazard Estimates for Sixty-Nine Nuclear Power Plant Sites East of the Rocky Mountains*, US Nuc. Reg. Comm, Rept. NUREG-1488, Apr.

USNRC (1973). *Design Response Spectra for Seismic Design of Nuclear Power Plants*, US Nuc. Reg. Comm, Reg. Guide 1.60, Rev. 1, Dec.

USNRC (1997). *Identification and Characterization of seismic sources and determination of safe shutdown earthquake ground motion*, US Nuc. Reg. Comm., Reg. Guide 1.165, March.

USNRC (2002). *Perspectives Gained from the Individual Plant Examination of External Events,* US Nuc. Reg. Comm., NUREG-1742, Vol. 2, April.

A

RISK (PERFORMANCE-GOAL) BASED APPROACH FOR ESTABLISHING THE DESIGN-BASIS RESPONSE SPECTRUM FOR FUTURE NUCLEAR POWER PLANTS[1]

Appendix A was written by Robert P. Kennedy

A.1 Introduction

It is proposed that the Design Response Spectrum (DRS) for future nuclear power plants be established following the Risk (Performance-Goal) Based Approach defined in ASCE (2005) Standard. The standard is a professional consensus committee developed standard. This standard is formally constructed to produce designs that achieve a target acceptable seismic risk goal, defined as the annual probability of seismic induced unacceptable performance. The first step in this process is to develop a risk-consistent or Uniform Risk Response Spectrum (URRS) which will be used as the DRS. When these URRSs are used as the DRSs, plants at different sites (all designed to the same design criteria, such as NUREG 0800, for their particular site-specific DRSs) should have consistent seismic risks. In contrast, this risk-consistency goal is not achieved when, as now, a Uniform Hazard Response Spectrum (UHRS) is used as the DRS; the UHRS fails to reflect the fact that the seismic hazard curves at different sites have substantially different slopes, and consideration of these slopes is critical to obtaining risk-consistent seismic designs. As described below, the URRS does depend on both the UHRS and these slopes.

The risk-consistent approach presented in ASCE (2005) to define the DRS was first recommended in 1994 in the Commentary of DOE-STD-1020-94 (USDOE, 1994) for risk-consistent seismic design of High Consequence (PC4) DOE facilities. The detailed basis was given in Kennedy and Short (1994). Therefore, this approach has been in existence and has been used for about 10 years. Very similar risk-consistent approaches for defining the DRS are presented in Kennedy (1997) and Kennedy (1999). A more liberal risk-consistent approach for defining the DRS was proposed and studied in NUREG/CR-6728 (REI, 2001). The ASCE (2005) Standard approach instead of that in NUREG/CR-6728 is recommended for nuclear power plant application because the ASCE Standard definition of the DRS is more conservative and because this Standard is a professional consensus standard.

[1] This paper has benefited from review comments provided by Dr. Carl Stepp, Earthquake Hazards Solutions, and Dr. Allin Cornell, Stanford University.

The purpose of this paper is to amplify upon the Commentary of ASCE (2005) in explaining the basis and assumptions behind the ASCE Standard approach for defining the risk-consistent DRS. To do so this paper has extracted extensive material from ASCE (2005), USDOE (1994), Kennedy and Short (1994), Kennedy (1997), Kennedy (1999), Kennedy (1999a), and REI (2001).

Four issues must be addressed in order to establish the criteria for computing the risk-consistent DRS. These issues are:

1. What is the target seismic risk goal P_{FT} that is to be aimed at by the specified seismic criteria? This goal needs to be defined in terms of both a quantitative target acceptable annual probability of unacceptable performance P_{FT}, and a qualitative description as to what constitutes unacceptable performance. This issue is further discussed in Section A.4.
2. What is the level of conservatism implied by use of the specified seismic design criteria? In particular, to what degree does NUREG-0800 provide seismic margin in the structures, systems and components designed to its criteria? And how is this represented? This issue will be discussed in Section A.5.
3. To maintain the convention of using a UHRS, the DRS will be calculated by

   $$DRS = DF * UHRS \qquad \textbf{Equation A-1}$$

   where UHRS is a "reference" Uniform Hazard Response Spectrum and DF is the Design (Scale) Factor used to define the DRS relative to the UHRS. Given this basis, at what reference seismic hazard exceedance frequency H should the reference UHRS be defined? As discussed above there is a unique DRS at a site that will provide risk consistency. But there are clearly many pairs of UHRS levels and DF factors that will produce the same DRS. Therefore there is some latitude in the selection of the value of H to be used. For practical reasons it should be within the bounds of 2 to 20 times P_{FT}, as described in Section A.6. However, once the value of H is chosen the required DF to be used in Equation A-1 will be a function of the Probability Ratio R_P defined by:

   $$R_P = \frac{H}{P_{FT}} \qquad \textbf{Equation A-2}$$

   Clearly the larger the value of H the lower the UHRS and the larger DF needs to be to give the unique DRS. Therefore DF is an increasing function of R_P. In addition, DF is a decreasing function of the conservatism of the seismic design criteria (Issue #2) and a decreasing function of the amplitude of the (negative) slope of the seismic hazard curve. This issue of selecting the value of H is discussed in Section A.6.
4. Having defined P_{FT} (Issue #1), conservatism of seismic design criteria (Issue #2), and H (Issue #3), the equation for DF needs to be developed which insures that the performance goal P_{FT} is achieved with the DRS defined by Equation A-1 when UHRS is defined at the exceedance frequency H. This step involves first using a basic probabilistic analysis to find an analytical equation for the P_{FT} as a function of a seismic hazard curve and a fragility curve of a typical component, and then re-arranging and empirically simplifying this result to form

the equation for DF for use in application. Section A.3 will present the derivation of the underlying theoretical equations used to develop the equation for the Design Factor DF. The ASCE (2005) Standard equation for DF is derived and discussed in Section A.7 for R_P=10 which is proposed herein.

A.2 Summary of ASCE (2005) Standard Approach for Defining Risk Based Design Response Spectrum DRS

A fundamental assumption is that Seismic Category 1 Structures, Systems, and Components (SSCs) in a nuclear power plant will be designed for the DRS utilizing the seismic capacity, seismic demand, and seismic design criteria laid out by the U.S. NRC for nuclear power plants in NUREG-0800 (USNRC, No Date), Regulatory Guides, and professional design codes and standards referenced therein. The U.S. NRC criteria are very similar to the criteria presented in the ASCE (2005) Standard for the most stringent Seismic Design Category SDC-5D. Therefore, the criteria specified in the ASCE Standard for SDC-5D are used to define the DRS for nuclear power plants.

For SDC-5D, the quantitative target acceptable annual probability of unacceptable performance P_{FT} is[2]:

$$P_{FT} = mean\ 1x10^{-5} / yr \qquad \textbf{Equation A-3}$$

The qualitative description of acceptable performance for SDC-5D is to not exceed Limit State D which is defined in the ASCE Standard as "Essentially Elastic Behavior." Thus, the definition of unacceptable performance for SDC-5D is the "onset of significant inelastic deformation."

Thus, the DRS is established at a level such that SSCs designed to meet U.S. NRC criteria for nuclear power plants will have a target mean annual frequency[3] of $1x10^{-5}$/yr for seismic-induced onset of significant inelastic deformation (FOSID).

It should be noted that Limit State D is well short of damage that might interfere with functionality, which generally corresponds to Limit States B or C. Furthermore, the onset of significant cyclic strength reduction in structures also corresponds to Limit States B or C, and the onset of collapse corresponds to beyond Limit State A defined in the ASCE Standard. The mean annual frequency of exceeding Limit States C, B, or A which might lead to core damage are less than $1x10^{-5}$ by increasingly larger factors.

[2] The term "mean" in front of the probability here and elsewhere means that the *mean* estimate of this probability should be used, in contrast to, for example, Reg Guide 1.165, which calls for the median estimate.

[3] The terms "annual frequency" and "annual probability", while not strictly equivalent, are used interchangeably here as they are numerically equivalent at these low levels.

In order to achieve the above defined target performance goal for SDC-5D, the ASCE Standard defines the DRS by Equation A-1, where the reference UHRS is defined at a reference seismic hazard exceedance frequency H of:

$$H = \text{mean } 1x10^{-4}/yr \qquad \textbf{Equation A-4}$$

Next, the required Design Factor DF is computed as follows. First, at each spectral frequency at which the UHRS is defined, an Amplitude Ratio A_R is computed from:

$$A_R = \frac{SA_{0.1H}}{SA_H} \qquad \textbf{Equation A-5}$$

where SA_H is the spectral acceleration at the mean exceedance frequency H and $SA_{0.1H}$ is the spectral acceleration at 0.1H (i.e., the spectral accelerations at $1x10^{-4}$, and $1x10^{-5}$/yr). Then the Design Factor, DF, at each spectral frequency is given by

$$DF = \text{Maximum } (DF_1 , DF_2) \qquad \textbf{Equation A-6}$$

where

$$DF_1 = 1.0 \qquad \textbf{Equation A-7}$$

and

$$DF_2 = 0.6(A_R)^{0.80} \qquad \textbf{Equation A-8}$$

which correspond to the appropriate DF_1 and DF_2 from Table 2.2-1 of the ASCE (2005) Standard for $R_P = 10$ from Equation A-2.

Furthermore, for SDC-5D, the ASCE Standard specifies a lower bound on the DRS peak ground acceleration (PGA) of 0.10g. For nuclear power plant applications, the lower bound on the DRS should be a Reg. Guide 1.60 response spectrum anchored to a PGA of 0.10g.

A.3 Theoretical Derivation of Design Factor DF

This section develops an equation for the DF from an analytical result for the risk, that is, the probability of unacceptable performance (or "failure[4]").

[4] As used herein, "failure" consists of unacceptable FOSID

A.3.1 Rigorous Seismic Risk Equation

Given a mean seismic hazard curve and a mean fragility curve, then the mean seismic risk P_F can be obtained by numerical convolution of the mean seismic hazard curve and mean fragility curve by either of two analytically equivalent equations:

$$P_F = -\int_0^{+\infty} P_F(a)\left(\frac{dH(a)}{da}\right) da \qquad \textbf{Equation A-9}$$

$$P_F = \int_0^{+\infty} H(a)\left(\frac{dP_F(a)}{da}\right) da \qquad \textbf{Equation A-10}$$

where $P_F(a)$ is the conditional probability of failure given the ground motion level a, which, by definition, is the mean fragility curve, and $H(a)$ is the mean hazard exceedance frequency corresponding to ground motion level a. For example, in words, the first says loosely that the probability of failure is the probability that the ground motion has value a times the probability of component failure given that level, integrated over all possible levels of a. (The minus sign is a result of "correcting" for the derivative of $H(a)$ being negative. Recall the $H(a)$ is the probability of exceeding a so it decreases as a increases.)

The mean fragility curves used can be that for failure (i.e., unacceptable performance) of an individual SSC or for a plant damage state such as core damage.

A.3.2 Simplified Seismic Risk Equation

Typical seismic hazard curves are close to linear when plotted on a log-log scale (for example see Figure A-1). Thus over any (at least) ten-fold difference in exceedance frequencies such hazard curves may be approximated by a power law:

$$H(a) = K_I a^{-K_H} \qquad \textbf{Equation A-11}$$

where $H(a)$ is the annual frequency of exceedance of ground motion level a, K_I is an appropriate constant, and K_H is a slope parameter defined by:

$$K_H = \frac{1}{\log(A_R)} \qquad \textbf{Equation A-12}$$

in which A_R is the ratio of ground motions corresponding to a ten-fold reduction in exceedance frequency, Equation A-5.

So long as the fragility curve $P_F(a)$ is lognormally distributed and the hazard curve is defined by Equation A-11, a rigorous closed-form solution exists for the seismic risk (Equations A-9 or A-10). This closed-form solution is derived in Appendix B as:

$$P_F = H\ M_{50\%}^{-K_H}\ e^{\alpha}$$ **Equation A-13**

in which

$$M_{50\%} = \frac{C_{50\%}}{C_H}$$ **Equation A-14**

and

$$\alpha = \tfrac{1}{2}(K_H\beta)^2$$ **Equation A-15**

where H is any reference exceedance frequency, C_H is the UHRS ground motion level that corresponds to this reference exceedance frequency H from the seismic hazard curve, $C_{50\%}$ is the median fragility capacity, and β is the logarithmic standard deviation of the fragility.

Equation A-13 is referred to here as the simplified seismic risk equation. The only approximations in its derivation are that the hazard curve is approximated by Equation A-11 over the exceedance frequency range of interest and the fragility curve is lognormally distributed.

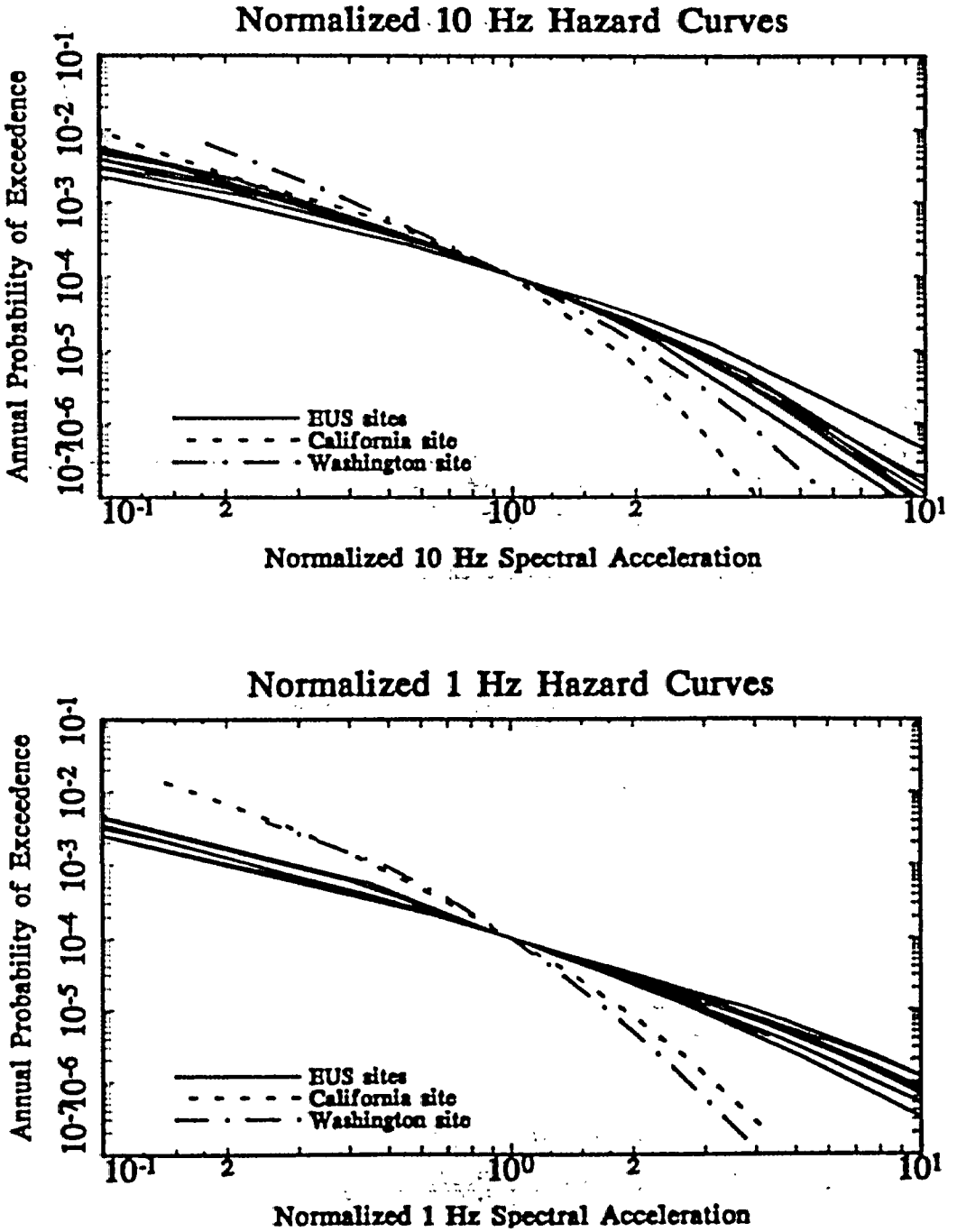

Figure A-1
SA (10 Hz) and SA (1 Hz) Hazard Curves for the Eleven Sites Normalized by the Acceleration Value Corresponding to Mean 10^{-4} Annual Probability. (From Figs. 7.7 and 7.8 of REI, 2001)

A.3.3 Design Factor Equation

With the Probability Ratio R_P defined by Equation A-2, Equation A-13 can be rearranged to define the median fragility capacity $C_{50\%}$ required to achieve a desired Probability Ratio R_P:

$$C_{50\%} = C_H\left[R_p e^{-\alpha}\right]^{1/K_H} \qquad \textbf{Equation A-16}$$

The conservatism introduced by the seismic design criteria such as NUREG-0800 can be defined by a seismic margin factor F_P given by:

$$F_P = \frac{C_P}{DRS} \qquad \textbf{Equation A-17}$$

where C_P, defined more formally below, is a value on the fragility curve corresponding to a conditional failure probability, P, i.e., C_p is a fractile of the fragility curve. In words, if one designs a component by some set of seismic criteria (e.g., NUREG-0800) for a design ground motion level DRS, those criteria will insure that this C_P fractile is F_P times larger than DRS. Next, defining the DRS by Equation A-1 and recognizing that C_H=UHRS, then:

$$F_P = \frac{C_P}{DF * C_H} \qquad \textbf{Equation A-18}$$

Lastly, the C_P fractile or "seismic capacity point" on a lognormal fragility curve can be defined in terms of the median fragility capacity $C_{50\%}$ and logarithmic standard deviation β by:

$$C_P = C_{50\%} e^{X_p \beta} \qquad \textbf{Equation A-19}$$

where X_P is the standard normal variable associated with P percent non-exceedance probability (NEP). For example, $C_{1\%}$, is factor $e^{-2.326}$ times the median fragility capacity.

Combining Equations. A-16, A-18 and A-19:

$$DF = \frac{\left[R_p e^{-f}\right]^{1/K_H}}{F_P} \qquad \textbf{Equation A-20}$$

in which

$$f = X_P(K_H\beta) - \frac{1}{2}(K_H\beta)^2 \qquad \textbf{Equation A-21}$$

Equation A-20 defines the required Design Factor DF to achieve any desired Probability Ratio R_P. As anticipated above, DF is an increasing function of R_P. For a given target P_{FT} the larger

you set H (i.e., the lower you make the UHRS), the larger R_P and DF must be to compensate for this higher H. But how strongly it depends on R_P depends on K_H, the hazard curve slope (Equation A-12).

Note, too, that the required DF is a complicated but generally decreasing function of the slope parameter K_H and a simple inverse function of the seismic conservatism factor F_P of the seismic design criteria. Again there is latitude in that the factor F_P can be defined in terms of any conditional failure probability P point on the fragility curve. The value chosen has practical implications, however. If P is defined in the 1% to 20% failure probability range, DF is only moderately sensitive to β. This insensitivity is exploited in practical seismic guidelines, such as ASCE (2005), as it permits DF to be defined effectively independently of β. The X_P values corresponding to various failure probability P levels at which F_P is to be defined are:

Table A-1
X_p Values for Different Failure Probabilities

P	X_P
1%	2.326
5%	1.645
10%	1.282
20%	0.842

As an example, if the seismic conservatism factor is defined at the 1% probability of failure level $F_{1\%}$, then:

$$DF = \frac{\left[R_P e^{-f}\right]^{1/K_H}}{F_{1\%}} \qquad \text{Equation A-22}$$

$$f = 2.326K_H\beta - \frac{1}{2}(K_H\beta)^2 \qquad \text{Equation A-23}$$

Equation A-22 will be used in Section A.7 to develop the simplified equation for the ASCE Standard Design Factor in Equation A-6 given in Section A.2 for R_P=10.

A.4 Basis for Target Performance Goal

As discussed in Section A.2, the target performance goal for the ASCE (2005) Standard SDC-5D SSCs, which was adopted herein for nuclear power plant application, is a mean frequency of $1x10^{-5}$ for seismic induced onset of significant inelastic deformation (FOSID).

The basis for selecting a quantitative target performance goal P_T of mean $1x10^{-5}$/yr is that mean $1x10^{-5}$/yr represents approximately the average seismic-induced Core Damage Frequency (CDF) reported for those nuclear power plants which have performed seismic probabilistic risk

assessments (SPRAs) and presented their results to the U.S. NRC. For example, Table A-2 shows the mean seismic CDF for 25 plants which performed SPRAs using EPRI-type hazard curves as reported in NUREG 1742 (USNRC, 2001). The reported mean seismic CDFs range from approximately $2x10^{-7}$/yr to $2x10^{-4}$/yr with a median value of $1.2x10^{-5}$/yr and a mean value of $2.5x10^{-5}$/yr. For these 25 plants, 7 plants report mean seismic CDF values significantly less than $1x10^{-5}$/yr and 7 plants report values significantly higher than $1x10^{-5}$/yr. The mean seismic CDF values for the remaining 11 plants are all close to $1x10^{-5}$/yr.

Table A-2
Mean Seismic CDF for Plants Performing Seismic PRA from Table 2.2 from NUREG 1742, Vol. 2

Plant	Mean Seismic CDF (EPRI)*	Plant	Mean Seismic CDF (EPRI)*
South Texas Project 1 & 2	1.90E-07	Seabrook	1.20E-05
Nine Mile Point 2	2.50E-07	Beaver Valley 1	1.29E-05
La Salle 1 & 2	7.60E-07	Indian Point 2	1.30E-05
Hope Creek	1.06E-06	Point Beach 1 & 2	1.40E-05
D.C. Cook 1 & 2	3.20E-06	Catawba 1 & 2	1.60E-05
Salem 1 & 2	4.70E-06	San Onofre 2 & 3	1.70E-05
Oyster Creek	4.74E-06	Columbia (Washington Nuclear Project No. 2)	2.10E-05
Surry 1 & 2	8.20E-06	TMI 1	3.21E-05
Millstone 3	9.10E-06	Oconee 1, 2, and 3	3.47E-05
Beaver Valley 2	1.03E-05	Diablo Canyon 1 & 2	4.20E-05
Kewaunee	1.10E-05	Pilgrim 1	5.80E-05
McGuire 1 & 2	1.10E-05	Indian Point 3	5.90E-05
		Haddam Neck	2.30E-04

Median of Mean Seismic CDF Value (EPRI Results)	1.20E-05
Mean of Mean Seismic CDF Value (EPRI Results)	2.50E-05
* CDF Values reported are for EPRI hazard curves. LLNL hazard curves produced substantially higher CDF results	

Additionally, a conservative bias is introduced by choosing the onset of significant inelastic deformation as the qualitative performance goal. This performance goal corresponds to significantly less damage than would be required to reach core damage. Therefore, holding the FOSID to a target of mean $1x10^{-5}$/yr insures that the CDF will be significantly below mean $1x10^{-5}$/yr. It is expected that the CDF will be between $4x10^{-6}$/yr and $0.6x10^{-6}$/yr. The basis for this expectation is presented in Section A.8.

A.5 Level of Conservatism of Specified Seismic Design Criteria

A.5.1 Factor of Conservatism for the Onset of Significant Inelastic Deformation

As noted in Section A.2, a fundamental assumption is that Seismic Category 1 SSCs will be designed for the DRS utilizing the seismic capacity, seismic demand, and seismic design criteria laid out by the U.S. NRC for nuclear power plants in NUREG-0800 (USNRC, No Date), Regulatory Guides, and professional design codes and standards referenced therein. It was also noted that these U.S. NRC criteria are very similar to the criteria presented in the ASCE (2005) Standard for SDC-5D SSCs. This ASCE Standard states that the seismic demand and structural capacity evaluation criteria presented therein are aimed at having sufficient conservatism to reasonably achieve *both* of the following:

1. Less Than About a 1% Probability of Unacceptable Performance for the Design Basis Earthquake Ground Motion, and

2. Less Than About a 10% Probability of Unacceptable Performance for a Ground Motion Equal to 150% of the Design Basis Earthquake Ground Motion

The basis for these estimated factors of Conservatism is presented in the Commentary Section C1.3 of ASCE (2005) Standard.

In computing the required DF for determining the DRS, these same factors of conservatism against the onset of significant inelastic deformation will be used for nuclear power plant Seismic Category I SSCs designed to meet NRC criteria. Even for the onset of significant inelastic deformation, the above factors of conservatism are expected to be conservatively underestimated because designers do not typically design an SSC to just barely satisfy the acceptance criteria. Additional margin or conservatism is generally included. However, no credit is taken for this added margin when determining the required DF.

Seismic fragility (i.e., the conditional probability of failure versus ground motion levels, $P_F(a)$) is typically defined as being lognormally distributed so that it can be fully described by two parameters, such as a seismic margin factor F_P corresponding to a conditional failure probability P_{FC} (Equation A-17), and an estimate of the capacity variability (i.e., the logarithmic standard deviation β). The two ASCE target levels of conservatism defined above result in the following seismic margin factors $F_{1\%}$, $F_{5\%}$, $F_{10\%}$, and $F_{50\%}$, corresponding to a 1%, 5%, 10%, and 50% conditional probability of unacceptable behavior, respectively:

Table A-3
Seismic Margin Factors for Different β Values

β	$F_{1\%}$	$F_{5\%}$	$F_{10\%}$	$F_{50\%}$
.30	1.10	1.35	1.5	2.2
.4	1	1.31	1.52	2.54
.5	1	1.41	1.69	3.2
.6	1	1.5	1.87	4.04

Note that for a logarithmic standard deviation less than 0.39, the second of the two conditional probability goals controls the fragility. For β greater than 0.39, the first goal controls. By specifying both goals, the following margins are achieved:

- $F_{1\%} \geq 1.0$
- $F_{5\%} \geq 1.3$
- $F_{10\%} \geq 1.5$
- $F_{50\%}$ increases with increasing β

The required Design Factor DF will be computed in Section A.7 for the above values of β which range from 0.3 to 0.6, and the corresponding seismic factors of conservatism F_P.

From EPRI (1994) and past SPRA studies, for structures and major passive mechanical components mounted on the ground or at low elevations within structures, β typically ranges from 0.3 to 0.5. For active components mounted at high elevations in structures the typical β range is 0.4 to 0.6. Therefore, the range 0.3 to 0.6 covers the practical range for β.

A.5.2 Expected Factor of Conservatism for Core Damage Fragility

The seismic design criteria factors of conservatism defined in Section A.5.1 are for the unacceptable performance defined as the onset of significant inelastic deformation. These margin factors are substantially too low for a Core Damage definition of unacceptable performance.

For the new Standard Plant designs, the U.S. NRC staff has required that a study be performed to show that the Core Damage HCLPF[5] margin factor is at least 1.67 times the DRS. The HCLPF point on the fragility curve computed in accordance with EPRI (1991) corresponds to the mean 1% conditional probability of failure point on the Core Damage fragility curve. Thus, for Core Damage:

$$F_{1\%} = 1.67 \qquad \text{Equation A-24}$$

[5] HCLPF is short for "High Confidence of a Low Probability of Failure".

For the above reason, NUREG/CR-6728 used the more liberal $F_{1\%}$=1.67 HCLPF margin when computing risk-consistent DRS.

Section A.8 computes the mean Core Damage Frequency (CDF) when the DRS is defined by the ASCE Standard method described in Section A.2 and a Core Damage $F_{1\%}$=1.67 is used.

A.6 Reference Mean Hazard Exceedance Frequency H Used to Define the Reference UHRS

For SDC-5D SSCs, the ASCE (2005) Standard defines the reference mean hazard exceedance frequency H to be:

$$H = \text{mean } 1 \times 10^{-4}/\text{yr} \qquad \textbf{Equation A-25}$$

and defines the Design Factor DF so as to achieve a Probability Ratio R_P of 10; together these two values achieve the target FOSID Performance Goal of P_{FT}= mean $1x10^{-5}$/yr.

While the ratio of H/R_p is important to obtaining the final Performance Goal, this particular choice of H and R_p values is, as discussed above, rather arbitrary. Any hazard exceedance frequency H between mean $2x10^{-4}$/yr and $2x10^{-5}$/yr could have been used to achieve P_{FT}= mean $1x10^{-5}$/yr, but for a different H value the value of R_P would have to change correspondingly. That would be done by changing the value of DF. The result would be essentially the same Design Response Spectrum (DRS) for any H and R_P pair. Therefore the reasons for a particular choice of H (and hence R_P) is practical convenience.

The primary reason for choosing R_P=10 is to insure that the DF is never less than unity, which would be an unfamiliar value for a structural load factor. For Western U.S. sites near major tectonic plate boundaries, the mean hazard curve has a steep slope so that the Amplitude Ratio A_R defined by Equation A-5 is less than 1.9 implying the slope K_H is greater than 3.6. For these Western U.S. sites DF=1.0 (as given by Equation A-6) so that the DRS simply equals the mean $1x10^{-4}$ UHRS. For Central and Eastern U.S. (CEUS) sites the mean hazard curve slope is shallower so that A_R typically lies in the range of 1.9 to 4.0 so that the DF ranges from 1.0 to 1.8. For these CEUS sites the DF is always equal to or greater than 1.0, but never excessively large. Thus, the proposed method never ends up with a DRS less than the mean $1x10^{-4}$ UHRS nor likely to be larger than 1.8 times the mean $1x10^{-4}$ UHRS.

A.7 Assessment of ASCE Standard Design Factor DF for Probability Ratio R_P of 10

The ASCE Standard DF is computed by Equation A-6 which was obtained by an empirical fit. In this section we assess how well the simplified formula works by comparing these DFs with those obtained from the more precise formula, Equation A-22, and by comparing how close the failure probabilities implied by use of Equation A-6 are to the target acceptable failure probability. The latter computation will be done two ways, using the analytical approximation (Equation A-13) and by numerical integration of the exact integrals.

A.7.1 Computation of Required DF for Comparison with ASCE Standard DF

The required Design Factors DF computed using Equation A-22 to achieve R_P=10 for the onset of significant inelastic deformation $F_{1\%}$ and β combinations defined in Section A.5.1 are shown in Table A-4 for an Amplitude Ratio A_R range from 1.5 to 6.0. These required DF factors are compared with ASCE Standard DF given by Equation A-6. The ASCE Standard DF Equation A-6 was empirically developed to closely fit these required DF values.

Table A-4
Design Factor DF Values Required to Achieve A Probability Ratio R_P = 10

A_R	DF				DF
	$F_{1\%}$=1.1 β = .3	$F_{1\%}$=1.0 β = .4	$F_{1\%}$=1.0 β = .5	$F_{1\%}$=1.0 β = .6	Eqn (A-6)
1.5	0.88	0.93	0.95	1.03	1.0
1.75	0.96	0.96	0.91	0.91	1.0
2	1.05	1.03	0.95	0.9	1.04
2.25	1.16	1.11	1	0.93	1.15
2.5	1.27	1.21	1.07	0.97	1.25
2.75	1.38	1.3	1.14	1.03	1.35
3	1.50	1.4	1.22	1.08	1.44
3.25	1.61	1.5	1.3	1.14	1.54
3.5	1.73	1.6	1.38	1.21	1.63
3.75	1.84	1.7	1.46	1.27	1.73
4	1.96	1.8	1.54	1.34	1.82
4.25	2.07	1.9	1.62	1.4	1.91
4.5	2.19	2.01	1.7	1.47	2.0
4.75	2.30	2.11	1.79	1.54	2.09
5	2.42	2.21	1.87	1.6	2.17
5.25	2.54	2.31	1.95	1.67	2.26
5.5	2.65	2.42	2.04	1.74	2.35
5.75	2.77	2.52	2.12	1.8	2.43
6	2.88	2.62	2.2	1.87	2.52

It can be seen that the ASCE Standard DFs given by Equation A-6 are conservatively biased on average. For the practical A_R range from 1.5 to 4.0, these Equation A-6 DF values range between 93% for β=0.3 and 136% for β=0.6 of the required DF. This shows that there is only a moderate sensitivity of DF to the logarithmic standard deviation of the fragility curve. Hence it could, for practical purposes, be dropped from appearing in the ASCE Standard definition.

A.7.2 Comparison of the Target Risk Goal, P_{FT}, with the Computed Risk, P_{FC}, Using the DF Defined by Equation A-6

A.7.2.1 Using the Simplified Risk Equation

The Simplified Risk Equation, Equation A-13, was derived assuming the hazard curve can be approximated by Equations A-11 and A-12. From Equation A-13, the computed mean unacceptable performance annual probability P_{FC} can be obtained by recasting Equation A-22 to:

$$(P_{FC}/H) = e^{-f}[DF * F_{1\%}]^{-K_H} \qquad \textbf{Equation A-26}$$

where f is obtained from Equation A-23.

Table A-5 presents P_{FC} results computed from Equation A-26 with the ASCE Standard DF defined by Equation A-6 and $F_{1\%}$ defined in Section A.5.1 for various logarithmic standard deviations β. The conclusion is that with the ASCE Standard DRS defined as described in Section A.2 the annual frequency of onset of significant inelastic deformation (FOSID) for an SSC that barely meets the acceptance criteria with no additional margin lies in the range of:

$$\text{FOSID} = \text{mean } 1.2\text{x}10^{-5}/\text{yr to } 0.5\text{x}10^{-5}/\text{yr} \qquad \textbf{Equation A-27}$$

which on average is safely less than the target performance goal and never is higher than 120% of the target goal.

Table A-5
Individual SSC Seismic Risk P_{FC} (FOSID) Obtained Using Equation A-6 Design Factors

(P_{FC} values shown should be multiplied times $0.1*H_D$)

A_R	P_{FC}			
	$F_{1\%}$=1.1 β = .3	$F_{1\%}$=1.0 β = .4	$F_{1\%}$=1.0 β =.5	$F_{1\%}$=1.0 β = .6
1.5	0.47	0.67	0.76	1.2
1.75	0.82	0.84	0.69	0.68
2	1.03	0.95	0.72	0.61
2.25	1.03	0.92	0.68	0.55
2.5	1.04	0.92	0.68	0.53
2.75	1.06	0.92	0.69	0.54
3	1.08	0.93	0.7	0.55
3.25	1.09	0.95	0.71	0.56
3.5	1.1	0.96	0.73	0.57
3.75	1.12	0.97	0.74	0.59
4	1.13	0.98	0.76	0.6
4.25	1.14	1	0.77	0.61
4.5	1.15	1.01	0.78	0.62
4.75	1.16	1.02	0.79	0.64
5	1.17	1.02	0.81	0.65
5.25	1.17	1.03	0.82	0.66
5.5	1.18	1.04	0.83	0.67
5.75	1.19	1.05	0.83	0.68
6	1.19	1.05	0.84	0.68

This degree of variability in achieved P_{FC} cannot be avoided for any simple criteria that are independent of β because P_{FC} varies by about a factor of two as a function of β. The goal has been to specify DF values that accurately achieve the target performance goal for low variability failure modes (β between 0.3 and 0.4) while accepting increased conservatism for larger variability failure modes (β larger than 0.4).

A.7.2.2 Using Rigorous Numerical Convolution of Fragility and Actual Hazard Curves

Figure A-1 shows some representative normalized hazard curves taken from Figs 7.7 and 7.8 of NUREG/CR-6728 (REI, 2001). These hazard curves are all normalized to unity spectral acceleration at the reference hazard exceedance frequency H = mean $1x10^{-4}$/yr for ease of visualizing the differences in hazard curve slopes. Table A-6 presents the tabulated normalized

spectral acceleration values SA at 1 Hz and 10 Hz for one Eastern U.S. hazard curve and for the California hazard curve.

Table A-6
Typical Normalized Spectral Acceleration Hazard Curve Values

Hazard Exceedance Frequency $H_{(SA)}$	Eastern U.S.		California	
	1 Hz SA	10 Hz SA	1Hz SA	10 Hz SA
5×10^{-2}	0.014	0.018	0.087	0.046
2×10^{-2}	0.027	0.034	0.13	0.072
1×10^{-2}	0.045	0.055	0.175	0.100
5×10^{-3}	0.07	0.089	0.236	0.139
2×10^{-3}	0.143	0.169	0.351	0.215
1×10^{-3}	0.235	0.275	0.474	0.334
5×10^{-4}	0.383	0.424	0.629	0.511
2×10^{-4}	0.681	0.709	0.814	0.762
1×10^{-4}	1.00	1.0	1.0	1.0
5×10^{-5}	1.46	1.41	1.23	1.22
2×10^{-5}	2.35	2.13	1.61	1.51
1×10^{-5}	3.27	2.88	1.89	1.76
5×10^{-6}	4.38	3.65	2.2	2.05
2×10^{-6}	6.44	4.62	2.68	2.42
1×10^{-6}	8.59	5.43	3.1	2.72
5×10^{-7}	10.34	6.38	3.58	3.06
2×10^{-7}	13.21	7.9	4.24	3.56
1×10^{-7}	15.9	9.28	4.67	3.84

The approximate hazard curves used in the simplified risk analysis of Section A.7.2.1 are defined by Equations A-11 and A-12 with A_R defined by Equation A-5. These approximate hazard curves would appear as a straight line on the log-log plots of Figure A-1 with the amplitude and slope defined by the spectral accelerations at $1x10^{-4}$/yr and $1x10^{-5}$/yr hazard exceedance frequencies. However, all actual seismic hazard curves have a downward curvature similar to those shown in Figure A-1 when plotted on log-log plots. The intent of this section is to study the effect of this downward curvature on the P_{FC} computed by rigorous numerical convolution versus the P_{FC} computed in Section A.7.2.1 using the simplified risk equation method.

For each of the four normalized hazard curves tabulated in Table A-6, Table A-7 shows the Amplitude Factor A_R computed by Equation A-5, the ASCE Standard Design Factor DF computed by Equation A-6, and the resulting DRS spectral accelerations computed by Equation A-1. The SSC fragility curves are defined by conservatism factors given in Section A.5.1 times

the normalized DRS for each case considered. The actually achieved P_{FC} values are also shown in Table A-7.

Table A-7
Individual SSC Seismic Risks P_{FC} (FOSID) Achieved for Representative Hazard Curves

Hazard Curve	UHRS SA_{UHRS}	A_R	DF	DRS SA_{DRS}	SSC Seismic Risk P_{FC} ($*10^{-5}$)			
					$F_{1\%}$=1.1 β = 0.30	$F_{1\%}$=1.0 β = 0.40	$F_{1\%}$=1.0 β = 0.50	$F_{1\%}$=1.0 β = 0.60
EUS 1Hz	1.00	3.27	1.55	1.55	1.09	0.93	0.69	0.52
EUS 10 Hz	1.00	2.88	1.40	1.40	1.03	0.87	0.62	0.46
Calif 1 Hz	1.00	1.89	1.00	1.00	1.04	0.96	0.73	0.61
Calif 10 Hz	1.00	1.76	1.00	1.00	0.84	0.78	0.58	0.48

By comparing the P_{FC} values presented in Table A-7 with those presented in Table A-5 for the same A_R and β cases, one can see that the simplified risk equation approach used in Section A.7.2.1 for Table A-5 introduces a slight, but negligible, conservative bias for the computed P_{FC} so long as A_R is defined by Equation A-5 and the extrapolation beyond the range where A_R is defined is not large.

Therefore, the FOSID conclusion reached in Section A.7.2.1 and presented in Equation A-27 remains valid.

A.8 Estimation of Core Damage Frequency (CDF) When DRS is Defined by ASCE Standard Method

Section A.5.2 indicates that for new Standard Plant designs the Core Damage HCLPF seismic margin factor $F_{1\%}$ is at least 1.67. With the DRS defined by the ASCE Standard for SDC-5D SSCs, it was shown in Section A.7 that the FOSID will lie within the range of 0.5×10^{-5}/yr and 1.2×10^{-5}/yr. The Core Damage Frequency (CDF) will be much less assuming a HCLPF seismic margin $F_{1\%}$=1.67. Table A-8 shows the CDF obtained from numerically convolving hazard curves and lognormal fragility curves. The fragility curves have HCLPF seismic margin $F_{1\%}$=1.67 and logarithmic standard deviations β in the range of 0.3 to 0.6. The four normalized hazard curves are defined in Table A-6.

Table A-8
Core Damage Frequency (CDF) for DRS Defined by ASCE Standard 43-5 Method and HCLPF Seismic Margin of 1.67

Hazard Curve	DRS	CDF (*10^{-6})			
	SA_{DRS}	β=0.30	β=0.40	β=0.50	β=0.60
EUS 1Hz	1.55	4.3	2.9	2.1	1.6
EUS 10 Hz	1.40	3.1	2.0	1.4	1.1
Calif 1 Hz	1.00	1.8	1.2	1.0	0.9
Calif 10 Hz	1.00	1.1	0.8	0.7	0.6

The CDF values are in the range of 4.3×10^{-6}/yr to 0.6×10^{-6}/yr. These CDF values are in the low range of CDF values shown in Table A-2 for existing plants.

A.9 References

ASCE (2005). *Seismic Design Criteria for Structures, Systems, and Components in Nuclear Facilities*, Amer. Soc. Civil Engrs, Rept. ASCE/SEI 43-05.

EPRI (1991). *A Methodology for Assessment of Nuclear Power Plant Seismic Margin,* EPRI NP-6041-SL, Revision 1, Electric Power Research Institute, August.

EPRI (1994). *Methodology for Developing Seismic Fragilities,* EPRI TR-103959, Electric Power Research Institute, June.

Kennedy, R.P. and Short, S.A. (1994). *Basis for Seismic Provisions of DOE-STD-1020,* UCRL-CR-111478, U.S. Dept. of Energy, April.

Kennedy, R.P. (1997). *Establishing Seismic Design Criteria To Achieve an Acceptable Seismic Margin,* Plenary/5, Transactions of the 14th International Conference on Structural Mechanics in Reactor Technology, Lyon, France, August.

Kennedy, R.P. (1999). *Development of Risk-Based Seismic Design Criterion,* Proceedings of the OECD-NEA Workshop on Seismic Risk, Tokyo, Japan, August.

Kennedy, R.P. (1999a). *Overview of Methods for Seismic PRA and Margin Assessments Including Recent Innovations,* Proceedings of the OECD-NEA Workshop on Seismic Risk, Tokyo, Japan, August 1999.

Risk Engineering, Inc, (REI) (2001). *Technical Basis for Revision of Regulatlory Guidance on Design Ground Motions: Hazard- and Risk-consistent Ground Motion Spectra Guidelines*, US Nuc. Reg. Comm. Rept NUREG/CR-6728, October.

USDOE (1994). *Natural Phenomena Hazards Design and Evaluation Criteria for Department of Energy Facilities,* DOE-STD-1020-94, U.S. Dept. of Energy, April.

USNRC (No Date). *Standard Review Plan,* NUREG-0800, U.S. NRC.

USNRC (2001). *Perspective Gained From the Individual Plant Examination of External Events (IPEEE) Program,* NUREG-1742, Volumes 1 and 2, U.S. NRC, Sept.

B
DERIVATION OF CLOSED FORM SOLUTION TO RISK EQUATION

Appendix B was written by Robert P. Kennedy

Assuming a lognormally distributed fragility curve with median capacity, C_{50}, and logarithmic standard deviation β, and defining the hazard exceedance probability $H_{(a)}$ by Equation A-11, then from Equation A-10 one obtains[6]:

$$P_F = \int_0^{\infty} \left\{K_I a^{-K_H}\right\} \left[\left(a\beta\sqrt{2\pi}\right)\exp\left\{\frac{(\ell n\, a - M)^2}{2\beta^2}\right\}\right]^{-1} da \qquad \textbf{Equation B-1}$$

in which

$$M = \ell n \;\; C_{50} \qquad \textbf{Equation B-2}$$

Defining $x = \ell n\, a$, Equation B.1 becomes:

$$P_F = \frac{K_I}{\beta\sqrt{2\pi}} \int_{-\infty}^{+\infty} \left[\exp\left\{K_H x - \left(\frac{(x-M)^2}{2\beta^2}\right)\right\}\right] dx \qquad \textbf{Equation B-3}$$

Many statistical textbooks[1] provide the solution to the definite integral shown in Equation B-3. The result is:

$$P_F = K_I \exp\left\{-K_H M + \tfrac{1}{2}(K_H\beta)^2\right\} \qquad \textbf{Equation B-4}$$

or from the previous definition of M:

$$P_F = K_I C_{50}^{-K_H} e^{\frac{1}{2}(K_H\beta)^2} \qquad \textbf{Equation B-5}$$

Defining H as any reference exceedance frequency, C_H is the ground motion level that corresponds to this reference exceedance frequency H, then from Equation A-11:

---

[6] Elishakoff, I., Probabilistic Methods in the Theory of Structures, John Wiley & Sons, 1983

$$K_I = H[C_H]^{K_H}$$ **Equation B-6**

from which:

$$P_F = HF_{50\%}^{-K_H} e^{\alpha}$$ **Equation B-7**

$$F_{50\%} = \frac{C_{50\%}}{C_H}$$ **Equation B-8**

$$\alpha = \frac{1}{2}(K_H \beta)^2$$ **Equation B-9**

Export Control Restrictions

Access to and use of EPRI Intellectual Property is granted with the specific understanding and requirement that responsibility for ensuring full compliance with all applicable U.S. and foreign export laws and regulations is being undertaken by you and your company. This includes an obligation to ensure that any individual receiving access hereunder who is not a U.S. citizen or permanent U.S. resident is permitted access under applicable U.S. and foreign export laws and regulations. In the event you are uncertain whether you or your company may lawfully obtain access to this EPRI Intellectual Property, you acknowledge that it is your obligation to consult with your company's legal counsel to determine whether this access is lawful. Although EPRI may make available on a case-by-case basis an informal assessment of the applicable U.S. export classification for specific EPRI Intellectual Property, you and your company acknowledge that this assessment is solely for informational purposes and not for reliance purposes. You and your company acknowledge that it is still the obligation of you and your company to make your own assessment of the applicable U.S. export classification and ensure compliance accordingly. You and your company understand and acknowledge your obligations to make a prompt report to EPRI and the appropriate authorities regarding any access to or use of EPRI Intellectual Property hereunder that may be in violation of applicable U.S. or foreign export laws or regulations.

Printed on recycled paper in the United States of America

The Electric Power Research Institute (EPRI)

The Electric Power Research Institute (EPRI), with major locations in Palo Alto, California, and Charlotte, North Carolina, was established in 1973 as an independent, nonprofit center for public interest energy and environmental research. EPRI brings together members, participants, the Institute's scientists and engineers, and other leading experts to work collaboratively on solutions to the challenges of electric power. These solutions span nearly every area of electricity generation, delivery, and use, including health, safety, and environment. EPRI's members represent over 90% of the electricity generated in the United States. International participation represents nearly 15% of EPRI's total research, development, and demonstration program.

Together...Shaping the Future of Electricity

Program:

Technology Innovation

1012044

ELECTRIC POWER RESEARCH INSTITUTE

3420 Hillview Avenue, Palo Alto, California 94304-1395 • PO Box 10412, Palo Alto, California 94303-0813 USA

800.313.3774 • 650.855.2121 • askepri@epri.com • www.epri.com